Evolution of the eccentricity and orbital inclination caused by planet-disc interactions

Jean Teyssandier

UPMC SORBONNE UNIVERSITÉS

THÈSE DE DOCTORAT
DE L'UNIVERSITÉ PIERRE ET MARIE CURIE

Spécialité : Physique

École doctorale : ASTRONOMIE ET ASTROPHYSIQUE D'ÎLE-DE-FRANCE

réalisée à

l'Institut d'Astrophysique de Paris

présentée par

Jean TEYSSANDIER

pour obtenir le grade de :

DOCTEUR DE L'UNIVERSITÉ PIERRE ET MARIE CURIE

Sujet de la thèse :

Évolution de l'excentricité et de l'inclinaison orbitale due aux interactions planètes-disque

soutenue le 16 Septembre 2014

devant le jury composé de :

Bruno Sicardy	**Président**
Carl Murray	**Rapporteur**
Sean Raymond	**Rapporteur**
Alessandro Morbidelli	**Examinateur**
Clément Baruteau	**Examinateur**
Caroline Terquem	**Directrice de thèse**

Une mathématique bleue
Dans cette mer jamais étale
D'où nous remonte peu à peu
Cette mémoire des étoiles

Léo Ferré, *La mémoire et la mer*

Remerciements

Mes remerciements vont tout d'abord à Caroline, pour avoir accepté de diriger cette thèse. Ca a été un plaisir de pouvoir profiter du large spectre de ses connaissances, et de tant apprendre à son contact. Je lui suis aussi redevable pour la rigueur qu'elle a imposée à mon travail et qui ne pourra que m'être bénéfique pour la suite. Je la remercie enfin de m'avoir laissé une grande liberté dans mes recherches, m'encourageant à explorer mes propres pistes et développer mes idées, et de toujours avoir laissé sa porte ouverte à la discussion. C'est aussi grâce à elle et Steve Balbus que j'ai pu passer deux si belles années à Oxford. Les aléas de la recherche ont parfois du bon!

Je remercie aussi Carl Murray et Sean Raymond d'avoir accepté de servir en tant que rapporteurs de cette thèse, ainsi que Bruno Sicardy, Alessandro Morbidelli et Clément Baruteau pour avoir accepté d'en être les examinateurs.

Je remercie aussi Frederic Rasio et Smadar Naoz de m'avoir accueilli à l'Université de Northwestern durant les stages qui ont précédé ma thèse. Ce sont eux qui m'ont définitivement donné le goût pour la dynamique des exoplanètes. Je remercie aussi John Papaloizou pour la collaboration qu'il a apportée à l'un des papiers publiés dans cette thèse.

Cette thèse n'aurait pas été une si belle expérience sans toutes les rencontres qu'elle a occasionnées en chemin. Il y a d'abord les anciens du M2 de l'Observatoire, Élodie, Andy, Jessica, Claire-Line, Alex, Élise et les autres. À l'IAP, c'est toujours un plaisir de revenir passer du temps avec Vincent, Flavien et tous les autres doctorants. À Oxford, je remercie Suzanne Aigrain de m'avoir accueilli dans son groupe, avec à la clé les fameux déjeuners du vendredi! C'est un plaisir d'avoir côtoyé ses étudiants, en particulier Tom, Ed et Ruth. Enfin, la vie à Oxford n'aurait pas été la même sans Thibaut, Rich et Shravan. Un grand merci au passage à Rich, pour avoir relu quelques bouts de ma thèse. Plus généralement, ce fut un plaisir de partager durant deux ans la vie du groupe d'astrophysique d'Oxford.

Peu de choses durant mon séjour à Oxford m'ont fait plus plaisir que de recevoir la visite de mon frère et ma soeur. J'espère qu'ils auront l'occasion de venir à Cambridge voir si les pubs sont si différents de ceux d'Oxford... Enfin, cette thèse est dédiée à mes parents, pour leur soutien inconditionnel durant toute la poursuite de mes études. Si j'en suis arrivé là, c'est surtout grâce à eux.

Abstract

Since the discovery of the first planet orbiting a main-sequence star outside the solar system in 1995, the field of exoplanet studies has grown rapidly, both from the observational and theoretical sides. Despite the fact that we are still lacking a global picture for the formation and evolution of planetary systems, it is now commonly accepted that planets form in protoplanetary discs and interact with them in the early stages of their evolution. This thesis aims at studying some of these interactions.

The observations of extrasolar planets have brought several puzzling results to the attention of the community. One of them is the existence of hot Jupiters, giant gaseous planets which orbit their parent star with a period of a few days only. The commonly accepted scenario is that they formed in the outer parts of the disc and migrated inward. Furthermore, a significant number of planets detected so far, especially by the method of radial velocities, have high eccentricities. This is in contrast with our own solar system where giant planets have quasi-circular orbits. Such a distribution of eccentricities may be the signature of strong dynamical interactions between the different components of a same planetary system. Finally, there are short-period planets whose orbits is misaligned with the axis of rotation of their host star, which could possibly argue against the smooth migration of planets in their disc.

Therefore, it is important to disentangle between the orbital characteristics that planets acquired through mutual dynamical interactions, and the ones they acquired when they interacted with the disc. Firstly, it gives constraints on the physical parameters of protoplanetary discs. Secondly, it is interesting to know the properties of the system of planets after the disc has dissipated, and what sort of initial conditions one can expect when planets start to interact freely one with each other. For instance, one can ask if it is possible for planets to reach large eccentricities and inclinations when the disc was still present, and whether they could maintain them or not.

The first topic that we study in this thesis is the interaction between a planet and a disc, when the orbit of the planet has a large inclination with respect to the mid-plane of the disc. If the initial inclination of the orbit is larger than some critical value, the gravitational force exerted by the disc on the planet leads to a Kozai cycle in which the eccentricity of the orbit is pumped up to large values and oscillates with time in antiphase with the inclination. On the other hand, both the inclination and the eccentricity are damped by the frictional force that the planet is subject to when it crosses the disc. Typically, Neptune or lower mass planets would remain on inclined and eccentric orbits over the disc lifetime, whereas orbits of Jupiter or higher mass planets would align and circularize.

A mechanism that could explain this primordial misalignment between planets and discs, and more generally, the population of planets with large spin-orbit misalignments, is that of resonant migration. When two planets migrate in a disc, it is possible that they enter a configuration where the ratio of their orbital periods is equal to the ratio between two small integers. This configuration is referred to as mean motion resonance. If the resonance is maintained during the migration, the eccentricities can grow to high values. Simulations have shown that, in some cases, the inclinations could also grow to high values. However, the disc tends to damp the eccentricities and inclinations and keep them to low values. In this thesis we study, analytically and numerically, the conditions needed for a system of two migrating planets trapped in a 2:1 mean motion resonance to enter an inclination–type resonance. We show that this resonance can be achieved only after the eccentricities have reached a critical value. However the maximum value reached by the eccentricities is limited by the disc damping. We show that the criterion for triggering an inclination–type resonance is a function of the ratio between the eccentricity damping timescale and the orbital migration timescale. If this ratio is larger than a few tenths, the system can enter an inclination–type resonance. However, both observations and theory suggest that this ratio probably cannot exceed a few hundredths. We conclude that excitation of inclinations through the type of resonance described here is very unlikely to happen in a system of two planets migrating in a disc.

Résumé

Depuis la découverte de la première planète orbitant une étoile de la séquence principale autre que le Soleil en 1995, ce champ de recherche a connu une croissance vertigineuse, tant au niveau des observations, que des modèles théoriques développés en parallèle. Même si la formation et l'évolution des systèmes planétaires restent encore mal comprises dans leur globalité, Il est à peu près certain que les planètes se forment dans des disques protoplanétaires et interagissent avec ces derniers durant la phase primordiale de leur évolution. Cette thèse s'attache à décrire certains aspects de ces interactions.

Parmi les problèmes soulevés par les nombreuses observations d'exoplanètes, on peut citer l'existence des Jupiter chaudes, géantes gazeuses dont la révolution autour de leur étoile s'effectue en quelques jours à peine. Il est communément admis qu'elles se sont formées dans les parties externes du disque, pour ensuite migrer vers l'intérieur. Cependant , les processus de migration restent encore débattus. On pourra aussi noter qu'un nombre important de planètes détectées, notamment par la méthode des vitesses radiales, présentent de fortes excentricités. Cette observation contraste avec celle de notre propre Système Solaire, où les planètes géantes ont des orbites quasi-circulaires. Cette distribution d'excentricités témoigne probablement d'une certaine richesse dans les interactions dynamiques entre les planètes d'un même système. Un autre résultat majeur des quelques dernières années est l'observation de planètes à faible période orbitale dont l'orbite n'est pas alignée avec l'axe de rotation de leur étoile. Cette observation pourrait potentiellement remettre en question l'idée selon laquelle ces planètes acquièrent leur faible période par le biais de la migration au sein du disque.

Par conséquent, il est important de pouvoir différencier quelles sont les caractéristiques observationelles des exoplanètes qui sont le fruit de leurs interactions mutuelles, et celles qui peuvent être expliquées lors de la phase d'interaction avec le disque protoplanétaire. D'une part, cela permet d'imposer des contraintes sur la physique des disques protoplanétaires. D'autre part, il est in-

téressant de savoir à quoi ressemble le système de planètes une fois que le disque se dissipe, et à quelles conditions intiales peut-on s'attendre lorsque les planétes commencent à interagir entre elles sans la présence du disque. Par exemple, est-il possible pour une ou des planètes d'acquérir de l'excentricité et de l'inclinaison au sein du disque, et de les maintenir par la suite? De plus, il est certain que le disque domine l'évolution des planètes au stage primordial de leur vie, mais jusqu'à quel point cela limite-t-il les interactions entre les planètes?

Le premier effet étudié dans cette thèse concerne l'évolution d'une planète dont l'orbite serait inclinée par rapport au plan du disque protoplanétaire. Si l'inclinaison relative entre les deux plans est plus grande qu'une certaine valeur critique, le potentiel gravitationnel du disque provoque d'importantes variations de l'excentricité et de l'inclinaison de la planète, par le biais de cycles de Kozai. Cependant, l'excentricité et l'inclinaison sont tous deux amorties par la force de friction qui s'exerce sur la planète quand elle traverse le plan du disque. La planète a donc tendance à se réaligner avec le disque, sur une orbite circulaire. Nous montrons que pour des planètes de la taille de Jupiter et plus, ce réalignement se fait en un temps plus court que la durée de vie du disque. Cependant, les planètes de la taille de Neptune restent inclinées par rapport au plan du disque, et acquièrent même de l'excentricité grâce à l'effet Kozai.

Un mécanisme pouvant expliquer ce non-alignement primordial entre le disque et la planète, et qui pourrait plus généralement expliquer l'observation de planètes dont l'orbite est inclinée par rapport à l'axe de rotation de l'étoile, est connu sous le nom de migration résonante. Lorsque deux planètes migrent dans un disque, il peut arriver qu'elles entrent dans une configuration où le rapport de leurs périodes orbitales est aussi le rapport entre deux petits nombres entiers. Ce phénomène est connu sous le nom de résonance de moyen mouvement. Lorsque la résonance est maintenue au cours de la migration, l'excentricité des planètes augmente. Dans certains cas, des simulations ont montré que l'inclinaison pouvait aussi augmenter significativement. Cependant, là encore, le disque cherche à maintenir l'excentricité et l'inclinaison à des faibles valeurs. Dans cette thèse, nous étudions, analytiquement et numériquement, les conditions requises pour que le système rentre dans une résonance d'inclinaison au cours de la migration. Nous montrons que cette résonance ne peut être atteinte que si l'excentricité est plus grande qu'une certaine valeur critique. Cependant, la valeur maximale que peut atteindre l'excentricité est limitée par l'amortissement dû au disque, qui freine la croissance. Nous montrons que la possibilité d'entrer en résonance d'inclinaison est fonction du rapport entre le temps d'amortissement de l'excentricité et le temps de migration orbitale. Si le rapport entre ces deux

temps est plus grand que quelques dixièmes, alors il devient possible pour le système d'entrer en résonance d'inclinaison. Cependant, un certain nombre d'études, appuyées par des observations, ont montré que le rapport entre ces deux temps n'excède probablement pas quelques centièmes. Par conséquent, il semble difficile pour deux planètes d'atteindre de fortes excentricités et inclinaisons lors de la phase où elles interagissent avec le disque.

Table of symbols and abbreviations

Symbol	Signification	Value in International System of Units
AU	Astronomical unit	1.4960×10^{11} m
G	Gravitational constant	6.6738×10^{-11} m^3 kg^{-1} s^{-2}
c	Speed of light in vacuum	299792458 m s^{-1}
$M_\odot$	Solar Mass	1.9891×10^{30} kg
M_J	Jupiter Mass	1.8981×10^{30} kg
M_N	Neptune Mass	1.0243×10^{26} kg
$M_\oplus$	Earth Mass	5.9722×10^{24} kg
$R_\odot$	Solar radius	6.963×10^{8} m
R_J	Jupiter radius	6.991×10^{7} m
R_N	Neptune radius	2.462×10^{7} m
$R_\oplus$	Earth radius	6.371×10^{6} m

Contents

Chapter 1

Introduction

Contents

1.1 Historical overview

The thrilling idea that other worlds may exist in the Universe is not new, and has fascinated Mankind for a long time. In fact, it can be traced back to ancient times. For instance, Metrodorus of Chios (4th century BC) reportedly wrote that "to suppose that Earth is the only populated world in infinite space is as absurd as to believe that in an entire field sown with millet, only one grain will grow". According to some writings by Archimedes, another Greek astronomer, Aristarchus of Samos, presented around 300 BC the first heliocentric model. However, the prevalent model remained for centuries the geocentric construction of Ptolemy. While his work was improved and criticized by Arab astronomers throughout the Middle Ages, the revolution in Europe came from Copernicus, who proposed the first complete heliocentric model during the sixteenth century. The monk Giordano Bruno saw further application to this model and imagined the Sun as being a small star among many others. He famously wrote " [God] is glorified not in one, but in countless suns; not in a single earth, a single world, but in a thousand thousand, I say in an infinity of worlds" in *De l'infinito universo et Mondi* (1584). At the same time, Galileo Galilei first pointed a telescope to the sky and showed that Jupiter was itself orbited by many moons, strongly arguing against the geocentric view of the Universe. The centuries that followed were a golden age for astronomy, with Kepler and Newton understanding the motion of planets. Improvements in optics and observation methods lead to the detection of Uranus by William Herschel in 1781. In parallel, Laplace published his *Traité de Mécanique Céleste*, the first modern treaty of celestial mechanics, based on calculus rather than geometry (a point of

view which Newton adopted). The triumph of celestial mechanics in the 19th century came with the discovery of Neptune by Adams and Le Verrier in the 1840's, based only on observations of irregularities in the motion of Uranus.

However, for most of the 19th and 20th century, celestial mechanics mainly remained devoted to the study of the solar system. The possibility of detecting life outside the solar system, however philosophically important, has not become a major goal of science until recently, mainly because of the technical difficulties that go along with it. However, the idea that planets could be detected around other stars is also quite old. As noted by Howell et al. (1999), Dionysius Lardner noted in his *Lardner's Handbooks of Natural Philosophy and Astronomy* (1858) that "periodical obscuration or total disappearance of the star, may arise from transits of the star by its attendant planets", which is the underlying idea for the transit detection method (see section 2.1.2). Belorizky (1938) later noted that, seen from outside the solar system, Jupiter would induce a variation of the radial velocity curve of the Sun of about 13 m/s, which was far beyond the detection limit of its instruments, and its light would be completely shadowed by that of the Sun, making direct observation impossible. He was also aware of the fact that the transit of Jupiter would induce a photometric variation of about 1% in the light curve of the Sun. He concluded " Toutes ces considérations nous incitent à penser que c'est peut-être dans la photométrie des étoiles avec une précision de 1/100 de magnitude que se trouve le moyen de découvrir *l'existence d'autres systèmes planétaires*" [1]

The confirmed discovery of the first exoplanets was made by Wolszczan and Frail (1992), with at least two planets orbiting the pulsar PSR1257+12. It relied on a detection method called pulsar timing and that can therefore only be applied to pulsars. Given the extreme regularity of the pulsar rotation period, any variation could be easily detected, which lead to this discovery. It allowed the discovery of small objects (2.8 and 3.4 Earth masses) with relatively long periods (66.6 and 98.2 days). Because of the rather unusual method and result, and because planets around pulsars could hardly sustain life, the discovery had little impact. The discovery that really set a milestone in exoplanet astronomy was that of Mayor and Queloz (1995) of a planet around the star 51 Peg. First, the method utilized to detect this planet, the so-called radial velocity method, would remain the main method for detecting exoplanets for at least a decade. Second, the host star 51 Peg is a main-sequence star, which looks very much like our own Sun, with a mass of 1.06 solar mass. However the orbital properties of the planet 51 Peg b has opened a new era in our understanding of planet formation and evolution. Indeed the rather massive planet (at least 0.47 Jupiter mass) has a very short period of 4.23 days, making it the first member of subset of planets now known as the *hot Jupiters*. As we will see, such planets could hardly form so close to their

[1] All these considerations encourage us to think that it is maybe in the photometry of stars with a precision of 1/100 is the way to discover *the existence of other planetary systems.*

star, and a migration mechanism must be invoked to explain their presence. During the two decades that follow this first discoveries, the number of planets detected has being growing exponentially, dramatically changing our view of planet formation and evolution.

1.2 Problematic

Before the detection of the first exoplanet, the only constraints we had on planet formation and evolution came from the solar system. The latter consists in well-spaced, quasi-aligned and circular to moderately eccentric planets. In addition, the four inner planets are small and telluric, whereas the four outer ones are giant and gaseous. The good alignment between all the orbits argues in favour of all the planets forming in the same, thin disc. Abundance of material in the outer parts allowed for formation of the giant planets, while the growth of the inner planets was limited by the lack of material. The discovery of 51 Peg in 1995, a giant planet on a short-period orbit, did not argue in favour of this idealistic picture. Fortunately, theories developed in the 1980's were able to give a natural description of this phenomenon: planets interact with their disc, which usually causes inward migration on a timescale shorter than the disc's lifetime. This scenario usually implies that the planet maintains a low eccentricity and remains in the plane of the disc. Some planets were found to be on eccentric and inclined orbits, and could be explained by a competing scenario in which planets acquire short periods by dynamical interactions: a system of several planets would evolve through their mutual interactions until one of them is put on a very eccentric orbit. At this point, close encounters with the star dissipate its orbital energy by tidal effects, resulting in its period shrinking to the observed value. Such scenario naturally forms inclined and eccentric orbits, but also comes with drawbacks, which we will review in the next chapter.

Therefore, one of the majors goals of exoplanetary sciences nowadays is to provide a general framework that can conciliate all theses theories and reproduce the wide diversity of exoplanets. It should be noted that, for instance, the two competing scenarios for the formation of hot Jupiter are not incompatible. It is possible that some of these planets form by disc migration, while the others form by high-eccentricity migration. A global theory, however, should be able to answer the question: "what fraction is formed by which scenario?". In addition, observations (of our own solar system, to start with), indicate that planet migration does not always take place, or at least does not always form a hot Jupiter. A possibility would be that the planets interact with each other as they interact with the disc. The goal of this thesis is to highlight some of the disc-planet interactions, and derive constraints on the interactions that may have taken place in the early stages of planet formation and evolution, while they cohabit with the disc.

1.3 Plan of the thesis

Because this thesis has been motivated by the harvest of exoplanets and their huge diversity, we devote the second chapter to give a summary of the detection techniques, and the statistical properties of exoplanets that can be deduced from the current sample. We also review the main theories regarding the formation and evolution of extrasolar planets, and see how they can be related to the observations. In the third chapter we introduce some of the main tools of celestial mechanics that we use in this thesis. We focus on some applications of perturbation theory in order to correctly model the resonant and secular evolution of planetary systems. In the fourth chapter we study the interaction between a planet on an inclined orbit and a disc. We make use of an aspect of secular theory developed in chapter 3, the so-called Kozai mechanism, and how it is triggered by the disc gravitational potential when the inclination is above a critical value. Because the planet crosses the disc, its eccentricity and inclination are damped, and we show that massive planets realign with the disc. However, low-mass planets remain on inclined and eccentric orbits throughout the disc's lifetime. In the fifth chapter, we study the resonant interaction between two planets migrating in a disc. We investigate, analytically and numerically, how this process can naturally lead to eccentric orbits. When the eccentricity reaches a critical value, inclinations can be excited to high values through a second-order resonant effect. However the growth of eccentricity is limited by the damping from the disc, and we derive a criterion for the onset of inclination resonances. We show that this criterion is unlikely to be fulfilled for realistic disc parameters. Finally, in the sixth chapter, we conclude and give perspectives for future works.

Chapter 2

Extrasolar planets

Contents

In this section we review some of the main results that 20 years of study of exoplanets have taught us. We start with the detection methods and some statistical properties that can be learnt from the current sample of exoplanets. Then we summarize the mains theories about planet formation and planet migration.

2.1 Detection methods

2.1.1 Direct Imaging

This method is perhaps the most natural to apprehend, as it simply consists in measuring the light we directly receive from a planet. Its advantage is that it can, in principle, give accurate information about the orbit of the planet. Moreover the direct observation of the planetary spectrum gives access to its atmospheric composition. The improvement in adaptive optics technologies allows us, for near-by stars, to obtain an angular resolution high enough to resolve planetary systems. The main problem comes from the very high contrast between the luminous flux from the star and that of the planet, which results in the light of the latter often being hidden. Moreover, estimations of the planetary mass rely on the knowledge of the stellar age, and can be poorly constrained. So far, this method can account for the discovery of Jupiter-mass (and higher) planets with orbital separations of several tens or hundreds of astronomical units (AU[1]). In the very near future, the Gemini Planet Imager will achieve high contrast resolution, aiming at detecting gas giants with semi-major axes of 5-30 AU.

2.1.2 Transit Photometry

The principle behind the transit method is known for a long time in the Solar System. When an object passes between an observer and the Sun, the luminosity of the latter decreases. It is the principle of solar eclipses and Venus transits, for instance. The same principle can be applied to extrasolar planets. If the orbital plane of a planet is well aligned with the line of sight from the observer to the star, the former can measure a decrease in the light flux of the latter. This decrease is proportional to the surface ratio of the stellar and planetary discs, thus the square of the ratio of the radii. Therefore this method favours planets with large radii: a Jupiter-like planet around a Sun-like star will lead to a decrease of luminosity of about 1% in the light curve of the star. For an Earth-size planet the decrease

[1]For a list of symbols and abbreviations used throughout this thesis, and their meaning, see the table page 11

will only be of 0.01%. In addition, active bright stars will have proper luminosity variations, which can mimic a planetary transit. In addition to properly model the stellar activity, it is necessary to observe a large number of transits, which requires long-term follow-up for long-period planets. Moreover, other periodic phenomena, like a stellar companion with a grazing orbit, or an eclipsing binary in the field of view can produce the same signal as a transiting planet. Therefore, because of the limited lifetime of observational programs, only short-period planets can be easily detected (an observer outside our own Solar System will have to wait at least 12 years in order to observe 2 transits of Jupiter). This technique gives access to the period of the planet, and to its radius. In addition, observing the transit at different wavelengths can tell us about the atmospheric composition of the planet. The first planet detected by transit was the hot Jupiter transiting HD 209458 (Henry et al., 2000; Charbonneau et al., 2000). Since then, this method has been successfully applied by ground-based telescopes such as SuperWASP, and by the space-based telescopes CoRoT and Kepler. Despite the small probability of observing a planet transiting around a given star, the large number of planets observed by these telescopes has allowed for the detection of a large number of planets.

2.1.3 Radial velocities

This is an indirect method for which we detect the planet through the gravitational influence it exerts on the star around which it gravitates. In a N-body system (here, the star and one or several planets), the motion of each body occurs around the centre of mass of the system. For the central star, this motion is small but detectable. Indeed the radial component of the stellar velocity will lead to a shift in the stellar spectrum: a blue shift if the star is coming toward the observer, or a red shift if it is going away from it. It is a direct application of the Doppler-Fizeau effect. This method (hereafter radial velocity method, or RV) led to the first detection of a planet around a main-sequence star, 51 Peg (Mayor and Queloz, 1995). It favours the detection of massive planets on short-period orbits. It is also more efficient for low-mass, nearby, main-sequence stars. Indeed, low-mass stars will be more sensitive to the planet's influence. Main-sequence stars will also tend to rotate slower than young active star, producing a clearer spectrum. A degeneracy exists because the inclination of the orbital plane with respect to the line of sight is not known. As a consequence the true mass $M_{\rm p}$ of the planet is unknown, only the the quantity $M_{\rm p}\sin(i_o)$ can be measured, where i_o is the inclination of the orbital plane with respect to the plane of the sky. The degeneracy can be broken if the planet also transits the star, In this case $i_o \sim 90^\circ$ and we get a very good estimation of the planetary mass.

For a single planet around a star of mass M_*, the semi-amplitude of the sinusoidal variations is given by

$$K = \left(\frac{2\pi G}{P}\right)^{1/3} \frac{M_{\rm p}\sin(i_o)}{M_*^{2/3}} \frac{1}{\sqrt{1-e^2}}, \tag{2.1}$$

where G is the gravitational constant, and P and e are the orbital period and eccentricity of the planet, respectively. From this formula, it clearly appears that the RV method will be more sensitive to massive planets on short-period orbits. For a circular Jupiter-mass planet with orbital period of a year around a Sun-like star, the semi-amplitude variation of the RV curve is $K = 28.4$ m s^{-1}. For an Earth-like planet with the same characteristics, it falls to 9 cm s^{-1}. At the time of writing, spectrometer like HARPS at the ESO 3.6 meter telescope in La Silla Observatory, Chile, or HIRES at the Keck telescopes are reaching accuracy of about 1 m s^{-1} and somewhat below. Next-generation spectrometers such as ESPRESSO (successor of HARPS) will aim to detect variations of 10 cm s^{-1} and below, giving access to Earth-like planets in the habitable zone.

2.1.4 Astrometry

As we just saw, the presence of planets around a star leads to a small stellar motion which causes variations in the stellar spectrum. However it only gives access to the radial velocity component of the motion. The so-called astrometric measurement of a star tracks the motion of the star on the plane of the sky. Therefore two components of the motion are known and it breaks the degeneracy caused by the unknown orbital inclination with respect to the line of sight. Therefore it gives access to all the orbital parameters and the planetary mass. Contrary to the transit or radial velocity method, the astrometric detection is more sensitive to massive planets far away from their star. At the moment, the transit and RV methods hardly reach this population of planets, and astrometric detections could represent an interesting complementary method. It is expected that the Gaia mission will detect some planets via this method.

2.1.5 Gravitational microlensing

The light from a distant star, as observed from Earth, can be magnified when another star passes in front of it. This is because the gravitational field from the foremost star acts like a lens when the two stars and the observer are exactly aligned. This effect is called gravitational microlensing. The gravitational field of an hypothetical planet around the foremost star will also contribute to the lensing. The method has proved successful for planets with large orbital separations around distant stars, and does not rely on the system being seen edge-on. Therefore it is a good complement to the transit and RV methods. The major drawback of this method relies in the uniqueness of the event. Because such events are also usually quite distant, it is hard to do follow-up observations with a more conventional method. It gives access to the physical distance between the star and the planet at the time of observation. For an eccentric orbit, this distance could be quite different from the semi-major axis. The mass estimated with this method usually comes with large error bars. However the occurrence of gravitational microlensing events could tell us about the abundance

of planets around stars in our galaxy, as well as the abundance of free-floating planets. For instance, Cassan et al. (2012) have inferred from microlensing surveys that there could be as high as one or more bound planets per star in our Galaxy.

2.1.6 Transit Timing Variations

If a star is orbited by a single, non-perturbed planet, the frequency at which transits occurs remains constant. Irregularities in the periodicity of the transit occurrence (usually called transit timing variations, hereafter TTV) can reveal the presence of an unseen, non transiting companion. Notably, companions on orbits in mean motion resonance produce large-amplitude TTV. It can also give a good estimate on the mass and eccentricity of the unseen planet. It has proven useful in order to get more informations for a system containing at least one transiting planet, especially regarding the Kepler mission.

2.1.7 Other methods

Other methods exist, and are often used to confirm and constraint the previously mentioned methods (mainly RV and transits). Such methods usually rely on the variation of the brightness of the star as the planet orbits around it. They are only of marginal importance in the current arsenal of detection methods, and we shall only mention them: variation of the total brightness caused by the thermal emission of the reflected light of the planet, relativistic beaming effect which changes the density of photons, and ellipsoidal variations caused by massive planets tidally distorting their parent stars. In addition, a few methods will apply only in specific cases. This is the case of the pulsar timing method, used to discover the first exoplanet. However its range of applications being rather limited, we will not develop it further in the present work.

2.1.8 The Rossiter-McLaughlin effect

Here we also mention an interesting measurement that can be made when we can obtain radial velocity data for a transiting planet. As we observe the rotating star, one of its hemispheres is coming toward us, appearing blueshifted in the spectrum, while the other is going away from us, appearing redshifted. Planets transiting in the prograde direction will first occult the blue part of the spectrum, then the red part, and vice-versa for retrograde planets. This is called the Rossiter-McLaughlin effect (hereafter RM effect; Rossiter, 1924; McLaughlin, 1924). Asymmetries in the RM effect provide informations about the projected angle between the stellar spin and the orbital inclination (see figure 2.1 for an illustration). As we will see, the spin-orbit angle, measured using the RM effect, gives important constraints about planet formation and evolution. We note here that the spin-orbit angle can also be obtained via asteroseismologic measurements.

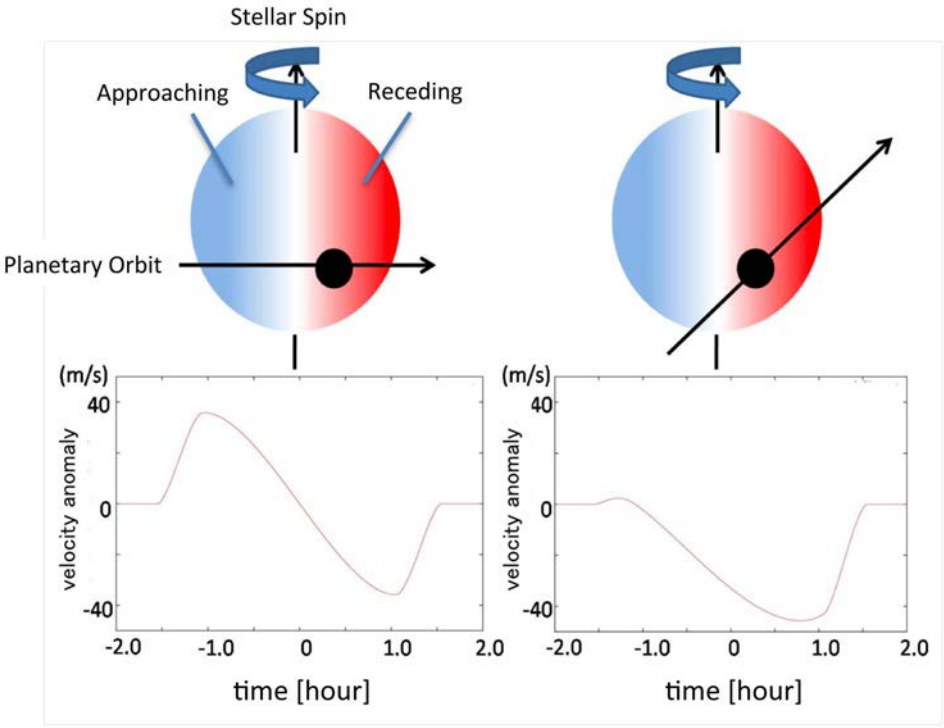

Figure 2.1: Illustration of the Rossiter-McLaughlin Effect. ©Subaru Telescope, NAOJ

2.2 The diversity of exoplanets

As of June 2014, 1518 exoplanets have been found, forming a total of 926 planetary systems. Among them, 1037 have been detected using the transit photometry method, and 439 using the RV method[2]. The range of masses, periods, eccentricities and inclinations they span is so wide that planet formation and evolution theories had to be revised and completed in order to try to provide a more global picture. Here we review the main features of exoplanet systems.

2.2.1 Period distribution

Probably the most surprising result that came along with the detection of 51 Peg b was its very short orbital period of 4.23 days (orbital separation of 0.0527 AU). This is twenty times shorter than Mercury's period. At the time of writing, the current sample of exoplanets spans about 6 orders of magnitudes in periods, ranging from a few hours to several hundred years.

On figure 2.2 we show the current distribution of periods for all the known extrasolar planetary systems, including data from all the detection methods (thick black line). This distribution looks roughly bimodal, with a peak between at 3-4 days, and another one, smaller, at around 1 year. The lack of planets beyond periods of $\sim 10^3$ yr is more of an observational bias than a real dearth of planets. Indeed, we saw that most detection methods fail to detect long-period planets, because of a lack of sensitivity and the inability to repeat observations.

[2]Data extracted from *http://exoplanets.org*

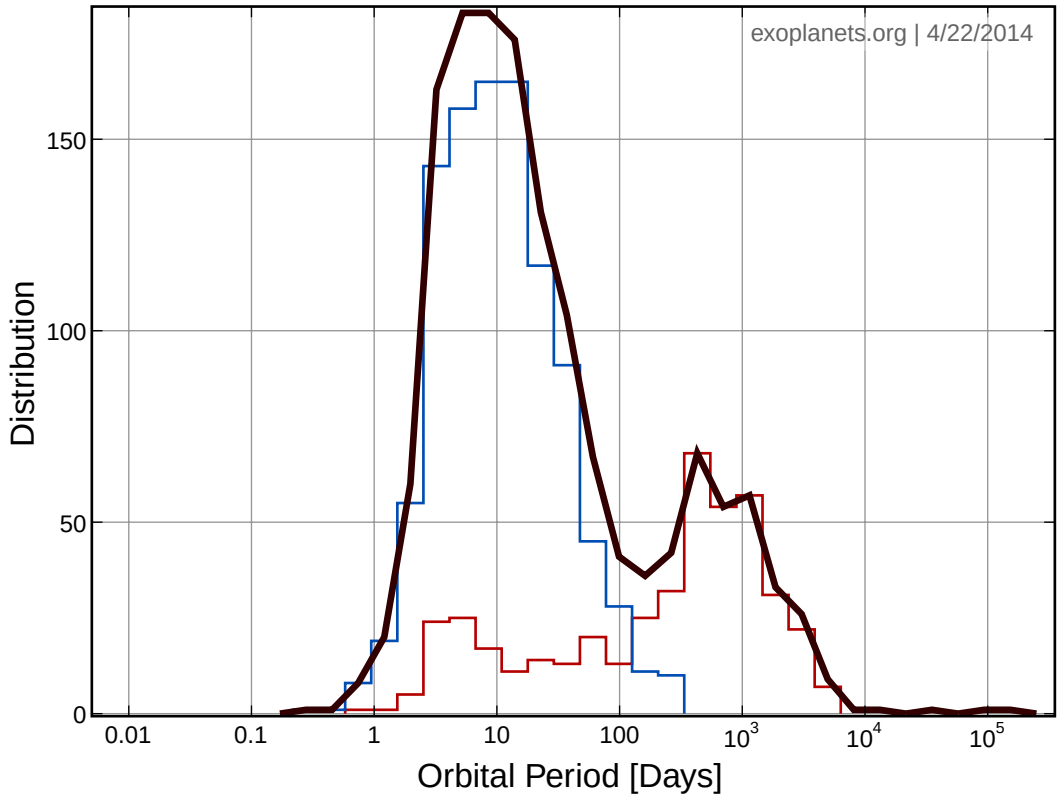

Figure 2.2: Period distribution for the current catalogue of exoplanets. The thick black curve shows the period distribution of all exoplanets, regardless of the detection method. The blue histogram shows the planets detected by the transits method, and the red histogram shows the planets detected by the RV method. Plot made using tools provided by *exoplanets.org*

The peak at a few days is more interesting. A lot of planets in this peak come from the over-abundance of short-period planets detected by the transit method. Although the RV method is more sensitive to short-period planets, it has detected a large number of planets with periods larger than 100 days. However, the RV method still finds a slight over-abundance of short-period planets (period smaller than 10 days). This is illustrated in figure 2.2 where planets detected by the RV method are shown by the red histogram. This figure also shows that the RV and transit methods account for the vast majority of the planets detected so far.

It is very unlikely that these short-period planets have formed so close to their host star, as we will explain in section §2.3. Hence, one must invoke some migration scenario to bring them here from the outer parts of the system (typically at period of a few hundred days and above, in the region where RV observation seem to find a significant number of planets). We will detail these processes in section §2.4

2.2.2 Mass distribution

In figure 2.3 we represent the mass of exoplanets as a function of their orbital period. The bi-modal distribution seen in figure 2.2 is still apparent, but additional features are also present. First, we remark that the sample of detected planets is biased toward massive planets (around one Jupiter mass), which is not surprising: RV measurements are sensitive to the planetary

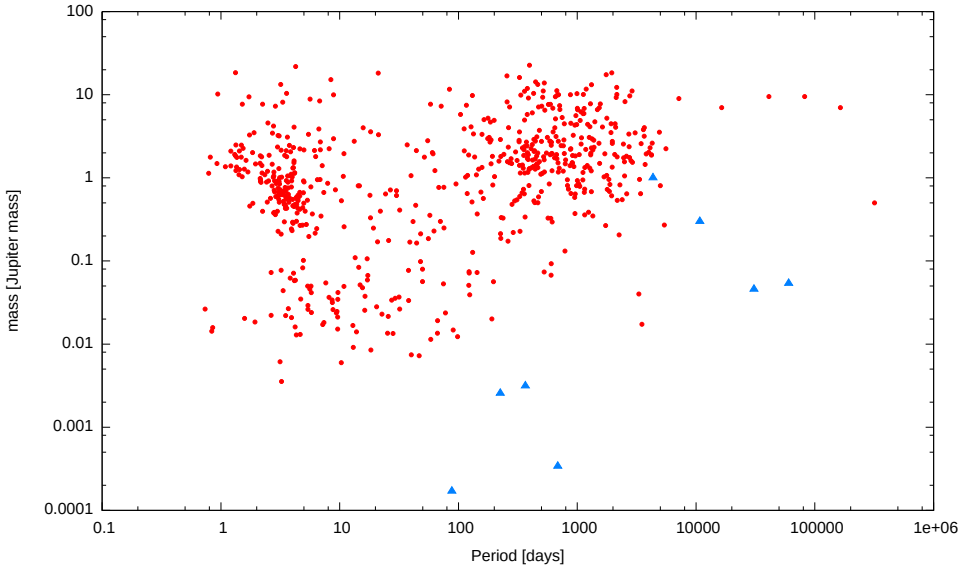

Figure 2.3: Mass vs. period relation for the current catalogue of exoplanets. Blue triangles represent the Solar System planets. Data extracted from *exoplanets.org*

mass (see eq. (2.1)) and transits are sensitive to the radius (which usually correlates with the mass). The group of planets at periods of a few days and Jovian masses are the so-called *hot Jupiters*. They have attracted considerable attention since the discovery of the first member of their kind, 51 Peg b. This is because not only were they the easiest planets to detect, but they also challenged formation theories in several ways, as we will see later in this chapter.

On figure 2.3 we also represent the planets of the Solar System with blue triangle. The current level of accuracy of detection methods fails to find equivalents to our own Solar System. Especially, Earth-like planets (small mass and moderate periods) and Neptune-like planets (long-period subgiants) are out of reach for our current instruments.

2.2.3 Eccentricity distribution

One surprising result revealed by the observation of extrasolar planets is the large range of orbital eccentricities, as shown in figure 2.4. The highest known eccentricity is that of HD 20782 b (O'Toole et al., 2009), reported to be 0.97. By comparison, the most eccentric planet in the Solar System is Mercury with 0.2, and all the other ones are below 0.1 (and basically below 0.05, apart from Mars). As we will see, high eccentricities can hardly be achieved in the configuration of a single planet migrating in a disc, and are likely to be caused by gravitational interaction in multiple systems. The architecture of systems with an eccentric planet is likely to be quite different from that of systems with quasi-circular orbits, for stability reasons. We will investigate this point in more details later in this chapter.

A noticeable feature of figure 2.4 is the dearth of very eccentric planets at short periods. More precisely, the higher the eccentricity, the further from the star the innermost planet is located. Eccentric planets on short-period orbits will either: i) have their eccentricity damped to zero through tidal interactions with the star, or ii) be tidally disrupted or even

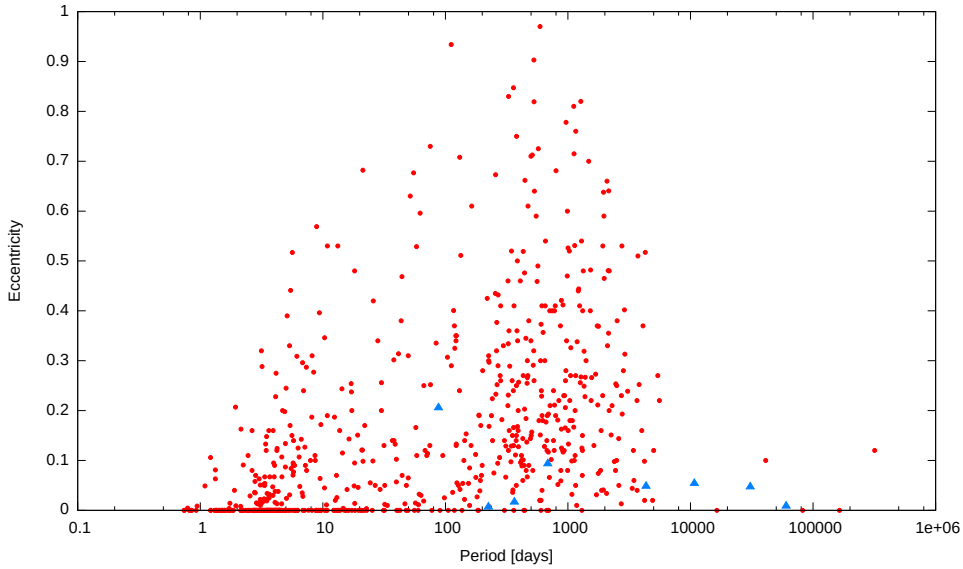

Figure 2.4: Eccentricity vs. period relation for the current catalogue of exoplanets. Blue triangles represent the Solar System planets. Data extracted from *exoplanets.org*

swallowed by the star.

2.2.4 Spin-orbit angle distribution

As we have seen in section §2.1.8, in some cases we can access the angle between the spin of the star and the orbital angular momentum of the planet around it. As we will see in sections §2.3 and §2.4, if a planet has formed in a disc, it can naturally undergo disc migration which would bring it on a closer orbit. However, when the disc forms by the flattening of the protostellar envelop, one can assume that it is roughly aligned with the equatorial plane, by mean of total angular momentum conservation. This statement is supported by i) our own Solar System, where all the planets lie within a few degrees of the Sun's equator, and ii) measurements of the angle between the stellar rotation axis inclination angles and the geometrically measured debris–disc inclinations for a sample of eight debris-disc by Watson et al. (2011), which shows no evidence for a misalignment between the two (see also Greaves et al., 2014).

The first measurement of the spin–orbit angle during a planetary transit was made by Queloz et al. (2000), who found no significant evidence of misalignment for the planet HD 209458 b, supporting the disc-migration scenario. Later on, Hébrard et al. (2008) suggested that the planet XO-3 b was possibly significantly misaligned, a result soon confirmed by Winn et al. (2009). Since then, many more hot Jupiters have proved to be misaligned (see, e.g., Triaud et al., 2010; Albrecht et al., 2012). The current distribution is represented in figure 2.5. Some measurements come with large error bars and it is hard to define the minimum angle from which we can classify a system as being misaligned. At the time of writing, out of the 66 exoplanets for which the spin-orbit angle has been measured, 33 show a misalignment larger than $15°$, and 10 are in retrograde orbits (spin–orbit angle larger than

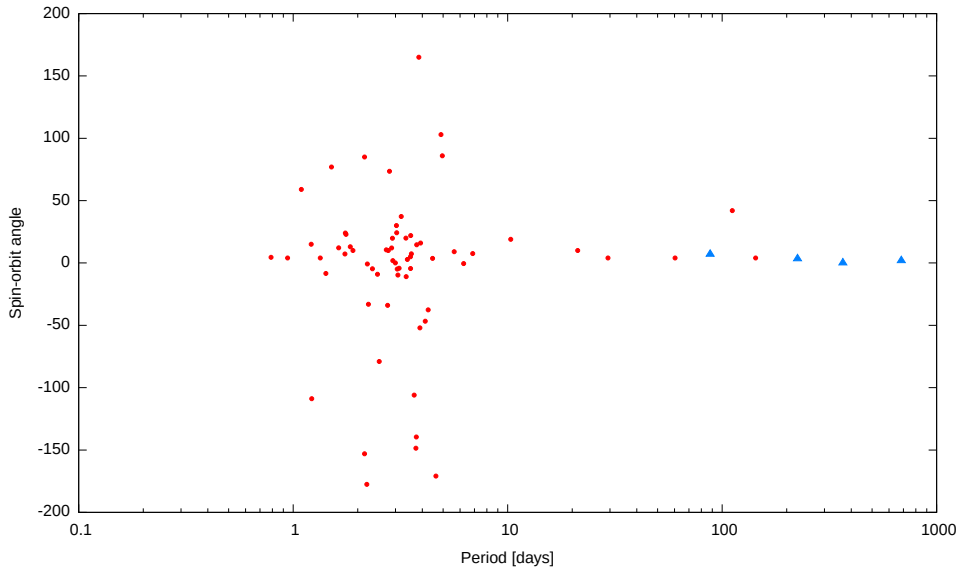

Figure 2.5: Spin-orbit angle vs. period relation for the current catalogue of exoplanets. Blue triangles represent the Solar System planets. Data extracted from *exoplanets.org*

90°). Such a significant number can hardly be explained within the disc migration scenario, and other models have been developed, mainly invoking gravitational multiple-body interactions. Note that this does not mean that the disc-migration scenario has been ruled out by observation, but only that different processes could be at work in different systems. Strong constraints could be put on each mechanism responsible for misalignment by looking at the outer parts of the systems containing a hot Jupiter, in order to evaluate which fraction contains an outer companion (planet at large separation, stellar binary companion...). Long-term RV surveys are currently running, performing follow-up observations of systems containing a hot Jupiter, and trying to detect a linear trend in the RV curve (see, e.g., Knutson et al., 2014).

2.2.5 Multiple systems

A significant fraction of planets are actually part of multiple-planet systems. Several trends have appeared in the last few years, regarding the architecture of planetary systems. For example, multiple-planet systems detected by the satellite Kepler appear to be mainly populated by Super-Earth and Neptune-like planets on relatively tight orbits. Moreover, Fabrycky et al. (2012) have estimated that most of these systems present a high degree of co-planarity, supporting the disc-formation scenario. For stability reasons, the tightly packed systems of Kepler should also contain planets with very low eccentricities. This could also support a disc-migration scenario, where the planets would have achieved a tight configuration while their eccentricities remained damped to low values by the disc (see §2.4). On the other hand, a recent analysis by Steffen et al. (2012) showed that most hot Jupiters from the Kepler data appear to have no nearby, coplanar companions (within a period ratio of a few); however, planetary companions at larger separations and large inclinations cannot be ex-

cluded (especially since an outer companion with an orbital period ratio of $\sim$10 and a 60° mutual inclination would have a detection likelihood of less than 5% by transit methods). This suggests a different evolutionary path for hot Jupiters and smaller planets. For instance, independently of the process by which a Jupiter-like planet will migrate, it is likely to scatter away most planetesimals and small-mass planets.

Although pairs of planets mostly have random orbital period ratios, some of them are located near mean motion resonance. For these planets, the ratios seem to have a small excess just outside the resonance, and a small deficit just inside. These multiple-planet systems (mainly consisting of super-Earth and Neptune-like planets) are also more tightly packed than our own Solar System. Note that the period ratio of two adjacent planets can be quite similar compared to that of the planets in the Solar System, but their physical mutual distance is much smaller. This requires very low eccentricities in order for the systems to remain stable.

2.2.6 Statistical properties of exoplanets

Combining results from the different detection methods, we are now able to draw a few conclusions on the content and architecture of planetary systems. More details can be found in Fischer et al. (2013) and references therein. When considering planets with periods of less than 50 days, small planets (Earth to Neptune size) outnumber large ones (gas giants). For instance, hot Jupiters are found around only 0.5 to 1% of Sun–like stars, despite the fact that they are easy to detect and therefore well characterized. They also tend to be the only planet orbiting their star, within observational limits. On the other hand, RV surveys indicate that 15% of Sun-like stars are orbited by planets with projected mass $M_{\rm p} \sin i_o$ in the range $3 - 30 M_\oplus$ at less than 0.25 AU. The HARPS survey also found that, in total, at least 50% of stars contain a planet at a period of less than 100 days, regardless of the mass of the planet. Results from the Kepler mission indicate that small-mass planets remain abundant up to periods of 250 days. 23% of the stars in the Kepler catalogue that contain one transiting planet actually host two or more planets. Hence, although finding an analogue of our Solar System remains challenging at the time of writing, mainly because of observational limitations, it makes little doubts now that planetary objects populate a large number of stars in our Galaxy. The large range of properties and architectures that they already exhibit, and the constant improvements in observational techniques have challenged, and keeps challenging, our views on planet formation and evolution. In the next section, we review some of the main results in this field.

2.3 Planet Formation

2.3.1 The protostellar nebulae

Back in the 18^{th} century, Kant (developing an original idea from Swedenborg) pictured the Solar System as having formed in a primordial gaseous nebulae. He argued that the spinning nature of the nebulae would flatten the orbits of gas particles and lead to the formation of a disc. Gravitational interactions inside the nebulae would lead to the formation of clumps that would become the Sun and the planets. The idea was further developed by Laplace 50 years later, where he explained how the slow-rotating, quasi-spherical nebulae would cool down, leading to its contraction. As it collapses, it spins faster in order to conserve angular momentum. It then flattens in the plane perpendicular to the spin axis, forming a succession of rings of material, in which the planets will form. Criticism arose quickly, especially owing for the fact that, in this model, the Sun should carry most of the angular momentum of the system, because it contains most of its mass. This is in contradiction with observations which show that the planet, via there orbital angular momentum, carry 99% of the total angular momentum of the Solar System.

However some of the underlying ideas of the primordial nebulae hypothesis are still considered to be correct. Stars form via direct gravitational collapse of the gas in large molecular clouds, and the remaining material forms a protoplanetary disc. This scenario has received support from both the theory and observation sides.

2.3.2 Properties of protoplanetary discs

An excellent review of the properties of protoplanetary discs, both from observations and theory, can be found in Williams and Cieza (2011). Here we review some of the main results, which we may use throughout this thesis. On average, the mass of a disc is about 1% of the mass of its host star, and discs tend to extend to a few hundred AU. The outer part of the disc emits weakly and is difficult to observe, but taking the outer radius to be of the order of 100 AU seems reasonable. Discs lifetime ranges from 1 to 10 Myr, with a median around 2 to 3 Myr. Two main processes dictate the mass evolution and the geometry of a protoplanetary disc: photoevaporation (mass loss at the outer edge) and accretion (mass loss at the inner edge). Beyond a critical radius (about 10 AU for solar mass stars), the thermal velocity of the ionized hydrogen becomes larger than its escape velocity and the material is lost. Photoevaporation causes mass loss at the outer edge of the disc, at a rate of the order of $10^{-8} M_{\odot}$ yr^{-1}. On the other hand, the inner part of the disc accretes material onto the star, and the inner cavity remains small (0.01 AU). The outer disc supplies material to the inner disc. The mass loss in the inner disc due to accretion is also about $10^{-8} M_{\odot}$ yr^{-1}. However, when photoevaporation has expelled most of the outer disc (i.e when the outer disc's mass has dropped from 10 to 1-2 M_{J}), the latter cannot provide the inner disc with enough material any more. On a timescale of 10^5 yr the inner disc vanishes and a cavity of

a few AU is formed.

2.3.3 Grains and planetesimals formation

The disc originally contains gas and small grains, of micrometer size. This dust tends to be slowed down by the gaseous medium as it goes through the equatorial plane of the disc. Overall, it tends to condensate in this plane. The cooling down and condensation of ice grains is only possible at distances larger than the so-called snow line. Inside the snow line, radiation and temperature are too important and prevent condensation of ice to occur (however, heavier elements such as silicates and metals can condensate in the inner parts, but they are not the dominant elements of the disc's material). When grains can condensate, they grow by accumulating more materials, through collisions with each others. On a relatively short timescale (a few 10^3 yr) centimeter to meter-sized particle are formed. The process which leads from these grains to kilometer-sized planetesimals remains unclear, and is still an active domain of research. Because gas drag causes an important orbital decay for meter-sized grains, the process has to occur rather quickly (a meter-sized body at 1 AU would drift towards the Sun in a few hundred years). Another issue is that an important collision-rate at high relative velocities would prevent the growth of planetesimals.

2.3.4 Rocky planets formation

When kilometer-sized bodies are formed, they are big enough to become decoupled from the gas. They now have Keplerian speeds around the central star, and their evolution is that of a gravitational N-body system (if we neglect the tidal interactions with the gaseous medium; we will review this process later, in the framework of disc migration). Planetesimals eccentricities increase as they encounter each others, leading to collisions and agglomerations. It follows that a so-called "runaway accretion" takes place, where the more massive body accrete faster than the less massive ones. These few massive embryos accrete most of the material inside their sphere of influence, and reach the state of protoplanets after a few 10^4 years. This process leaves the system with a small number of rocky cores that interact with each others. A last phase of merging, from embryos of typical masses of about $10^{-2}\ M_\oplus$, to Earth-mass rocky planets, then takes place on a much longer timescale. Some of these cores will then accrete gas by a process described below in order to form giant planets, on a timescale limited by the disc's lifetime ($\sim 10^6$ yr). After the disc dissipates, collisions between rocky planetesimals continue for a few 10^8 years.

2.3.5 Giant planets formation

Observations show that the gas in the disc dissipates on a timescale of a few million years. Hence, while rocky planets can keep forming on a much longer timescale via merger of rocky planetesimals, giant gaseous planets have to form rapidly, as they need to accrete gas

from the disc. There are currently two main scenarios aiming at explaining the formation of giant planets. The first one is called the "core accretion" model (Pollack et al., 1996). In this scenario it is assumed that a solid core of a few Earth masses has formed according to the scenario described above. In addition to the accretion of planetesimals, the solid core also gravitationally accretes gas, which forms an atmosphere. At first, the gas accretion is rather slow, up to a few million years. However, when the mass of gas contained in the atmosphere becomes comparable to the mass of the solid core (around $10\ M_{\oplus}$), the growth becomes much quicker, and a Jupiter–mass planet can be formed before the disc dissipates. The growth stops when the planet has accreted all the gas on its orbit. This scenario can also explain Neptune-like planets, who can be described as "failed" giants, whose growth was stopped by the lack of gas, probably because they started accreting too late and the disc has been dissipated before they could reach a larger size.

The second scenario for forming giant planets is usually referred to as the "gravitational instability" scenario (see, e.g., Boss, 1997, and references therein), which is similar to that envisioned by Laplace, and that is at work in star formation processes. In this scenario, the disc (or, at an even earlier stage, the protostellar envelop) would start to fragment into dense clumps under gravitational instabilities. The gravitational collapse of these over-dense regions can potentially form giant planets in a few thousand years. However, in its current form, it suffers several major drawbacks, and remains less commonly accepted than the core accretion model. First, it requires a massive disc, whose mass would be 10% of the stellar mass. However we saw that the mass of the disc is estimated to be about 1% of the stellar mass. In addition this scenario tends to form massive gaseous planets far from the star ($\gtrsim 50$ AU), and cannot explain Neptune-mass gaseous planets. Finally, it struggles to explain the lack of heavy elements in the chemical composition of the atmosphere of Jupiter and Saturn.

2.4 Planet migration

As we saw, planets have to form in a region where condensation of the grains is possible (i.e., for giant planets, further than the snow line, located at a few AU from the star), and have to accrete the gas quickly, in gas-rich regions. In addition, the inner part of the disc (<0.1 AU) has a complicated structure: high temperatures tend to cause evaporation and ionization, stellar winds blow away material (making the region rather gas-poor), and the stellar magnetic field is thought to truncate the disc at a distance of a few stellar radii. Hence, the formation of giant, gaseous, planets seems very unlikely so close to the star. In consequence, it seems natural to invoke a migration scenario to explain the population of giant planets at orbital distances below 0.1 AU (the hot Jupiters population)

2.4.1 Disc migration

We first consider the evolution of small planets embedded in a gaseous disc (we will quantify what we mean by "small" more precisely in the following section, but let us consider here anything smaller than a few Earth masses). In this case, first considered by Goldreich and Tremaine (1979, 1980), one can develop the gravitational potential of the planet using a Fourier expansion in the azimuthal angle, leading to terms proportional to $\exp im(\phi - \Omega_p t)$. Here m is the Fourier mode number, ϕ is the azimuthal angle and Ω_p the orbital frequency of the planet, which we assume to be on a circular Keplerian orbit at a distance r_p. It is then possible to study the response of the disc to this perturbation, and then sum over all the modes in order to derive the torque applied by the disc on the planet. The complete derivation is non-trivial, and one of the major results is that the torque is exerted at discrete locations in the disc, and vanished away from these locations. These locations come in two flavours: *corotation* resonance and *Lindblad* resonances. If we denote by $\Omega(r)$ the orbital frequency of a particle of gas orbiting at a distance r, the corotation resonance is defined by $\Omega(r) = \Omega_p$ (i.e., particles orbiting in the vicinity of the planet's orbit). In a frame of reference orbiting with a parcel of gas at a frequency $\Omega(r)$, the perturbation caused by the Fourier mode m occurs at a frequency $\omega = m(\Omega_p - \Omega(r))$. A Lindblad resonance occurs when $\omega = \kappa$, where κ is the *epicyclic* frequency. This frequency, defined by $\kappa(r)^2 = r\mathrm{d}(\Omega^2)/\mathrm{d}r + 4\Omega^2$, simply becomes $\kappa(r) = \Omega(r)$ for a Keplerian disc. It appears naturally when one considers the small perturbation acting on a gas particle (for which the unperturbed state would be a circular orbit). The particle oscillates around this circular orbit (often referred as the *guiding centre*) at the frequency κ. It is easy to show that for a Keplerian disc, the Lindblad resonance corresponding to a mode m is located at a radius

$$r_L = \left(1 \pm \frac{1}{m}\right) r_p. \tag{2.2}$$

Note that the Lindblad torques seem to pile-up at the location $r = r_p$ for large m. However, an effect know as "torque cut-off", beyond the scope of this thesis, tends to suppress all the torques for which $m \gtrsim r/H$, where H is the disc height (Artymowicz, 1993). In conclusion, the total torque exerted by the planet is a combination of a corotation torque and a series of Lindblad torques.

2.4.1.1 Type I migration

When considering small planets, one can assume that the global structure of the disc will not be affected by the planet. However, at the location of the Lindblad resonances, density waves are excited and propagate in the disc. Constructive interferences between the superposition of the waves launched at Lindblad resonances give rise to a one-armed spiral density wave, often referred to as the wake (Ogilvie and Lubow, 2002). It propagates outside of the location of the resonance, i.e., at $r < r_{\mathrm{ILR}}$ (resp,. $r > r_{\mathrm{OLR}}$), where r_{ILR} is

the location of the inner Lindblad resonance (resp., where $r_{\rm OLR}$ is the location of the outer Lindblad resonance). Because of the differential rotation, the outer density wave trails behind the planet, therefore exerting a negative torque on the planet (and the opposite for the inner density wave). This is illustrated in the left panel of figure 2.6. Ward (1997) showed that the torque exerted by the outer part of the disc is larger than the inner torque. This is because the outer Lindblad resonance is located slightly closer to the planet than the inner one, because of the disc geometry. Therefore, the planet tends to loose angular momentum to the disc and migrate inward. The typical migration timescale, given by Ward (1997) is

$$t_{\rm mig} \approx 10^8 \left(\frac{M_p}{M_\oplus}\right)^{-1} \left(\frac{\Sigma}{g\ cm^{-2}}\right)^{-1} \left(\frac{r}{\rm AU}\right)^{-1/2} \times 10^2 \left(\frac{H}{r}\right)\ {\rm yr}, \tag{2.3}$$

where Σ is the disc's surface density. Type I migration typically occurs on a timescale of 10^5 years for a 1 $M_\oplus$ planet at 1 AU. The torque acting on the planet will also modify its eccentricity. For small eccentricities, the net effect will be a damping of the eccentricity. Papaloizou and Larwood (2000) provide a fit for the migration timescale $t_{\rm mig}$ and the eccentricity damping $t_{\rm e}$ the 2D case, given by (see also Papaloizou and Terquem, 2010):

$$t_{\rm mig} = 146.0 \left[1 + \left(\frac{e}{1.3H/r}\right)^5\right] \left[1 - \left(\frac{e}{1.1H/r}\right)^4\right]^{-1} \times \left(\frac{H/r}{0.05}\right)^2 \frac{M_\odot}{M_{\rm d}} \frac{M_\oplus}{M_{\rm p}} \frac{a}{1{\rm au}}\ {\rm yr}, \tag{2.4}$$

$$t_{\rm e} = 0.362 \left[1 + 0.25 \left(\frac{e}{H/r}\right)^3\right] \left(\frac{H/r}{0.05}\right)^4 \frac{M_\odot}{M_{\rm d}} \frac{M_\oplus}{M_{\rm p}} \frac{a}{1{\rm au}}\ {\rm yr}, \tag{2.5}$$

where a and e are the semi-major axis and eccentricity of the planet, respectively, and $M_{\rm d}$ is the disc mass contained within the planetary orbit. These authors also estimated that the orbital inclination of the planet should be damped on a timescale $t_{\rm i}$ similar to $t_{\rm e}$. The damping timescale is much shorter than the migration timescale, so we can conclude that low-mass planets will tend to remain on circular and planar orbits as they migrate.

2.4.1.2 Type II migration

Type I migration causes small planets to migrate inward but leaves most of the disc unaffected by the planet's presence. However we can expect massive planets to affect the gas, at least in the vicinity of their orbit. When a particle is orbiting inside the orbital radius of the planet ($r < r_p$), the net effect of the planet will be to speed it up. Thus, angular momentum is transferred from the particle to the planet, and the particle is pushed inward. If one simply considers the impulse received by a particle as it approaches the planet, and the subsequent deflection, one can deduce that the rate of transfer of angular momentum between the disc's

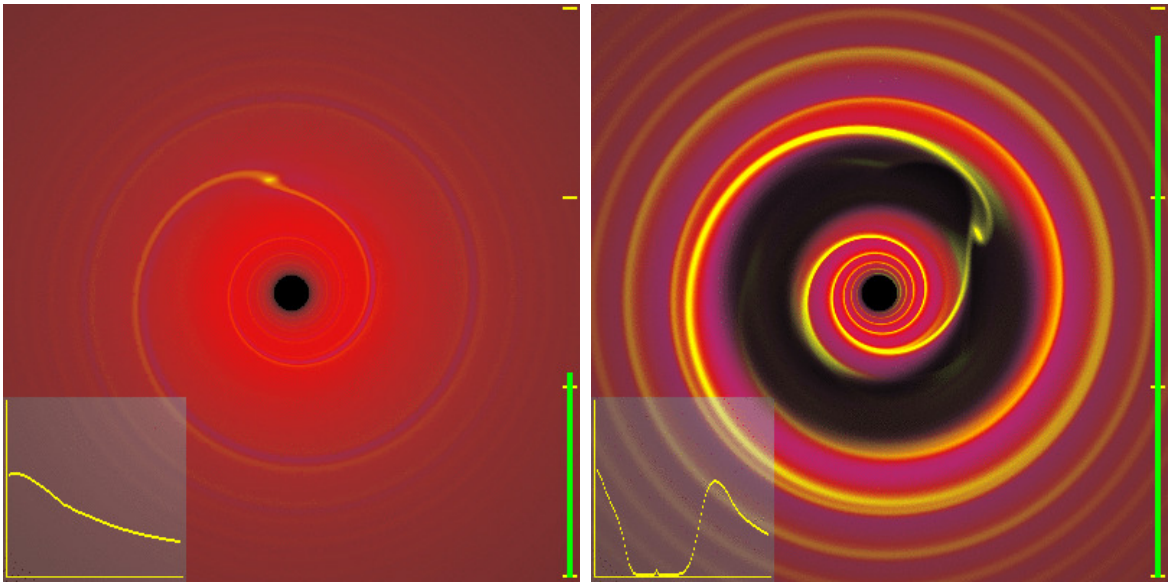

Figure 2.6: *Left panel:* a low mass planet embedded in a protoplanetary disc launches a trailing spiral wave in the disc. The surface density of the disc is not significantly modified by the presence of the planet. *Right panel:* a massive planet has cleared a large gap in the disc, where the surface density is almost zero. In each panel, the bottom left corner shows the surface density of the disc. The gap opening is clearly apparent for massive planets. Plot from *http://jila.colorado.edu/~pja/planet_migration.html*.

particles inside the planetary orbit and the planet is given by:

$$\frac{\mathrm{d}J}{\mathrm{d}t} = \frac{8G^2 M_\mathrm{p}^2 r\Sigma}{27\Omega_p^2 a_\mathrm{min}^3}, \tag{2.6}$$

where a_min is the distance of minimal approach between the particles and the planet (Lin and Papaloizou, 1979). Note that the sign is positive, leading indeed to the particles being pushed inward. A similar analysis can be done for the particle exterior to the planet's orbital radius ($r > r_p$), with a similar result, except that the sign is opposite. Hence material outside the orbit of the planet is pushed outward. In conclusion the planet tends to push the material away, and can clear a gap in the disc, where the density drops significantly. However, viscous diffusion in the disc tends to transport angular momentum, at a rate

$$\frac{\mathrm{d}J_\mathrm{visc}}{\mathrm{d}t} = 3\pi\nu\Sigma r^2\Omega_p \tag{2.7}$$

where ν is the kinematic viscosity. The viscous timescale associated with this flow of angular momentum is given by

$$t_\mathrm{visc} = \frac{r^2}{\nu} = \left(\frac{H}{r}\right)^{-2} \frac{1}{\alpha\Omega} \tag{2.8}$$

Here we have assumed that the viscosity follows the model developed by Shakura and Sunyaev (1973). In this model, viscosity is dominated by turbulence in the gas. The largest turbulence scale should be of the order of disc height H, and propagates with a characteristic speed smaller than the sound speed $c_s = H/\Omega$. Hence we write $\nu = \alpha c_s H$, where α is a

dimensionless constant parameter, which can be constrained to be in the range $10^{-3} - 10^{-2}$ in order for type II migration to occur within the lifetime of protoplanetary discs.

The net effect of this viscous transport will be to refill the gap. Hence, from these considerations, we can deduce that a gap will open if

$$\frac{\mathrm{d}J}{\mathrm{d}t} > \frac{\mathrm{d}J_{\mathrm{visc}}}{\mathrm{d}t}. \tag{2.9}$$

This condition can be re-written as

$$\frac{M_{\mathrm{p}}}{M_*} > \frac{40\nu}{r^2\Omega_p}. \tag{2.10}$$

For typical disc models, a gap can be opened for planets of the mass of Saturn and higher (see illustration in the right panel of figure 2.6, where a massive planet opens a large gap).

Once the gap is opened, the corotation torque is cancelled due to the lack of material in the vicinity of the planet, and the total Lindblad torque exerted on the planet is zero, because the latter positions itself at the equilibrium point in the gap where the inner torque cancels the outer one. In the inner parts of the disc, accretion onto the central star causes the gas to move inward. The planet will simply follow this accretion flow, because there is still transfer of angular momentum from the inner parts to the outer parts, and migrate inward on the viscous timescale. For a planet starting at 5 to 10 AU, the viscous timescale is of the order of a few 10^5 years, and the planet is therefore expected to migrate inward on a timescale shorter than the disc's lifetime. It is important to remark the fundamental difference between type I and type II migration. In the case of type I migration, low-mass planets migrate *in* the disc, leaving the latter mostly unaffected. In type II migration, massive planets migrate *with* the disc, and affect its structure by opening a gap. Type II migration is often invoked to explain the population of hot Jupiters. It is interesting to notice that this process (as well as type I migration), was foreseen long before the detection of the first hot Jupiter, mainly by Lin and Papaloizou (1986).

Even if disc-driven eccentricity growth seems possible, in particular for planets of several Jupiter masses (see, e.g., Papaloizou et al., 2001), in general the outcome of disc–planet interactions is to damp the eccentricity of the planet (Bitsch and Kley, 2010). Eccentricity damping is often related to the migration timescale through the following parametrization:

$$\left|\frac{\dot{e}}{e}\right| = K\left|\frac{\dot{a}}{a}\right|, \tag{2.11}$$

where K is a dimensionless constant. Numerical investigations find $K > 1$, with values possibly as high as $K = 100$. Hence, like in the case of type I migration, the eccentricity is damped quicker than the migration timescale. In addition, Bitsch and Kley (2011) find that the orbital inclination is also damped on a timescale that is shorter than the migration timescale, for moderate inclinations (of the order of the disc aspect ratio). The evolution of

eccentricity and inclination for planets with large initial inclinations is studied in detail in Teyssandier et al. (2013b), which is the subject of Chapter 4 of this thesis.

If hot Jupiters are really the result of type II migration, then it requires that the migration stops before the planet falls into the star. Several mechanisms have been proposed in order to stop type II migration. For instance, it is likely that the disc is truncated at a few stellar radii because of the stellar magnetic field (Bouvier et al., 2007). In addition, Terquem (2003) argued that the presence of a magnetic field in the disc could change the total torque and slow down the migration. Trilling et al. (1998) suggested that a planet affected by tides from the star would overflow its Roche lobe and transfer part of its mass to the star. Conservation of angular momentum would then cause the planet to move away from the star. It is also thought that the first generation of planets would eventually merge with their star, and only planets that have been formed later could survive, because of the subsequent lack of material in the disc. One should also keep in mind that we have studied the migration of a single planet in a disc. However, observations support the idea of multiple-planet systems. Mutual interactions between migrating planets could affect the migration. One aspect of the mutual interaction between two migrating planets is the possibility of mean motion resonance locking. This effect and its consequences on the eccentricities and inclinations are studied by Teyssandier and Terquem (2014), presented in Chapter 5.

2.4.1.3 Type III migration

So far we have mostly neglected the corotation torque: For type I migration, the main contribution to the total torque comes from the Lindblad torque, and for type II migration, the planet has opened a gap and cleared all the material that could give rise to a corotation torque.

Material that is in corotation with the planet exhibits so-called horseshoe orbits (as seen from a reference frame rotating with the planet, see illustration in figure 2.7), which corresponds to libration around the Lagrange equilibrium points L_4 and L_5. Particles originally located at a distance $r_p + \delta r$ experience a U-turn in the vicinity of the planet, which brings them to a distance $r_p - \delta r$. By doing so, they loose angular momentum, which is communicated to the planet. Symmetrically, particles originally located at a distance $r_p - \delta r$ take angular momentum away from the planet. By symmetry, the net effect should be zero.

As we saw, low-mass planets do not clear a gap, contrary to massive planets. The transition occurs for Saturn-mass planets. Such planets are expected to clear only a partial gap, and material will keep flowing through the orbit, passing by the corotation radius, and therefore exerting a strong corotation torque. Masset and Papaloizou (2003) were the first to study this effect. As the planet migrates inward, material from the inner disc get trapped in the horseshoe streamline and goes to the outer disc. In doing so, they remove angular momentum from the planet. On the other hand, as the material is trapped in the corotation region, it drifts inward with the planet, loosing angular momentum. The two effects

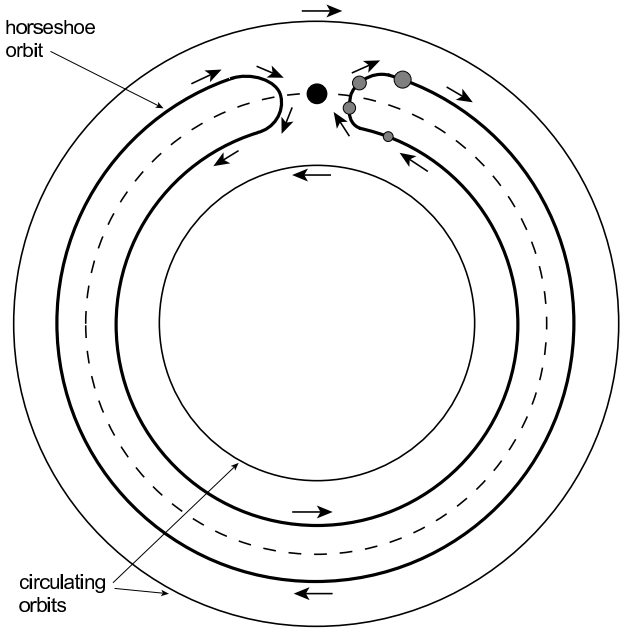

Figure 2.7: Different trajectories of gas particles as seen in a frame of reference where the planet (represented by the black dot) remains fixed. Particles trapped in horseshoe trajectories make a U-turn in the vicinity of the planet. Figure extracted from Kley and Nelson (2012)

do not cancel out, and give rise to a net torque which acts to assist the migration. This is why this effect is often referred to as *runaway migration*. This process is likely to occur for Saturn-mass planets embedded in massive discs, and causes migration on the timescale of a few hundred orbits. Note that if the planet was originally migrating outward, the net torque would again act to assist outward migration.

2.4.2 Migration via scattering of planetesimals

In our Solar System, the existence of the Kuiper Belt and the Oort cloud provide evidences that planetesimals have been gravitationally scattered by the giant planets. For instance one could imagine that Neptune, as the outermost planet, perturbs some planetesimals and increases their eccentricities. Their small perihelion brings them closer to second outermost planet (Uranus), which then dominates their evolution. Because the planetesimal migrated inward, Neptune had to migrate outward. The process is likely to continue until Jupiter finally sends the planetesimals into almost parabolic orbits, hence creating the Oort cloud. Because of its high mass, Jupiter would be only weakly affected, while Neptune could migrate outward by a few AU. By doing so, it can enter a mean-motion resonance with some planetesimals, as observed in the Kuiper Belt (e.g., the 3:2 resonance with Pluto) and excite their eccentricities (also an observational fact in the Kuiper Belt). Note that in this scenario, Saturn, Uranus and Neptune would migrate outward as they send the planetesimals to the inner parts of the system, while Jupiter would (slightly) migrate inward as it sends them to the Oort Cloud. This scenario (see, e.g., Fernandez and Ip, 1984; Hahn and Malhotra, 1999) is one of the underlying ideas behind the so-called Nice model (Morbidelli et al., 2007),

which aims to explain the formation of the Solar System. More generally, Levison et al. (2007) found that when two planets interact with a disc of planetesimals, the inner one is likely to migrate inward while the outer one would migrate outward.

2.4.3 High-eccentricity induced migration

There exists an alternative theory for planet migration, which does not rely on disc-planet interactions. The underlying idea behind this mechanism would be as follows: Once the disc has been swept out, only the planets (and some planetesimals, which we ignore here) would remain. Therefore the dynamical evolution of the system is dominated by planet–planet gravitational interactions. If such interactions could excite the eccentricity of one of the planet to large values, the perihelion of this planet would be located very close to the star. At each perihelion passage, the planet would loose orbital energy to the star, because of tidal interactions. As a result, it would circularize at a short period, possibly forming a hot Jupiter. The ways the eccentricity of a planet can be pumped up to high values come in different flavours, which we briefly review here.

2.4.3.1 Orbital relaxation

Papaloizou and Terquem (2001) considered a scenario in which a large number of giant planets (several Jupiter masses) rapidly form through the fragmentation of a thick protoplanetary disc or a protostellar envelope (due to gravitational instabilities), and start interacting with each other, leading to rapid dynamical relaxation on a timescale of a few hundred orbits. They found that, almost independently of the initial number of planet (between 5 and 100), most objects escape, and only 2 or 3 planets remain bound to the star, with various eccentricities and inclinations. Interestingly, the innermost planet often undergoes tidal circularization and ends up having a short period. Such scenario could then account for the eccentric planets, as well as some of the hot Jupiters. Terquem and Papaloizou (2002) refined the scenario by including low-mass, inner planets. Such planets were assumed to have formed via the core accretion model, and remain tidally bound to the disc, before being perturbed by the outer, dynamically relaxed, planets, leading again to eccentric, close-in planets. Adams and Laughlin (2003) considered a similar scenario and focused on the statistical outcome of a large number of simulations of dynamical relaxations. They found that it is difficult to exactly reproduce the distribution of short–period planets, because in order for the planet to move inward (losing orbital energy), it requires to scatter away a large number of low-mass objects (hence increasing their orbital energy).

2.4.3.2 Planet–planet scattering

Shortly after the discovery of the planet around 51 Peg, Rasio and Ford (1996) and Weidenschilling and Marzari (1996) proposed the following mechanism to explain this unusual

discovery: shortly after the protoplanetary disc dissipates, the system is left with several planets in a tight configuration. Because the disc is not here any more to damp the eccentricities and inclinations, the planets now interact freely one with each other. In some case, this leads to strong gravitational interactions, where the semi-major axis, eccentricities and inclinations of the planets change dramatically on a short timescale. The outcome is quite similar to that of orbital relaxation, with most planets being expelled from the system, and only a few left on eccentric and inclined orbits. This scenario also struggles to explain alone some of the observed properties of extrasolar planets (see, e.g., Davies et al., 2013, and references therein)

2.4.3.3 Secular chaos

Wu and Lithwick (2011) proposed an alternative scenario for the formation of hot Jupiters. They set up a system of 3 massive planets, where the outer planet is the most massive and most eccentric. On a secular timescale, much longer than that of planet–planet scattering, the outer planet chaotically diffuses its eccentricity and inclination to the inner parts of the system. The innermost planet eventually reaches a quasi-parabolic orbit and is subsequently tidally locked to the star, at large inclination. Note that the initial conditions required for such mechanism to occur could be the result of an early phase of planet–planet scattering. The diffusion of eccentricity from outer, massive, planets, to inner, less massive ones, could aslo explain why Mercury has the highest eccentricity of all the planets in the Solar System (Lithwick and Wu, 2011)

2.4.3.4 The Kozai mechanism

The Kozai mechanism (Kozai, 1962; Lidov, 1962) will be studied in details in the next chapter. In this scenario, an inner planet is perturbed by an outer, far-away, more massive body, such as a planet, a brown-dwarf, or a star. If the inclination between the two orbits is larger than a critical value ($\sim 40^\circ$), the inner planet reaches very high eccentricities and can eventually be tidally circularized to its host star. Naoz et al. (2011) showed that when the perturber is on an eccentric orbit, the inner planet can naturally flip from prograde to retrograde orbits, which could naturally account for some of the highly misaligned hot Jupiters. Because a significant number of stars are thought to be part of binary systems, a stellar companion could naturally raise Kozai oscillations on a planet (see, e.g., Fabrycky and Tremaine, 2007). However this mechanism could be killed by the presence of additional planets in the system. Teyssandier et al. (2013a) showed that a planetary companion, at orbital distances ranging from 50 to 150 AU, eccentricities between 0.25 and 0.7 and a mass larger than $2\ M_{\rm J}$ could drive an inner Jupiter-mass planet at 5 AU from a circular to a quasi-parabolic orbit, where tidal circularization at periastron could take place.

Chapter 3

Basics of celestial mechanics

Contents

3.1 The two-body problem

In this thesis we are interested in the orbital evolution of planetary systems. In this section we recall some of the main results of celestial mechanics that we will use throughout this work. First, we quickly present the point mass two-body problem, which allows us to introduce our notations. This introduction roughly follows that of Murray and Dermott (1999)

3.1.1 The planar case

We consider the evolution of two point mass of mass m_1 et m_2, for which the positions with respect to an origin O are respectively given by the vectors $\mathbf{r}_1$ and $\mathbf{r}_2$. Similarly we can study the motion of m_2 with respect to m_1. The relative position vector $\mathbf{r}$ is defined by $\mathbf{r} = \mathbf{r}_2 - \mathbf{r}_1$.

The motion of **r** with time is the solution of the following equation:

$$\frac{\mathrm{d}^2\mathbf{r}}{\mathrm{d}t^2} = -\mu\frac{\mathbf{r}}{r^3}, \tag{3.1}$$

where $\mu = G(m_1 + m_2)$, with G the gravitational constant. It is straightforward to show that the quantity $\mathbf{h} \equiv \mathbf{r} \times \dot{\mathbf{r}}$ is a constant of the motion, because of the radial nature of the force involved in equation (3.1). Therefore the motion is restricted to the plan defined by the vectors **r** and $\dot{\mathbf{r}}$. In a polar coordinate system where the vector **r** is given by the coordinates (r, θ), we get that the norm of **h** is $h = r^2\dot{\theta}$, which is a constant of motion.

The solution of equation (3.1) is well known: it is a conic of equation:

$$r = \frac{h^2/\mu}{1 + \frac{Ah^2}{\mu}\cos(\theta - \theta_0)}. \tag{3.2}$$

Here, A et θ_0 are two constants of integration. We can define the conic parameter p by $p = h^2/\mu$, and the eccentricity by $e = Ah^2/\mu$. We also define the true anomaly$f$ by $f = \theta - \theta_0$. Hence:

$$r = \frac{p}{1 + e\cos f}. \tag{3.3}$$

The nature of the trajectory will depend on the value of e. Indeed the total energy of the system E, divided by the reduced mass, takes the form:

$$E = \frac{1}{2}\left(\frac{\mathrm{d}\mathbf{r}}{\mathrm{d}t}\right)^2 - \frac{\mu}{r}. \tag{3.4}$$

The total energy is then:

$$E = -\frac{\mu}{2p}(1 - e^2). \tag{3.5}$$

We will focus on closed trajectories only (negative total energy), i.e, solutions for which $e \in [0; 1[$. The trajectory is an ellipse (or a circle if $e = 0$) of semi-major axis $a = (1/2)(r_{\max} + r_{\min})$, where $r_{\max}$ and $r_{\min}$ are the values of r for which $f = \pi$ and $f = 0$ respectively. It follows that $a = p/(1 - e^2)$. $r_{\min} = a(1 - e)$ is called the *pericenter*, while $r_{\max} = a(1 + e)$ is the *apocenter*. We indicate them respectively by P and Q on figure 3.1 We note that the total energy is now simply:

$$E = -\frac{\mu}{2a}. \tag{3.6}$$

During an infinitesimal increment along the ellipse, the area swept out by the orbital radius vector is $\mathrm{d}A = \frac{1}{2}r^2\mathrm{d}\theta$. This leads to the so-called Kepler's second law:

$$\frac{\mathrm{d}A}{\mathrm{d}t} = \frac{1}{2}h. \tag{3.7}$$

Because h is constant, equal areas are swept out in equal times. If we define T as the orbital period, we find that the total area of the ellipse is $A = hT/2$. Geometrically, the area

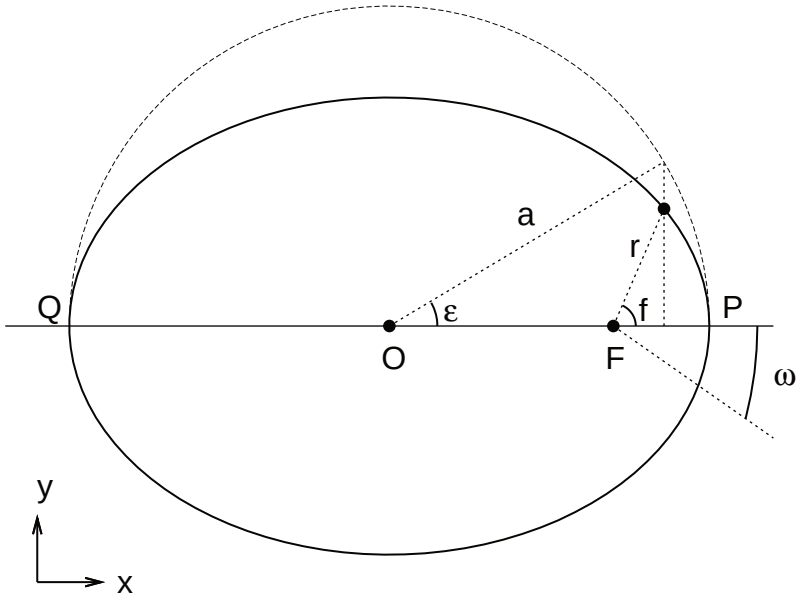

Figure 3.1: Geometrical representation of the orbital elements in the elliptical case.

is also $A = \pi a^2\sqrt{1-e^2}$. We deduce Kepler's third law:

$$\mu = n^2 a^3, \tag{3.8}$$

where we have defined $n = 2\pi/T$. The quantity n is usually called the mean motion.

Geometrically, the angle f gives the position of the body on the ellipse, at a given time, measured from one focus F of the ellipse and with respect to the line of apses (the line that connects the pericenter to the apocenter), as shown on figure 3.1. However, we will see that the line of apses can vary in time under the effect of perturbations. We define the angle ω, which we call the argument of pericenter, and which gives the direction of the pericenter with respect to a reference direction. We can choose as a direction of reference the line of apses at the time $t = 0$. The angle ω is shown on figure 3.1.

The knowledge of the quantities a, e, ω and f gives the position and speed of the body on the ellipse at any given time, and is therefore equivalent to the knowledge of the position and velocity vectors $\mathbf{r} = (x, y)$ and $\dot{\mathbf{r}} = (\dot{x}, \dot{y})$.

The set of variables (a, e, ω, f) is only one possible representation. In particular we can use an angle different from the true anomaly f. We could for example define the circumcircle of the ellipse as the circle of radius a and sharing the same centre O as the ellipse. The eccentric anomaly, given by the angle ϵ in figure 3.1, is the angle between the direction of pericenter, and the projection of the point on this circle. True an eccentric anomalies are related by the following formula:

$$\tan\frac{f}{2} = \sqrt{\frac{1+e}{1-e}}\tan\frac{\epsilon}{2}. \tag{3.9}$$

We also have the useful relation:

$$r = a(1 - e\cos\epsilon). \tag{3.10}$$

Note that, while the set of variables (a, e, ω, f) can give the position of the body on the ellipse, the time variable does not explicitly appear in the equations of motion. In celestial mechanics it is common to replace the time variable by a dimensionless variable called the mean anomaly, noted M and defined by:

$$M = n(t - t_0). \tag{3.11}$$

Here t_0 is the time of passage at pericenter. This variable does not have a simple geometrical interpretation, but has the dimension of an angle and is an increasing linear function of time. It is related to the eccentric anomaly through Kepler's equation:

$$M = \epsilon - e\sin\epsilon. \tag{3.12}$$

This equation is fundamental as it gives the position of the body on the ellipse (given by ϵ) as a function of time (given by M).

Finally we give some useful relations. Differentiating Kepler's equation, we get

$$\mathrm{d}M = (1 - e\cos\epsilon)\mathrm{d}\epsilon. \tag{3.13}$$

Then, it can be shown that :

$$\mathrm{d}M = \frac{(1-e^2)^{3/2}}{(1+e\cos f)^2}\mathrm{d}f. \tag{3.14}$$

These relations will prove useful every time we wish to average a quantity over its orbital period.

3.1.2 Three-dimensional orbit

We saw that the two-body problem for mass point objects is a planar problem, and it was therefore natural to choose a coordinate system in which the vertical component z and the associated velocity $\dot{z}$ are thoroughly zero. The motion is characterized by a, e, ω and f. In space, the motion needs to be characterized by two additional variable. The set of six variable will be equivalent to the six Cartesian components that form the position and velocity vectors. First we can define the inclination I between the plane of the orbit and a plane of reference. Then we define the longitude of ascending node Ω as the angle between the intersection of the orbital plane and the plane of reference, with respect to a reference direction (see figure 3.2). In space, we define the longitude of pericenter ϖ as $\varpi = \Omega + \omega$, even though the angles ω and Ω do not lie in the same plane. We can also define the mean longitude λ as $\lambda = M + \varpi$. The set of variables a, e, I, ϖ, Ω and λ allows us to characterize

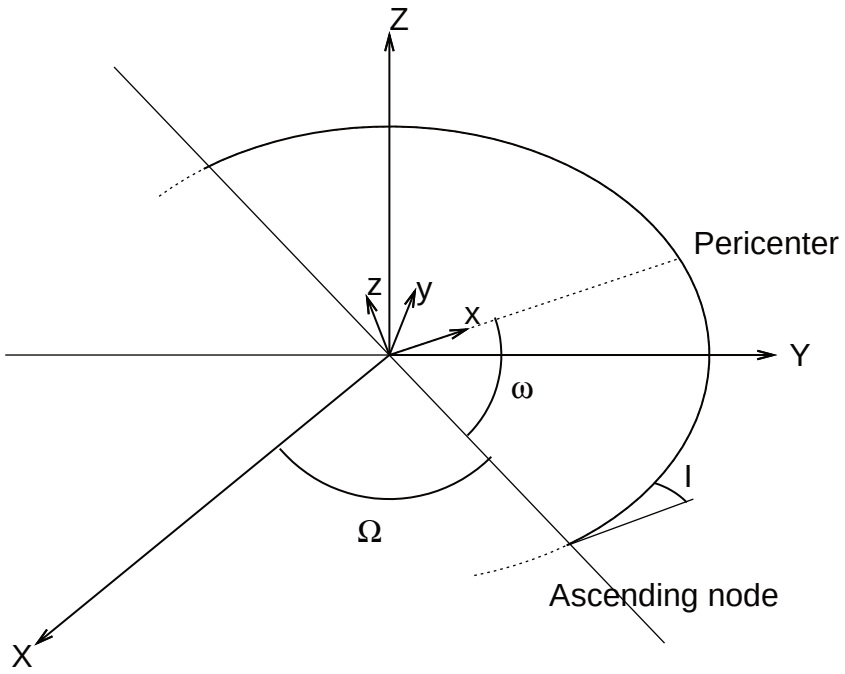

Figure 3.2: Elliptical orbital elements with respect to a system of reference (X, Y, Z). The system of reference used in the planar case is represented by (x, y, z).

the elliptic trajectory at any given time in space.

If we consider a coordinate system in which the x axis is defined by the direction of the semi-major axis, and the y axis perpendicular to it (in the orbital plane), such as in figure 3.2, then the planet has a position vector **r** defined by:

$$\mathbf{r} = r \begin{pmatrix} \cos f \\ \sin f \end{pmatrix}. \tag{3.15}$$

If the x axis now lies along the line of ascendig node, and the y axis is still in the orbital plane, then we have:

$$\mathbf{r} = r \begin{pmatrix} \cos(\omega + f) \\ \sin(\omega + f) \end{pmatrix}. \tag{3.16}$$

This vector can then be projected onto the axis (X, Y, Z) of an arbitrary reference frame such as represented in figure 3.2. It follows that:

$$\mathbf{r} = r \begin{pmatrix} \cos(\omega + f)\cos\Omega - \sin(\omega + f)\sin\Omega\cos I \\ \cos(\omega + f)\sin\Omega + \sin(\Omega + f)\cos\Omega\cos I \\ \sin(\omega + f)\sin I \end{pmatrix}. \tag{3.17}$$

3.2 Perturbation theory

As we saw, the problem of two isolated point mass is integrable. This situation is known as the “Keplerian problem”. Unfortunately, this solution offers only a pale representation of

the dynamics of celestial bodies. When studying, for example, the long term evolution of the solar system, it is necessary to take into account (at least) the mutual interactions between the 8 planets, in addition to their Keplerian motion around the Sun. Furthermore, if one tries to correctly model the motion of an artificial satellite around the Earth, the latter cannot be considered as a point mass: its deviation from a perfect sphere has to be taken into account, in order to correctly model its gravitational field. Unfortunately, the general N-body problem does not offer simple solutions. This is why the main effort of celestial mechanics in the last centuries has been to focus on so-called "perturbed" solutions. Starting from an integrable problem, for instance the Keplerian motion of a planet around a star, we add a small perturbation, arising for instance from an external planet. By modelling the perturbation as a small deviation from the integrable problem, we will try to seek approximate solutions.

3.2.1 Keplerian orbits perturbed by an extra force

We wish to know how an orbit changes when a small extra force is acting on it. Following Burns (1976) we start with the equation of motion

$$\frac{\mathrm{d}^2\mathbf{r}}{\mathrm{d}t^2} = -\mu\frac{\mathbf{r}}{r^3}, \tag{3.18}$$

and add a little perturbation in the form of a small force **dF**. We write $\mathbf{dF} = R\mathbf{e}_R + T\mathbf{e}_T + N\mathbf{e}_N$ where $\mathbf{e}_R$ pointing radially outwards, $\mathbf{e}_T$ is orthogonal to $\mathbf{e}_R$, lying in the orbital plane and positive in the direction of the motion, and $\mathbf{e}_N$ normal to the orbital plane such as the three vectors form a direct set of unit base vectors. The variation of energy $E = -\mu/2a$ and angular momentum $\mathbf{H} = r^2\dot{\theta}\mathbf{e}_N$ (per unit of mass) is given by:

$$\frac{\mathrm{d}E}{\mathrm{d}t} = \dot{\mathbf{r}}.\mathbf{dF}, \tag{3.19}$$

$$\frac{\mathrm{d}H}{\mathrm{d}t} = \mathbf{r} \times \mathbf{dF}. \tag{3.20}$$

It follows that the orbital energy E varies as:

$$\frac{\mathrm{d}E}{\mathrm{d}t} = \sqrt{\frac{\mu}{a(1-e^2)}}\left[Re\sin f + T(1+e\cos f)\right], \tag{3.21}$$

The angular momentum $\mathbf{H}$ changes as $\dot{\mathbf{H}} = rT\mathbf{e}_N - rN\mathbf{e}_T$. Since $\mathbf{H}$ lies along $\mathbf{e}_z$, the rN component changes its direction, and the change of magnitude is $\dot{H} = rT$. Hence:

$$\frac{\mathrm{d}H}{\mathrm{d}t} = \frac{a(1-e^2)}{1+e\cos f}T \tag{3.22}$$

It follows that the six orbital elements can be written as a function of the components R, T and N. We give here the equations for a, e, I and ω:

$$\frac{\mathrm{d}a}{\mathrm{d}t} = 2\sqrt{\frac{a^3}{\mu(1-e^2)}}\left[Re\sin f + T(1+e\cos f)\right], \tag{3.23}$$

$$\frac{\mathrm{d}e}{\mathrm{d}t} = \sqrt{\frac{a}{\mu}(1-e^2)}\left[R\sin f + T(\cos f + \cos\epsilon)\right], \tag{3.24}$$

$$\frac{\mathrm{d}I}{\mathrm{d}t} = \frac{rN\cos(\omega+f)}{H}, \tag{3.25}$$

$$\frac{\mathrm{d}\omega}{\mathrm{d}t} = \frac{1}{e}\sqrt{\frac{a(1-e^2)}{\mu}}\left[-R\cos f + T\sin f(2+e\cos f)\right] - \dot{\Omega}\cos I. \tag{3.26}$$

Equations (3.23)–(3.26) will prove very useful when dealing with dissipative forces. However, in the case of the point mass three-body problem, an other set of equations is prefered, which we present now.

3.2.2 The disturbing function and Lagrange's equations

Let us consider the motion of two planets around a central star. For $j = 1, 2$, we note $\mathbf{r}_j$ the position vector between the planet j (mass m_j) and the central star of mass M. The equations of motion for planet 1 and 2 take the form;

$$\frac{\mathrm{d}^2\mathbf{r}_1}{\mathrm{d}t^2} + G(M+m_1)\frac{\mathbf{r}_1}{r_1^3} = Gm_2\left(\frac{\mathbf{r}_2-\mathbf{r}_1}{|\mathbf{r}_2-\mathbf{r}_1|^3} - \frac{\mathbf{r}_2}{r_2^3}\right), \tag{3.27}$$

$$\frac{\mathrm{d}^2\mathbf{r}_2}{\mathrm{d}t^2} + G(M+m_2)\frac{\mathbf{r}_2}{r_2^3} = Gm_1\left(\frac{\mathbf{r}_1-\mathbf{r}_2}{|\mathbf{r}_1-\mathbf{r}_2|^3} - \frac{\mathbf{r}_1}{r_1^3}\right). \tag{3.28}$$

The right-hand side of equation (3.27) (resp., equation [3.28]) derives from a potential $\mathcal{R}_1$ (resp. $\mathcal{R}_2$), with:

$$\mathcal{R}_1 = Gm_2\left(\frac{1}{|\mathbf{r}_2-\mathbf{r}_1|} - \frac{\mathbf{r}_1.\mathbf{r}_2}{r_2^3}\right), \tag{3.29}$$

$$\mathcal{R}_2 = Gm_1\left(\frac{1}{|\mathbf{r}_1-\mathbf{r}_2|} - \frac{\mathbf{r}_1.\mathbf{r}_2}{r_1^3}\right). \tag{3.30}$$

If Ψ is the angle between $\mathbf{r}_1$ and $\mathbf{r}_2$, it is well-known that the quantity $|\mathbf{r}_2-\mathbf{r}_1|^{-1}$ can be written in term of the Legendre polynonials P_l:

$$\frac{1}{|\mathbf{r}_2-\mathbf{r}_1|} = \frac{1}{\mathbf{r}_2}\sum_{l=0}^{\infty}\left(\frac{r_1}{r_2}\right)^l P_l(\cos\Psi). \tag{3.31}$$

Similarly, the term involving $\mathbf{r}_1.\mathbf{r}_2$ is also a function of Ψ. Using these developments, considerable efforts have been put to express the disturbing function using orbital elements only. We will skip the details, but it has been shown that the disturbing function can take the

very general form (Murray and Dermott, 1999)

$$\mathcal{R}_1 = Gm_2 \sum_{j_1,\dots,j_6} \frac{f(\alpha)}{a_2} e_1^{|j_3|} e_2^{|j_4|} s_1^{|j_5|} s_2^{|j_6|} \cos(j_1\lambda_1 + j_2\lambda_2 + j_3\varpi_1 + j_4\varpi_2 + j_5\Omega_1 + j_6\Omega_2) \quad (3.32)$$

and a similar form for $\mathcal{R}_2$. Here $\alpha = a_1/a_2$ and $f(\alpha)$ is a function of the Laplace coefficients (see appendix §A). We also have introduce the notation $s_k = \sin(I_k/2)$ for $k = 1, 2$. Summation is made over the six integers j', which obey the d'Alembert relation:

$$\sum_{i=1}^{6} j_i = 0, \quad (3.33)$$

coming from the fact that the disturbing function has to remain invariant under global rotation.

In order to conveniently use the disturbing function, one needs to know the variation of the orbital elements under the action of the disturbing function. We shall go straight to result, which is referred to as the Lagrange's planetary equations:

$$\frac{\mathrm{d}a}{\mathrm{d}t} = \frac{2}{na}\frac{\partial R}{\partial \lambda}, \quad (3.34)$$

$$\frac{\mathrm{d}e}{\mathrm{d}t} = -\frac{\sqrt{1-e^2}}{na^2 e}\frac{\partial R}{\partial \varpi} - \frac{e\sqrt{1-e^2}}{na^2(1+\sqrt{1-e^2})}\frac{\partial R}{\partial \lambda}, \quad (3.35)$$

$$\frac{\mathrm{d}I}{\mathrm{d}t} = -\frac{1}{na^2\sqrt{1-e^2}\sin I}\frac{\partial R}{\partial \Omega} - \frac{\tan(I/2)}{na^2\sqrt{1-e^2}}\left(\frac{\partial R}{\partial \varpi} + \frac{\partial R}{\partial \lambda}\right), \quad (3.36)$$

$$\frac{\mathrm{d}\varpi}{\mathrm{d}t} = \frac{\sqrt{1-e^2}}{na^2 e}\frac{\partial R}{\partial e} + \frac{\tan(I/2)}{na^2\sqrt{1-e^2}}\frac{\partial R}{\partial I}, \quad (3.37)$$

$$\frac{\mathrm{d}\Omega}{\mathrm{d}t} = \frac{1}{na^2\sqrt{1-e^2}\sin I}\frac{\partial R}{\partial I}, \quad (3.38)$$

$$\frac{\mathrm{d}\lambda}{\mathrm{d}t} = n - \frac{2}{na}\frac{\partial R}{\partial a} + \frac{e\sqrt{1-e^2}}{na^2(1+\sqrt{1-e^2})}\frac{\partial R}{\partial e} + \frac{\tan I/2}{na^2\sqrt{1-e^2}}\frac{\partial R}{\partial I}. \quad (3.39)$$

Note that these equations can be used with any disturbing function, not only with that arising from the three-body problem. A complete derivation of these equations can be found, e.g., in Brouwer and Clemence (1961).

3.2.3 Laplace-Lagrange theory of secular perturbations

We consider the evolution of two planets of mass m_1 and m_2 orbiting a central star of mass m_0 ($m_0 \gg m_1$ and $m_0 \gg m_2$) and we only take into account the secular interactions between the two planets.

We follow Murray & Dermott (1999): for $j = 1, 2$, let a_j, e_j, I_j, n_j, ϖ_j and Ω_j be the semi-major axis, eccentricity, inclination, mean motion, longitude of pericenter and longi-

tude of ascending node of planet j, respectively. Let also $\mathcal{R}_j$ be the disturbing function of planet j, in this case the secular perturbation from planet $k = 1, 2,\ k \neq j$. To second order in inclinations and eccentricities we have

$$\begin{aligned}\mathcal{R}_j = n_j a_j^2 \Bigg[& \frac{1}{2} A_{jj} e_j^2 + A_{jk} e_1 e_2 \cos(\varpi_1 - \varpi_2) \\ & + \frac{1}{2} B_{jj} I_j^2 + B_{jk} I_1 I_2 \cos(\Omega_1 - \Omega_2) \Bigg]\end{aligned} \tag{3.40}$$

where the A's and B's are functions of the Laplace coefficients (see appendix A)

Because we are only interested in the secular variations of the system, we have averaged out to zero all the terms containing the mean longitudes λ. Therefore, given the Lagrange's equations, the semi-major axis remain constant throughout secular evolution. We have only kept the lowest order terms in eccentricities and inclinations, and the disturbing function becomes fully decoupled: the variations of the $(e; \varpi)$ variables is independent from the variation of the $(I; \Omega)$ variables. The problem reduces to that of finding two sets of eigenvalues and eigenfrequencies. The general solution reads, for planet j:

$$e_j \sin \varpi_j = \sum_{k=1}^{2} e_{jk} \sin(g_k t + \beta_k), \qquad e_j \cos \varpi_j = \sum_{k=1}^{2} e_{jk} \cos(g_k t + \beta_k), \tag{3.41}$$

and

$$I_j \sin \Omega_j = \sum_{k=1}^{2} I_{jk} \sin(f_k t + \gamma_k), \qquad I_j \cos \Omega_j = \sum_{k=1}^{2} I_{jk} \cos(f_k t + \gamma_k). \tag{3.42}$$

The e_{jk} and I_{jk} are components of the kth eigenvector, and the g_k and f_k the corresponding eigenvalues. The phases β_k and γ_k, as well as the amplitude of the eigenvectors, are given by the initial conditions. Note that in the case of the inclination vectors, one eigenfrequency is zero, owing for the conservation of total angular momentum. Note also that the formulas above can be generalized to N planets.

The eccentricities and inclinations of each planet vary sinusoidally with time, and the longitudes of pericenters and ascending nodes precess on timescales of order g_k^{-1} and f_k^{-1}, respectively. A secular resonance arises when two secular frequencies match each other, or are equal to a precession frequency induced by another mechanism (e.g., the precession induced by the oblateness of the central star).

This theory applied well in the early studies of the Solar System, where the major planets have moderate eccentricities and inclinations, and are not locked into any first-order mean-motion resonances. The simple, long-term, exchange of angular momentum which arise from this theory let astronomers to believe that the Solar System could be long-term stable. In extrasolar planetary systems, however, planets can have large eccentricities and/or inclinations, and be very close to mean-motion resonances, making this theory poorly ap-

plicable. However the precession timescales are very useful, as they can be compared to other timescales arising from other kind of perturbations. Such first-order analysis can give a quick glance at which mechanism is going to dominate the evolution of the system.

3.2.4 Hierarchical systems and the Kozai mechanism

Here we review another example of secular interaction that does not fit in the framework of the Laplace-Lagrange theory. We wish to study a system in which a tight binary (e.g., a planet of mass m_1 around a star of mass m_0) is orbited by an outer, far-away, companion (e.g., a planet of mass m_2), such as the ratio of semi-major axis remains small ($a_1/a_2 \ll 1$). Such system is called hierarchical. Once again we will average out over the orbital periods, in order to focus on the secular evolution only. However, the system studied here presents a major difference with the Laplace-Lagrange theory. Here we restrict ourselves to the case $a_1/a_2 \ll 1$ but we have no restrictions on the values which can be taken by the eccentricities and inclinations. In the Laplace-Lagrange theory, the expansion would be valid for any a_1/a_2 (as long as it is not located on a low-order MMR) but would be valid for small eccentricities and inclinations only.

Perturbation theory in the framework of hierarchical systems is discussed in Valtonen and Karttunen (2006), and some applications can be found in Innanen et al. (1997). Let us consider the case where $m_1 \ll m_2$, therefore the disturbing function that is of interest for us is:

$$\mathcal{R} = Gm_2 \left(\frac{1}{|\mathbf{r}_2 - \mathbf{r}_1|} - \frac{\mathbf{r}_1.\mathbf{r}_2}{r_2^3} \right). \tag{3.43}$$

We note ψ the angle between $\mathbf{r}_1$ and $\mathbf{r}_2$. The quantity $|\mathbf{r}_2 - \mathbf{r}_1|^{-1}$ can be expanded to second order in r_1/r_2 to give

$$\frac{1}{|\mathbf{r}_2 - \mathbf{r}_1|} = \frac{1}{r_2} \left[1 + \frac{r_1}{r_2} \cos\psi - \frac{1}{2} \left(\frac{r_1}{r_2} \right)^2 \left(1 - 3\cos^2\psi \right) \right]. \tag{3.44}$$

It follows that:

$$\mathcal{R} = \frac{Gm_2}{r_2} \left[1 - \frac{1}{2} \left(\frac{r_1}{r_2} \right)^2 \left(1 - 3\cos^2\psi \right) \right]. \tag{3.45}$$

In order to study the secular interaction between the two planets, we have to average the disturbing function $\mathcal{R}$ over the orbital period of the two planets, in order to get the secular disturbing function $\mathcal{R}_{sec}$:

$$\mathcal{R}_{sec} = \int_0^{2\pi} \int_0^{2\pi} \mathcal{R} \mathrm{d}M_1 \mathrm{d}M_2.$$

First of all we need to express $\mathcal{R}$ as a function of the orbital elements of the two planets.

We can use eq. (3.17) to calculate the term $\cos\psi = \mathbf{r}_1.\mathbf{r}_2/(r_1 r_2)$. We obtain:

$$\begin{aligned}\cos\psi = &(\cos\omega_1\cos\omega_2 + \sin\omega_1\sin\omega_2\cos I_1\cos I_2)\cos(\Omega_1-\Omega_2)\\ &+ (\cos\omega_1\sin\omega_2\cos I_2 - \sin\omega_1\cos\omega_2\cos I_1)\sin(\Omega_1-\Omega_2)\\ &+ \sin\omega_1\sin\omega_2\sin I_1\sin I_2.\end{aligned} \tag{3.46}$$

We can choose a plane of reference (X, Y, Z) such as Z is aligned with the (constant) total angular momentum of the system (in this case, the sum of the orbital angular momentum of the two planets), and X and Y lie in the plane perpendicular to this axis. Conservation of angular momentum imposes $\Omega_2 - \Omega_1 = \pi$, such as

$$\cos\psi = -(\cos\omega_1\cos\omega_2 + \sin\omega_1\sin\omega_2\cos I_1\cos I_2) + \sin\omega_1\sin\omega_2\sin I_1\sin I_2. \tag{3.47}$$

In addition we have assumed that $m_1 \ll m_2$ and $a_1 \ll a_2$. Thus m_2 carries most of the angular momentum of the system, and we have $\sin I_2 \simeq 0$. Finally we get

$$\cos\psi = -(\cos\omega_1\cos\omega_2 + \sin\omega_1\sin\omega_2\cos I_1) \tag{3.48}$$

Using equations (3.3), (3.14) and (3.48) we can carry the integration over the outer orbit's period. After some tedious algebra, or making use of a symbolic computational software like *Mathematica* we get:

$$\frac{1}{2\pi}\int_0^{2\pi}\mathcal{R}\mathrm{d}M_2 = \frac{Gm_2}{a_2}\left[1 + \left(\frac{r_1}{a_2}\right)^2 \frac{1 + 3\cos(2I_1) + 6\cos 2(\omega_1+f_1)\sin^2 I_1}{16\left(1-e_2^2\right)^{3/2}}\right] \tag{3.49}$$

Because the semi-major axis are constant in the secular approximation, we can drop the additive term Gm_2/a_2, and carry the integration over the inner orbit's period to get:

$$\mathcal{R}_{sec} = \frac{Gm_2a_1^2}{32a_2^3(1+e_2^2)^{3/2}}\left[(2+3e_1^2)(1+3\cos(2I_1)) + 30e_1^2\cos(2\omega_1)\sin^2 I_1\right]. \tag{3.50}$$

which we can re-write, using trigonometric formulas:

$$\mathcal{R}_{sec} = \frac{Gm_2a_1^2}{8a_2^3(1+e_2^2)^{3/2}}\left[2 + 3e_1^2 - 3\sin^2 I_1(1 - e_1^2 + 5e_1^2\sin^2\omega_1)\right]. \tag{3.51}$$

In this disturbing function, the orbital elements of the perturbing body appear only in the overall multiplicative factor. Therefore they will only change the timescale on which the interactions take place. Because we have averaged over the orbital periods, we have eliminated all short-term interactions in the disturbing function (3.51).

Using eq. (3.51), Lagrange planetary equations for the secular problem give:

$$\begin{aligned}
\frac{\mathrm{d}I}{\mathrm{d}\tau} &= -\frac{15}{8}\frac{e^2}{\sqrt{1-e^2}}\sin 2\omega \sin I\cos I,\\
\frac{\mathrm{d}e}{\mathrm{d}\tau} &= \frac{15}{8}e\sqrt{1-e^2}\sin 2\omega \sin^2 I,\\
\frac{\mathrm{d}\omega}{\mathrm{d}\tau} &= \frac{3}{4}\frac{1}{\sqrt{1-e^2}}\left[2(1-e^2)+5\sin^2\omega(e^2-\sin^2 I)\right].
\end{aligned} \tag{3.52}$$

where we have dropped the subscript "1" for the inner planet, and where we have defined a dimentionless time parameter τ as

$$\tau = \frac{Gm_2}{a_2^3(1-e_2^2)^{3/2}n}t.$$

We assume that the inner eccentricity is initially small, so that we can neglect all the terms in e^2:

$$\begin{aligned}
\frac{\mathrm{d}I}{\mathrm{d}\tau} &= 0,\\
\frac{\mathrm{d}e}{\mathrm{d}\tau} &= \frac{15}{8}e\sin 2\omega \sin^2 I,\\
\frac{\mathrm{d}\omega}{\mathrm{d}\tau} &= \frac{3}{4}\left[2-5\sin^2\omega\sin^2 I)\right].
\end{aligned} \tag{3.53}$$

Since $\mathrm{d}I/\mathrm{d}\tau = 0$, we can define a new constant quantity A by

$$A = 5\sin^2 I - 2.$$

In appendix B, we show that the equation $\mathrm{d}\omega/\mathrm{d}\tau = a + b\sin^2\omega$ can be solved to give

$$\omega = \begin{cases} \arctan\left[\sqrt{\frac{2}{A}}\frac{\mathrm{e}^{\frac{3}{2}\sqrt{2A}\tau}+1}{\mathrm{e}^{\frac{3}{2}\sqrt{2A}\tau}-1}\right] & \text{if } I > 39.23^\circ \\ \arctan\left[\sqrt{\frac{2}{-A}}\tan\left(\frac{3}{4}\sqrt{-2A}\tau\right)\right] & \text{if } I < 39.23^\circ. \end{cases} \tag{3.54}$$

We now study the behavior of this solution, depending whether $I < 39.23^\circ$ or $I > 39.23^\circ$.

Case $I < 39.23^\circ$

We first consider the case $I < 39.23^\circ$, the solution for ω is

$$\tan\omega = \tan\left[\sqrt{\frac{2}{-A}}\tan\left(\frac{3}{4}\sqrt{-2A}\tau\right)\right].$$

Therefore ω periodically circulates. As I is constant, the Lagrange equation for e takes the form

$$\frac{\mathrm{d}e}{e} = C\sin(2\omega)\mathrm{d}\omega$$

where C is a constant. The solution for e will take the form

$$e = e_0 \exp\left[-\frac{C}{2}\cos 2\omega\right].$$

and therefore e will remain bounded around its initial small value.

Case $I > 39.23°$

We now consider the case $I > 39.23°$. When looking at the secular evolution of the system, we consider timescales much larger than the orbital period, i.e. $t \gg T$. Therefore we can use the approximation $\frac{e^{\frac{3}{2}\sqrt{2A}\tau}+1}{e^{\frac{3}{2}\sqrt{2A}\tau}-1} \simeq 1$. With this approximation, ω becomes a constant and therefore $\frac{d\omega}{d\tau} = 0$. Given the Lagrange planetary equation for ω we deduce

$$5\sin^2\omega\sin^2 I = 2$$

Hence the Lagrange equation for e is:

$$\frac{de}{d\tau} = \frac{15}{4}e\sqrt{\frac{2}{5}\left(\sin^2 I - \frac{2}{5}\right)}. \tag{3.55}$$

Note that there is also a negative solution if $\cos\omega$ and $\sin\omega$ are of opposite signs. Noting e_0 the initial (small) eccentricity, this equation is easily integrated to give

$$e(t) = e_0 \exp\frac{15}{4}\sqrt{\frac{2}{5}\left(\sin^2 I - \frac{2}{5}\right)}\,\tau. \tag{3.56}$$

Therefore the growth of e from e_0 is exponential. Very quickly the approximation stating that I is constant is not valid anymore. However, as e increases, the quantity

$$\sqrt{1-e^2}\cos I \tag{3.57}$$

has to remain constant. It can be seen from calculating $\frac{d}{dt}\sqrt{1-e^2}\cos I$ using Eq.(3.34). This quantity is sometimes referred to as the *Kozai integrale*. Physically it is the dimensionless z-component of the angular momentum of the inner orbit. Equation (3.57) clearly indicates that when e is maximum, I is minimum and vice-versa. We saw that the minimum of I occurs for $\sin^2 I = 2/5$, therefore $\cos I = \sqrt{3/5}$. At this point the eccentricity reaches its maximal value $e_{\max}$:

$$\sqrt{1-e_0^2}\cos I_0 = \sqrt{1-e_{\max}^2}\sqrt{\frac{3}{5}}$$

where I_0 is the initial inclination. Therefore, recalling that e_0 is very small, one gets

$$e_{\max} = \sqrt{1-\frac{5}{3}\cos^2 I_0} \tag{3.58}$$

After reaching its maximum, e will decrease until it reaches e_0, and so on. Meanwhile, I will vary accordingly, in order to keep $\sqrt{1-e^2}\cos I$ constant. This long-term periodic variations are call *Kozai cycles*. On figure 3.3 we show an example of such cycles. We carry out the numerical integration of equations (3.52) for a system of two planets around a star of $1\ M_\odot$. The inner planet has a mass of $0.1\ M_\mathrm{J}$ at 4 AU on a circular orbit, and is inclined by $60°$. The perturber is a planet of $10\ M_\mathrm{J}$ on a circular orbit at 80 AU, with no inclination. Numerically, the eccentricity reaches a maximum $e_{1,\max} = 0.7638$, in very good agreement with eq. (3.58). When this maximum is reached, the inclination reaches a minimum of $39.23°$, which is the Kozai critical angle.

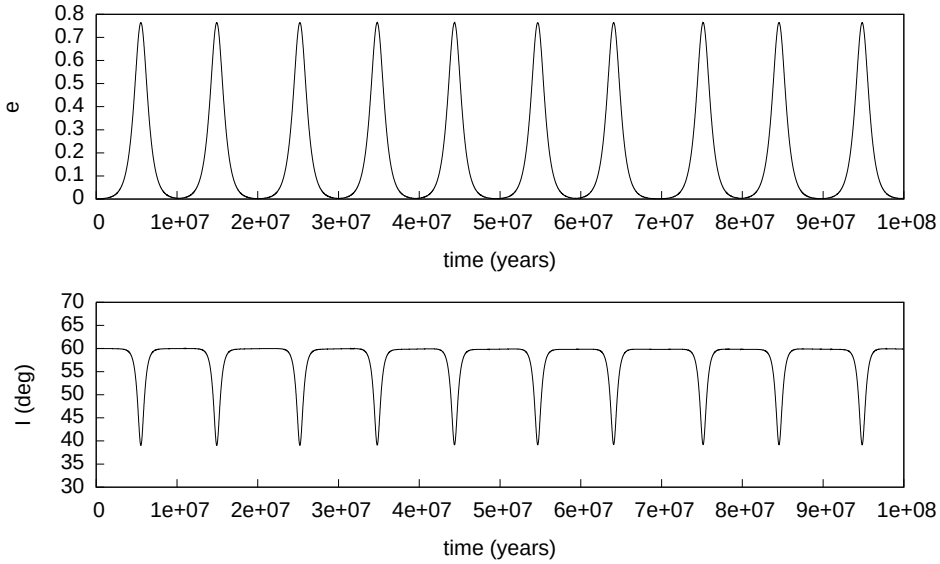

Figure 3.3: Evolution of the eccentricity (top panel) and inclination (bottom panel) for a planet undergoing Kozai cycles. The planet has a mass of $0.1\ M_\mathrm{J}$ at 4 AU on a circular orbit, and is inclined by $60°$. The perturber is a planet of $10\ M_\mathrm{J}$ on a circular orbit at 80 AU, with no inclination. The cycles of equal period clearly appear. As the eccentricity reaches its maximum, the inclination reaches its minimum, and vice-versa. These maximum and minimum values satisfy those predicted by the theory.

According to equation (3.56) the eccentricity increases to reach its maximum on a timescale τ_e given by

$$\tau_\mathrm{e} = 0.42 \left(\sin^2 I_0 - \frac{2}{5}\right)^{-1/2} \ln\left(\frac{e_\mathrm{max}}{e_0}\right). \tag{3.59}$$

Therefore a complete cycle will take place on a timescale at least twice as large as this. In units of times, we can define the Kozai timescale as

$$T_K = \left(\frac{a_2}{a_1}\right)^3 \frac{m_0}{m_2}(1-e_2^2)^{3/2}\frac{T_1}{2\pi} \tag{3.60}$$

where T_1 is the orbital period of the inner planet. Therefore the period of a Kozai oscillation is at least $2\tau_\mathrm{e}T_K$ (Innanen et al., 1997, found that the period of oscillations is actually slightly larger than that). For example, when applied to the system in figure 3.3, it gives a period of

$1.3\ 10^7$ yr, which is in good agreement with the numerical period.

The first applications of this so-called Kozai (or Kozai-Lidov) mechanism can be found in Kozai (1962) and Lidov (1962). Kozai's work was motivated by the dynamical study of asteroids orbiting the Sun and perturbed by Jupiter, while Lidov was interested in artificial satellites in the Earth-Moon system. Since then, this mechanism has been applied to a large variety of astrophysical problems, from solar system dynamics to binary black holes, and of course including extrasolar planets (for an extensive bibliographical review of the astrophysical applications of secular dynamics in hierarchical three-body system, we refer the reader to Naoz et al., 2013).

To conclude, we remark that the onset of the Kozai mechanism is based on a very slow precession of the argument of pericenter. This is therefore possible in systems in which there are no other sources of strong variations of the argument of pericenter. For instance, the action of a fourth body, the oblateness of the star, or post-Newtonian effects (see §3.2.6), could lead to rapid variations of this argument, and hence suppress the Kozai mechanism.

We note that the author has participated in series of papers devoted to the Kozai mechanism (Naoz et al., 2011, 2013; Teyssandier et al., 2013a) at a higher level of approximation. When relaxing the assumptions of test particle for the inner body and circular orbit for the outer body, higher-order terms in the Hamiltonian become important (often referred to as *octupole* terms). The inner planet can reach eccentricities arbitrary close to unity, and spans a wide spectrum of inclinations. The high value reached by the eccentricity means that when tides arising from the star are taken into account, the planet undergoes strong orbital energy dissipation at pericenter. The result is a circularized, highly inclined planets on a very short orbit. This can account for the population of observed misaligned hot Jupiters.

3.2.5 Resonant perturbations

A mean motion resonance (hereafter MMR) arises when the ratio of the mean motions of two bodies (say, two planets orbiting a star) is close to the ratio of two integers. Namely, a $(p+q):p$ MMR is a configuration that will obey

$$\frac{n_2}{n_1} = \frac{p}{p+q} \tag{3.61}$$

where p and q are positive integers, with $p \neq 0$, and n denotes the mean motion. The simplest case is the case $q = 0$. This is often referred to as a corotation (or co-orbital) resonance. An example of such resonance can be found in the Solar System, with the Trojan asteroids which share the orbit of Jupiter, but are situated roughly $\pm 60^\circ$ away from the planet. In general, q is called the order of the resonance. For instance, in a 2:1 MMR, the inner planet will orbit the star twice while the outer planet orbits it once. Every qth conjunction occur at the same longitude, which results in the planets exerting a strong gravitational influence on each other, causing important exchanges of angular momentum, which can gradually lead to

unstable orbits. In other circumstances the resonant configuration helps the orbits to remain stable.

Following the excellent review of Peale (1976) (see also Greenberg, 1977), we introduce some important physical concepts of MMRs. Let us consider the case of two planets orbiting a central star and experiencing repeated conjunctions. We assume that the two planets have masses m_1 and m_2, with $m_1 \gg m_2$. The two orbits are coplanar, and the inner mass is assumed to on a circular orbit, unaffected by the lower mass outer planet (hereafter, the particle) on an eccentric orbit. We are interested in exchange of angular momentum between the planets and the stable configuration that could arise. It is useful to keep in mind equation (3.22), which gives the relation between the variation of orbital angular momentum, orbital radius and tangential force as

$$\frac{\mathrm{d}H}{\mathrm{d}t} = rT.$$

Let us first consider the case where conjunction occurs exactly at apocenter or pericenter. By symmetry, the tangential force exerted by the massive planet on the particle before and after conjunction will be of equal magnitude and opposite sign. Hence the effect of the tangential force averages out to zero and there is no net transfer of angular momentum.

Now, let us examine the situation where conjunctions occur at any other location on the orbits. On figure 3.4 we show one such example where the conjunction occurs slightly before apocenter. As the particle is coming toward apocenter, its angular velocity will be faster before conjunction than after. Therefore it will be closer to the inner planet's angular velocity before than after. Hence the tangential force is applied longer before conjunction than after. In addition, the tangential force will tend to be larger before conjunction than after, as the two orbits quickly diverge one from the other after conjunction passage. Therefore the largest tangential force will be the one acting against the motion of the particle, leading to a total torque being negative. Hence, angular momentum is lost by the particle, slowing down its period. This causes the next conjunction to occur slightly later, i.e, closer to the apocenter.

Similarly, let us consider the situation where conjunction occurs just before pericenter. The particle coming toward pericenter, its angular velocity increases, being faster just after conjunction. Hence the tangential force will act longer after conjunction than before. Because the two orbits diverge slowly, the net torque is positive, and the period of the particle's orbits shrinks. Thus the next conjunction occurs slightly sooner, i.e, closer to apocenter again.

The same argument can be applied to show that conjunctions occurring just after apocenter and just after pericenter will also bring the followings conjunctions to occur closer to apocenter. Conjunction at apocenter then appears to be the stable equilibrium configuration of the system. Murray and Dermott (1999) showed that in the other configuration, i.e, the particle being on the inner eccentric orbit, then pericenter conjunction is the stable equilibrium configuration.

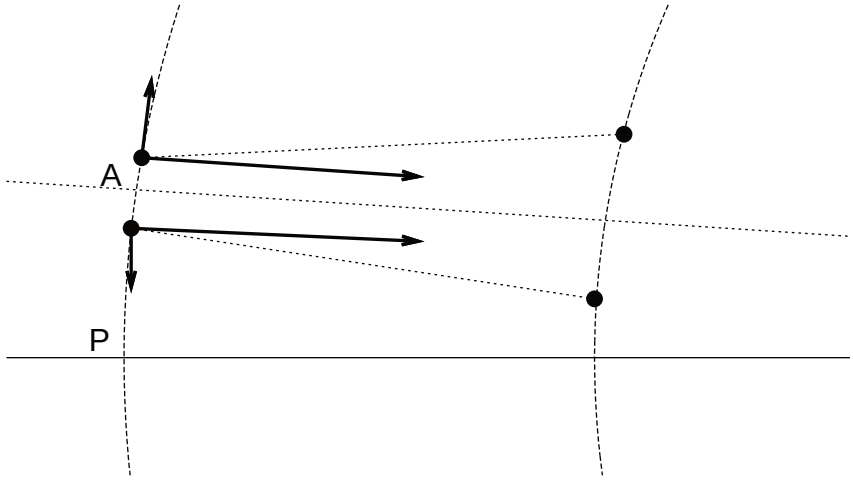

Figure 3.4: Resonant encounter at conjunction at point A, just before pericenter (point P). Arrow pointing up and down are the tangential forces, whereas arrows pointing to the right are radial forces exerted by the inner planet on the outer one, just before and just after conjunction.

Much like a pendulum can oscillate around its equilibrium position or go around it doing a full circle, the resonant conjunction can oscillate around the line of apses (libration) or do a full 360° motion around it (circularization). As long as the conjunction is maintained, so will be the ratio of orbital periods.

Conjunction will occur at a longitude given by $\lambda_{\rm conj} = (p+q)\lambda_2 - p\lambda_1$. As we just saw, the longitude of conjunction tends to align with the line of apses. However the later can precess because of the interactions between the two planets. Therefore, provided the line of apses varies on timescale longer than the orbital periods, the longitude of conjunction will match its variations, such as the angle $(p+q)\lambda_2 - p\lambda_1 - q\varpi_1$ remains roughly constant. Note that the coefficients of this argument follow the relation (3.33). Such angle is called a *resonant argument*, and measures the displacement of the longitude of conjunction with respect to the line of apses. Although the relation $n_2/n_1 = p/(p+q)$ denotes a *nominal* resonance, an *exact* resonance will occur when the time derivative of a resonant argument is exactly zero. The exact location of a resonance will hence be slightly shifted from the position of the exact resonance. In the case of two massive planets, ϖ_2 can also be subject to variations, and several distinct resonances can arise. For instance, in the 2:1 resonance, the two obvious resonant angles will be $2\lambda_2 - \lambda_1 - \varpi_1$ and $2\lambda_2 - \lambda_1 - \varpi_2$. However, other resonant angles exist which can be formed as linear combination of these ones, such as $4\lambda_2 - 2\lambda_1 - 2\varpi_1$, $4\lambda_2 - 2\lambda_1 - 2\varpi_2$ and the mixed angle $4\lambda_2 - 2\lambda_1 - \varpi_1 - \varpi_2$.

However, a term like $4\lambda_2 - 2\lambda_1 - 2\varpi_1$ will contribute to a lower extend than a term like $2\lambda_2 - \lambda_1 - \varpi_1$. Indeed we saw in equation (3.32) that a general term of the disturbing

function takes the form

$$\frac{f(\alpha)}{a_2} e_1^{|j_3|} e_2^{|j_4|} s_1^{|j_5|} s_2^{|j_6|} \cos(j_1\lambda_1 + j_2\lambda_2 + j_3\omega_1 + j_4\omega_2 + j_5\Omega_1 + j_6\Omega_2).$$

Therefore, $4\lambda_2 - 2\lambda_1 - 2\varpi_1$, having $q = 2$, has an amplitude of the order e^2, compared to $2\lambda_2 - \lambda_1 - \varpi_1$ which has an amplitude of order e. For low eccentricities, the latter will dominate. For the same reason, a 31:15 MMR, although in appearance very similar to a 2:1 MMR, has an order $q = 16$, meaning that the associated terms in the disturbing function, being of order e^{16} at least, will be of insignificant contribution.

Similarly to the eccentricity-type resonance we have just presented, there exists inclination-type resonances. They are characterized by libration of the conjunction around the longitudes of nodes. As we saw in equation (3.25), only the normal component of perturbative forces will affect the inclinations. The normal component of the force being very small for low inclinations, there are no inclination-type resonances for low inclinations (Greenberg, 1977). More generally, inclinations terms only appear in even powers of the disturbing function, in order to insure physical invariance under the permutation of the vertical axis.

3.2.6 Post-Newtonian perturbations

In 1859, Urbain le Verrier analysed 150 years of Solar System observations and compared them with the existing theory for the motion of planets (basically, an expansion of the Laplace-Lagrange theory including higher-order terms). He found that the gravitational precession of Mercury was about 40 arcsec/century faster than the theoretical value, which included perturbation by the seven other planets. The result stood against all theories until Einstein applied its newly created General Relativity and solved the problem.

This effect is now taken into account in every theory that aims at studying the long-term stability of the Solar System. It was also found to play a part in the dynamics of some exoplanets. Indeed, hot Jupiters are orbiting so close to their star that this effect is greatly enhanced. As we saw, the Kozai mechanism is based on the slow variation of the argument of pericenter. Therefore, if the relativistic precession were occurring on a timescale shorter than the Kozai timescale, the latter would be "killed". Here we quickly introduce the main results of this effect.

We consider a planet of mass m_1 orbiting a star of mass m_0 at a distance r_1. The potential due to the first-order post-Newtonian term reads (see, e.g., Nobili and Roxburgh, 1986):

$$\Phi_{\rm GR} = -\frac{3G^2 m_0^2}{r_1^2 c^2}, \tag{3.62}$$

where c is the speed of light. The force that derives from this potential reads:

$$\Gamma_{\rm GR} = -\frac{6G^2 m_0^2}{c^2} \frac{\mathbf{r}_1}{|\mathbf{r}_1|^4}. \tag{3.63}$$

The long-term variation of the argument of pericenter ω_1 caused by this force is

$$\left\langle \frac{\mathrm{d}\omega_1}{\mathrm{d}t} \right\rangle = \frac{1}{2\pi} \int_0^{2\pi} \frac{\mathrm{d}\omega_1}{\mathrm{d}t} \mathrm{d}M_1. \tag{3.64}$$

where $\dot{\omega}_1$ is given by equation (3.26). The integration can be carried out once we substitute $\mathrm{d}M_1$ by $\mathrm{d}f_1$ via equation (3.14). We get

$$\left\langle \frac{\mathrm{d}\omega_1}{\mathrm{d}t} \right\rangle = \frac{3G^{3/2}m_0^{3/2}}{a_1^{5/2}c^2(1-e_1^2)}. \tag{3.65}$$

The argument of pericentre is the only element affected by this precession. For all the other elements, the effect averages out to zero. It follows that an estimate for the relativistic precession timescale is

$$\tau_{\mathrm{GR}} = 2\pi \frac{a_1^{5/2}c^2(1-e_1^2)}{3G^{3/2}m_0^{3/2}}. \tag{3.66}$$

This timescale can then be compared with other timescales (Kozai, Laplace-Lagrange...) in order to determine the dominant effect.

Chapter 4

Interactions between an inclined planet and a disc

Contents

4.1 Planets on inclined orbits

In this chapter we are interested in planets whose orbit is misaligned with respect to a protoplanetary disc. In chapter 2, we have seen that some planets have been observed with a large angle between their orbital plane and the stellar equatorial plane. If the total angular momentum of the protoplanetary disc is aligned with the stellar spin (a statement currently supported by observations, see, e.g., Watson et al., 2011), this would indicate that the orbital plane of the planet, as we observe it today, is no longer in the plane where the disc was once located. In this chapter, we aim at determining the fate of a planet whose orbit is inclined

with respect to the disc. Mainly, we examine under which conditions will it realign with the plane of the disc, and whether it could leave some observational evidences.

The evolution of a planet whose orbit is inclined with respect to a disc has been studied by Terquem and Ajmia (2010) and Rein (2012). We note that Vokrouhlicky and Karas (1998) have also used the same approach when looking at stellar orbits around a central galactic black hole, surrounded by an accretion disc. In particular, both Vokrouhlicky and Karas (1998) and Terquem and Ajmia (2010) have shown that the gravitational potential of the disc can raise Kozai oscillations on the planet (or any other orbiting celestial body), provided that the angle between the orbital plane and the mid-plane of the disc is above a critical angle.

There is currently no evidence of such a primordial misalignment between a disc and a planet, but Barnes et al. (2013) reported a possible misaligned hot Jupiter orbiting the pre-main-sequence star PTFO 8-8695, whose age of less than 3 Myr could be compatible with the presence of a disc. In addition, models suggest that a primordial misalignment could be possible. For instance Papaloizou and Terquem (2001) envisioned a scenario in which a large number of massive planetary size objects formed out of the disc through a fragmentation process occurring in the protostellar envelope while it collapses on to the protostar. Most of them are rapidly ejected during a phase of dynamical relaxation, and only a handful remain, with various inclinations and eccentricities. They could later on interact with the protoplanetary disc. Another scenario could invoke interactions in dense stellar clusters where the system originated: capture of free-floating planets, or of planets from another system during a stellar flyby are possible (Malmberg et al., 2011), and could result in the planet being inclined and eccentric. In the next chapter we will also study a scenario in which planets can be put on inclined orbits with respect to a disc, via resonant migration of a pair of planets.

In the present chapter we first study the gravitational perturbation that the disc induces on the planet, and show that it naturally leads to Kozai oscillations. Then we study the dissipative processes that result from the frictional forces exerted by the disc particles on the planet, as its orbit crosses the plane of the disc. We then combine these effects to study the interactions between an inclined planet and a disc. These results are presented in a paper published in MNRAS in 2013 (Teyssandier, Terquem & Papaloizou). Finally we look at systems of two planets and a disc.

4.2 The disc potential

We study a system of a star of mass M_*, orbited by a planet of mass M_p. The star is also surrounded by a protoplanetary disc of mass M_d. In all this chapter, we assume that the angular momentum of the disc is large compared to that of the planet's orbit. Therefore the disc is not affected by the planet. We justify this more precisely in the appendix of

Teyssandier et al. (2013b). We work in a coordinate system centred on the star.

4.2.1 The 2D case

The gravitational interaction between a two-dimensional disc and an inclined planet was studied in Terquem and Ajmia (2010). Here, we review in details some of their results. We first assume that the disc is a two-dimensional ring of material, located in the equatorial plane of the star. We choose this plane to be the plane of reference, so that the disc's inclination is zero. The disc extends from an inner radius R_i to an outer radius R_o. Using spherical coordinates, the planet is at a location (r_p, ϕ_p, θ_p), where ϕ_p is the azimuthal angle and θ_p the polar angle. If we consider a small portion of material in the disc at the location (r, ϕ), then the distance between this material and the planet is $(r^2 + r_p^2 - 2rr_p \cos\phi \sin\theta_p)^{1/2}$. Therefore, the gravitational potential exerted by the disc on the planet is

$$\Phi = -\int_{R_i}^{R_o} \int_0^{2\pi} \frac{G\Sigma(r) r}{(r^2 + r_p^2 - 2rr_p \cos\phi \sin\theta_p)^{1/2}} \mathrm{d}r\mathrm{d}\phi. \tag{4.1}$$

Here $\Sigma(r)$ is the surface density of the disc. We assume that the density profile follows:

$$\Sigma(r) = \Sigma_0 \left(\frac{r}{R_0}\right)^{-n}. \tag{4.2}$$

The constant Σ_0 is defined through the total mass of the disc. We have

$$M_\mathrm{d} = \int_{R_i}^{R_o} \int_0^{2\pi} \Sigma(r) r \mathrm{d}r\mathrm{d}\phi, \tag{4.3}$$

which imposes

$$\Sigma_o = \frac{(-n+2) M_\mathrm{d}}{2\pi R_o^2 \left(1 - \eta^{-n+2}\right)}. \tag{4.4}$$

Here $\eta \equiv R_i/R_o$. The quantity n, which characterizes the density profile, usually varies between $1/2$ and $3/2$.

In order to capture the main features of the gravitational interaction, we assume that the planet is gravitating inside the inner cavity of the disc, so that $r_p \ll R_i$, thus $r_p \ll r$ for any r in the disc. A similar reasoning, although less restrictive, can be applied if we assume that most of the disc's mass is contained in the outer parts of the disc, so that the gravitational interaction mainly arises from the parts of the disc satisfying $r \gg r_p$. In any case, we get, to second order in r/r_p:

$$(r^2 + r_p^2 - rr_p \cos\alpha \sin\theta_p)^{-1/2} = \frac{1}{r}\left[1 + \frac{r_p}{r}\cos\alpha\sin\theta_p - \frac{r_p^2}{2r^2}\left(1 - 3\cos^2\alpha \sin^2\theta_p\right)\right]. \tag{4.5}$$

It follows that

$$\int_0^{2\pi} (r^2 + r_p^2 - r r_p \cos\alpha \sin\theta_p)^{-1/2} = \frac{1}{r}\left[1 - \frac{r_p^2}{2r^2}\left(1 - \frac{3}{2}\sin^2\theta_p\right)\right]. \tag{4.6}$$

The integration on dr can be completed, and we finally get:

$$\Phi = -\frac{2-n}{1-\eta^{-n+2}}\frac{GM_\mathrm{d}}{R_o}\left[\frac{1-\eta^{1-n}}{1-n} - \frac{-1+\eta^{-1-n}}{1+n}\frac{r_p^2}{2R_o^2}\left(1 + \frac{3}{2}\sin^2\theta_p\right)\right] \tag{4.7}$$

If the planet has a semi-major a, eccentricity e, inclination I, argument of periapsis ω and true anomaly f, we get the following relation:

$$\cos\theta_p = \sin(\omega + f)\sin I. \tag{4.8}$$

If we want to study the secular evolution of the planet perturbed by the disc, we have to average Φ over the orbital period of the planet. We have to calculate the quantity:

$$\frac{1}{2\pi}\int_0^{2\pi} r_p^2\left(1 - \frac{3}{2}\sin^2\theta_p\right)\mathrm{d}M.$$

We use relations (3.3), (3.14) and (4.8), and compute the final integrale to get the average potential:

$$\langle\Phi\rangle = \frac{(2-n)(-1+\eta^{-1-n})}{(1+n)(1-\eta^{-n+2})}\frac{GM_\mathrm{d}a^2}{8R_o^3}\left(2 + 3e^2 - 3\sin^2 I(1 - e^2 + 5e^2\sin^2\omega)\right), \tag{4.9}$$

where we have dropped a constant additive term. Up to a constant multiplicative factor, this potential is equivalent to that given by eq. (3.51) if the perturber was a planet of mass M_d on a circular orbit at a distance R_o. Therefore we can expect that the disc should raise Kozai-like oscillations on an inclined planet. The multiplicative factor in equation (4.9) gives us the modified timescale of the disc-Kozai cycles:

$$T_{K,\mathrm{disc}} = \frac{(1+n)(1-\eta^{-n+2})}{(2-n)(-1+\eta^{-1-n})}\left(\frac{R_o}{a}\right)^3\frac{M_*}{M_\mathrm{d}}\frac{T}{2\pi}. \tag{4.10}$$

4.2.2 The 3D case

Previously, we modelled the disc as a two-dimensional ring of material without any vertical structure. This assumption could prove to be useful when studying a planetary ring, such as that of Saturn. However, protoplanetary discs, which we are interested in, can have a significant vertical structure. We define the aspect ratio $H_0 \equiv H(r)/r$, where $H(r)$ is the height of the disc at the radius r. Both observation and theory suggest that the disc aspect ratio is quite small, in the range $10^{-2} - 10^{-1}$. It has been suggested that $H \propto r^\gamma$, with γ of the order unity (D'Alessio et al., 1998, for example, suggest $\gamma \approx 5/4$). Here we will assume

that $H \propto r$, such as H_0 is constant. Note that we define H from the mid-plane of the disc, so that the total thickness of the disc is $2H$.

We consider again a planet of mass M_p, orbiting a star of mass M_*, and whose position is given, in cylindrical coordinates, by (r_p, ϕ_p, z_p), in a coordinate system centred on the star. The star is also surrounded by a disc of mass M_d, whose mid-plane lies in the equatorial plane defined by $z = 0$. The disc has a vertical structure defined by its semi-thickness $H(r)$. It extends from an inner radius R_i to an outer radius R_o. This disc exerts a gravitational potential on the planet, which takes the form

$$\Phi(r_p, z_p) = -G \int_{R_i}^{R_o} \int_{-H}^{H} \int_0^{2\pi} \frac{\rho(r', z') r' \mathrm{d}r' \mathrm{d}z' \mathrm{d}\phi'}{\left(r_p^2 + r'^2 - 2 r_p r' \cos\phi' + (z_p - z')^2\right)^{1/2}}, \tag{4.11}$$

where $\rho(r, z)$ is the mass density in the disc.

If one wants to integrate numerically the orbit of a planet perturbed by the disc, then one needs to express the gravitational force that derives from equation (4.11), which is $-\nabla\Phi$. This is detailed in Teyssandier et al. (2013b).

4.3 Frictional forces

When the planet crosses the disc, it has a relative velocity with respect to the particles in the disc, and thus suffers a frictional force. We will assume that the disc particles have a Keplerian speed. At the distance r from the disc, their angular velocity is given by $\Omega = \sqrt{GM_*/r^3}$, where M_* is the stellar mass. If the planet has a position $\mathbf{r} = (x_p, y_p, z_p)$ and a velocity $\mathbf{v} = (\dot{x}_p, \dot{y}_p, \dot{z}_p)$, the relative velocity between the planet and the disc particles at location $r = |\mathbf{r}|$ is $\mathbf{v}_\mathrm{rel} = \dot{x}_p + \Omega y_p, \dot{y}_p - \Omega x_p, \dot{z}_p$, with $v_\mathrm{rel} = |\mathbf{v}_\mathrm{rel}|$.

4.3.1 Aerodynamic drag

The first kind of friction that acts on the planet is caused by direct collisions with the particles of the gaseous medium. This effect, called the aerodynamic drag, is proportional to the surface of the planet. It is also likely to be a function of the relative speed between the planet and the gas particles $\mathbf{v}_\mathrm{rel}$, the fluid density ρ and the viscosity ν. A dimensional analysis, usually referred as the Buckingham π theorem, can be conducted in order to arrange these quantities in order to write down a functional form for the drag force. One finds that the force per unit of mass reads:

$$\mathbf{\Gamma}_\mathrm{aero} = -\frac{1}{2M_\mathrm{p}} C \pi R_p^2 \rho(r, z) v_\mathrm{rel} \mathbf{v}_\mathrm{rel}, \tag{4.12}$$

where C is a dimensionless coefficient related to the Reynolds number, and therefore dependant on the viscosity and geometry of the problem. In our case we will adopt a coefficient of unity.

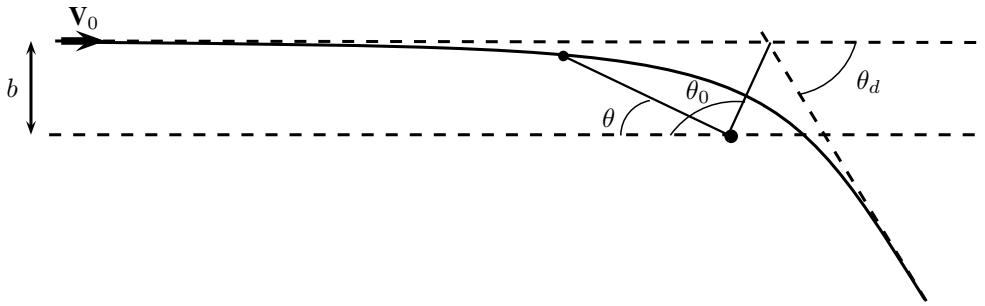

Figure 4.1: Geometry of a close encounter between the planet and a particle, and the subsequent deflection of the trajectory.

4.3.2 Dynamical Friction

We consider the motion of a planet of mass M_p in a gaseous medium consisting of particle of masses $m \ll M_\mathrm{p}$. In order to evaluate the outcome of an encounter between the planet an a single particle, we follow Binney and Tremaine (1987). Then we will integrate to take into account the interaction with the entire medium.

Let $(\mathbf{x}_\mathrm{p}, \mathbf{v}_\mathrm{p})$ and $(\mathbf{x}_\mathrm{m}, \mathbf{v}_\mathrm{m})$ be the positions and velocities of the planet and the particle, respectively. Their relative position is $\mathbf{r} = \mathbf{x}_\mathrm{m} - \mathbf{x}_\mathrm{p}$, and their relative speed is $\mathbf{V} = \dot{\mathbf{r}}$. The relative motion of the reduced system follow the equation of motion (3.1). During the encounter, the velocities are going to change by a value $\Delta\mathbf{v}_\mathrm{p}$ and $\Delta\mathbf{v}_\mathrm{m}$. We note $\Delta\mathbf{V} = \Delta\mathbf{v}_\mathrm{m} - \Delta\mathbf{v}_\mathrm{p}$. The position $\mathbf{R}$ of the center mass of the two bodies is given by $(m + M_\mathrm{p})\mathbf{R} = m\mathbf{x}_\mathrm{m} + M_\mathrm{p}\mathbf{x}_\mathrm{p}$. Because $\ddot{\mathbf{R}} = \mathbf{0}$, it follows that

$$m\Delta\mathbf{v}_\mathrm{m} + M_\mathrm{p}\Delta\mathbf{v}_\mathrm{p} = \mathbf{0}. \tag{4.13}$$

Hence we have

$$m\Delta\mathbf{v}_\mathrm{m} = -\left(\frac{m}{m + M_\mathrm{p}}\right)\Delta\mathbf{V}. \tag{4.14}$$

As represented on figure 4.1, we note $\mathbf{V}_o$ the initial relative velocity and b the impact parameter. In such a reduced system, the angular momentum per unit of mass h is conserved. Evaluated at $t \to -\infty$ (assuming the encounter occurs at $t = 0$), it gives $h = bV_o$. Rewriting eq. (3.2), the hyperbolic trajectory reads:

$$\frac{1}{r} = A\cos(\theta - \theta_0) + \frac{G(M_\mathrm{p} + m)}{b^2 V_0^2}, \tag{4.15}$$

where A and θ_0 are set by initial conditions. It follows that

$$\frac{\mathrm{d}r}{\mathrm{d}t} = Ar^2\dot{\theta}\sin(\theta - \theta_0). \tag{4.16}$$

We assume $\theta(t \to \infty) = 0$ and $\frac{\mathrm{d}r}{\mathrm{d}t}(t \to -\infty) = -V_0$ and we recall that $h = r^2\dot{\theta}$. Thus we

have

$$-V_0 = AbV_0 \sin -\theta_0. \tag{4.17}$$

In addition we assume $r^{-1}(t \to \infty) = 0$, such as

$$A \cos\theta_0 + \frac{G(M_\mathrm{p} + m)}{b^2 V_0^2} = 0. \tag{4.18}$$

Finally we obtain:

$$\tan\theta_0 = \frac{-bV_0^2}{G(M_\mathrm{p} + m)}. \tag{4.19}$$

Because the encounter is symmetrical about the point of closest approach (given by $\theta = \theta_0$, solution of $\dot{r} = 0$), the geometry of the problem gives the relation between θ_0 and the deflection angle θ_d as $2(\pi - \theta_0) + \theta_d = \pi$, which can be written

$$\theta_d = 2\theta_0 - \pi. \tag{4.20}$$

If we write

$$\Delta\mathbf{V} = V_0 \cos\theta_d \hat{\mathbf{e}}_x - V_0 \sin\theta_d \hat{\mathbf{e}}_y - V_0 \hat{\mathbf{e}}_x \tag{4.21}$$

it is natural to define the two components of $\Delta\mathbf{V}$, $\Delta\mathbf{V}_\perp$ and $\Delta\mathbf{V}_\parallel$ as being perpendicular and parallel to the initial $\mathbf{V}_0$. It follows that

$$|\Delta\mathbf{V}_\perp| = |V_0 \sin\theta_d|, \tag{4.22}$$

$$|\Delta\mathbf{V}_\parallel| = |V_0(1 - \cos\theta_d)|. \tag{4.23}$$

Using eq. (4.19), we get:

$$|\Delta\mathbf{V}_\perp| = \frac{2bV_0^3}{G(M_\mathrm{p} + m)} \left(1 + \frac{b^2 V_0^4}{G^2(M_\mathrm{p} + m)^2}\right)^{-1}, \tag{4.24}$$

$$|\Delta\mathbf{V}_\parallel| = 2V_0 \left(1 + \frac{b^2 V_0^4}{G^2(M_\mathrm{p} + m)^2}\right)^{-1}. \tag{4.25}$$

Using eq. (4.14) we can write:

$$|\Delta\mathbf{v}_{\mathrm{p}\perp}| = \frac{2mbV_0^3}{G(M_\mathrm{p} + m)^2} \left(1 + \frac{b^2 V_0^4}{G^2(M_\mathrm{p} + m)^2}\right)^{-1}, \tag{4.26}$$

$$|\Delta\mathbf{v}_{\mathrm{p}\parallel}| = \frac{2mV_0}{M_\mathrm{p} + m} \left(1 + \frac{b^2 V_0^4}{G^2(M_\mathrm{p} + m)^2}\right)^{-1}. \tag{4.27}$$

These equations give the variation of the velocity of the planet after an encounter with a particle of mass m. Although very tiny, this effect will be amplified if M_p is travelling in homogeneous medium consisting in a large number of particles of masses m. By symmetry, the average change of velocity $\langle\Delta\mathbf{v}_{\mathrm{p}\perp}\rangle$ will be zero. On the other hand, the change $\langle\Delta\mathbf{v}_{\mathrm{p}\parallel}\rangle$

does not average out to zero. It forms a density wake trailing behind the planet, which will tend to slow it down. This effect is called dynamical friction.

As it travels at a speed $\mathbf{V}$ relative to the medium, the planet encounters particles in a cylinder of radius $b + \mathrm{d}b$ at a rate $2\pi b\mathrm{d}b \times V \times n(r, z)$. Here n is the number of particles per unit of volume, and we use cylindrical coordinates. The total variation of $\mathbf{v}_\mathrm{p}$ is then:

$$\frac{\mathrm{d}\mathbf{v}_p}{\mathrm{d}t} = -\int_{b_\mathrm{min}}^{b_\mathrm{max}} \mathbf{V} n(r, z) |\Delta \mathbf{v}_{p\|}| 2\pi b \mathrm{d}b \tag{4.28}$$

where the $-$ sign represents the fact that dynamical friction opposes the motion. Carrying the integration gives

$$\frac{\mathrm{d}\mathbf{v}_p}{\mathrm{d}t} = -2\pi \mathbf{V} n(r, z) \frac{G^2 m(m + M_\mathrm{p})}{V^3} \ln \left(\frac{1 + \frac{b_\mathrm{max}^2 V^4}{G^2 (M_\mathrm{p}+m)^2}}{1 + \frac{b_\mathrm{min}^2 V^4}{G^2 (M_\mathrm{p}+m)^2}} \right) \tag{4.29}$$

The minimum impact parameter can be taken as $b_\mathrm{min} = R_p$, the planetary radius. The minimum orbital velocity, V_min is given by $(GM_\mathrm{p}/R_p)^{1/2}$, and represents the minimum velocity necessary to keep a body in orbit. Therefore $b_\mathrm{min} V^2/(GM_\mathrm{p}) = V^2/V_\mathrm{min}^2$ and this quantity is much larger than 1. In a disc of height H, it is natural to choose $b_\mathrm{max} = H$, and we can assume that $H > R_p$. Therefore the two quantities $b_\mathrm{min} V^2/(GM_\mathrm{p})$ and $b_\mathrm{max} V^2/(GM_\mathrm{p})$ are larger than 1, so that the logarithm can be approximated by $2\ln(H/R_p)$.

In addition, if there are N particles of mass m in the medium, then the quantity $n(r, z) \times m$ is the density $\rho(r, z)$. Finally the dynamical friction force per unit of mass takes the form:

$$\mathbf{\Gamma}_\mathrm{dyn} = -4\pi G^2 M_\mathrm{p} \rho(r, z) \ln \left(\frac{H}{R_p} \right) \frac{\mathbf{v}_\mathrm{rel}}{v_\mathrm{rel}^3}, \tag{4.30}$$

where we now use the notation $\mathbf{v}_\mathrm{rel}$ for the relative velocity, and we have use the approximation $m + M_\mathrm{p} \simeq M_\mathrm{p}$.

4.3.3 Comparison of the two forces

The aerodynamic drag and the dynamical friction differ in several ways. For instance Γ_aero is proportional to v_rel^2 whereas Γ_dyn is proportional to v_rel^{-2}. In addition Γ_aero is strongly dependant on the size of the planet, through R_p^2, but scales down with M_p. Therefore we could expect Γ_aero to be more important for planetesimals and small mass planets.

If we assume that the disc particles and the planet are on circular keplerian orbits, their orbital velocity at an orbital distance r will be $\sqrt{GM_*/r}$. If we note I the inclination between the midplane of the disc and the orbital plane of the planet, then we get

$$v_\mathrm{rel}^2 = \frac{2GM_*}{r} \sin^2 I. \tag{4.31}$$

When the orbital inclination is significantly large, we get that the relative speed is of the

order $v_{\rm rel}^2 \simeq GM_*/r$. Thus, the ratio of the two frictional forces can be written as:

$$\frac{\Gamma_{\rm aero}}{\Gamma_{\rm dyn}} = \frac{1}{8\ln\frac{H}{R_p}} \left(\frac{M_*}{M_{\rm p}}\right)^2 \left(\frac{R_p}{r}\right)^2 . \tag{4.32}$$

Here H is the height for the disc at location r. We assume the ratio H/r, called the disc aspect ratio, to be constant. Values of H/r for protoplanetary discs are usually of a few 10^{-2}. On figure 4.2 we show the variation of the ratio given by eq. (4.32) as a function of the orbital distance, for different three different planets, for which we have taken the mass and radius of the Earth, Neptune and Jupiter. We also take $H/r = 0.025$ and $M_* = 1M_\odot$. The aerodynamical drag is only significant for Earth-like planets at orbital separations lower than 2 AU. Here we focus on planets with masses equal to or larger than that of Neptune. Therefore, despite the fact that we include both forces in our model and in our simulations, any quantitative analysis, such as finding the damping timescales associated with friction, can be done taking only the dynamical friction into account.

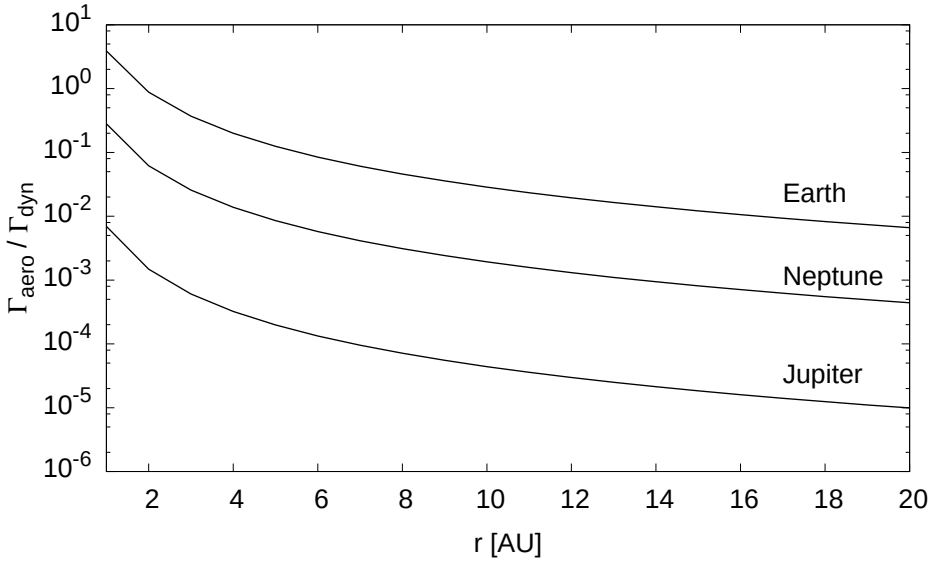

Figure 4.2: Ratio of the aerodynamic drag over the dynamical friction as a function of the orbital distance, for planets with the mass and radius of the Earth, Neptune and Jupiter.

4.4 Publication I - Orbital evolution of a planet on an inclined orbit interacting with a disc

In the previous sections of this chapter we have introduced different forces that can be exerted by a disc on a planet. The forces introduced here are well suited if one wants to study the evolution of a planet whose orbit is significantly inclined with regard to the mid-plane of a protoplanetary disc. First, let us consider the gravitational potential of a disc. We showed that it takes the same form, at least up to the first order, as the Kozai potential in the case of a

three-body problem. It is not surprising if one remembers that the Kozai effect was derived in the secular approximation. The averaging over the orbital periods reduces the problem to that of two rings of mass exchanging angular momentum. A protoplanetary disc can be seen, approximatively, as a continuum of such rings of mass. Specifically, in both cases, the potential is considered to be axisymmetric. Therefore we expect the disc to raise Kozai cycles on the planet, which will excite its eccentricity and inclination. However, depending on the location of the inner radius of the disc compared to the orbital parameters of the planet, it is possible that, when crossing the plane of the disc, the planet encounters some gas, and thus suffers friction, as previously described. Friction is expected to damp the eccentricity and inclination of the planet. These parameters are expected to be excited by the Kozai mechanism, and the following publication aims at studying the combined effects of these two processes and what constraints does it give on a possible primordial misalignment between a planet and the disc.

Note that in our approach, the disc is modelled only by its gravitational potential and frictional forces. We make the underlying assumption that it preserves the same structure during the simulations. The first thing that could perturb the disc's structure is the planet itself, that could potentially generate a warp, or carve a gap at the location where it crosses the disc. In the appendix of the following paper, we study the response of the disc to a linear perturbation from the planet. We show that the torque exerted by the planet rapidly vanishes away from it. Therefore the deformation is just local and does not affect the global structure of the disc. Different authors (Xiang-Gruess and Papaloizou, 2013; Bitsch et al., 2013) have also shown that only massive planets (several Jupiter mass) can open a partial gap in a disc when they are inclined with respect to the latter. Thus we neglect the perturbations raised by the disc on the planet. The second effect that could modify the structure of the disc is its own evolution. Mass loss of the disc usually comes in two ways: photoevaporation of the outer parts, and accretion of the inner parts onto the star. However, neglecting these effects should not massively change the results presented below: if planets realign on a timescale much shorter than the disc's lifetime, then accretion and photoevaporation do not have time to significantly affect the structure of the disc. If planets realign on a timescale much longer than the disc's lifetime, then the disc's mass loss will only enhance this process. The only situation where it could become significant is if the planet realigns on a timescale comparable to the disc's lifetime. However, as we will see, it is not the case for the planets we study here.

Monthly Notices
of the
ROYAL ASTRONOMICAL SOCIETY

MNRAS **428,** 658–669 (2013) doi:10.1093/mnras/sts064

Orbital evolution of a planet on an inclined orbit interacting with a disc

Jean Teyssandier,[1]⋆ Caroline Terquem[1]⋆ and John C. B. Papaloizou[2]⋆

[1]*Institut d'Astrophysique de Paris, UMR 7095, CNRS, UPMC Univ Paris 06, 98 bis bd Arago, F-75014 Paris, France*
[2]*Department of Applied Mathematics and Theoretical Physics, Centre for Mathematical Sciences, University of Cambridge, Wilberforce Road, Cambridge CB3 0WA*

Accepted 2012 September 21. Received 2012 September 14; in original form 2012 July 25

ABSTRACT

We study the dynamics of a planet on an orbit inclined with respect to a disc. If the initial inclination of the orbit is larger than some critical value, the gravitational force exerted by the disc on the planet leads to a Kozai cycle in which the eccentricity of the orbit is pumped up to large values and oscillates with time in antiphase with the inclination. On the other hand, both the inclination and the eccentricity are damped by the frictional force that the planet is subject to when it crosses the disc. We show that, by maintaining either the inclination or the eccentricity at large values, the Kozai effect provides a way of delaying alignment with the disc and circularization of the orbit. We find the critical value to be characteristically as small as about 20°. Typically, Neptune or lower mass planets would remain on inclined and eccentric orbits over the disc lifetime, whereas orbits of Jupiter or higher mass planets would align and circularize. This could play a significant role in planet formation scenarios.

Key words: celestial mechanics – planets and satellites: general – planetary systems – planets and satellites: formation – planet-disc interactions.

1 INTRODUCTION

At the time of writing, more than 800 extrasolar planets have been detected around main-sequence stars. Most of these objects have been observed through radial velocity measurements, and about one-third of them have also been detected through transit measurements. In addition, the Kepler mission has so far released about 2300 planet candidates (Borucki et al. 2011; Batalha et al. 2012). Only a few of these objects have been confirmed by radial velocity measurements so far, but the number of false positives is expected to be very small. The rate at which extrasolar planets are being discovered is accordingly increasing very sharply.

The angle between the sky projections of the stellar spin axis and the orbit normal (that we will call hereafter the *projected inclination angle*) has been measured using the Rossiter–McLaughlin effect for 53 planets (Albrecht et al. 2012, and references therein). About one-third display significant misalignment with retrograde orbits being indicated in some cases. Misalignment, therefore, is common, at least for short-period systems for which measurements have been made. Note however that the planets in this sample are rather massive. The lightest one has a mass of about 25 $M_\oplus$, whereas the other planets in the sample have masses ranging from a few tenths of a Jupiter mass to several Jupiter masses. By performing duration ratio statistics on the Kepler planetary candidates, Fabrycky et al. (2012) have concluded that pairs of planets in their sample are aligned to within a few degrees. As the Kepler catalogue contains a majority of super-Earth and Neptune-like planets, it is possible that misalignment is less common for lower mass planets.

According to the commonly accepted core accretion scenario, in which planets form in a disc through the accretion of solid material into a core followed, in the case of giant planets, by the capture of a gaseous atmosphere, the orbit of planets should lie in the disc, and therefore in the equatorial plane of the star. In this model, migration due to tidal interaction between disc and planets can be invoked to explain the presence of giant planets on very short orbits. However, such an interaction would not account for the occurrence of any inclination of the orbit. Therefore, this scenario is not likely to apply to the hot Jupiters that are observed to be on inclined orbits. Planet formation through fragmentation of the disc might be considered, but in that case the orbits are also expected to lie in the plane of the disc.

One scenario that has been proposed for misaligning the orbits of hot Jupiters that have formed in a disc lying in the stellar equatorial plane relies on gravitational interaction with a distant stellar or planetary companion that takes place after the disc has dissipated. When the two orbits are not coplanar, the secular perturbation exerted by the companion produces a Kozai cycle in which the eccentricity and the inclination of the inner planet's orbit vary in antiphase. If the pericentre distance gets small enough, the orbit may become circularized because of the tidal interaction with the central star, and the orbit shrinks while, in some circumstances, keeping a high inclination (Fabrycky & Tremaine 2007; Wu, Murray & Ramsahai

⋆ E-mail: teyssand@iap.fr (JT); caroline.terquem@iap.fr (CT); J.C.B.Papaloizou@damtp.cam.ac.uk (JCBP)

2007; Naoz et al. 2011). In this model, a distant companion is needed which, however, may not always be present in reality. Other models rely on planet–planet scattering (Chatterjee et al. 2008) or secular chaos (Wu & Lithwick 2011).

It has been proposed that the disc itself may be misaligned with respect to the stellar equatorial plane. This could happen if the disc, at later times, were accreting material with angular momentum misaligned with that of the star, as considered by Bate, Lodato & Pringle (2010). If at that stage there was enough mass in the disc to form planets, their orbits would naturally be inclined with respect to the stellar equatorial plane. A similar scenario was studied by Thies et al. (2011), who pointed out that close encounters of a disc accreting from an extended envelope with another star could result in the disc plane becoming tilted, possibly even to a retrograde orientation with respect to its original one. Planetary orbits inclined with respect to the stellar equatorial plane would also result if the stellar spin axis were tilted due to interaction with the disc (Foucart & Lai 2011; Lai, Foucart & Lin 2011). Note however that by comparing stellar rotation axis inclination angles with the geometrically measured disc inclinations for a sample of eight debris discs, Watson et al. (2011) have seen no evidence of a misalignment between the two.

Another possibility would be that the misaligned planets have formed out of the disc through a fragmentation process occurring in the protostellar envelope while it collapses on to the protostar, as envisioned by Papaloizou & Terquem (2001) and Terquem & Papaloizou (2002). In this scenario, a population of planetary objects form rapidly enough that their orbits can undergo dynamical relaxation on a time-scale of the order of a few 10^4 yr. During the relaxation process, most of the objects are ejected, while one to a few planets become more bound to the central star. Formation of hot Jupiters through tidal circularization by the central star of a highly eccentric orbit may occur (Papaloizou & Terquem 2001). The orbits of the planets that are left in the system at the end of the relaxation process display a range of eccentricities and inclinations (Adams & Laughlin 2003). In this context, the misaligned planets interact with the disc that has formed around the star during the protostellar envelope collapse. It is the subsequent dynamics of a system of this type, consisting of a gaseous disc together with a planet with an orbital plane misaligned with its mid-plane, that we propose to investigate here. Note that we do not expect low-mass planets to form according to the scenario of Papaloizou & Terquem (2001). On the other hand, in the scenario proposed by Bate et al. (2010), it may happen that subsequent discs with different inclinations form and dissipate, so that planets formed early in a disc may interact at later time with a disc with different orientation.

In this paper, we focus on a system with only one planet. Multiple systems will be studied in future publications. Some preliminary work on the interaction of a planet on an inclined orbit with a disc has been carried out by Terquem & Ajmia (2010). It was found that the gravitational force exerted by the disc on to the planet leads to a Kozai cycle in which the eccentricity and the inclination of the orbit vary periodically with large amplitudes. This indicates that a planet's orbit which is inclined to start with may achieve high eccentricity. In their calculations, Terquem & Ajmia (2010) adopted a two-dimensional flat disc model and ignored the frictional force felt by the planet as it passes through the disc. In this paper, we extend this work by modelling the disc in three dimensions and including the frictional force. Our goal is to understand under what circumstances inclined orbits can be maintained when the disc is present. We consider planets with masses ranging from Neptune mass to several Jupiter masses. The plan of the paper is as follows.

In Section 2.1, we describe the three-dimensional disc model used in the numerical simulations and the calculation of the gravitational force exerted by the disc on a planet in an inclined orbit. A computationally convenient formulation, in terms of elliptic integrals, is presented in Appendix B. We go on to give a brief review of the Kozai mechanism in Section 2.2. In Section 2.3, we give an expression for the frictional force exerted by the disc on the planet and derive a damping time-scale based on a simplified analysis in Section 2.4. In Section 3, we present the results of numerical simulations of the interaction between a planet on an inclined orbit and a disc. We first perform simulations without the frictional force in Section 3.1 and compare the results to those of Terquem & Ajmia (2010) that were obtained for a two-dimensional flat disc model. In Section 3.2, we include friction. We show that when the planet's orbit starts with a low inclination (less than about 23°) with respect to the disc, it becomes aligned with the disc plane and circularized by the frictional force. However, when the inclination is initially high enough, the Kozai effect is present. This pumps up the eccentricity of the planet's orbit maintaining either the inclination or the eccentricity at large values. As a consequence, alignment of the orbital and disc planes, as well as circularization of the orbit resulting from the frictional force, is delayed. In some cases, the orbit stays misaligned over the disc lifetime. More massive planets and planets further away from the star align faster. In addition, more massive discs favour alignment. In Section 4, we discuss our results in the light of the observations that have been reported so far.

2 INTERACTION BETWEEN A PLANET ON AN INCLINED ORBIT AND A DISC

2.1 Gravitational potential and disc model

We consider a planet of mass M_p orbiting around a star of mass $M_\star$ which is itself surrounded by a disc of mass M_d. The disc's mid-plane is in the equatorial plane of the star, whereas the orbit of the planet is inclined with respect to this plane. We denote by I the angle between the orbital plane and the disc's plane. We suppose that the angular momentum of the disc is large compared to that of the planet's orbit so that the effect of the planet on the disc is negligible: the disc does not precess and its orientation is invariable (see Appendix A). We denote by (x, y, z) the Cartesian coordinate system centred on the star and by (r, φ, z) the associated cylindrical coordinates. The (axisymmetric) disc is in the (x, y) plane, its inner radius is R_i, its outer radius is R_o and its thickness (defining the region within which the mass is confined) at radius r is $2H(r)$.

The gravitational potential exerted by the disc at the location (r, z) of the planet is

$$\Phi(r,z) = -G\int_{R_\mathrm{i}}^{R_\mathrm{o}}\int_{-H}^{H}\int_{0}^{2\pi}\frac{\rho(r',z')\,r'\mathrm{d}r'\mathrm{d}z'\mathrm{d}\phi'}{\sqrt{r^2+r'^2-2rr'\cos\phi'+(z-z')^2}}, \tag{1}$$

where G is the gravitational constant and ρ is the mass density in the disc.

We assume that ρ falls off exponentially with z^2 near the mid-plane with a cutoff at $|z| = H(r)$, while decreasing as a power of r. Thus, we adopt

$$\rho(r,z) = \left[\mathrm{e}^{\frac{1}{2}(1-z^2/H(r)^2)}-1\right]\left(\frac{r}{R_\mathrm{o}}\right)^{-n}\frac{\rho_0}{\mathrm{e}^{1/2}-1}, \tag{2}$$

where ρ_0 is a constant. We have $\rho = 0$ at the surface of the disc, i.e. when $|z| = H$ and $\rho(r, 0) = \rho_0(r/R_\mathrm{o})^{-n}$ in the mid-plane. This z

dependence of ρ has been chosen for simplicity, but we note that the details of how ρ varies with z do not matter. What is important is the local disc surface density at the location the planet passes through. This largely determines the change in orbital energy resulting from the dynamical drag force (as is apparent from equation 11 of Section 2.3).

The mass density given above is discontinuous at $r = R_\mathrm{i}$ and R_o, as ρ is zero outside the disc. We have found that this could introduce some numerical artefacts in the calculation of the disc's gravitational force, so that in some runs we have replaced ρ by $\rho \times f(r)$ with

$$f(r) = \left[1 - \left(\frac{R_\mathrm{i}}{r}\right)^{10}\right]\left[1 - \left(\frac{r}{R_\mathrm{o}}\right)^{20}\right]. \tag{3}$$

The exponents 10 and 20 ensure that the edges are rather sharp, so that we get quantitatively the same orbital evolution whether the factor f is used or not.

In the calculations presented below, we choose a value of the disc mass M_d and calculate ρ_0 using $M_\mathrm{d} = \int\int\int_\mathrm{disc} \rho \mathrm{d}V$. For the disc's semithickness, we choose a constant aspect ratio,

$$H(r) = H_0 r, \tag{4}$$

where H_0 is a constant. The gravitational force per unit mass exerted by the disc on to the planet is $-\nabla\Phi$. In Appendix B, we give convenient expressions for $-\nabla\Phi$ in terms of elliptic integrals which can be readily computed.

2.2 The Kozai mechanism

The Kozai effect (Kozai 1962; Lidov 1962) arises when an inner body on an inclined orbit is perturbed by a distant companion. First derived by Kozai to study the motion of inclined asteroids around the Sun under perturbations from Jupiter, it has since found many applications in astrophysics. We are interested here in the cases where the inner body is a planet of mass M_p. We denote by a its semimajor axis, M' the mass of the outer companion, assumed to be on a circular orbit, and a' its semimajor axis. We consider the case $a' \gg a$. The secular perturbation from the outer companion causes the eccentricity e of the inner planet and the mutual inclination I of the two orbits to oscillate in time in antiphase provided that the initial inclination angle I_0 is larger than the critical angle I_c given by

$$\cos^2 I_\mathrm{c} = \frac{3}{5}. \tag{5}$$

The maximum value reached by the eccentricity is then given by

$$e_\mathrm{max} = \left(1 - \frac{5}{3}\cos^2 I_0\right)^{1/2}, \tag{6}$$

and the time t_evol it takes to reach e_max starting from e_0 is (Innanen et al. 1997)

$$\frac{t_\mathrm{evol}}{\tau} = 0.42\left(\sin^2 I_0 - \frac{2}{5}\right)^{-1/2} \ln\left(\frac{e_\mathrm{max}}{e_0}\right), \tag{7}$$

with the time τ defined by

$$\tau = \left(\frac{a'}{a}\right)^3 \left(\frac{M_\star}{M'}\right) \frac{T}{2\pi}, \tag{8}$$

where T is the orbital period of the inner planet. If the eccentricity oscillates between e_min and e_max, then the period of the oscillations P_osc is given by $P_\mathrm{osc} = 2t_\mathrm{evol}$ with $e_0 = e_\mathrm{min}$ in equation (7).

Since the two orbits are well separated, the component of the angular momentum of the inner orbit perpendicular to the orbital plane is constant. As it is proportional to $\sqrt{1-e^2}\cos I$, the oscillations of I and e are in antiphase. Hereafter, we will refer to this mechanism as the *classical Kozai effect*.

Terquem & Ajmia (2010) found that the Kozai effect extends to the case where the inner orbit is perturbed by the gravitational potential of a disc, even when the orbit of the planet crosses the disc, provided most of the disc mass is beyond the planet's orbit. In that case, I is the angle between the orbital plane and the disc's plane. They also showed that, in agreement with equations (7) and (8), the period of the oscillations decreased with a. It was also found to decrease with increasing disc mass. When the semimajor axis of the planet is small compared to the disc's inner radius, the evolution time-scale is of the same form as that given by equation (7) but with

$$\tau \propto \left(\frac{R_\mathrm{o}}{a}\right)^3 \left(\frac{M_\star}{M_\mathrm{d}}\right) \frac{T}{2\pi}, \tag{9}$$

where the coefficient of proportionality depends on the functional form of ρ and on the ratio $R_\mathrm{i}/R_\mathrm{o}$.

2.3 Friction

When the planet crosses the disc, as it has a relative velocity with respect to the particles in the disc, it suffers a frictional force. There are two types of drag acting on the planet: (i) an aerodynamic drag, due to the fact that the planet has a finite size and suffers direct collisions with the particles in the disc, and (ii) a dynamical drag, due to the fact that particles in the disc are gravitationally scattered by the planet.

Adopting a drag coefficient of unity, the aerodynamic drag force per unit mass exerted on the planet located at (r, φ, z), or equivalently (x, y, z), can be written as

$$\boldsymbol{\Gamma}_\mathrm{aero} = -\frac{1}{2M_\mathrm{p}} \pi R_\mathrm{p}^2 \rho(r, z) v_\mathrm{rel} \boldsymbol{v}_\mathrm{rel}, \tag{10}$$

where R_p is the planet's radius and $\boldsymbol{v}_\mathrm{rel}$ is the relative velocity of the planet with respect to the particles in the disc at the location (x, y, z). If we denote by $\boldsymbol{v} = (v_x, v_y, v_z)$ the velocity of the planet, then $\boldsymbol{v}_\mathrm{rel} = (v_x + y\Omega, v_y - x\Omega, v_z)$, where $\Omega = \sqrt{GM_\star/r^3}$.

The dynamical drag is the gravitational force exerted by the particles in the disc on the planet that is associated with the scattering and change of location that occurs as a result of the passage of the planet. The main contribution to this force comes from the particles located in the vicinity of the planet at the time it crosses the disc. Note that the gravitational force from these particles has already been included in $-\nabla\Phi$ (see Section 2.1), but as we have ignored the motion of the particles in the disc relative to the planet when calculating this force, it is conservative and does not capture the change of energy of the planet's orbital motion. The problem is similar to dynamical friction in a collisionless medium (e.g. Binney & Tremaine 1987).

When the inclination angle of the planet's orbit with respect to the disc is not very small, $v_\mathrm{rel} \sim \sqrt{GM_\star/a}$, with a being the semimajor axis of the planet's orbit, is supersonic. In this case, the dynamical friction force per unit mass acting on the planet can be written as (Ruderman & Spiegel 1971; Rephaeli & Salpeter 1980; Ostriker 1999)

$$\boldsymbol{\Gamma}_\mathrm{dyn} = -4\pi G^2 M_\mathrm{p} \rho(r, z) \left|\ln\frac{H(r)}{R_\mathrm{p}}\right| \frac{\boldsymbol{v}_\mathrm{rel}}{v_\mathrm{rel}^3}. \tag{11}$$

The ratio of the two frictional forces is thus

$$\frac{\Gamma_{\rm aero}}{\Gamma_{\rm dyn}} \sim \frac{1}{8\left|\ln\frac{H(r)}{R_{\rm p}}\right|}\left(\frac{R_{\rm p}}{a}\right)^2\left(\frac{M_\star}{M_{\rm p}}\right)^2, \tag{12}$$

where we have replaced $v_{\rm rel}^2$ by $GM_\star/a$. In this paper, we will focus on planets with masses at least that of Neptune, for which the previous expression gives $\Gamma_{\rm aero}/\Gamma_{\rm dyn} \ll 1$ for the orbital parameters we consider. Therefore, friction is dominated by the dynamical term even though a large value of unity was adopted for the drag coefficient.

2.4 Evolution time-scale

The velocity v of the planet is, in first approximation, the Keplerian velocity around the star, i.e. $v \simeq \sqrt{GM_\star/a}$. To simplify matters, we approximate the relative velocity by its vertical component so that $v_{\rm rel} \sim v_z \simeq v \sin I \simeq \sqrt{GM_\star/a}\sin I$.

When the planet's orbit has a significant eccentricity, the relative velocity is in general larger as the planet crosses the disc closer to pericentre than apocentre and its horizontal components (in the disc's plane) are then important. We define a damping time-scale for the planet in the absence of forces other than friction as

$$\tau_{\rm damp} = \left(\frac{1}{v}\frac{{\rm d}v}{{\rm d}t}\right)^{-1} = \frac{v}{\Gamma_{\rm dyn}}. \tag{13}$$

This is the characteristic time-scale in which the frictional force $\mathbf{\Gamma}_{\rm dyn}$ damps the velocity of the planet. Note that $\tau_{\rm damp} = 2a({\rm d}a/{\rm d}t)^{-1}$. With the above approximation for $v_{\rm rel}$ and $|\ln(H/R_{\rm p})| \simeq 6$, which corresponds to giant planets at around 10 au in a disc with $H(r) = 2.5\times10^{-2}r$, as we consider below in the numerical calculations, we get

$$\tau_{\rm damp} \sim \frac{M_\star^2\sin^2 I}{24\pi M_{\rm p}a^3\rho(r,z)}\frac{T}{2\pi}, \tag{14}$$

where T is the orbital period of the planet.

To proceed further, for the purpose of getting a convenient analytical estimate of $\tau_{\rm damp}$, we approximate the vertical dependence of the mass density by a δ function in z and set $\rho(r,z) = 2\delta(z)H(r)\rho_0(r/R_{\rm o})^{-n}$. Then, we get $\Sigma(r) = \int_{-H}^{H}\rho(r,z)\,{\rm d}z = 2\rho_0(r/R_{\rm o})^{-n}H(r)$. Using equation (4), we can then calculate the disc mass to be $M_{\rm d} = \int_{R_{\rm i}}^{R_{\rm o}}\Sigma(r)2\pi r{\rm d}r \simeq 8\pi\rho_0 H_0 R_{\rm o}^3/3$, where we have used $n = 3/2$, as in the numerical simulations below. This allows us to express ρ_0 in term of $M_{\rm d}$, such that $\rho_0 \simeq 3M_{\rm d}/(8\pi H_0 R_{\rm o}^3)$. In accordance with equation (2), we identify the mid-plane mass density as $\rho(r,0) = \rho_0(r/R_{\rm o})^{-n} \simeq 3M_{\rm d}(r/R_{\rm o})^{-n}/(8\pi H_0 R_{\rm o}^3)$.

We now suppose that the planet's orbit is not too eccentric so that ρ can be evaluated at $r = a$ in the expression of $\tau_{\rm damp}$. Finally, equation (14) gives

$$\tau_{\rm damp} \sim \frac{M_\star^2}{9M_{\rm p}M_{\rm d}}\left(\frac{R_{\rm o}}{a}\right)^{3/2}H_0\sin^2 I\frac{T}{2\pi}. \tag{15}$$

This expression may not give the correct quantitative value of the damping time-scale, because of the approximations that have been used in deriving it, but it gives the scaling of $\tau_{\rm damp}$ with the different parameters. Also, although the dependence on the eccentricity has not been taken into account in this expression, as pointed out above, we expect the damping time-scale to be larger when the eccentricity is larger.

3 NUMERICAL SIMULATIONS

To study the evolution of the system (star, planet, disc), we use the *N*-body code described in Papaloizou & Terquem (2001) in which we have added the gravitational and frictional forces exerted by the disc on the planet.

The equation of motion for the planet is

$$\frac{{\rm d}^2\boldsymbol{r}}{{\rm d}t^2} = -\frac{GM_\star\boldsymbol{r}}{|\boldsymbol{r}|^3} - \nabla\Phi + \mathbf{\Gamma}_{\rm aero} + \mathbf{\Gamma}_{\rm dyn} + \mathbf{\Gamma}_{t,r} - \frac{GM_{\rm p}\boldsymbol{r}}{|\boldsymbol{r}|^3}. \tag{16}$$

The last term on the right-hand side is the acceleration of the coordinate system based on the central star. It arises because the centre of mass of the system does not coincide with that of the star. This term takes into account only the force exerted by the planet on to the star and neglects the net force of the disc on the central star, which would of course require a calculation of the disc response to the planet's perturbation. Tides raised by the star in the planet and relativistic effects are included through $\mathbf{\Gamma}_{t,r}$, but they are unimportant here as the planet does not approach the star closely. Equation (16) is integrated using the Bulirsch–Stoer method. The integrals over ϕ involved in $\nabla\Phi$ are calculated using elliptic integrals (see Appendix B). The integrals over r and z are calculated with the Romberg method (Press et al. 1993).

The planet is set on a circular orbit at the distance $r_{\rm p}$ from the star. When the planet does not pass through the disc, e.g. when there is no friction, the orbital energy is conserved and $r_{\rm p}$ is equal to the planet's semimajor axis a throughout the evolution of the system. The initial inclination angle of the orbit with respect to the disc is I_0. In the simulations reported here, we have taken $M_\star = 1\,{\rm M}_\odot$, a radial power law with exponent $n = 3/2$ for the disc mass density ρ (see equation 2), a disc aspect ratio $H_0 = 2.5\times10^{-2}$ and a disc outer radius $R_{\rm o} = 100$ au.

We will consider a planet with either (i) $M_{\rm p} = 10^{-3}\,{\rm M}_\odot \equiv 1\,M_{\rm J}$ and $R_{\rm p} = 7\times10^9$ cm (Jupiter), (ii) $M_{\rm p} = 5\times10^{-5}\,{\rm M}_\odot \equiv 1\,M_{\rm N}$ and $R_{\rm p} = 2.5\times10^9$ cm (Neptune) or (iii) $M_{\rm p} = 10^{-2}\,{\rm M}_\odot = 10\,M_{\rm J}$ and $R_{\rm p} = 8.4\times10^9$ cm, i.e. 1.2 times Jupiter's radius. These latter values approximately correspond to the mass and radius of the planet XO–3 b, which has been detected both in transit and using radial velocity measurements (Johns-Krull et al. 2008; Winn et al. 2008).

3.1 Gravitation only

To get a benchmark, we first consider the evolution of the planet's orbit in the case where friction is ignored (i.e. $\Gamma_{\rm aero}$ and $\Gamma_{\rm dyn}$ are set to zero in equation 16). This applies when the planet's distance to the star is at all times smaller than the disc inner radius (e.g. planet orbiting in a cavity). These calculations are similar to those performed by Terquem & Ajmia (2010), and a comparison is made below.

Fig. 1 shows the time evolution of the eccentricity e and inclination I for $M_{\rm p} = 1\ M_{\rm J}$, $r_{\rm p} = 5$ au, $M_{\rm d} = 10^{-2}\,{\rm M}_\odot$, $R_{\rm i} = 10$ au and $I_0 = 50^\circ$.

The inclination angle varies between $I_{\rm min} = I_{\rm c}$ and $I_{\rm max}$, where $I_{\rm c}$ is the critical value of I_0 below which eccentricity growth is not observed. The fact that $I_{\rm min} = I_{\rm c}$ is illustrated in Fig. 2, which shows the time evolution of the inclination I for $M_{\rm p} = 1\ M_{\rm J}$, $r_{\rm p} = 7$ au, $M_{\rm d} = 10^{-2}\,{\rm M}_\odot$, $R_{\rm i} = 1$ au and I_0 varying between 23° and 50°. For these parameters, oscillations of the eccentricity and inclination disappear once I_0 becomes smaller than 23°, which means that $I_{\rm c} = 23^\circ$. For values of I_0 well above $I_{\rm c}$, the inclination is seen to oscillate between $I_{\rm min} = I_{\rm c}$ and $I_{\rm max}$. When I_0 decreases, however,

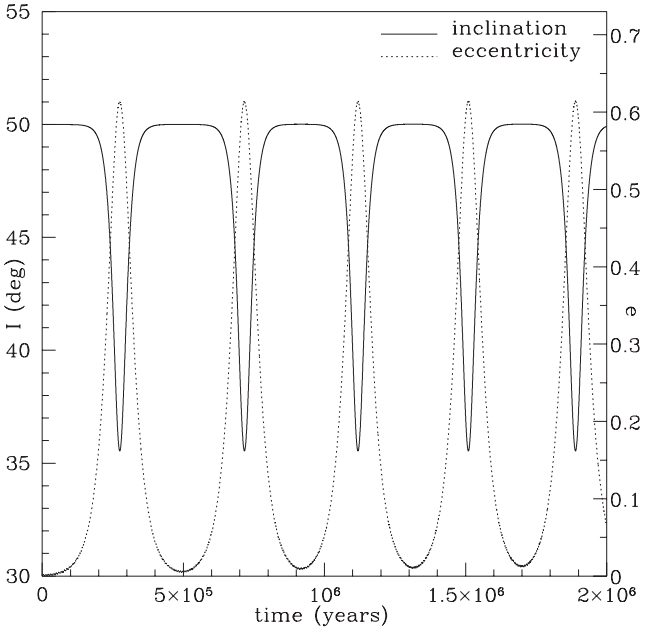

Figure 1. Eccentricity e (dotted line) and inclination angle I (in degrees, solid line) versus time (in yr) in the absence of friction for $M_p = 1\ M_J$, $r_p = 5$ au, $M_d = 10^{-2}\,M_\odot$, $R_i = 10$ au and $I_0 = 50^\circ$.

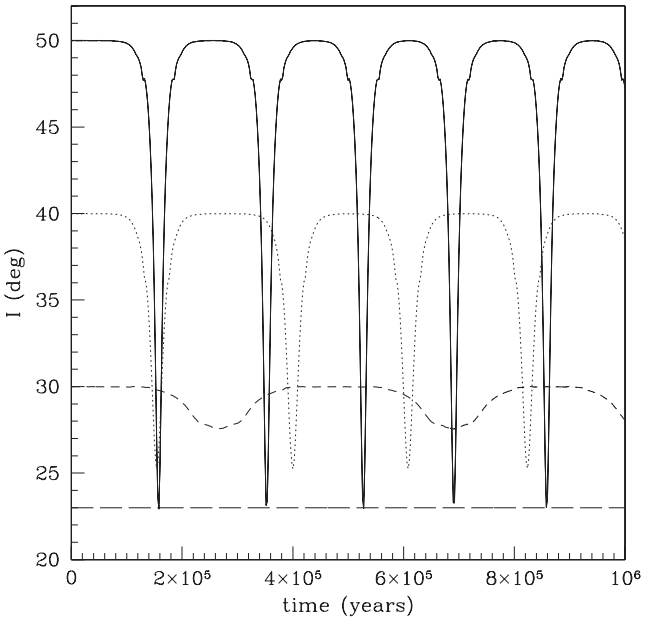

Figure 2. Inclination I (in degrees) versus time (in yr) in the absence of friction for $M_p = 1\ M_J$, $r_p = 7$ au, $M_d = 10^{-2}\,M_\odot$, $R_i = 1$ au and $I_0 = 50^\circ$ (solid line), 40° (dotted line), 30° (short dashed line) and 23° (long dashed line). For these parameters, $I_c = 23^\circ$. No oscillations are present for $I_0 < I_c$.

the amplitudes of the oscillations are such that I_{min} gets a bit larger than I_c.

As already noted by Terquem & Ajmia (2010), since I_c depends on the gravitational force exerted on to the planet, it varies with the initial position of the planet r_p. When $r_p \ll R_i$, the conditions are similar to the classical Kozai effect and the gravitational force from the disc can be approximated by a quadrupole term. In this case, it can be shown that $I_c = 39^\circ$ (equation 5). When r_p is larger

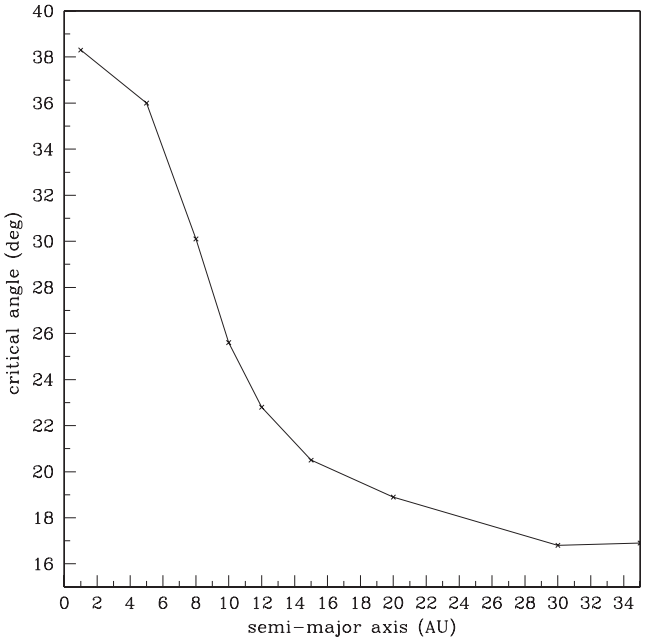

Figure 3. I_c (in degrees) versus r_p (in au) in the absence of friction for $M_p = 1\ M_J$, $M_d = 10^{-2}\,M_\odot$, $R_i = 10$ au and r_p varying between 1 and 35 au. For $r_p \ll R_i$ au, we recover the classical Kozai value $I_c = 39^\circ$.

though, the quadrupole approximation is not valid anymore and I_c gets smaller. This is illustrated in Fig. 3, which shows the critical angle I_c as a function of r_p, which here is the same as the planet's semimajor axis since the orbit is initially circular and there is no energy dissipation. These calculations are done for $M_p = 1\ M_J$, $M_d = 10^{-2}\,M_\odot$, $R_i = 10$ au and r_p varying between 1 and 35 au. For these parameters, the Kozai effect disappears when r_p becomes larger than $\sim$40 au, as most of the mass is then no longer outside the orbit of the planet (Terquem & Ajmia 2010).

For comparison, we have also run the case displayed in Fig. 1 by modelling the disc in two dimensions only, as in Terquem & Ajmia (2010). The gravitational potential is then calculated as arising from a distribution of mass with surface density $\Sigma_{2D}(r) \propto r^{-p}$. We take $p = 1/2$ as in the three-dimensional calculations we have $\Sigma(r) \sim \rho(r)H(r) \propto r^{-1/2}$. There is very good agreement between the two sets of calculations. The extrema of I and e and the period of the oscillations are roughly the same.

In the three-dimensional case, we have also checked that the vertical structure of the disc does not affect the oscillations. Indeed, when the disc mass is kept constant but H_0 is varied in equation (4), the oscillations are unchanged.

3.2 The effect of friction

We are now going to study the effect of friction on the evolution of the planet's orbit by taking into account Γ_{aero} and Γ_{dyn} in equation (16).

Fig. 4 shows the time evolution of the orbital parameters I, e, semimajor axis a and distance to pericentre $a(1-e)$ for $M_p = 1\ M_N$, $r_p = 7$ au, $M_d = 10^{-2}\,M_\odot$, $R_i = 1$ au and for two different values of I_0. For these parameters, $I_c = 23^\circ$ (the critical angle does not depend on the mass of the planet and therefore is the same as in Fig. 2). As discussed in Section 2.4, the damping time-scale increases with I and e. Therefore, when $I_0 > I_c$, as at all times one of these parameters has a large value because of the Kozai cycle,

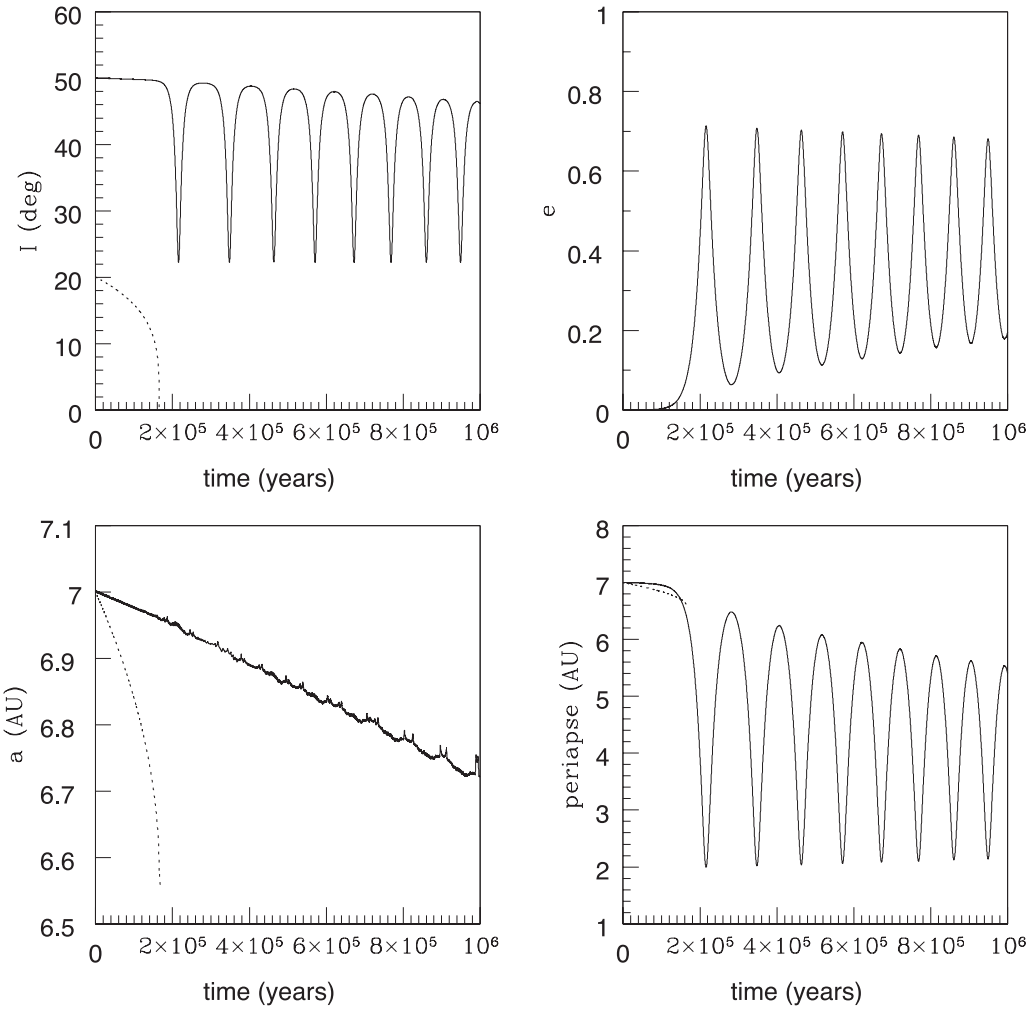

Figure 4. Inclination I (in degrees, upper-left plot), eccentricity e (upper-right plot), semimajor axis a (in au, lower-left plot) and pericentre distance $a(1-e)$ (in au, lower-right plot) versus time (in yr) for $M_{\rm p} = 1\ M_{\rm N}$, $r_{\rm p} = 7$ au, $M_{\rm d} = 10^{-2}\,{\rm M}_{\odot}$, $R_{\rm i} = 1$ au and $I_0 = 50^\circ$ (solid line) and 20° (dotted line). For these parameters, $I_{\rm c} = 23^\circ$. When $I_0 = 20^\circ$, $e = 0$ throughout the evolution so the curve does not show on the plot. The Kozai effect provides a way of pumping up e and maintaining either e or I at large values, and therefore delays circularization and alignment with the disc of the orbit.

the damping time-scale is longer than in the case $I_0 < I_{\rm c}$ and $e = 0$. This is illustrated in Fig. 4, where we see that a decreases much more rapidly when $I_0 = 20^\circ$ than when $I_0 = 50^\circ$. In the case where there is no Kozai cycle, the orbit stays circular and I is damped faster as it becomes smaller, so that the orbit aligns with the disc on a very short time-scale. When $I_0 > I_{\rm c}$, Kozai oscillations are present as expected, but the oscillations are damped because of friction. We observe that damping is much less efficient than in the $I_0 = 20^\circ$ case, even though the inclination I does reach values that are not much larger than 20° and for which the damping time-scale would be similar if the orbit were circular. When the Kozai cycle is present though, the eccentricity of the orbit is large when I is minimum, which results in the damping time-scale being maintained at large values. Contrary to what happens when $I_0 < I_{\rm c}$ then, the damping time-scale stays roughly constant. This is illustrated in the plot of Fig. 4 that shows a versus time. Ultimately, if the disc were present long enough, the orbit of the planet would align with the disc and would be circularized (I and e vanish). For a Neptune mass planet and the parameters used here though, we find that misalignment can be maintained over the disc lifetime, which is of a few million years. A Jupiter mass planet would align faster, as discussed below.

These calculations show that, by pumping up the eccentricity of the planet's orbit and maintaining either I or e at large values, the Kozai effect provides a way of delaying alignment with the disc and circularization of the orbit.

We see in Fig. 4 that the period of the oscillations decreases with time. If there were no dissipation, this period would stay constant. In the classical Kozai cycle, when the orbit of the inner planet has a semimajor axis a, the time it takes to reach $e_{\rm max}$ starting from $e_{\rm min}$ is proportional to $a^{-3/2}\ln(e_{\rm max}/e_{\rm min})$ (see equations 7 and 8). Although this formula has been derived for a quadrupolar gravitational potential, it may be expected to give a general trend in the disc case as well. Friction reduces a, which tends to increase this time-scale. But the amplitude of the cycle also decreases ($e_{\rm min}$ increases and $e_{\rm max}$ decreases), so that the net effect is a shorter time-scale.

As pointed out in Section 2.3, the expression for dynamical friction given by equation (11) is valid only when the relative velocity of the planet with respect to the particles in the disc is supersonic. This is not the case when I is close to zero and, therefore, the part of the curves in Fig. 4 corresponding to I close to zero can be interpreted only qualitatively.

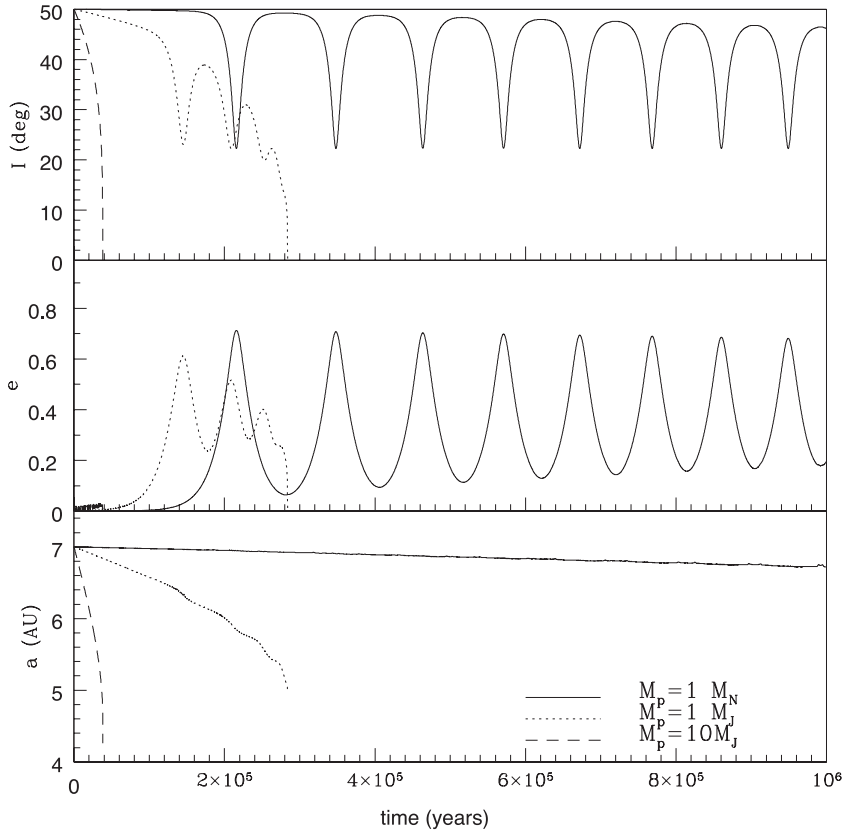

Figure 5. Inclination I (in degrees, upper plot), eccentricity (middle plot) and semimajor axis a (in au, lower plot) versus time (in yr) for $r_p = 7$ au, $M_d = 10^{-2}\,M_\odot$, $R_i = 1$ au, $I_0 = 50^\circ$ (same parameters as in Fig. 4) and $M_p = 1\,M_N$ (solid line), $1\,M_J$ (dotted line) and $10\,M_J$ (dashed line). For these parameters, $I_c = 23^\circ < I_0$ so that we are in the regime where Kozai cycles are present. Friction damps the oscillations more efficiently for larger mass planets. Alignment of the orbit with the disc may not happen over the disc lifetime for smaller mass planets.

3.2.1 Influence of the planet's mass

We now study the influence of the planet's mass on the evolution of the orbit. Fig. 5 shows the time evolution of the inclination I, eccentricity e and semimajor axis a for the same parameters as in Fig. 4, i.e. $r_p = 7$ au, $M_d = 10^{-2}\,M_\odot$, $R_i = 1$ au, $I_0 = 50^\circ$ and three different values of M_p. As $I_c = 23^\circ$ for these parameters, we are in the regime where Kozai cycles are present. As shown by equation (15), the damping time-scale τ_{damp} is proportional to $1/M_p$. The period P_{osc} of the Kozai cycle, on the other hand, does not depend on the planet's mass (see equations 8 and 9). We therefore expect friction to be very efficient for high-mass planets for which the damping time-scale τ_{damp} would be smaller than P_{osc}, and much less efficient for low-mass planets for which $\tau_{damp} \gg P_{osc}$. This is borne out by the results displayed in Fig. 5. Friction dominates the evolution for the planet with $M_p = 10\,M_J$, for which τ_{damp} is smaller than P_{osc}. For a Jupiter mass planet, the two time-scales are comparable and the orbit aligns after a few oscillations, i.e. after a few 10^5 yr. For a Neptune mass planet, $\tau_{damp} \gg P_{osc}$ and I decreases very slowly. In that case, the orbit would stay misaligned over the disc lifetime.

As stated above, P_{osc} does not depend on the planet's mass. However, we see from Fig. 5 that the oscillations for $M_p = 1\,M_J$ and $M_p = 1\,M_N$ do not have the same period. This is because, as noted above, P_{osc} decreases as damping reduces the amplitudes of the oscillations.

The fact that dynamical drag leads to faster alignment of the orbits for more massive planets was seen in the numerical simulations of Rein (2012) who considered planets on highly inclined orbits but without taking into account the gravitational interaction with the disc.

3.2.2 Influence of the disc's mass

Fig. 6 shows the time evolution of the inclination I and semimajor axis a for $M_p = 1\,M_N$, $r_p = 7$ au, $R_i = 1$ au, $I_0 = 50^\circ$ (as in Fig. 4) and three different values of M_d ranging from 10^{-2} to $0.1\,M_\odot$. Terquem & Ajmia (2010) showed that I_c does not depend on M_d when the other parameters are kept fixed, so that we have $I_c = 23^\circ$ here. Since $I_0 = 50^\circ$, we are therefore in the regime of Kozai cycles. From equation (15), we see that $\tau_{damp} \propto M_d^{-1}$. On the other hand, we also have $P_{osc} \propto M_d^{-1}$, as expected from the classical Kozai effect and verified in the disc's case by Terquem & Ajmia (2010). It follows that alignment of the orbit with the disc, when it occurs, should happen after the same number of oscillations whatever the disc's mass. This is confirmed by the curves in Fig. 6 which are all a time-scaled version of each other, with the more massive disc showing the shortest evolution time-scale. It is therefore easier to keep a planet on an inclined orbit in the presence of a less massive disc.

3.2.3 Influence of the planet's initial semimajor axis

Finally, we study the effect of the initial semimajor axis on the orbital evolution. Fig. 7 shows the time evolution of the inclination

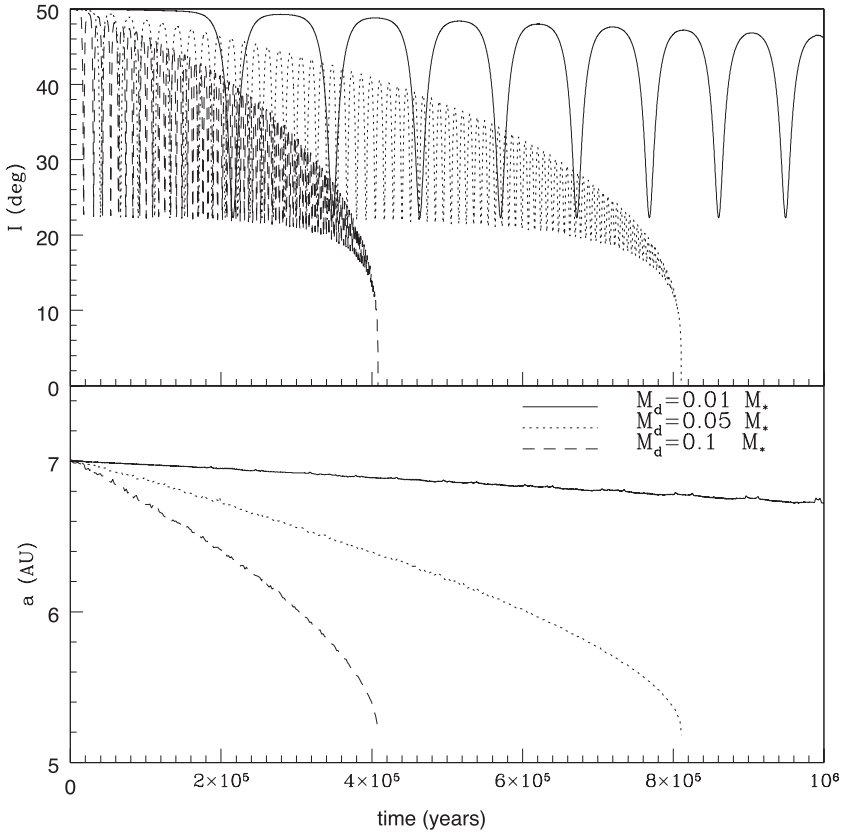

Figure 6. Inclination I (in degrees, upper plot) and semimajor axis a (in au, lower plot) versus time (in yr) for $M_p = 1\ M_N$, $r_p = 7$ au, $R_i = 1$ au, $I_0 = 50^\circ$ (same parameters as in Fig. 4) and $M_d = 0.1\,M_\odot$ (dashed line), $5 \times 10^{-2}\,M_\odot$ (dotted line) and $10^{-2}\,M_\odot$ (solid line). For these parameters, $I_c = 23^\circ < I_0$ so that we are in the regime where Kozai cycles are present. It is easier to keep a planet on an inclined orbit in the presence of a less massive disc.

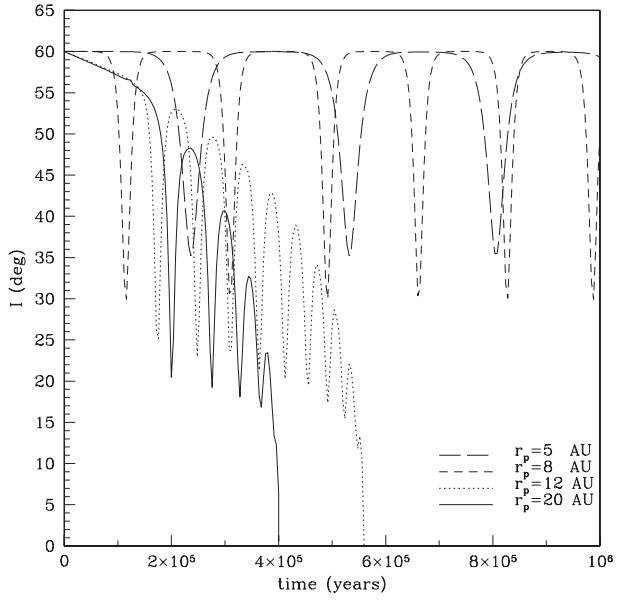

Figure 7. Inclination I (in degrees) versus time (in yr) for $M_p = 1\ M_J$, $M_d = 10^{-2}\,M_\odot$, $R_i = 10$ au, $I_0 = 60^\circ$ and $r_p = 20$ au (solid line), 12 au (dotted line), 8 au (short dashed line) and 5 au (long dashed line). For these parameters, we are in the regime of Kozai cycles. Alignment of the orbit with the disc is faster at larger distances from the star.

I for $M_p = 1\ M_J$, $M_d = 10^{-2}\,M_\odot$, $R_i = 10$ au, $I_0 = 60^\circ$ and four different values of r_p ranging from 5 to 20 au. For these parameters, we are in the regime of Kozai cycles. For $r_p = 5$ au, the planet stays in the disc's inner cavity so that it never experiences frictional forces when it goes through the disc's plane. The orbital evolution is therefore that of a Kozai cycle with no friction and a minimum angle of 37°, consistent with the results of Fig. 3. For $r_p = 8$ au, although the distance to the star does get larger than R_i when $e > 0.25$, as it happens the planet is always in the disc's inner cavity when it crosses the disc's plane, so that here again friction does not play a role. Like in the previous case, the minimum angle for this cycle is consistent with the results of Fig. 3. As noted above, $P_{osc} \propto a^{-3/2}$ in the classical Kozai case. We verify here that P_{osc} does indeed decrease when a increases [in agreement with Terquem & Ajmia (2010). For $r_p = 12$ and 20 au, the planet crosses the disc so that the oscillations are damped by the frictional force. As shown by equation (15), the damping time-scale τ_{damp} does not depend on a. This is consistent with the curves displayed in Fig. 7 at early times, before the eccentricity of the orbits grows, as they show that the damping time-scale is indeed the same for $r_p = 12$ and 20 au. But as the inclination gets smaller for the larger value of r_p (I_{min} is smaller and the planet spends more time in the disc), τ_{damp} also gets shorter for this value of r_p. Alignment of the orbit with the disc is then faster at larger distances from the star.

4 DISCUSSION

We have investigated the dynamics of a planet on an orbit inclined with respect to a disc. If the initial inclination of the orbit is larger than some critical value, the gravitational force exerted by the disc on the planet leads to a Kozai cycle in which the eccentricity of the orbit is pumped up to large values and oscillates with time in antiphase with the inclination. On the other hand, when the planet goes through the disc, it suffers a frictional force that results in a loss of orbital energy. As a consequence, the inclination and the eccentricity of the orbit are damped and the semimajor axis decreases. The goal of this paper was to study on what time-scale orbits inclined with respect to a disc would align with it.

The calculations presented in this paper show that, by pumping up the eccentricity of the planet's orbit and maintaining either I or e at large values, planets in orbits undergoing Kozai cycles maintain large velocities relative to the disc as they pass through it, so delaying alignment with the disc and circularization of the orbit.

For the parameters used in this paper, which are typical of protostellar discs, it was found that Neptune mass planets would remain on inclined orbits over the disc lifetime. Jupiter mass planets, however, tend to align faster, as the damping time-scale is shorter for more massive planets. Note however that we have not taken into account the fact that the disc dissipates progressively over time. As damping is less efficient in less massive discs, Jupiter mass planets could remain misaligned if the disc's mass were decreasing sufficiently fast. We have also found that alignment of the orbits was faster at larger distances from the star.

So far, the only planets that have been found on inclined orbits are rather massive (with a mass $\sim M_{\rm J}$) and on short-period orbits. This of course is a result of observational bias, as the inclination is measured so far only for transiting planets. As the results of this paper suggest, if these planets had been on inclined orbits when the disc was present, they probably would have aligned if they had crossed the disc. Therefore, either (i) the orbits became inclined after the disc had dissipated, (ii) the disc in which the planets formed was misaligned with the stellar equatorial plane or (iii) the planets formed on inclined orbits with short enough periods that they crossed the disc's plane only in an inner cavity. Jupiter mass planets formed on inclined orbits at large distances from the star would be expected to have aligned with the disc unless the formation took place near the end of the life of the disc.

The planets in the Kepler sample seem to have both low inclinations (Fabrycky et al. 2012) and low eccentricities (Kane et al. 2012). Radial velocity surveys also show lower eccentricities for lower mass planets. According to the results of our paper, this strongly suggests that these planets, with masses mainly at most $\sim M_{\rm N}$, have formed and stayed in the original disc. Had they been in a sufficiently inclined orbit at some point, this would have recurred over the disc lifetime, and the orbit would have had episodes of high eccentricity. Thus, a population in both highly eccentric and inclined orbits would be expected. Measurement of inclination angles for longer period orbits will enable the evaluation of proposed aspects of planet formation scenarios.

Finally, we remark that in this paper we have considered only one planet interacting with the disc. In a subsequent paper, we will investigate the dynamics of multiple systems.

REFERENCES

Adams F. C., Laughlin G., 2003, Icarus, 163, 290
Albrecht S., Winn J. N., Johnson J. A. et al., 2012, ApJ, 757, 18
Batalha N. M., Rowe J. F., Bryson S. T. et al., 2012, eprint arXiv:1202.5852
Bate M. R., Lodato G., Pringle J. E., 2010, MNRAS, 401, 1505
Binney J., Tremaine S., 1987, Galactic dynamics. Princeton Univ. Press, Princeton, NJ
Borucki W. J., Koch D. G., Basri G. et al., 2011, ApJ, 736, 19
Chatterjee S., Ford E. B., Matsumura S., Rasio F. A., 2008, ApJ, 686, 580
Fabrycky D. C., Tremaine S., 2007, ApJ, 669, 1298
Fabrycky D. C., Lissauer J. J., Ragozzine D. et al., 2012, ApJ, eprint arXiv:1202.6328
Foucart F., Lai D., 2011, MNRAS, 412, 2799
Innanen K. A., Zheng J. Q., Mikkola S., Valtonen M. J., 1997, AJ, 113, 1915
Johns-Krull C. M. et al., 2008, ApJ, 677, 657
Kane S. R., Ciardi D. R., Gelino D. M., von Braun K., 2012, MNRAS, 425, 757
Kozai Y., 1962, AJ, 67, 591
Lai D., Foucart F., Lin D. N. C., 2011, MNRAS, 412, 2790
Larwood J. D., Nelson R. P., Papaloizou J. C. B., Terquem C., 1996, MNRAS, 282, 597
Lidov M. L., 1962, Planet. Space Sci., 9, 719
Naoz S., Farr W. M., Lithwick Y., Rasio F. A., Teyssandier J., 2011, Nat, 473, 187
Nelson R. P., Papaloizou J. C. B., 1999, MNRAS, 309, 929
Ostriker E. C., 1999, ApJ, 513, 252
Papaloizou J. C. B., Terquem C., 1995, MNRAS, 274, 987
Papaloizou J. C. B., Terquem C., 2001, MNRAS, 325, 221
Press W. H., Teukolsky S. A., Vetterling W. T., Flannery B. P, 1993, Numerical Recipes in Fortran. Cambridge Univ. Press, Cambridge
Rein H., 2012, MNRAS, 422, 3611
Rephaeli Y., Salpeter E. E., 1980, ApJ, 240, 20
Ruderman M. A., Spiegel E. A., 1971, ApJ, 165, 1
Terquem C., Ajmia A., 2010, MNRAS, 404, 409
Terquem C., Papaloizou J. C. B., 2002, MNRAS, 332, L39
Thies I., Kroupa P., Goodwin S. P., Stamatellos D., Whitworth A. P., 2011, MNRAS, 417, 1817
Watson C. A., Littlefair S. P., Diamond C., Collier Cameron A., Fitzsimmons A., Simpson E., Moulds V., Pollacco D., 2011, MNRAS, 413, L71
Winn J. N. et al., 2008, ApJ, 683, 1076
Wu Y., Lithwick Y., 2011, ApJ, 735, 109
Wu Y., Murray N. W., Ramsahai J. M., 2007, ApJ, 670, 820

APPENDIX A: RESPONSE OF THE DISC TO THE GRAVITATIONAL INTERACTION WITH THE PLANET

We here estimate the warping response of a disc of the type we consider to a planet in an inclined circular orbit. The disc is assumed to contain significantly more angular momentum than the planet and obey a barotropic equation of state. We show that provided the inverse of the orbital precession frequency is less than the local disc sound crossing time and the mass of the planet is less than the disc mass in its neighbourhood, the range of inclinations excited is expected to be small.

A1 Governing equations

The basic governing equations are the equations of continuity and motion for a barotropic gas in the form

$$\frac{\partial \rho}{\partial t} + \nabla \cdot \rho \boldsymbol{v} = 0, \tag{A1}$$

$$\frac{\partial \boldsymbol{v}}{\partial t} + \boldsymbol{v}\cdot\nabla\boldsymbol{v} = -\frac{1}{\rho}\nabla P - \nabla\Phi - \nabla\Phi_\star, \tag{A2}$$

where $\Phi_\star = -GM_\star/|\boldsymbol{r}|$ is the gravitational potential due to the central star and

$$\Phi = -\frac{GM_\mathrm{p}}{\sqrt{r^2+R^2-2rR\cos(\phi-\phi_\mathrm{p})+(z-z_\mathrm{p})^2}} \tag{A3}$$

is the potential due to the planet which is treated as a perturbation for which we calculate the linear response below (the indirect term does not contribute to the warping and so may be dropped). Here the cylindrical coordinates of the planet are $(R, \phi_\mathrm{p}, z_\mathrm{p})$.

We adopt a Fourier decomposition in azimuth and time of the form

$$\Phi = \sum_{m>0}\Phi_m \exp[\mathrm{i}(m\phi+\omega_{p,m}t)] + cc, \tag{A4}$$

where $+cc$ indicates the addition of the complex conjugate, m is the azimuthal mode number and $\omega_{p,\,m}$ is an associated frequency corresponding to a pattern speed $-\omega_{p,\,m}/m$. For global warps we are interested in $m=1$ and pattern speeds that correspond to a slow precession of the planetary orbit. The precession period of the line of nodes, which for the purposes of this section is assumed to be given, is related and comparable to the period of Kozai oscillations when these occur. We adopt the time or orbit average of the coefficient Φ_1 which is appropriate for a discussion of the secular evolution of global warps. We perform a corresponding Fourier decomposition for the response perturbations to the disc which are taken to have ϕ and t dependences through a multiplicative factor $\exp[\mathrm{i}(m\phi+\omega_{p,\,m}t)]$. From now on, this factor will be taken as read and we drop the subscript m on quantities as this is taken to be unity.

A2 The disc inclination response

Denoting perturbations with a prime, linearization of the equations of motion (A2) for the response to the perturbing potential, Φ, gives

$$\begin{aligned}
\mathrm{i}(\omega_\mathrm{p}+\Omega)v_r' - 2\Omega v_\phi' &= -\frac{\partial W}{\partial r}\\
\mathrm{i}(\omega_\mathrm{p}+\Omega)v_\phi' + \frac{\kappa^2}{2\Omega}v_r' &= -\frac{\mathrm{i}W}{r}\\
\mathrm{i}(\omega_\mathrm{p}+\Omega)v_z' &= -\frac{\partial W}{\partial z},
\end{aligned} \tag{A5}$$

where $W = P'/\rho + \Phi$ and κ is the epicyclic frequency. Solving for the velocity perturbations, we obtain

$$\begin{aligned}
v_r' &= -\mathrm{i}\frac{(\omega_\mathrm{p}+\Omega)\partial W/\partial r + 2\Omega W/r}{\kappa^2-(\omega_\mathrm{p}+\Omega)^2}\\
v_\phi' &= \frac{(\kappa^2/(2\Omega))\partial W/\partial r + (\omega_\mathrm{p}+\Omega)W/r}{\kappa^2-(\omega_\mathrm{p}+\Omega)^2}.
\end{aligned} \tag{A6}$$

As we are interested in a disc that is close to Keplerian rotation, with $\omega_\mathrm{p} \ll \Omega$ and $\kappa \sim \Omega$, we neglect ω_p and set $\kappa = \Omega$ in the numerators above, and replace $\kappa^2-(\omega_\mathrm{p}+\Omega)^2$ by $2\Omega(\kappa-\omega_\mathrm{p}-\Omega)$ in the denominators to obtain

$$\begin{aligned}
v_r' &= -\mathrm{i}\frac{\partial W/\partial r + 2W/r}{2(\kappa-\omega_\mathrm{p}-\Omega)}\\
v_\phi' &= \frac{\partial W/\partial r + 2W/r}{4(\kappa-\omega_\mathrm{p}-\Omega)}.
\end{aligned} \tag{A7}$$

Following our previous work (e.g. Papaloizou & Terquem 1995; Larwood et al. 1996; Nelson & Papaloizou 1999), we seek a solution for which v_z' is independent of z to within a correction of the order of $(H/r)^2$. Then to within the same order of accuracy we may integrate the linearized z component of the equation of motion to give

$$W = -\mathrm{i}(\omega_\mathrm{p}+\Omega)zv_z'. \tag{A8}$$

We now write down the linearized continuity equation in the form

$$\frac{\mathrm{i}(\omega_\mathrm{p}+\Omega)\rho(W-\Phi)}{c_s^2} = -\nabla\cdot(\rho\boldsymbol{v}'), \tag{A9}$$

where we have used $P' = c_s^2\rho'$, with $c_s^2 = \mathrm{d}P/\mathrm{d}\rho$. Multiplying (A9) by z and integrating over the vertical extent of the disc, we get

$$\begin{aligned}
\int_{-\infty}^{\infty}\frac{\mathrm{i}(\omega_\mathrm{p}+\Omega)\Phi\rho z}{c_s^2}\,\mathrm{d}z = &\int_{-\infty}^{\infty}\frac{(\omega_\mathrm{p}+\Omega)^2 v_z'\rho z^2}{c_s^2}\mathrm{d}z\\
&-\int_{-\infty}^{\infty}v_z'\rho\,\mathrm{d}z + \nabla_\perp\cdot\left(\int_{-\infty}^{\infty}z\boldsymbol{v}_\perp'\rho\,\mathrm{d}z\right),
\end{aligned} \tag{A10}$$

where the perpendicular velocity perturbation is $\boldsymbol{v}_\perp' = (v_r', v_\phi', 0)$. Making use of equations (A7) and (A8) with ω_p neglected in the latter, and vertical hydrostatic equilibrium for the unperturbed state, we obtain

$$\begin{aligned}
&\frac{\partial}{\partial r}\left(\frac{\mu\Omega}{\omega_\mathrm{p}+\Omega-\kappa}\frac{\partial g}{\partial r}\right) + \frac{4\omega_\mathrm{p}\Sigma g}{\Omega}\\
&\quad = \frac{2\mathrm{i}r^2}{GM_\star}\int_{-\infty}^{\infty}\rho\frac{\partial\Phi}{\partial z}\mathrm{d}z \sim \frac{2\mathrm{i}r^2\Sigma}{GM_\star}\left(\frac{\partial\Phi}{\partial z}\right)_{z=0},
\end{aligned} \tag{A11}$$

where

$$\mu = \int_{-\infty}^{\infty}\rho z^2\mathrm{d}z, \tag{A12}$$

$g = r^2\Omega v_z'/(r^3\Omega^2) \equiv v_z'/(r\Omega)$, and terms of the order of ω_p^2 have been neglected. Note that consistently with the approximations used here, where possible, we have adopted Keplerian rotation and taken $r^3\Omega^2 = GM_\star$ to be a constant in this expression. Thus, $2g$ becomes the local inclination of the disc [the factor of 2 arises from the form of the Fourier decomposition (A4)]. We remark that (A11) may also be written as

$$\frac{\partial}{\partial r}\left(\frac{\mu\Omega}{\omega_\mathrm{p}+\Omega-\kappa}\frac{\partial g}{\partial r}\right) + \frac{4\omega_\mathrm{p}\Sigma g}{\Omega} = \frac{1}{\pi GM_\star}\frac{\mathrm{d}T}{\mathrm{d}r}, \tag{A13}$$

where, for orbits with line of nodes coinciding with the y-axis as considered below, T is the torque due to the planet acting on the disc in the radial interval (r,∞) in the x direction. Thus, $T\to 0$ as $r\to\infty$.

A3 Solution for the disc inclination

We wish to solve (A13) for the inclination of the disc induced by a planet on an inclined orbit. As the unforced problem has solutions consisting of long-wavelength bending waves propagating with a speed that is a multiple of the sound speed (Nelson & Papaloizou 1999), a complete solution requires knowledge of the complete structure of the disc including boundary details which are beyond the scope of the modelling in this paper. To deal with this situation we assume that the disc extends to large radii and has much larger angular momentum content than the planet. We then look for a solution for which the inclination response is localized away from large radii having $g\to 0$, and $\mathrm{d}g/\mathrm{d}r\to 0$, for $r\to\infty$. These solutions are in fact regular as $r\to 0$ for the power-law discs we adopt here. However, inner boundary effects could possibly cause the excitation of a freely propagating bending wave that should

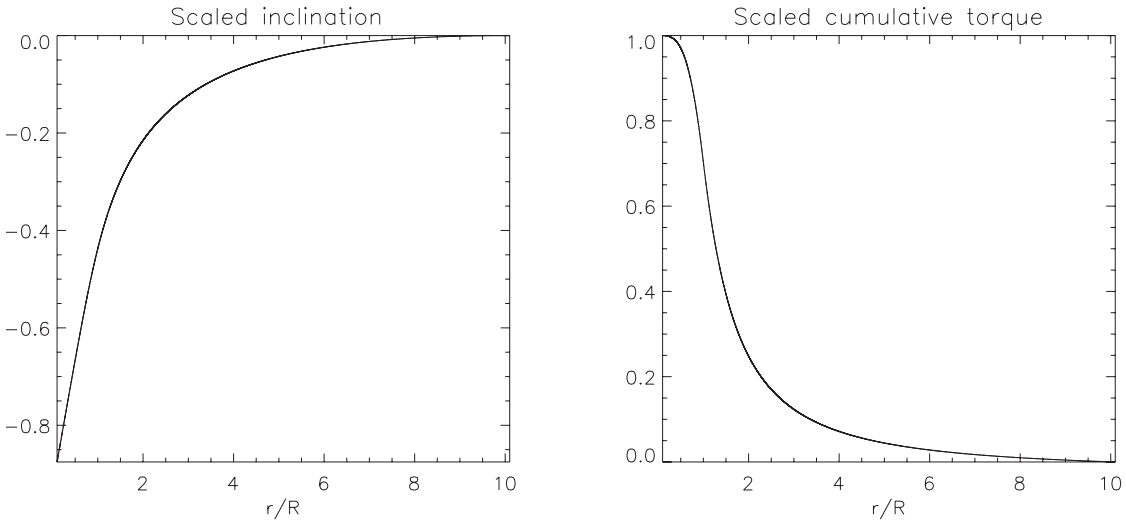

Figure A1. The left-hand panel shows the inclination, normalized by the factor $10^3(M_\mathrm{p}/M_\star)(0.05R/H(R))^2\omega_\mathrm{p}R^{3/2}/\sqrt{GM_\star}$, as a function of r/R for the calculation described in the text. This was calculated under the condition that it tended to zero as $r \to \infty$. The right-hand panel shows the function $T(r/R)/T(0)$ which represents the magnitude of the torque due to the planet acting on the disc in the radial interval (r, ∞) normalized by its value as $r \to 0$. For both panels the inclination of the circular planetary orbit of radius R to the plane of the disc was $\pi/4$.

be added. But this should not affect an estimate of the scale of the warping. To simplify matters further, we shall take $\kappa = \Omega$ as expected for a constant aspect ratio disc, under the gravitational potential due to a central point mass, and assume that ω_p/Ω is much less than H/r. The latter assumption, which is expected to lead to mild warping (e.g. Larwood et al. 1996 and see below), enables us to neglect the term $\propto g$ in equation (A13) which can then be easily integrated to give

$$\frac{\mu\Omega}{\omega_\mathrm{p}}\frac{\partial g}{\partial r} = \frac{1}{\pi G M_\star}T, \tag{A14}$$

and accordingly

$$g = -\omega_\mathrm{p}\int_r^\infty \frac{T}{\pi\mu\Omega G M_\star}\mathrm{d}r. \tag{A15}$$

We make a rough estimate of g as determined by (A15) by setting $\mu = \Sigma H^2$ and $T \sim \pi G M_\mathrm{p}\Sigma r \sim M_\mathrm{p}r^2\omega_\mathrm{p}\Omega$, where r is evaluated at a location where the planet intersects the disc. Then, we estimate

$$g \sim \frac{\omega_\mathrm{p}M_\mathrm{p}r^2}{\Omega M_\star H^2} \sim \left(\frac{\omega_\mathrm{p}^2 r^2}{\Omega^2 H^2}\right)\left(\frac{M_\mathrm{p}\Omega}{M_\star\omega_\mathrm{p}}\right). \tag{A16}$$

This implies that the inclination range is in general small. The first factor in brackets measures the square of the product of the precession frequency and local sound crossing time which is expected to be less than unity and so leads to only small warping (see Papaloizou & Terquem 1995; Larwood et al. 1996; Nelson & Papaloizou 1999). The second factor in brackets is expected to be the ratio of the planet mass to the characteristic disc mass contained within a length scale comparable to that of the orbit, which is expected to be less than of order unity particularly for low-mass planets.

We have evaluated the solution given by (A15) for a planet in a circular orbit of radius R, inclined at 45° to the plane of the disc and with line of nodes coinciding with the y-axis. We took $\Sigma \propto r^{-1/2}$ as in the main text and as the solution scales with the inverse square of the disc aspect ratio, H/r, that is left as a parameter. The left-hand panel of Fig. A1 shows the inclination in units of $10^3(M_\mathrm{p}/M_\star)(0.05R/H(R))^2\omega_\mathrm{p}R^{3/2}/\sqrt{GM_\star}$, as a function of r/R. The maximum value of this is of order unity indicating that, even for a Jovian mass planet in a disc with an aspect ratio of 0.05, the characteristic value of the inclination range is of the order of $\omega_\mathrm{p}R^{3/2}/\sqrt{GM_\star}$ which is expected to be of the order of the ratio of the mass of the disc to that of the central star and thus a small quantity. The right-hand panel of Fig. A1 shows the cumulative torque $T(r/R)/T(0)$ measured in the sense of increasing inwards. This indicates that the torque falls off rapidly at large radii.

APPENDIX B: EXPRESSION OF THE GRAVITATIONAL FORCE DUE TO THE DISC IN TERMS OF ELLIPTIC INTEGRALS

Here we develop expressions for the gravitational force per unit mass exerted by a disc on a planet that may be passing through it in terms of elliptic integrals. The resulting expressions require the evaluation of two-dimensional integrals with integrands that at worst contain a logarithmic singularity which is readily manageable numerically.

The gravitational potential exerted by the disc at the location (r, z) of the planet is given by equation (1) as

$$\Phi(r, z_\mathrm{p}) = -G\int_{R_\mathrm{i}}^{R_\mathrm{o}}\int_{-H}^{H}\int_0^{2\pi}\frac{\rho(r', z')\, r'\mathrm{d}r'\mathrm{d}z'\mathrm{d}\phi'}{\sqrt{r^2 + r'^2 - 2rr'\cos\phi' + (z - z')^2}}. \tag{B1}$$

As the disc is axisymmetric, the gravitational force per unit mass exerted by the disc on the planet has only a radial and a vertical component, given by $-\partial\Phi/\partial r$ and $-\partial\Phi/\partial z$, respectively. To calculate these, we first note that Φ is the solution of Poisson's equation, which is given by

$$\frac{\partial^2\Phi}{\partial r^2} + \frac{1}{r}\frac{\partial\Phi}{\partial r} + \frac{\partial^2\Phi}{\partial z^2} - \frac{m^2\Phi}{r^2} = 4\pi G\rho(r, z), \tag{B2}$$

with $m = 0$. In the general non-axisymmetric case, when the φ dependence of ρ is through a factor $\exp(\mathrm{i}\varphi)$, the azimuthal number m is non-zero and we have $\partial^2\Phi/\partial\varphi^2 = -m^2\Phi$. We now differentiate equation (B2), with $m = 0$, with respect to r to

obtain

$$\frac{\partial^2}{\partial r^2}\left(\frac{\partial\Phi}{\partial r}\right)+\frac{1}{r}\frac{\partial}{\partial r}\left(\frac{\partial\Phi}{\partial r}\right)-\frac{1}{r^2}\frac{\partial\Phi}{\partial r}+\frac{\partial^2}{\partial z^2}\left(\frac{\partial\Phi}{\partial r}\right)=4\pi G\frac{\partial\rho}{\partial r}. \tag{B3}$$

This shows that $\partial\Phi/\partial r$ satisfies Poisson's equation with $m=1$ and $\partial\rho/\partial r$ as the source term. The solution can be written as

$$\frac{\partial\Phi}{\partial r}=-G\int_{R_\mathrm{i}}^{R_\mathrm{o}}\int_{-H}^{H}\int_0^{2\pi}\frac{\frac{\partial\rho}{\partial r}(r',z')\,r'\mathrm{d}r'\cos\phi'\mathrm{d}z'\mathrm{d}\phi'}{\sqrt{r^2+r'^2-2rr'\cos\phi'+(z-z')^2}}+B_\mathrm{i}+B_\mathrm{o}. \tag{B4}$$

Here the domain of integration is the interior of the domain containing the mass distribution, and B_i and B_o are boundary terms that have to be taken into account when the disc's mass density is given by equation (2), as in that case $\partial\rho/\partial r$ is infinite at the radial boundaries of the disc. When the disc's mass density is made continuous by multiplication by the factor f defined in equation (3), these boundary terms are not included.

Expression (B4) can be recast in the form

$$\frac{\partial\Phi}{\partial r}=-G\int_{R_\mathrm{i}}^{R_\mathrm{o}}\int_{-H}^{H}\frac{\partial\rho}{\partial r}(r',z')H_r(r,r',z-z')\,r'\mathrm{d}r'\mathrm{d}z'+B_\mathrm{i}+B_\mathrm{o}, \tag{B5}$$

with

$$H_r(r,r',z-z')=\int_0^{2\pi}\frac{\cos\phi'\mathrm{d}\phi'}{\sqrt{r^2+r'^2-2rr'\cos\phi'+(z-z')^2}}. \tag{B6}$$

We define $a^2=r^2+r'^2+(z-z')^2$, $b^2=2rr'$ and $u=2b^2/(a^2+b^2)$. It is then straightforward to show that

$$H_r(r,r',z-z')=\frac{4\sqrt{a^2+b^2}}{b^2}\left[\frac{a^2}{a^2+b^2}K(u)-E(u)\right], \tag{B7}$$

where K and E are the elliptic integrals of the first and second kind, defined as

$$K(m)=\int_0^{\pi/2}\frac{\mathrm{d}\theta}{\sqrt{1-m\sin^2\theta}}, \tag{B8}$$

$$E(m)=\int_0^{\pi/2}\sqrt{1-m\sin^2\theta}\mathrm{d}\theta, \tag{B9}$$

with $m<1$.

We calculate the boundary terms B_i and B_o by assuming that ρ is continuous and supposing that ρ increases from 0 to $\rho(R_\mathrm{i},z)$ over a distance $\Delta r\to 0$ at the inner edge and decreases from $\rho(R_\mathrm{o},z)$ to 0 over the same distance at the outer edge, i.e.

$$B_\mathrm{i}=-G\int_{R_\mathrm{i}-\Delta r}^{R_\mathrm{i}}\int_{-H}^{H}\frac{\partial\rho}{\partial r}(r',z')H_r(r,r',z-z')\,r'\mathrm{d}r'\mathrm{d}z', \tag{B10}$$

$$=-G\int_{-H(R_\mathrm{i})}^{H(R_\mathrm{i})}\rho(R_\mathrm{i},z')R_\mathrm{i}H_r(r,R_\mathrm{i},z-z')\,\mathrm{d}z'. \tag{B11}$$

Similarly,

$$B_\mathrm{o}=-G\int_{R_\mathrm{o}}^{R_\mathrm{o}+\Delta r}\int_{-H}^{H}\frac{\partial\rho}{\partial r}(r',z')H_r(r,r',z-z')\,r'\mathrm{d}r'\mathrm{d}z', \tag{B12}$$

$$=+G\int_{-H(R_\mathrm{o})}^{H(R_\mathrm{o})}\rho(R_\mathrm{o},z')R_\mathrm{o}H_r(r,R_\mathrm{o},z-z')\,\mathrm{d}z'. \tag{B13}$$

We calculate $\partial\Phi/\partial z$ in a similar way by differentiating Poisson's equation (B2), with $m=0$, with respect to z, which leads to

$$\frac{\partial^2}{\partial r^2}\left(\frac{\partial\Phi}{\partial z}\right)+\frac{1}{r}\frac{\partial}{\partial r}\left(\frac{\partial\Phi}{\partial z}\right)+\frac{\partial^2}{\partial z^2}\left(\frac{\partial\Phi}{\partial z}\right)=4\pi G\frac{\partial\rho}{\partial z}. \tag{B14}$$

This shows that $\partial\Phi/\partial z$ satisfies Poisson's equation with $m=0$ and $\partial\rho/\partial z$ as the source term. The solution can be written as

$$\frac{\partial\Phi}{\partial z}=-G\int_{R_\mathrm{i}}^{R_\mathrm{o}}\int_{-H}^{H}\int_0^{2\pi}\frac{\frac{\partial\rho}{\partial z}(r',z')\,r'\mathrm{d}r'\mathrm{d}\phi'\mathrm{d}z'}{\sqrt{r^2+r'^2-2rr'\cos\phi'+(z-z')^2}}. \tag{B15}$$

This expression can be recast in the form

$$\frac{\partial\Phi}{\partial z}=-G\int_{R_\mathrm{i}}^{R_\mathrm{o}}\int_{-H}^{H}\frac{\partial\rho}{\partial z}(r',z')H_z(r,r',z-z')\,r'\mathrm{d}r'\mathrm{d}z', \tag{B16}$$

with

$$H_z(r,r',z-z')=\int_0^{2\pi}\frac{\mathrm{d}\phi'}{\sqrt{r^2+r'^2-2rr'\cos\phi'+(z-z')^2}}, \tag{B17}$$

or in terms of the elliptic function K as

$$H_z(r,r',z-z')=\frac{4}{\sqrt{a^2+b^2}}K(u). \tag{B18}$$

This paper has been typeset from a TEX/LATEX file prepared by the author.

4.5 Interplay between eccentricity and inclination

In this section, we wish to clarify a statement we have made in the publication above. In the abstract, we stated that "by maintaining either the inclination or the eccentricity at large values, the Kozai effect provides a way of delaying alignment with the disc and circularization of the orbit". Previous studies (see, e.g., Fendyke and Nelson, 2014, for low-mass planets) showed that eccentric planets embedded in discs are damped less rapidly than those on quasi-circular orbits. Here, the fact that the eccentricity is excited to high values by the disc argues in favour of the statement we made in the abstract. However, we remark that, because of the nature of the Kozai mechanism, the increase of eccentricity is correlated with a decrease of inclination. And the lower the inclination, the more time is spent in the disc during each orbit, and therefore the longer the planet undergoes dynamical friction. Hence, even inside the Kozai mechanism itself, two effects compete to decide how quickly the planet is going to realign. On figure 4.3 we show, in arbitrary units, the semi major axis, inclination and eccentricity of the run depicted in figure 5 of Teyssandier et al. (2013b) for a planet of $1\ M_{\rm J}$. As expected, the semi major axis decreases more rapidly at the peak of the Kozai mechanism (maximum eccentricity and minimum inclination). In figure 4.4 we redo the same run, removing the disc's gravitational potential (and therefore suppressing the Kozai oscillations, leaving only the friction). We show that inclination is damped slower without the Kozai oscillations. However the time on which the planet realigns with the disc is only slightly larger, and it does not affect our conclusion that massive planets realign within the disc's lifetime. Therefore we conclude that Kozai oscillations do not necessarily delay alignment.

4.6 Systems of two planets

Until now we have always assumed that there was only one planet orbiting around the star. Here we explore the possibility of having a system containing two planets misaligned with respect to a disc. We expect that additional planets will also be mainly perturbed by the disc. However, mutual perturbations between the planets could affect their evolution. The main source of mutual perturbations arises from the secular exchange of angular momentum between the two planets, which we have introduced in chapter 3 in the framework of the Laplace-Lagrange theory (see §3.2.3). We saw that the eccentricities and inclinations periodically vary in time, on a timescale given by the eigenfrequencies g_i and f_i, related to the precession of the argument of pericenter and longitude of ascending node, respectively. In chapter 2, we also saw that the Kozai mechanism can only be triggered if the variation of the argument of pericenter is slow. Hence, in the case where the variation of the arguments of pericenter caused by the mutual interaction between the planets would occur on a timescale shorter than the disc-Kozai induced variation, one could expect the planet-planet interaction to dominate the disc-planet interaction.

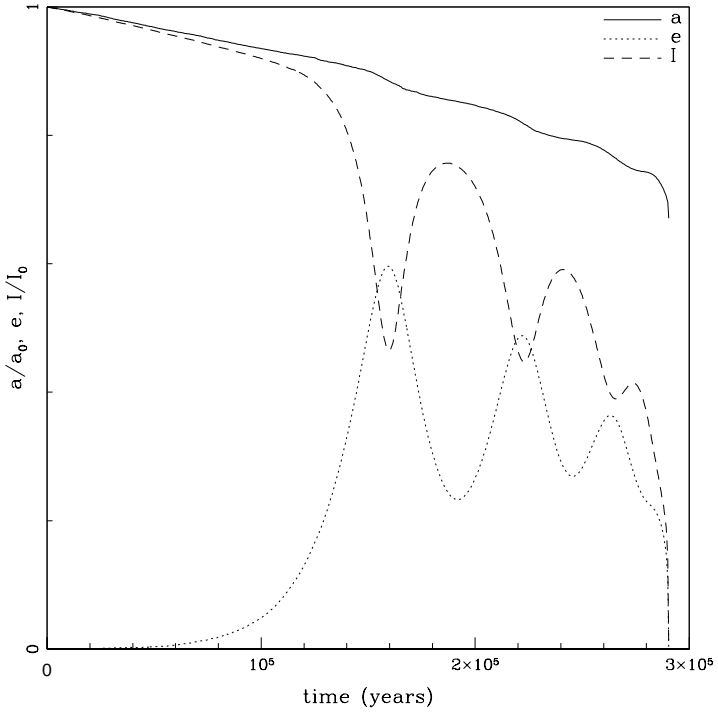

Figure 4.3: Semimajor axis (solid line, in units of the initial semimajor axis), eccentricity (dotted line) and inclination (dashed line, in units of the initial inclination) as a function of time, for the same set up at in figure 5 of Teyssandier et al. (2013b). The semimajor axis decreases because of the friction. At the peak of the Kozai cycle (maximum eccentricity, minimum inclination), the decrease of the semimajor axis is steeper (hence the friction is more important).

Takeda et al. (2008) proposed a dynamical classification for systems of two planets around a star, perturbed by a binary star companion. In our case, the pertuber is no longer a star, but the disc. Still, a similar classification can be done. For the i-th planet, where $i = 1\ , 2$ (with 1 denoting the inner planet), we note $t_{K,i}$ the timescale of the Kozai oscillations raised by the disc on planet i. In addition, we note $t_{\omega,i}$ the timescale of the Laplace-Lagrange precession of the argument of pericenter of planet i caused by the other planet. Similarly, $t_{\Omega,i}$ is the Laplace-Lagrange precession timescale of the longitude of ascending node of planet i. With the notations of section 3.2.3, we can write, for $i = 1, 2$:

$$t_{\omega,i} = \frac{2\pi}{g_i}, \quad t_{\Omega,i} = \frac{2\pi}{f_i}. \tag{4.33}$$

We recall that the inclination part of the problem is degenerate, which leads to $f_1 = f_2$. Therefore we have only one precession timescale of the ascending nodes, which we note t_Ω.With these notations, we classify the systems as follows:

- Decoupled systems: the two planets are not coupled one to each other, and are fully dominated by perturbations from the disc. In this case, $t_{K,i} < t_{\omega,i}$ for $i = 1, 2$, and the planets can develop independent disc-driven Kozai oscillations, provided their inclination with respect to the disc is above the critical angle. In this configuration,

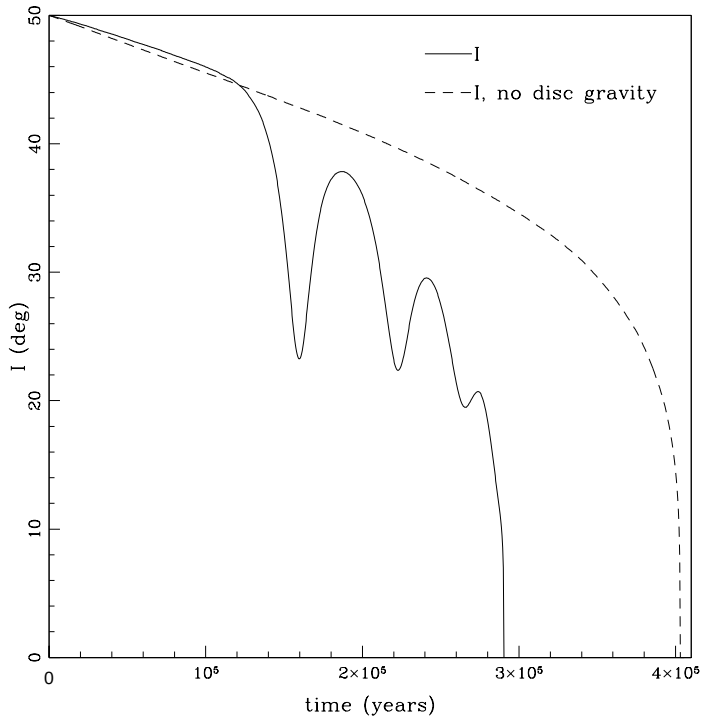

Figure 4.4: Solid line: inclination as a function of time for the same set up at in figure 5 of Teyssandier et al. (2013b). The dashed line shows the inclination for the same set up, but without the disc's gravitational potential. Because the Kozai cycles periodically bring the inclination to low values, where friction is more important (as the planet spends more time in the disc), the inclination is damped more rapidly in the presence of Kozai cycles. However in both cases, the inclination is damped much more rapidly than the disc's lifetime.

the ascending nodes of the two planets precess independently ($t_\Omega \gg t_{K,i}$), meaning that the planets can reach a large mutual inclination. However, even if this inclination is larger than the critical Kozai angle, Kozai oscillations between the two planets will not appear, as they are both independently evolving in the gravitational potential of the disc.

- Weakly coupled systems: here, the outer planet is dominated by the secular perturbations from the disc, and can undergo disc-Kozai osscillations. Meanwhile the inner planet is affected mainly by the outer planet. Large-amplitude nodal libration of the inner planet can lead to large mutual inclination and eccentricity. Because the inclination and eccentricity of the outer planet are already excited by the disc, this configuration can rapidly lead to chaotic behaviour.

- Strongly coupled systems: The two planets act as a "rigid body" and remain roughly coplanar, which is characterized by the two nodes varying at the same speed. Because, in the Kozai mechanism, the longitude of ascending node precesses at a speed similar

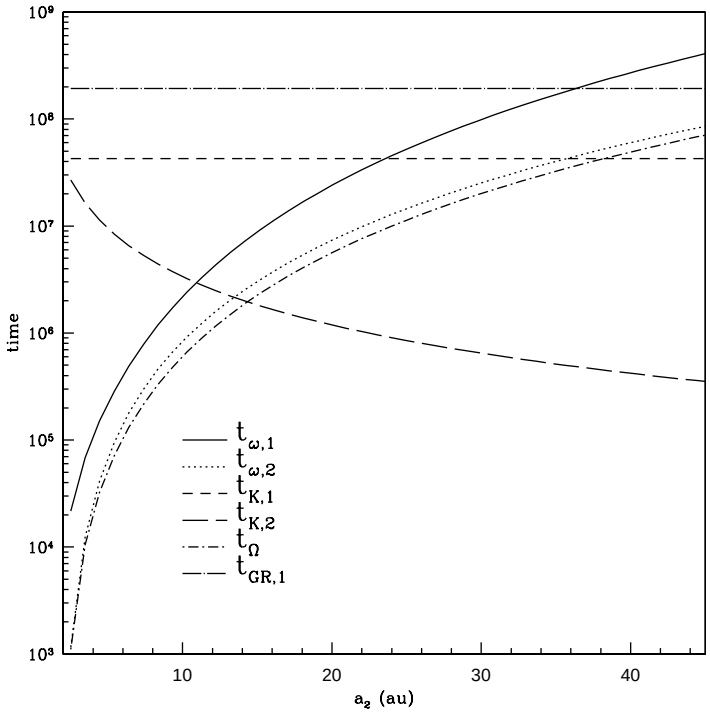

Figure 4.5: Comparison of different timescales as a function of the initial semi major axis of the outer planet. The inner planet is located at 2 AU. In this case, both planets have a mass of $0.5\ M_{\rm J}$. The disc extends from 50 to 500 AU with a mass of $5\ M_{\rm J}$. $t_{\omega,1}$ and $t_{\omega,2}$ are timescales associated with the precession of the pericenters, and t_Ω the nodal precession timescale, all derived in the framework of the Laplace-Lagrange theory. $t_{K,1}$ and $t_{K,2}$ are the timescale of the Kozai oscillations raised by the disc on planet 1 and 2, respectively. $t_{\rm GR,1}$ is General Relativity pericenter precession timescale of planet 1. We see two clear distinct regimes: when $a_2 < 14$ AU, the planets evolve through their mutual Laplace-Lagrange perturbations. When $a_2 > 14$ AU the shorter, dominant, timescale will be that of the Kozai oscillations raised by the disc on the outer planet.

to that of the argument of pericenter, a system will be strongly coupled when $t_\Omega \ll t_{K,i}$.

On figure 4.5 we show an example of such timescale analysis, where we compare the timescales of the pericenter and longitudes of ascending nodes precessions, in the framework of the Laplace-Lagrange theory, with the timescale of the Kozai oscillations raised by the disc on the planets. We also plot $t_{\rm GR,1}$, the timescale of the general relativity precession of the inner planet. Note that we have chosen a specific set of parameters to illustrate our analysis. In particular, we have assumed that the disc, despite being relatively massive, has cleared out a large inner cavity at $R_i = 50$ AU, which allows us to ignore the dynamical friction that we studied above. The disc extends to 500 AU with a mass of $5\ M_{\rm J}$. It appears that, as soon as the outer planet is sufficiently far away from the inner one, the disc is expected to dominate the evolution of the later.

On figure 4.6 we show an example where the disc has a mass of $5\ M_{\rm J}$ and extends from 50 to 500 AU. The star is orbited by two planets, both of them having a mass of $0.5\ M_{\rm J}$, eccentricities of 10^{-3} and inclinations of 50° and 55°, at 2 and 6 AU initially.

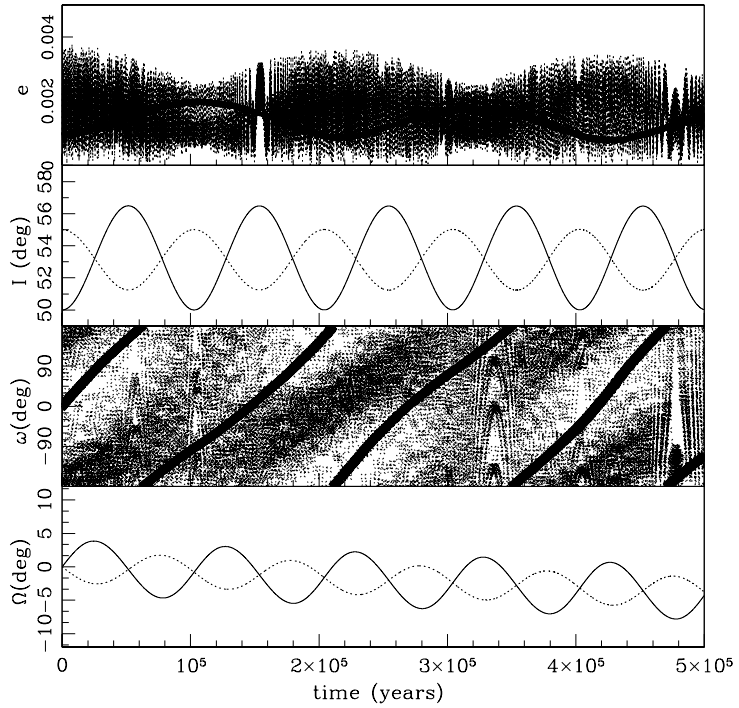

Figure 4.6: Evolution of the eccentricity, inclination, argument of pericenter, longitude of ascending node of two planets, at 2 and 6 AU, with masses of $0.5\ M_{\rm J}$, in the presence of a disc of $5\ M_{\rm J}$ extending from 50 to 500 AU. The planets evolve mainly through their mutual secular interactions, and the influence of the disc is negligible. Hence the two planets are dynamically rigid, as shown by the behaviour of the longitudes of ascending nodes.

Because they orbit in the inner cavity of the disc, friction does not need to be taken into account. As predicted by our timescale analysis in figure 4.5, the planets are dominated by their Laplace-Lagrange interaction. The eccentricities variations come in two flavours: an envelope that varies on a secular timescales, and some rapid variations in this envelope, that are not captured by our analysis. The inclinations show a clear, periodic, secular variation. The pericenter of the inner planet shows a regular circulation, while the pericenter of the outer planet shows a more chaotic behaviour, but tends to increase with time. The rigidity of the system is clearly illustrated by the two longitudes of ascending nodes, which show only small amplitude variations, on the same period as the inclinations.

On figure 4.7 we show the same simulation, but the outer planet has a semimajor axis of 42 AU. It is clear from our timescale analysis that the outer planet should be dominated by the disc-Kozai oscillations. Regarding the inner planet, secular variations, general relativity and disc-Kozai oscillations are all of the same order of magnitude. However they act on a timescale of about 10^8 yr, which is much longer than our integration time. Therefore we do not expect any important variations of the orbital elements of the inner planet, which is what we observe on figure 4.7.

The two examples that we have shown above illustrate well two extreme cases, one where the effect of the disc is negligible, and one where it completely dominates the evo-

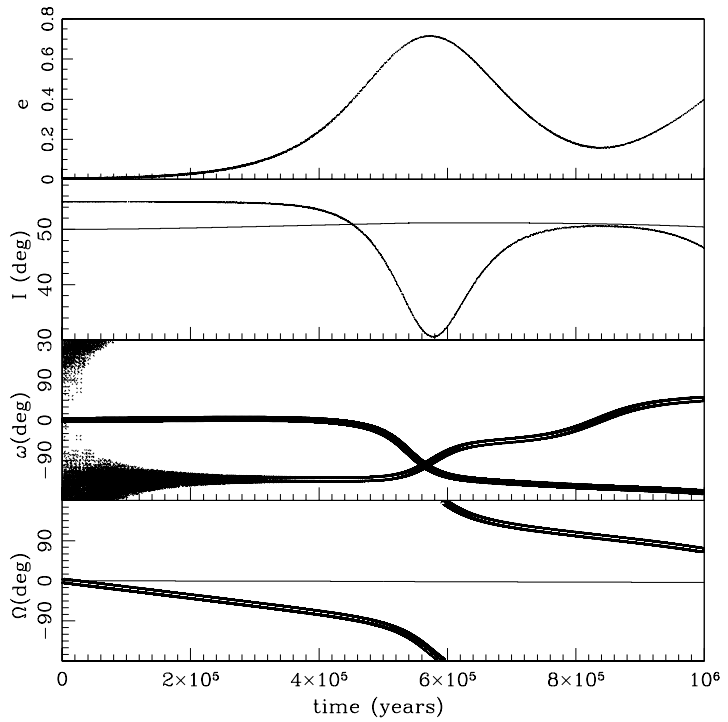

Figure 4.7: Evolution of the eccentricity, inclination, argument of pericenter, longitude of ascending node of two planets, at 2 and 42 AU, with masses of $0.5\ M_{\rm J}$, in the presence of a disc of $5\ M_{\rm J}$ extending from 50 to 500 AU. The outer planet exhibits large variations of eccentricity and inclination, caused by Kozai oscillations from the disc. The inner planet's eccentricity and inclination merely vary during the integration time (the eccentricity is invisible as it remains close to its initial value of 0.001).

lution of one of the planet, leaving the other unaffected on the timescale of the simulation. Note that we have chosen initial conditions (in particular the disc's parameters) that are convenient to illustrate our point. On figure 4.8 we show an example with a more realistic disc (but still ignoring friction). The disc extends from 10 to 100 AU, with a mass of $10\ M_{\rm J}$. The inner planet is located at 3 AU with a mass of $0.1\ M_{\rm J}$ and an inclination of $55°$, while the outer planet has a mass of $1\ M_{\rm J}$ and inclination of $65°$. Both planets are on circular orbits. In this case it clearly appears that the outer planet will always be dominated by Kozai oscillations from the disc, because it is too massive to be strongly perturbed by the inner planet. In addition, as the separation between the planets increases, the secular influence of the outer one on the inner one decreases and we expect that when $a_2 \gtrsim 10$ AU, the inner planet would also be dominated by Kozai-disc oscillations. Note that their could be some intermediate cases with interesting behavior: the inner planet would be dominated by secular perturbations from the outer one, causing the system to be rigid. In the meantime, the outer planet would be dominated by disc-Kozai variations. In this case the inner planet could "follow" the Kozai oscillations of the outer planet and undergo large eccentricity variations. However such configuration is expected to be quite unstable, because of the various sources of eccentricity excitation.

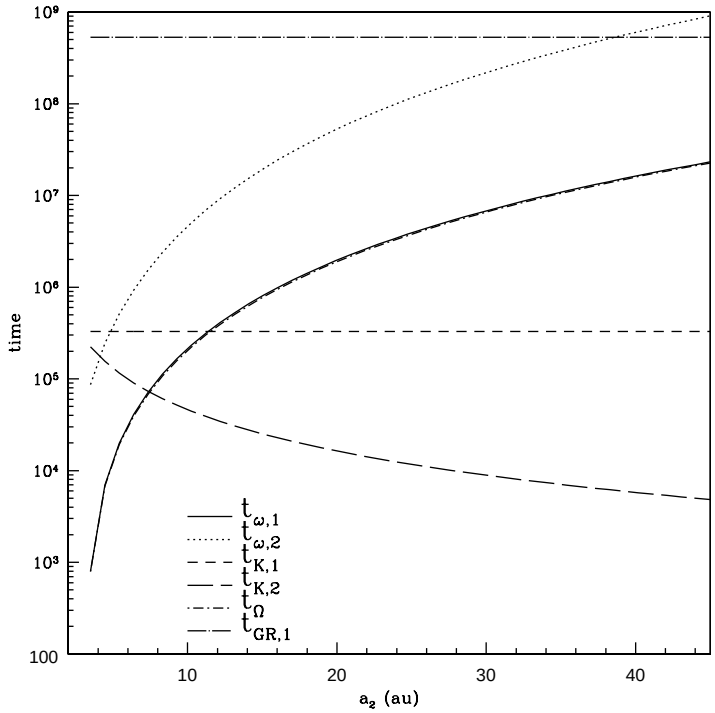

Figure 4.8: Comparison of different timescales as a function of the initial semi major axis of the outer planet. The inner planet is located at 3 AU. In this case, the inner planet has a mass of $0.1\ M_{\rm J}$, and the outer one $1\ M_{\rm J}$. $t_{\omega,1}$ and $t_{\omega,2}$ are timescales associated with the precession of the pericenters, and t_Ω the nodal precession timescale, all derived in the framework of the Laplace-Lagrange theory. $t_{K,1}$ and $t_{K,2}$ are the timescales of the Kozai oscillations raised by the disc on planet 1 and 2, respectively. $t_{\rm GR,1}$ is General Relativity pericenter precession timescale of the inner planet. The outer planet is dominated by the Kozai oscillations from the disc, mainly because the inner planet has a lower mass. When the two planets are well separated $(a_2 > 10$ AU$)$, we expect the inner planet to also be dominated by disc-Kozai oscillations

Finally we remark that we have neglected friction, mainly because we have considered simplistic cases where the planets orbit in an inner cavity. When friction is included, it will act to decrease the semi-major axis of the planets, meaning that the timescales we have derived will evolve in time. This makes the evolution of the system hard to predict, especially if the planets cross some secular resonances that could lead to chaotic behaviour.

Chapter 5

Resonant Migration

Contents

5.1 Migration and the capture in resonance

In the previous chapter we have analysed a configuration where a planet is inclined with respect to the mid-plane of a disc. In the present chapter, we study a mechanism that has been thought by several authors to cause a primordial misalignment between a pair of planets and their native disc. This mechanism, which also excites eccentricities, is referred to as *resonant migration*. It involves the planets being locked in a mean motion resonance (hereafter MMR, see section 3.2.5), where the ratio of their orbital period is the ratio of two small integers.

5.1.1 Observational evidences

Several stars have been found to be orbited by pairs of planets in, or close to, mean motion resonances. In particular, the star GJ 876 was found to host two giant planets in a 2:1 MMR (Marcy et al., 2001). The best-fit orbital solution (Rivera et al., 2010) gives periods of 30.4

and 61.1 days, with the inner planet having a mass of $0.7\ M_{\rm J}$ and an eccentricity of 0.26, while the outer one has a mass of $2.3\ M_{\rm J}$ and an eccentricity of 0.03. As pointed out by Lee and Peale (2002), this system contrasted with an other example of a 2:1 MMR, involving the satellites Io and Europa of Jupiter. In this case the resonant angles librate about 0° and 180°, and the apses are therefore anti-aligned. In the GJ 876 system, both resonant angles librate around 0° and the apses are aligned.

An other example consists in the two Saturn-like planets orbiting HD 45364, which were found to be in a 3:2 MMR (Correia et al., 2009). Because a system in a 3:2 MMR is likely to have crossed the 2:1 MMR first, fast migration is required in order to avoid trapping in this configuration (see section 5.2.1 below). Rein et al. (2010) argued that fast type III migration could account for this, and managed to produce an orbital solution and the associated light-curve that could fit the observations. There solution differs from that of Correia et al. (2009) and only subsequent observations will be able to disentangle between the two solutions.

The Kepler mission has revealed a large population of multiple systems, and a small fraction of them appear to be located in, or at least close to, MMRs. For these systems, the general trend is that the period ratio (outer period over inner period) is slightly larger than the exact resonant value. Terquem and Papaloizou (2007), Lithwick and Wu (2012), and Batygin and Morbidelli (2013) argued that tidal interactions with the star can increase the period ratio of two planets otherwise in a resonant configuration. However, this mechanism cannot explain why this trend is still observed for systems with the inner planet's period larger than 10 days, where tides are almost insignificant. More generally, the processes which, at the planet-disc level of interactions, can help or prevent the formation of resonances are still an active area of research.

5.1.2 Disc–driven migration of two planets

It is very unlikely that the pairs of resonant planets where formed in this configuration. The most natural explanation invokes convergent migration of the planets (Snellgrove et al., 2001). In fact, because the formation of MMR configurations is a natural outcome of the migration of a pair of planets, the observation of such systems could argue in support of disc migration. However, note that MMRs could also be an outcome of planet-planet scattering (Raymond et al., 2008).

If the orbits decay at rates such as the mutual separation between the two planets increases, then resonant capture cannot occur. However, if the two orbits converge, numerical simulations of planets embedded in protoplanetary discs reveal that resonant capture is possible. Figure 5.1 (from Kley and Nelson, 2012) shows an example of such hydrodynamical simulation where two giants planets clear out a mutual gap. The inner planet is pushed outward by the inner disc, while the outer planet is pushed inwards by the outer disc, resulting in convergent migration. Subsequently, the planets enter a resonant configuration. The 2:1 MMR is the first first-order resonance that two initially well-spaced planets may encounter,

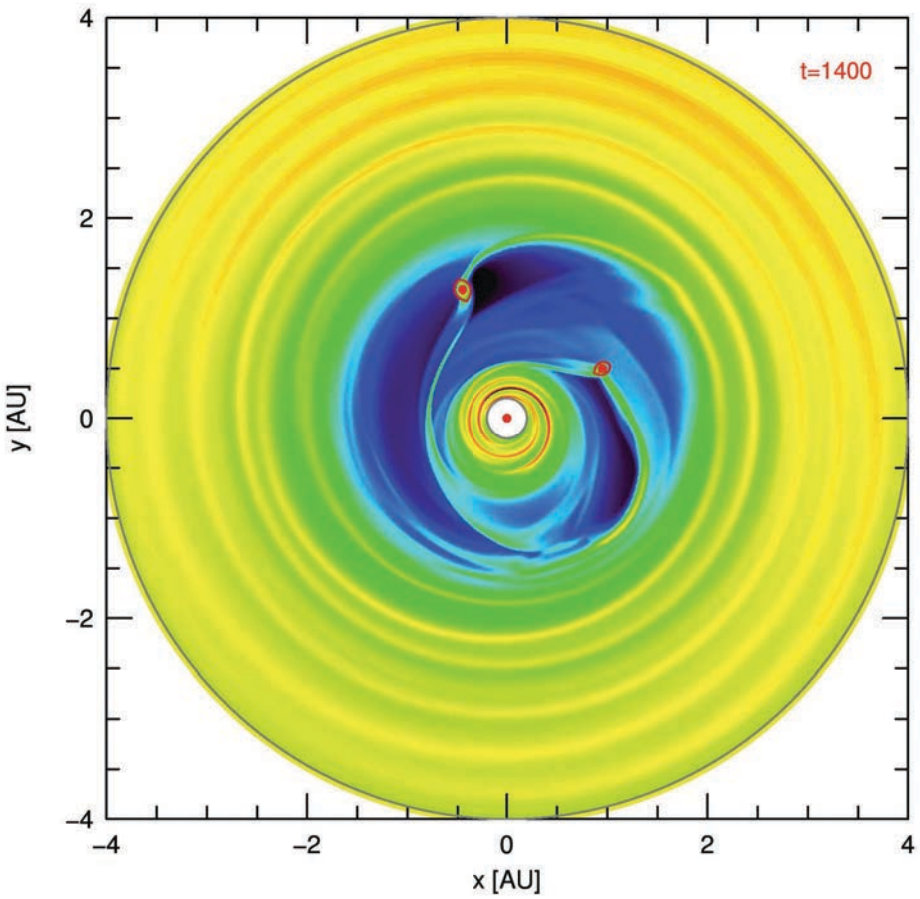

Figure 5.1: Disc-migration of two planets trapped in a 2:1 resonance, and the formation of a joint gap. The simulation is 2D, represented in a fixed Cartesian reference frame after 1400 orbits of the inner planet. Figure extracted from Kley and Nelson (2012).

and therefore represents the most likely outcome.

Note that in figure 5.1, there is still a flow of material from the outer disc to the inner one, mainly driven by the wake in the vicinity of the planets. Numerical simulations (Lubow and D'Angelo, 2006) indicate that the gap formation can significantly reduce this flow of material. In this case, the inner disc might accrete onto the star, significantly reducing the torque on the inner planet.

5.2 Resonant migration and orbital evolution

In this section we describe in details how the resonant migration can affect the orbital elements of the planets. We show that it can be associated with eccentricity and inclination growth. We first recall how the the disc affects the orbital elements and how we can model these effects. Then we use a more general model that takes into account first and second-order terms in eccentricities and inclinations. This development allows us to conduct a parametric study of the resonant migration. These results are presented in a paper published in MNRAS (Teyssandier and Terquem, 2014), in which we determine, analytically

and numerically, the conditions needed for a system of two migrating planets trapped in a 2:1 MMR to enter an inclination–type resonance, in which the inclinations can grow to high values, and eject the planets out of the plane of the disc. We also present a simple analytical solution for the eccentricities and semi-major axis in the case of of two planar orbits and strong eccentricity damping.

5.2.1 Probability of capture in resonance

In section 3.2.5, we have noted that the behaviour of a resonant angle resembles that of a pendulum. Close to the equilibrium point, the resonant angle librates, and circulates further away. To a given resonance, we can associate a *libration width*, which gives the size of the libration area. For a planet with a semi-major axis a_2, we note Δa the extent of the libration in terms of semi-major axis. Following Rein et al. (2010), we can get a first-order estimate of the possibility of capture in resonance for a migrating planet, based on simple physical considerations. If we consider that the planet is migrating inward at a constant rate on a timescale t_a, it can capture an inner planet in resonance, provided the time spent in the libration width is bigger than the period associated with the libration. More precisely, for a constant migration rate, the time Δt spent in the libration zone is given by

$$\Delta t = \frac{\Delta a}{a_2} t_a. \tag{5.1}$$

Hence, if $P_{\rm lib}$ is the libration period, resonant capture is possible as long as

$$t_a > \frac{a_2}{\Delta a} P_{\rm lib}. \tag{5.2}$$

The variation Δa can be related to the variation of the mean motion by Kepler's third law, to give:

$$\frac{2}{3}\Delta n = \frac{n_2}{a_2}\Delta a, \tag{5.3}$$

and for a resonant system, Δn can be directly related to $2\pi/P_{\rm lib}$, such as the resonant capture condition reads:

$$t_a > \frac{P_{\rm lib}^2}{P_2}. \tag{5.4}$$

where P_2 is the period of the outer planet.

However, expressing $P_{\rm lib}$ as a function of the orbital parameters is not trivial (see, e.g., Rein and Papaloizou, 2009). Quillen (2006) used a Hamiltonian model to study the probability of capture into mean motion resonance by a migrating planet, and give a simple expression for the minimum migration timescale that permits capture. Precisely, she showed that resonant capture can occur if the migration timescale t_a satisfies, in the case of the 2:1 MMR:

$$t_a \gtrsim 0.4 \mu^{-4/3} P_2 \tag{5.5}$$

where μ is the outer planet to star mass ratio. The resonant capture of an inner planet by an outer migrating planet of $1\ M_{\rm J}$ at 5 AU is possible as long as the migration timescale of the latter is larger than 4.7×10^4 yr. Because the viscous timescale, on which type II migration is supposed to occur, is of the order of a few 10^5 yr, resonant capture is likely to happen.

5.2.2 Physics of the resonant migration

As we have seen in section 3.2.5, resonant conjunctions tend to stabilize near one apse, and therefore librate around 0° or 180°. If the outer planet is now migrating inward, the next conjunction will be located slightly after the stable longitude. The net tangential force that results from this configuration leads to a small exchange of angular momentum. This exchange acts to prevent the conjunction to depart from the stable longitude. Therefore, the resonant configuration is maintained and the inner planet migrates inward along with the outer one. A similar reasoning shows that an inner planet that is migrating outward can capture another planet exterior to its orbit in a MMR. In the solar system, outward migration of natural satellites due to tidal interaction with their giant planet host can explain the large number of resonant configurations, for example around Saturn (Goldreich, 1965). However, an inner planet migrating inward cannot drag along with it an outer planet, because commensurability cannot be maintained.

Even if the commensurability is maintained, the conjunction for a libration state of the relevant argument of resonance still tends to occur after longitude of the line of apse. Would the conjunction happen exactly at apocenter or pericenter, the transfer of angular momentum from apocenter to pericenter would be exactly compensated by the transfer from pericenter to apocenter. The net transfer of angular momentum would average out to zero over one orbit, and their would be no change of eccentricity. Here, the symmetry is broken by the migration of the outer planet, which causes the conjunction to occur away from the apse. The radial impulse that results from this configuration will act to increase the eccentricities.

To summarize, one can expect the net effect of resonant capture of an inner planet by an outer, migrating one, to maintain the resonant commensurability, while exciting the two eccentricities. As we will see, such process can also, under specific conditions, excite the inclinations to large values.

5.2.3 Damping of the orbital elements by the disc

We have mentioned in section 2.4.1.2 that under disc migration, the disc tends to damp the orbital eccentricities and inclinations. The eccentricity damping is often parametrized in the following way

$$\left|\frac{\dot{e}}{e}\right| = K \left|\frac{\dot{a}}{a}\right|, \tag{5.6}$$

where K is a dimensionless parameter. The orbital decay on the right-hand side occurs on a viscous timescale of a few 10^5 years. Numerical simulations have put constraints on K,

ranging between 1 and 100. For instance, Lee and Peale (2002) showed that the GJ 876 system can only be reproduced with $K \sim 100$, whereas 2D hydrodynamical simulations from Kley et al. (2004) indicate K of the order unity.

Results from hydrodynamical simulations (see, e.g., Snellgrove et al., 2001; Kley et al., 2004) have shown that a prescription can be used to model the migration, which reproduces the same results. This prescription consists in adding extra forces to an N-body code, which allows for faster computation. Precisely, let us define the two following forces per unit of mass:

$$\mathbf{\Gamma}_{\mathrm{d,a}} = -\frac{1}{t_m}\frac{\mathrm{d}\mathbf{r}}{\mathrm{d}t}, \tag{5.7}$$

$$\mathbf{\Gamma}_{\mathrm{d,e}} = -\frac{2}{t_e|\mathbf{r}|^2}\left(\frac{\mathrm{d}\mathbf{r}}{\mathrm{d}t}\cdot\mathbf{r}\right)\mathbf{r}, \tag{5.8}$$

where $\mathbf{r}$ is the orbital distance from the planet to the star, t_m parametrizes the orbital decay, and t_e the eccentricity damping timescale. It is possible to show, using the equations of section 3.2.1, that $\mathbf{\Gamma}_{\mathrm{d,a}}$ leads to an exponential damping of the semi-major axis, of the form

$$\frac{\mathrm{d}a}{\mathrm{d}t} = -\frac{2}{t_m}a, \tag{5.9}$$

while $\mathbf{\Gamma}_{\mathrm{d,e}}$ leads to an exponential damping of the eccentricity, of the form

$$\frac{\mathrm{d}e}{\mathrm{d}t} = -\frac{1}{t_e}e. \tag{5.10}$$

Note that $\mathbf{\Gamma}_{\mathrm{d,e}}$ also contributes to the evolution of the semi-major axis, adding a term of the form

$$\frac{\mathrm{d}a}{\mathrm{d}t} = -\frac{2}{t_e}ae^2. \tag{5.11}$$

The details of the calculation can be found in the appendix of Teyssandier and Terquem (2014). We remark that the orbital decays of a single planet actually occurs on a timescale $t_m/2$, and we define $t_a = t_m/2$ as the effective migration timescale.

5.3 Publication II - Evolution of eccentricity and orbital inclination of migrating planets in 2:1 mean motion resonance

As we have mentioned earlier in this chapter, the resonant capture of a planet while it migrates in a disc is a well-known mechanism, and has been applied to real planetary systems such as GJ 876 and HD 45364. However, these studies remained focused on the planar evolution of migrating planets, without taking into consideration the possibility of vertical motion. This can be justified by the fact that planets are expected to remain in their

thin disc will migrating. However, Thommes and Lissauer (2003) found that if the planets reach high eccentricities, an inclination–type resonance can be triggered, and the inclinations grow to large values, of the order of several tens of degrees. They concluded that this could be responsible for a high degree of non-coplanarity in planetary systems. Their results were further developed by Lee and Thommes (2009), and extended to higher-order resonances by Libert and Tsiganis (2009). These works showed that the onset of inclination–type resonance was only possible if the eccentricity damping caused by the disc occurred on a timescale of the order of, or larger than, the migration timescale. In addition, their results were mostly numerical, and an in-depth analytical understanding was lacking.

In the following publication, we study the evolution of a pair of planets under the combined effect of the 2:1 MMR and disc-migration. Our work contains both an analytical and a numerical part. In order to analytically model the resonant effects, we follow section 3.2.5, and use a disturbing function that contains all the resonant and secular terms up to, and including, the second order in eccentricities and inclinations. This disturbing function is tabulated in Murray and Dermott (1999). The disc-migration mechanism is modelled by the forces introduced in section 5.2.3 above. Numerical integration can be done for the motion of the two planets, using a N-body integrator with a Bulirsch–Stoer scheme. Using N-body simulation instead of hydrodynamical simulations is less computational expensive, and allow us to conduct a large number of simulations and map the parameter space.

Monthly Notices
of the
ROYAL ASTRONOMICAL SOCIETY

MNRAS **443,** 568–583 (2014) doi:10.1093/mnras/stu1137

Evolution of eccentricity and orbital inclination of migrating planets in 2:1 mean motion resonance

Jean Teyssandier[1]★ and Caroline Terquem[1,2]

[1]*Institut d'Astrophysique de Paris, UPMC Univ Paris 06, CNRS, UMR7095, 98 bis bd Arago, F-75014 Paris, France*
[2]*Department of Astrophysics, University of Oxford, Keble Road, Oxford OX1 3RH, UK*

Accepted 2014 June 5. Received 2014 May 16; in original form 2014 March 26

ABSTRACT

We determine, analytically and numerically, the conditions needed for a system of two migrating planets trapped in a 2:1 mean motion resonance to enter an inclination-type resonance. We provide an expression for the asymptotic equilibrium value that the eccentricity $e_{\rm i}$ of the inner planet reaches under the combined effects of migration and eccentricity damping. We also show that, for a ratio q of inner to outer masses below unity, $e_{\rm i}$ has to pass through a value $e_{\rm i,\,res}$ of the order of 0.3 for the system to enter an inclination-type resonance. Numerically, we confirm that such a resonance may also be excited at another, larger, value $e_{\rm i,\,res} \simeq 0.6$, as found by previous authors. A necessary condition for onset of an inclination-type resonance is that the asymptotic equilibrium value of $e_{\rm i}$ is larger than $e_{\rm i,\,res}$. We find that, for $q \leq 1$, the system cannot enter an inclination-type resonance if the ratio of eccentricity to semimajor axis damping time-scales $t_{\rm e}/t_{\rm a}$ is smaller than 0.2. This result still holds if only the eccentricity of the outer planet is damped and $q \lesssim 1$. As the disc/planet interaction is characterized by $t_{\rm e}/t_{\rm a} \sim 10^{-2}$, we conclude that excitation of inclination through the type of resonance described here is very unlikely to happen in a system of two planets migrating in a disc.

Key words: celestial mechanics – planets and satellites: dynamical evolution and stability – planetary systems.

1 INTRODUCTION

At the time of writing, 98 extrasolar multiple-planet systems have been detected by radial velocity surveys and 420 by the *Kepler* mission (Lissauer et al. 2014; Rowe et al. 2014). A significant fraction of these systems contain planet pairs in or near a 2:1 mean motion resonance (MMR; Lissauer et al. 2011; Fabrycky et al. 2012, see also Petrovich, Malhotra & Tremaine 2013).

Capture in MMR is thought to be the result of convergent migration of planets (Snellgrove, Papaloizou & Nelson 2001). Several studies (Lee & Peale 2002; Beaugé, Ferraz-Mello & Michtchenko 2003; Lee 2004; Kley et al. 2005), focusing on the dynamics of the two planets in 2:1 MMR in the system GJ 876, were published soon after the discovery of this system (Marcy et al. 2001). They assume coplanar orbits and focus on explaining the unusual fact that the orbits of the two planets librate about apsidal alignment in this system (as opposed to anti-alignment in the Io–Europa system). The evolution of planetary systems in MMR has also been studied with three-dimensional simulations (Thommes & Lissauer 2003; Lee & Thommes 2009; Libert & Tsiganis 2009). It has been found that a system of planets in an eccentricity-type resonance may enter an inclination-type resonance if the eccentricity of the inner planet becomes large enough. In this context, very high orbital inclinations can be reached starting from nearly coplanar configurations.

Studies of resonant inclination excitation are important as this mechanism has been proposed to explain the fact that some extrasolar planets have an orbit which is inclined with respect to the stellar equatorial plane.

Other processes which have been put forward to produce such an inclination include interactions between the planet and a companion (Fabrycky & Tremaine 2007; Wu, Murray & Ramsahai 2007; Chatterjee et al. 2008; Naoz et al. 2011; Wu & Lithwick 2011), misalignment of the disc in which the planet forms (Bate, Lodato & Pringle 2010; Batygin 2012; Terquem 2013), tilting of the stellar spin axis due to interaction with the disc (Foucart & Lai 2011; Lai, Foucart & Lin 2011) or dynamical relaxation of a population of planets (Papaloizou & Terquem 2001).

The studies of inclination-type resonances published so far, which are numerical, have mapped to some extent the parameter space and have shown that the onset of resonant inclination excitation depends sensitively on the eccentricity damping time-scale and the ratio of the planets' masses.

★ E-mail: caroline.terquem@astro.ox.ac.uk

In this paper, we derive analytically a necessary condition for the onset of inclination-type resonance. The analysis has to be done to second order in eccentricities and inclinations. We also perform numerical simulations to investigate the regime of high eccentricities. We now review eccentricity- and inclination-type resonances before giving an outline of the plan of the paper.

1.1 Eccentricity- and inclination- type resonances

In this paper, we are interested in the case where convergent migration of two planets has led to capture into a 2:1 MMR. First-order eccentricity-type resonance involves only the resonant arguments $2\lambda_o - \lambda_i - \varpi_{i,o}$, where $\lambda_{i,o}$ and $\varpi_{i,o}$ are the mean longitudes and longitudes of pericentres of the inner and outer planets, respectively, and is not associated with a variation of the inclinations (see Section 2.2 below). Inclination-type resonance is of second order and involves the resonant arguments $4\lambda_o - 2\lambda_i - 2\Omega_{i,o}$ and $4\lambda_o - 2\lambda_i - \Omega_i - \Omega_o$, where $\Omega_{i,o}$ are the longitudes of ascending nodes of the planets. As shown by Thommes & Lissauer (2003), it requires the eccentricity of the inner planet to reach relatively large values to be excited.

Depending on the eccentricities and masses of the planets, stable eccentricity-type resonances can be (Beaugé et al. 2003; Lee 2004):

(i) symmetric with both resonant arguments librating about 0° (and $\varpi_o - \varpi_i$ librating about 0°, i.e. the apsidal lines are aligned and conjunction occurs when the planets are near pericentre),

(ii) antisymmetric with the resonant arguments librating about 0° and 180°, respectively (and $\varpi_o - \varpi_i$ librating about 180°, i.e. the apsidal lines are anti-aligned and conjunction occurs when one planet is near pericentre and the other near apocentre),

(iii) asymmetric with the resonant arguments librating about angles far from 0° and 180°.

Resonances are stable if the distance between the planets at conjunctions stays large enough. To understand the physics of resonance, let us consider the case of conjunction occurring when the planets are near an apse, i.e. librating about 0° or 180°. In that case, the tangential force exerted by one planet on to the other integrates to zero over an orbit and there is no exchange of angular momentum. The next conjunction therefore occurs at the same longitude. However, if the outer planet is migrating inwards (over a time-scale much longer than the orbital period), the conjunction occurs slightly away from the stable longitude. In that case, there is a net tangential force which results in the planets exchanging angular momentum in such a way that subsequent conjunctions will be closer to the stable longitude. Therefore, commensurability is maintained and the inner planet is pushed inwards (Goldreich 1965; Peale 1976). It can also be shown that during the migration process the radial perturbative force between the planets tends to increase their eccentricities (Lissauer, Peale & Cuzzi 1984).

If the eccentricities are small, the net tangential force exerted by one planet on to the other is small, and therefore, the transfer of angular momentum between the two planets is weak. However, in that case, the radial force is much more effective in changing the orientation (causing the regression) of the line of apses and therefore in maintaining the orientation of the apses with the conjunction longitude (Peale 1976; Greenberg 1977). The eccentricity-type resonance therefore exists even for small eccentricities.

For inclination-type resonances, conjunctions librate about the longitude of a node of one planet. There is however no resonance for low inclinations. This is because although the orientation of the lines of nodes can be more easily varied when the inclination is small, the normal perturbative force between the planets, which tends to vary the orientation of the lines of nodes, becomes smaller when the inclination decreases (Greenberg 1977).

1.2 Plan of the paper

In Section 2, we develop an analysis, valid to second order in eccentricities and inclinations, of a system of two planets embedded in a disc and in 2:1 MMR. We give an expression of the disturbing function in Section 2.1, write Lagrange's planetary equations in Section 2.2 and explain how migration and eccentricity damping are included in Section 2.3. We assume that the semimajor axis and the eccentricity of the outer planet are damped by interaction with the disc, and consider both the case where the eccentricity of the inner planet is damped and the case where it is not. In Section 2.4, we derive a necessary condition for the onset of inclination-type resonance. We find that, for a ratio q of inner mass to outer mass below unity, the eccentricity of the inner planet has to reach $e_{i,\,res} \sim 0.3$ for an inclination-type resonance to be excited. This cannot be achieved for $t_{ei}/t_a < 0.2$, where t_{ei} and t_a are the time-scales over which the eccentricity of the inner planet and the semimajor axis of the outer planet are damped. We also find that the onset of the inclination-type resonance requires the eccentricity of the outer planet to reach a critical value $e_{o,\,res}$. In Section 3, we present the results of N-body simulations. We write the equations of motion which are solved in the code in Section 3.1 and give the initial setting in Section 3.2. In Section 3.3, we describe three illustrative cases corresponding to three different values of the eccentricity damping time-scale in the case where the eccentricities of both planets are damped over the same time-scale t_e. We compare numerical and analytical results in Section 3.4, investigate how the onset of inclination-type resonance depends on q and t_e/t_a in Section 3.5 and study the influence of varying parameters in Section 3.6. In Section 3.7, we consider the case where eccentricity damping affects only the outer planet. The effect of inclination damping is discussed in Section 3.8. These simulations confirm the analysis and show that there is another, larger, value of $e_{i,\,res} \simeq 0.6$ (which was found by Thommes & Lissauer 2003). The simulations also show that the onset of inclination-type resonance requires the eccentricity of the outer planet to reach $e_{o,\,res} \sim 0.2$ when $q \lesssim 1$. The resonant argument ϕ_2 librates about 180° or 0° (while ϕ_1 librates about 0°) depending on whether the system enters an inclination-type resonance with $e_{i,\,res} \simeq 0.3$ or 0.6, respectively. Finally, in Section 4 we summarize and discuss our results.

2 ANALYSIS OF THE RESONANCE

2.1 Disturbing function

We consider two planets of masses m_i and m_o orbiting a star of mass $m_\star$. The subscripts 'i' and 'o' refer to the inner and outer planets, respectively. The orbital elements λ_i, a_i, e_i, I_i, ϖ_i and Ω_i denote the mean longitude, semimajor axis, eccentricity, inclination, longitude of pericentre and longitude of ascending node of the planet of mass m_i, with same quantities with subscript 'o' for the planet of mass m_o. We suppose that the two planets are close to or in a 2:1 mean motion commensurability, i.e. the ratio of the mean motions, n_i/n_o, is close or equal to 2. The dynamics is therefore dominated by the resonant and secular terms in the disturbing function, since all the other terms are short period and average out to zero over the orbital periods.

The perturbing functions for the inner and outer planets can be written under the form (Murray & Dermott 1999)

$$\langle \mathcal{R}_\mathrm{i} \rangle = \frac{Gm_\mathrm{o}}{a_\mathrm{o}} \left(\left\langle \mathcal{R}_\mathrm{D}^\mathrm{sec} \right\rangle + \left\langle \mathcal{R}_\mathrm{D}^\mathrm{res} \right\rangle + \alpha \langle \mathcal{R}_\mathrm{E} \rangle \right), \tag{1}$$

$$\langle \mathcal{R}_\mathrm{o} \rangle = \frac{Gm_\mathrm{i}}{a_\mathrm{o}} \left(\left\langle \mathcal{R}_\mathrm{D}^\mathrm{sec} \right\rangle + \left\langle \mathcal{R}_\mathrm{D}^\mathrm{res} \right\rangle + \frac{1}{\alpha^2} \langle \mathcal{R}_\mathrm{I} \rangle \right), \tag{2}$$

where G is the constant of gravitation, $\alpha \equiv a_\mathrm{i}/a_\mathrm{o}$, $\left\langle \mathcal{R}_\mathrm{D}^\mathrm{sec} \right\rangle$ and $\left\langle \mathcal{R}_\mathrm{D}^\mathrm{res} \right\rangle$ are the secular and resonant contributions to the direct part of the disturbing function, respectively, $\langle \mathcal{R}_\mathrm{E} \rangle$ is the indirect part due to an external perturber and $\langle \mathcal{R}_\mathrm{I} \rangle$ is the indirect part due to an internal perturber. The brackets indicate that the quantities are time averaged. Note that there is no secular contribution to $\langle \mathcal{R}_\mathrm{E} \rangle$ and $\langle \mathcal{R}_\mathrm{I} \rangle$.

When an expansion of the perturbing function in the orbital elements is carried out, the lowest orders at which eccentricities and inclinations appear are the first and second, respectively, and at second order, there are no terms in which eccentricities and inclinations are coupled. To study the inclination-type resonance, second-order terms in eccentricities need to be included. The expansion of the perturbing function to second order is (Murray & Dermott 1999)

$$\begin{aligned} \left\langle \mathcal{R}_\mathrm{D}^\mathrm{sec} \right\rangle = {} & K_1 \left(e_\mathrm{i}^2 + e_\mathrm{o}^2 \right) + K_2 e_\mathrm{i} e_\mathrm{o} \cos\left(\varpi_\mathrm{i} - \varpi_\mathrm{o} \right) \\ & + K_3 \left(s_\mathrm{i}^2 + s_\mathrm{o}^2 \right) + K_4 s_\mathrm{i} s_\mathrm{o} \cos\left(\Omega_\mathrm{i} - \Omega_\mathrm{o} \right), \end{aligned} \tag{3}$$

$$\begin{aligned} \left\langle \mathcal{R}_\mathrm{D}^\mathrm{res} \right\rangle = {} & e_\mathrm{i} f_1 \cos\phi_1 + e_\mathrm{o} f_2 \cos\phi_2 + e_\mathrm{i}^2 f_3 \cos\phi_3 \\ & + e_\mathrm{i} e_\mathrm{o} f_4 \cos\phi_4 + e_\mathrm{o}^2 f_5 \cos\phi_5 + s_\mathrm{i}^2 f_6 \cos\phi_6 \\ & + s_\mathrm{i} s_\mathrm{o} f_7 \cos\phi_7 + s_\mathrm{o}^2 f_8 \cos\phi_8, \end{aligned} \tag{4}$$

$$\langle \mathcal{R}_\mathrm{E} \rangle = -2 e_\mathrm{o} \cos\phi_2, \tag{5}$$

$$\langle \mathcal{R}_\mathrm{I} \rangle = -\frac{1}{2} e_\mathrm{o} \cos\phi_2, \tag{6}$$

where $s_{\mathrm{i,\,o}} = \sin\left(I_{\mathrm{i,\,o}}/2 \right)$, and the $f_i\,(i = 1, \ldots, 8)$ and $K_i\,(i = 1, \ldots, 4)$ are expressed in term of the Laplace coefficients and α. Their expression is given in Appendix A. The resonant angles $\phi_i\,(i = 1, \ldots, 8)$ are defined by

$$\phi_1 = 2\lambda_\mathrm{o} - \lambda_\mathrm{i} - \varpi_\mathrm{i}, \tag{7}$$

$$\phi_2 = 2\lambda_\mathrm{o} - \lambda_\mathrm{i} - \varpi_\mathrm{o}, \tag{8}$$

$$\phi_3 = 4\lambda_\mathrm{o} - 2\lambda_\mathrm{i} - 2\varpi_\mathrm{i}, \tag{9}$$

$$\phi_4 = 4\lambda_\mathrm{o} - 2\lambda_\mathrm{i} - \varpi_\mathrm{o} - \varpi_\mathrm{i}, \tag{10}$$

$$\phi_5 = 4\lambda_\mathrm{o} - 2\lambda_\mathrm{i} - 2\varpi_\mathrm{o}, \tag{11}$$

$$\phi_6 = 4\lambda_\mathrm{o} - 2\lambda_\mathrm{i} - 2\Omega_\mathrm{i}, \tag{12}$$

$$\phi_7 = 4\lambda_\mathrm{o} - 2\lambda_\mathrm{i} - \Omega_\mathrm{i} - \Omega_\mathrm{o}, \tag{13}$$

$$\phi_8 = 4\lambda_\mathrm{o} - 2\lambda_\mathrm{i} - 2\Omega_\mathrm{o}. \tag{14}$$

2.2 Lagrange's planetary equations

When the perturbing function is expanded to second order in the eccentricities and inclinations, Lagrange equations can be written as follows:

$$\frac{\mathrm{d}a_\beta}{\mathrm{d}t} = \frac{2}{n_\beta a_\beta} \frac{\partial \left\langle \mathcal{R}_\beta \right\rangle}{\partial \lambda_\beta}, \tag{15}$$

$$\frac{\mathrm{d}e_\beta}{\mathrm{d}t} = \frac{-1}{n_\beta a_\beta^2 e_\beta} \frac{\partial \left\langle \mathcal{R}_\beta \right\rangle}{\partial \varpi_\beta}, \tag{16}$$

$$\frac{\mathrm{d}\varpi_\beta}{\mathrm{d}t} = \frac{1}{n_\beta a_\beta^2 e_\beta} \frac{\partial \left\langle \mathcal{R}_\beta \right\rangle}{\partial e_\beta}, \tag{17}$$

$$\begin{aligned} \frac{\mathrm{d}\lambda_\beta}{\mathrm{d}t} = {} & n_\beta + \frac{1}{n_\beta a_\beta^2} \left(-2a_\beta \frac{\partial \left\langle \mathcal{R}_\beta \right\rangle}{\partial a_\beta} \right. \\ & \left. + \frac{e_\beta}{2} \frac{\partial \left\langle \mathcal{R}_\beta \right\rangle}{\partial e_\beta} + \tan\frac{I_\beta}{2} \frac{\partial \left\langle \mathcal{R}_\beta \right\rangle}{\partial I_\beta} \right), \end{aligned} \tag{18}$$

$$\frac{\mathrm{d}\Omega_\beta}{\mathrm{d}t} = \frac{1}{n_\beta a_\beta^2 \sin I_\beta} \frac{\partial \left\langle \mathcal{R}_\beta \right\rangle}{\partial I_\beta}, \tag{19}$$

$$\frac{\mathrm{d}I_\beta}{\mathrm{d}t} = \frac{-1}{n_\beta a_\beta^2 \sin I_\beta} \frac{\partial \left\langle \mathcal{R}_\beta \right\rangle}{\partial \Omega_\beta}, \tag{20}$$

where $\beta = \mathrm{i}, \mathrm{o}$. In equation (18), the derivative with respect to a_β has to be carried out by ignoring the fact that the angles $\phi_i\,(i = 1, \ldots, 8)$ depend on a_β through λ_i and λ_o (Roy 1978). We define a time-scale T such that

$$T = n_{\mathrm{o}0}^{-1} \frac{m_\star}{m_\mathrm{i}}, \tag{21}$$

where the subscript '0' denotes initial value. We consider planets with masses $m_{\mathrm{i,\,o}} \ll m_\star$, so that the mean motions are approximated by $n_{\mathrm{i,o}} = \left(Gm_\star / a_{\mathrm{i,o}}^3 \right)^{1/2}$.

Using the expression of the perturbing function given by equations (1)–(6), we can rewrite Lagrange equations (15)–(20) in the following dimensionless form:

$$\frac{\mathrm{d}a_\mathrm{i}}{\mathrm{d}\tau} = \mathcal{C}_\mathrm{i} 2a_\mathrm{i} \left[e_\mathrm{i} F_1 + e_\mathrm{o} F_2 - e_\mathrm{o} 2\alpha \sin\phi_2 + F_3 + \mathcal{O}(3) \right], \tag{22}$$

$$\frac{\mathrm{d}a_\mathrm{o}}{\mathrm{d}\tau} = \mathcal{C}_\mathrm{o}(-4a_\mathrm{o}) \left[e_\mathrm{i} F_1 + e_\mathrm{o} F_2 - \frac{e_\mathrm{o}}{2\alpha^2} \sin\phi_2 + F_3 + \mathcal{O}(3) \right], \tag{23}$$

$$\frac{\mathrm{d}e_\mathrm{i}}{\mathrm{d}\tau} = \mathcal{C}_\mathrm{i} \left[-F_1 + \mathcal{O}(2) \right], \tag{24}$$

$$\frac{\mathrm{d}e_\mathrm{o}}{\mathrm{d}\tau} = \mathcal{C}_\mathrm{o} \left[-F_2 + \frac{1}{2\alpha^2} \sin\phi_2 + \mathcal{O}(2) \right], \tag{25}$$

$$\begin{aligned} \frac{\mathrm{d}\varpi_\mathrm{i}}{\mathrm{d}\tau} = {} & \mathcal{C}_\mathrm{i} \left[\frac{1}{e_\mathrm{i}} f_1 \cos\phi_1 + 2 f_3 \cos\phi_3 + \frac{e_\mathrm{o}}{e_\mathrm{i}} f_4 \cos\phi_4 + 2K_1 \right. \\ & \left. + K_2 \frac{e_\mathrm{o}}{e_\mathrm{i}} \cos\left(\varpi_\mathrm{i} - \varpi_\mathrm{o} \right) + \mathcal{O}(1) \right], \end{aligned} \tag{26}$$

$$\frac{\mathrm{d}\varpi_\mathrm{o}}{\mathrm{d}\tau} = \mathcal{C}_\mathrm{o}\left[\frac{1}{e_\mathrm{o}}\left(f_2 - \frac{1}{2\alpha^2}\right)\cos\phi_2 + \frac{e_\mathrm{i}}{e_\mathrm{o}} f_4 \cos\phi_4 + 2 f_5 \cos\phi_5 + 2K_1 + K_2\frac{e_\mathrm{i}}{e_\mathrm{o}}\cos\left(\varpi_\mathrm{i} - \varpi_\mathrm{o}\right) + \mathcal{O}(1)\right], \tag{27}$$

$$\frac{\mathrm{d}\lambda_\mathrm{i}}{\mathrm{d}\tau} = \mathcal{C}_\mathrm{i}\left[\frac{1}{\alpha}\frac{m_\star}{m_\mathrm{o}} + \frac{1}{2}e_\mathrm{i} f_1 \cos\phi_1 + 4\alpha e_\mathrm{o}\cos\phi_2 - \Delta + \mathcal{O}(2)\right], \tag{28}$$

$$\frac{\mathrm{d}\lambda_\mathrm{o}}{\mathrm{d}\tau} = \mathcal{C}_\mathrm{o}\left[\frac{m_\star}{m_\mathrm{i}} + 2e_\mathrm{i} f_1 \cos\phi_1 + \frac{1}{2}e_\mathrm{o}\left(5 f_2 + \frac{3}{2\alpha^2}\right)\cos\phi_2 + \Delta + \mathcal{O}(2)\right], \tag{29}$$

$$\frac{\mathrm{d}\Omega_\mathrm{i}}{\mathrm{d}\tau} = \frac{\mathcal{C}_\mathrm{i}}{2}\left[K_3 + \frac{1}{2}\frac{s_\mathrm{o}}{s_\mathrm{i}}\left(K_4\cos(\Omega_\mathrm{i} - \Omega_\mathrm{o}) + f_7\cos\phi_7\right) + f_6\cos\phi_6 + \mathcal{O}(1)\right], \tag{30}$$

$$\frac{\mathrm{d}\Omega_\mathrm{o}}{\mathrm{d}\tau} = \frac{\mathcal{C}_\mathrm{o}}{2}\left[K_3 + \frac{1}{2}\frac{s_\mathrm{i}}{s_\mathrm{o}}\left(K_4\cos(\Omega_\mathrm{i} - \Omega_\mathrm{o}) + f_7\cos\phi_7\right) + f_8\cos\phi_8 + \mathcal{O}(1)\right], \tag{31}$$

$$\frac{\mathrm{d}I_\mathrm{i}}{\mathrm{d}\tau} = \mathcal{C}_\mathrm{i}\left[\frac{1}{2}\frac{s_\mathrm{o}}{c_\mathrm{i}}\left(K_4\sin(\Omega_\mathrm{i} - \Omega_\mathrm{o}) - f_7\sin\phi_7\right) - \frac{s_\mathrm{i}}{c_\mathrm{i}} f_6\sin\phi_6 + \mathcal{O}(2)\right], \tag{32}$$

$$\frac{\mathrm{d}I_\mathrm{o}}{\mathrm{d}\tau} = \mathcal{C}_\mathrm{o}\left[-\frac{1}{2}\frac{s_\mathrm{i}}{c_\mathrm{o}}\left(K_4\sin(\Omega_\mathrm{i} - \Omega_\mathrm{o}) + f_7\sin\phi_7\right) - \frac{s_\mathrm{o}}{c_\mathrm{o}} f_8\sin\phi_8 + \mathcal{O}(2)\right], \tag{33}$$

where $\tau = t/T$, $c_{\mathrm{i,\,o}} = \cos\left(I_{\mathrm{i,\,o}}/2\right)$, $\mathcal{C}_\mathrm{i} = \left(a_{\mathrm{o}0}/a_\mathrm{o}\right)^{3/2} m_\mathrm{o}/(m_\mathrm{i}\sqrt{\alpha})$, $\mathcal{C}_\mathrm{o} = \left(a_{\mathrm{o}0}/a_\mathrm{o}\right)^{3/2}$,

$$F_1 = f_1\sin\phi_1 + 2e_\mathrm{i} f_3\sin\phi_3 + e_\mathrm{o} f_4\sin\phi_4 - K_2 e_\mathrm{o}\sin\left(\varpi_\mathrm{i} - \varpi_\mathrm{o}\right), \tag{34}$$

$$F_2 = f_2\sin\phi_2 + 2e_\mathrm{o} f_5\sin\phi_5 + e_\mathrm{i} f_4\sin\phi_4 + K_2 e_\mathrm{i}\sin\left(\varpi_\mathrm{i} - \varpi_\mathrm{o}\right), \tag{35}$$

$$F_3 = 2s_\mathrm{i}^2 f_6\sin\phi_6 + 2s_\mathrm{i}s_\mathrm{o} f_7\sin\phi_7 + 2s_\mathrm{o}^2 f_8\sin\phi_8 \tag{36}$$

and

$$\Delta = 2\alpha\left(e_\mathrm{i}\frac{\partial f_1}{\partial\alpha}\cos\phi_1 + e_\mathrm{o}\frac{\partial f_2}{\partial\alpha}\cos\phi_2\right). \tag{37}$$

Note that, with a perturbing function expanded to second order in eccentricities and inclinations, the rate of change of $\varpi_{\mathrm{i,\,o}}$ and $\Omega_{\mathrm{i,\,o}}$ can be obtained only to zeroth order in eccentricities and inclinations.

The only orbital elements which are relevant when the orbits are coplanar are $a_{\mathrm{i,\,o}}$, $e_{\mathrm{i,\,o}}$, $\varpi_{\mathrm{i,\,o}}$ and $\lambda_{\mathrm{i,\,o}}$. At the order at which the above equations are valid, we note that their evolution is decoupled from that of $\Omega_{\mathrm{i,\,o}}$ and $I_{\mathrm{i,\,o}}$. Similarly, when the semimajor axes do not vary significantly, the variations of $\Omega_{\mathrm{i,\,o}}$ and $I_{\mathrm{i,\,o}}$ are decoupled from that of the other orbital elements.

2.3 Modelling of migration and eccentricity damping

We are interested in the case where the two planets capture each other in an MMR, which happens for instance if the outer planet migrates inwards due to its interaction with the disc at least as fast as the inner planet. To model this, we artificially decrease the semimajor axis of the outer planet by adding a damping term $-a_\mathrm{o}/\tau_\mathrm{a}$ on the right-hand side of equation (23), where τ_a is the (dimensionless) migration time-scale that can be freely specified. In principle, due to its interaction with the disc, the inner planet also migrates independently of the outer one. For simplicity, this is not taken into account here. It would not change the results presented in this paper as long as the inner planet were not migrating faster than the outer one. In this context, the time-scale τ_a can be thought of as the time-scale over which the outer planet migrates with respect to the inner one. Note that a diminution of a_i, although not being added artificially, will be induced by that of a_o (see below).

Interaction with the disc also leads to damping of the planets eccentricities. This is taken into account by adding a damping term $-e_\mathrm{i}/\tau_\mathrm{ei}$ and $-e_\mathrm{o}/\tau_\mathrm{eo}$ on the right-hand side of equations (24) and (25), respectively, where τ_ei and τ_eo are the (dimensionless) eccentricity damping time-scales. Eccentricity damping does in turn contribute to the damping of the semimajor axis by a term $-2a_{\mathrm{i,\,o}}e_{\mathrm{i,\,o}}^2/\tau_{\mathrm{ei,\,o}}$ (see Appendix B).

With migration and eccentricity damping taken into account, equations (22)–(25) become

$$\frac{\mathrm{d}a_\mathrm{i}}{\mathrm{d}\tau} = \mathcal{C}_\mathrm{i}2a_\mathrm{i}\left[e_\mathrm{i}F_1 + e_\mathrm{o}F_2 - e_\mathrm{o}2\alpha\sin\phi_2 + F_3 + \mathcal{O}(3)\right] - \frac{2a_\mathrm{i}e_\mathrm{i}^2}{\tau_\mathrm{ei}}, \tag{38}$$

$$\frac{\mathrm{d}a_\mathrm{o}}{\mathrm{d}\tau} = \mathcal{C}_\mathrm{o}(-4a_\mathrm{o})\left[e_\mathrm{i}F_1 + e_\mathrm{o}F_2 - \frac{e_\mathrm{o}}{2\alpha^2}\sin\phi_2 + F_3 + \mathcal{O}(3)\right] - \frac{a_\mathrm{o}}{\tau_\mathrm{a}} - \frac{2a_\mathrm{o}e_\mathrm{o}^2}{\tau_\mathrm{eo}}, \tag{39}$$

$$\frac{\mathrm{d}e_\mathrm{i}}{\mathrm{d}\tau} = \mathcal{C}_\mathrm{i}\left[-F_1 + \mathcal{O}(2)\right] - \frac{e_\mathrm{i}}{\tau_\mathrm{ei}}, \tag{40}$$

$$\frac{\mathrm{d}e_\mathrm{o}}{\mathrm{d}\tau} = \mathcal{C}_\mathrm{o}\left[-F_2 + \frac{1}{2\alpha^2}\sin\phi_2 + \mathcal{O}(2)\right] - \frac{e_\mathrm{o}}{\tau_\mathrm{eo}}. \tag{41}$$

In this paper, we will consider either the case $\tau_\mathrm{ei} = \tau_\mathrm{eo}$ or the case of infinite τ_ei (no damping on the inner planet) and finite τ_eo.

Inclination damping has not been included, as it is not relevant here (see Section 3.8).

2.4 Necessary condition for the onset of inclination-type resonance

In this section, we derive a necessary condition for a pair of planets in 2:1 MMR to enter an inclination-type resonance. We assume that the planets have captured each other in an exact resonance, so that

$\alpha \equiv a_\mathrm{i}/a_\mathrm{o} = 2^{-2/3}$ remains constant in time. In that case, it is useful to note that $2\alpha = 1/(2\alpha^2)$. We also define the mass ratio $q \equiv m_\mathrm{i}/m_\mathrm{o}$.

In this context, equations (38) and (39) can be combined to give

$$\frac{2}{a_\mathrm{i}}\frac{\mathrm{d}a_\mathrm{i}}{\mathrm{d}\tau} + \frac{1}{q\sqrt{\alpha}}\frac{1}{a_\mathrm{o}}\frac{\mathrm{d}a_\mathrm{o}}{\mathrm{d}\tau} = -\frac{1}{q\sqrt{\alpha}\tau_\mathrm{a}} - 4\frac{e_\mathrm{i}^2}{\tau_\mathrm{ei}} - \frac{2}{q\sqrt{\alpha}}\frac{e_\mathrm{o}^2}{\tau_\mathrm{eo}}. \quad (42)$$

Using $\alpha = a_\mathrm{i}/a_\mathrm{o}$, we obtain the following differential equation for a_i and a_o:

$$\left(1 + 2q\sqrt{\alpha}\right)\frac{1}{a_\mathrm{i,o}}\frac{\mathrm{d}a_\mathrm{i,o}}{\mathrm{d}\tau} = -\frac{1}{\tau_\mathrm{a}} - 4q\sqrt{\alpha}\frac{e_\mathrm{i}^2}{\tau_\mathrm{ei}} - 2\frac{e_\mathrm{o}^2}{\tau_\mathrm{eo}}. \quad (43)$$

To first order in eccentricities, the solutions are

$$a_\mathrm{i,o}(\tau) = a_\mathrm{i0,o0}\,\mathrm{e}^{-\tau/\left[(1+2q\sqrt{\alpha})\tau_\mathrm{a}\right]}. \quad (44)$$

This shows that, when $q = 0$, i.e. when the inner planet is treated as a test particle, both planets migrate at a rate τ_a. When q is non-zero, the migration is slightly slowed down by the mutual interaction between the two planets.

2.4.1 Eccentricity-type resonance

As a first step, we calculate the equilibrium values reached by the eccentricities under the combined effects of migration and eccentricity damping when the system is in an eccentricity-type resonance with zero inclinations.

Equations (40) and (41) can be combined to give

$$e_\mathrm{i}\frac{\mathrm{d}e_\mathrm{i}}{\mathrm{d}\tau} + \frac{e_\mathrm{i}^2}{\tau_\mathrm{ei}} + \frac{1}{q\sqrt{\alpha}}\left(e_\mathrm{o}\frac{\mathrm{d}e_\mathrm{o}}{\mathrm{d}\tau} + \frac{e_\mathrm{o}^2}{\tau_\mathrm{eo}}\right)$$
$$= -\mathcal{C}_\mathrm{i}\left[e_\mathrm{i}F_1 + e_\mathrm{o}F_2 - \frac{e_\mathrm{o}}{2\alpha^2}\sin\phi_2 + \mathcal{O}(3)\right]. \quad (45)$$

When the inclinations are zero, $F_3 = 0$. Using equations (39) and (43), we can then rewrite equation (45) under the form

$$\frac{\mathrm{d}e_\mathrm{i}^2}{\mathrm{d}\tau} + \frac{1+q\sqrt{\alpha}}{1+2q\sqrt{\alpha}}\frac{4e_\mathrm{i}^2}{\tau_\mathrm{ei}} + \frac{1}{q\sqrt{\alpha}}\left[\frac{\mathrm{d}e_\mathrm{o}^2}{\mathrm{d}\tau} + \frac{1+q\sqrt{\alpha}}{1+2q\sqrt{\alpha}}\frac{2e_\mathrm{o}^2}{\tau_\mathrm{eo}}\right]$$
$$= \frac{1}{\tau_\mathrm{a}(1+2q\sqrt{\alpha})}. \quad (46)$$

When $q \to 0$, e_o has to satisfy $\mathrm{d}e_\mathrm{o}^2/\mathrm{d}\tau + 2e_\mathrm{o}^2/\tau_\mathrm{eo} = 0$, which means that e_o is damped to zero whereas, in this limit, e_i reaches the equilibrium value $[\tau_\mathrm{ei}/(4\tau_\mathrm{a})]^{1/2}$.

2.4.1.1 Finite values of τ_ei and τ_eo: When the eccentricities of both planets are damped and $q \leq 1$, i.e. the outer planet is at least a massive as the inner one, we expect the eccentricity of the outer planet to grow less than that of the inner planet. We therefore neglect the terms involving e_o in equation (46), which then leads to the following equilibrium value (corresponding to $\tau \gg \tau_\mathrm{ei}$) for e_i:

$$e_\mathrm{i,eq} = \frac{1}{2}\left(\frac{\tau_\mathrm{ei}/\tau_\mathrm{a}}{1+q\sqrt{\alpha}}\right)^{1/2}. \quad (47)$$

In Fig. 1, we plot $e_\mathrm{i,\,eq}$ as a function of q for $\tau_\mathrm{ei}/\tau_\mathrm{a} = 1$, 0.2 and 0.1.

The numerical simulations presented in the next section confirm that neglecting e_o in equation (46) is a valid approximation for the parameters of interest in this paper. The numerical values found for $e_\mathrm{i,\,eq}$ also agree very well with that given by equation (47), as indicated in Fig. 6.

2.4.1.2 Finite value of τ_eo and $\tau_\mathrm{ei} \to \infty$: In some conditions that will be discussed in Section 3.7, damping due to tidal interaction with the disc acts only on the eccentricity of the outer planet, not on that of the inner planet. In that case, as the planets are in resonance, e_i still reaches an equilibrium value. This is shown by equation (24) in which $F_1 = 0$ when the resonant angles librate about 0° or 180°. By substituting $\mathrm{d}e_\mathrm{i}^2/\mathrm{d}\tau = 0$ and $\tau_\mathrm{ei} \to \infty$ in equation (46), we obtain the following equilibrium value (corresponding to $\tau \gg \tau_\mathrm{eo}$) for e_o:

$$e_\mathrm{o,eq} = \left[\frac{q\sqrt{\alpha}\;\tau_\mathrm{eo}/\tau_\mathrm{a}}{2\left(1+q\sqrt{\alpha}\right)}\right]^{1/2}. \quad (48)$$

In Fig. 2, we plot $e_\mathrm{o,\,eq}$ as a function of q for $\tau_\mathrm{eo}/\tau_\mathrm{a} = 0.2$, 0.05 and 0.01.

The numerical values found for $e_\mathrm{o,\,eq}$ agree very well with that given by equation (48), as indicated in Fig. 10.

2.4.2 Inclination-type resonance

We now calculate the values $e_\mathrm{i,\,res}$ and $e_\mathrm{o,\,res}$ that e_i and e_o, respectively, have to reach for the inclinations to start growing. A necessary condition for the system to enter an inclination-type resonance when both τ_ei and τ_eo are finite is $e_\mathrm{i,\,res} < e_\mathrm{i,\,eq}$, where $e_\mathrm{i,\,eq}$ is given by equation (47). When $\tau_\mathrm{ei} \to \infty$, a necessary condition is $e_\mathrm{o,\,res} < e_\mathrm{o,\,eq}$, where $e_\mathrm{o,\,eq}$ is given by equation (48).

Inclination-type resonance can be reached only after an eccentricity-type resonance has been established (Thommes & Lissauer 2003) and therefore all the resonant angles librate about some values. Due to eccentricity damping, libration of the resonant angles is actually offset from a fixed value (generally 0° or 180°) by a term of the order of $e_\mathrm{i}/\tau_\mathrm{ei}$ or $e_\mathrm{o}/\tau_\mathrm{eo}$ (Goldreich & Schlichting 2014). Because of the $1/\tau_\mathrm{ei}$ or $1/\tau_\mathrm{eo}$ factor, this term is much smaller than those retained in the analysis here, so that we will ignore it. Therefore, the time-derivative of the resonant angles is close to zero. Equations (7), (8), (12) and (14) then yield

$$\frac{\mathrm{d}\varpi_\mathrm{i}}{\mathrm{d}\tau} = \frac{\mathrm{d}\varpi_\mathrm{o}}{\mathrm{d}\tau} = \frac{\mathrm{d}\Omega_\mathrm{i}}{\mathrm{d}\tau} = \frac{\mathrm{d}\Omega_\mathrm{o}}{\mathrm{d}\tau}, \quad (49)$$

i.e. the nodes and pericentres all precess at the same rate. In the inclination-type resonance we consider here, as shown in the numerical simulations presented below, the resonant angles ϕ_6, ϕ_7 and ϕ_8 librate about 180°, 0° and 180°, respectively, and $\Omega_\mathrm{i} - \Omega_\mathrm{o}$ librates about 180°, in agreement with Thommes & Lissauer (2003). In the analysis that follows, we therefore use $\phi_7 = 0°$, $\phi_6 = 180°$, $\phi_8 = 180°$ and $\Omega_\mathrm{i} - \Omega_\mathrm{o} = 180°$.

We first write $\mathrm{d}\Omega_\mathrm{i}/\mathrm{d}\tau = \mathrm{d}\Omega_\mathrm{o}/\mathrm{d}\tau$ by equating equations (30) and (31). This leads to an algebraic equation for $s_\mathrm{i}/s_\mathrm{o}$. Using the fact that $f_6 = f_8$ and $K_3 - f_8 = (-K_4 + f_7)/2$ (see Appendix A), we can write the solution of this equation as

$$\frac{s_\mathrm{o}}{s_\mathrm{i}} = q\sqrt{\alpha}. \quad (50)$$

For values of q less than unity, the inclination of the inner planet is more easily excited than that of the outer planet. Note that the ratio of the inclinations does not depend on τ_a nor τ_ei or τ_eo.

We now write $\mathrm{d}\varpi_\mathrm{o}/\mathrm{d}\tau = \mathrm{d}\Omega_\mathrm{o}/\mathrm{d}\tau$ by equating equations (27) and (31) and $\mathrm{d}\varpi_\mathrm{i}/\mathrm{d}\tau = \mathrm{d}\Omega_\mathrm{i}/\mathrm{d}\tau$ by equating equations (26) and (30). In the resulting set of equations, we replace $s_\mathrm{i}/s_\mathrm{o}$ by the value found above. This set of two equations can now be solved to calculate $e_\mathrm{i,\,res}$ and $e_\mathrm{o,\,res}$, which are the values of e_i and e_o, respectively, when the inclination-type resonance is reached. This calculation requires the knowledge of ϕ_1 and ϕ_2 at the time when the inclination-type

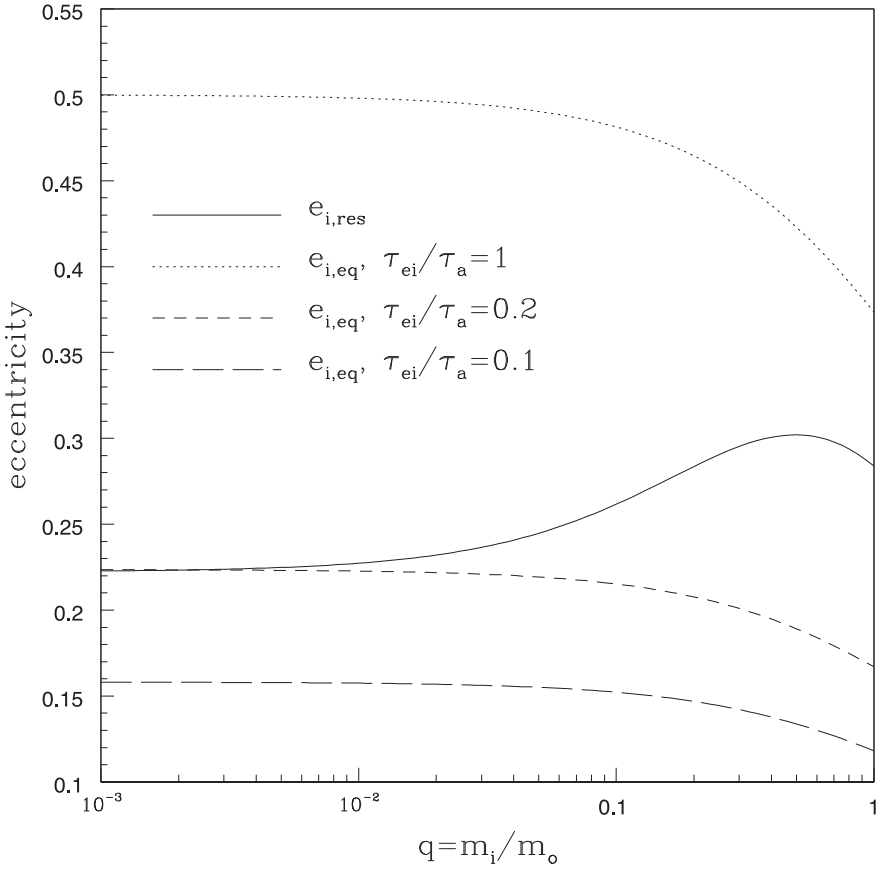

Figure 1. Solid line: eccentricity $e_{\rm i,\,res}$ of the inner planet when the system enters an inclination-type resonance versus q in logarithmic scale. This curve corresponds to equation (51) with $\cos^2\phi_2 = 1$. Also shown is the equilibrium eccentricity for $\tau_{\rm ei}/\tau_{\rm a} = 0.1$ (long dashed line), $\tau_{\rm ei}/\tau_{\rm a} = 0.2$ (short dashed line) and $\tau_{\rm ei}/\tau_{\rm a} = 1$ (dotted line). These curves correspond to equation (47). The system cannot enter an inclination-type resonance when $\tau_{\rm ei}/\tau_{\rm a} < 0.2$.

resonance is triggered. For two planets in 2:1 MMR, it has been found (e.g. Lee & Peale 2002) that, in general, $(\phi_1, \phi_2) = (0^\circ, 180^\circ)$ or $(0^\circ, 0^\circ)$, depending on whether the eccentricities are small or large, respectively ('large' meaning that second-order terms in the eccentricities are not negligible). Fixing $\phi_1 = 0^\circ$ and $\cos^2\phi_2 = 1$, we obtain

$$e_{\rm i,res} = \frac{-f_1\Delta_3 + \left(f_2 - \frac{1}{2\alpha^2}\right)(f_4 + K_2)}{-(f_4 + K_2)^2 + \Delta_3\Delta_4}, \tag{51}$$

$$e_{\rm o,res} = \frac{f_1(f_4 + K_2) - \Delta_4\left(f_2 - \frac{1}{2\alpha^2}\right)}{\Delta_3\Delta_4 - (f_4 + K_2)^2}\cos\phi_2, \tag{52}$$

where we have defined $\Delta_1 = K_3 + q\sqrt{\alpha}(f_7 - K_4)/2 - f_6$, $\Delta_2 = K_3 + (f_7 - K_4)/(2q\sqrt{\alpha}) - f_8$, $\Delta_3 = 2f_5 + 2K_1 - \Delta_2/2$ and $\Delta_4 = 2f_3 + 2K_1 - \Delta_1/2$.

We note that $e_{\rm i,\,res}$ and $e_{\rm o,\,res}$ do not depend on the damping time-scales. When $q \to 0$, equations (51) and (52) give $e_{\rm i,\,res} = f_1/[(K_3 - f_6)/2 - 2(f_3 + K_1)] \simeq 0.22$ and $e_{\rm o,\,res} = 0$, respectively.

Equation (52) gives a positive value of the eccentricity for $\phi_2 = 0^\circ$ but a negative value for $\phi_2 = 180^\circ$. When ϕ_2 evolves from libration about 0° to libration about 180°, the apsidal lines evolve from being aligned to being anti-aligned, i.e. the pericentre of the outer orbit is changed to apocentre. In that case, for the equation of the outer ellipse which was used in deriving Lagrange's equations to be preserved, $e_{\rm o}$ should be changed to $-e_{\rm o}$. The value of $e_{\rm o}$ corresponding to $\phi_2 = 180^\circ$ is therefore the opposite as that given by equation (52).

In Fig. 1, we plot the eccentricity $e_{\rm i,\,res}$ given by equation (51) as a function of q. For q varying between 0.1 and 1, we see that $e_{\rm i,\,res} \simeq 0.3$. The eccentricity $e_{\rm o,\,res}$ given by equation (52) is shown in Fig. 2. We see that $e_{\rm o,\,res}$ varies much more with q than $e_{\rm i,\,res}$.

The numerical results presented in the next section show that there are two regimes in which the system may enter an inclination-type resonance: (i) a *small eccentricity* regime, which is described by the analysis above (although the value of $e_{\rm o,\,res}$ found numerically is about twice as large as that found analytically), and (ii) a *large eccentricity* regime, in which inclination-type resonance is obtained for $e_{\rm i,\,res} \simeq 0.6$ and $e_{\rm o,\,res} \simeq 0.2$ for $q \lesssim 1$. The large eccentricity regime cannot be captured by the analysis above, as our equations are not developed up to a sufficient order in $e_{\rm i,\,o}$. As noted above, by expanding the perturbing function to second order in $e_{\rm i,\,o}$, we obtain $\mathrm{d}\varpi_{\rm i,o}/\mathrm{d}t$ and $\mathrm{d}\Omega_{\rm i,o}/\mathrm{d}t$ to zeroth order only in $e_{\rm i,\,o}$.

When both $\tau_{\rm ei}$ and $\tau_{\rm eo}$ are finite, we can find the values of q and $\tau_{\rm ei}/\tau_{\rm a}$ for which inclination-type resonance may occur by writing the necessary condition $e_{\rm i,\,res} < e_{\rm i,\,eq}$. Using equations (47) and (51) and ignoring the (weak) variation of $e_{\rm i,\,res}$ with q, this leads to

$$\frac{\tau_{\rm ei}/\tau_{\rm a}}{1 + q\sqrt{\alpha}} > 4e_{\rm i,res}^2. \tag{53}$$

Note that the above condition is necessary but not sufficient, as we have not taken into account the fact that $e_{\rm o}$ must also reach $e_{\rm o,\,res}$ (we cannot write this condition as we have not calculated $e_{\rm o,\,eq}$ when $\tau_{\rm ei}$ is finite). Fig. 1 shows that the system cannot enter an inclination-type resonance when $\tau_{\rm ei}/\tau_{\rm a} < 0.2$. When q decreases, the inclination-type resonance is reached for shorter eccentricity

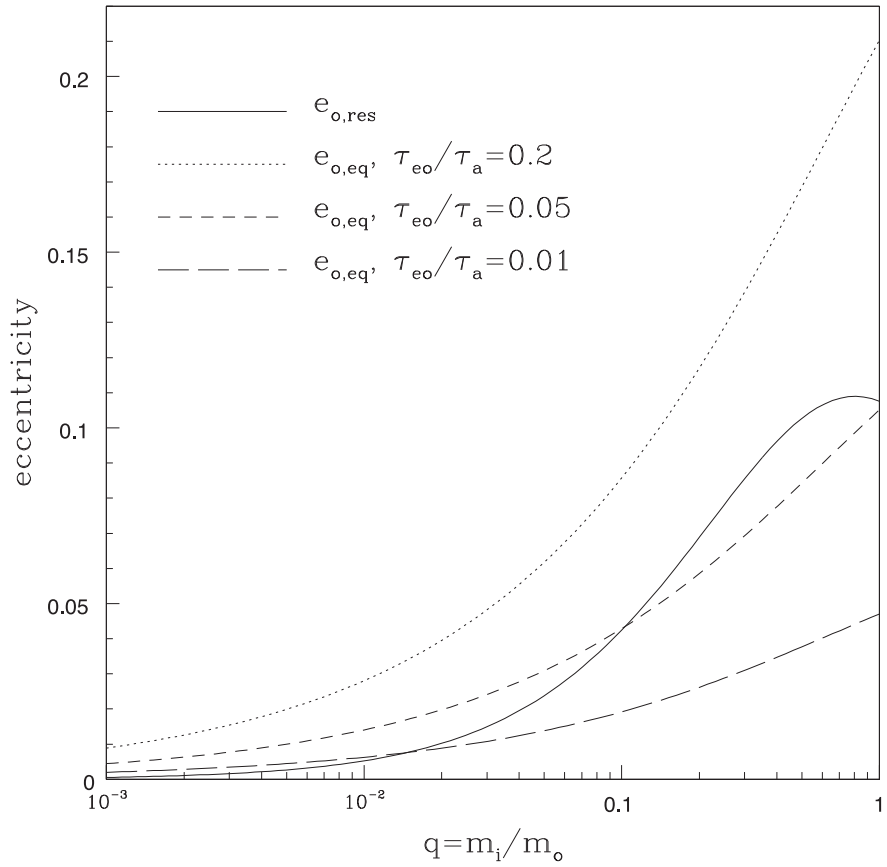

Figure 2. Solid line: eccentricity $e_{\mathrm{o,\,res}}$ of the outer planet when the system enters an inclination-type resonance versus q in logarithmic scale. This curve corresponds to equation (52) with $\cos^2\phi_2 = 1$. Also shown is the equilibrium eccentricity for $\tau_{\mathrm{ei}} \to \infty$ and $\tau_{\mathrm{eo}}/\tau_{\mathrm{a}} = 0.01$ (long dashed line), $\tau_{\mathrm{eo}}/\tau_{\mathrm{a}} = 0.05$ (short dashed line) and $\tau_{\mathrm{eo}}/\tau_{\mathrm{a}} = 0.2$ (dotted line). These curves correspond to equation (48). Note that the value of $e_{\mathrm{o,\,res}}$ found numerically for $q \lesssim 1$ is almost twice as large as that displayed here, being $\simeq 0.2$. In this context, and for $q \lesssim 1$, the system cannot enter an inclination-type resonance when $\tau_{\mathrm{eo}}/\tau_{\mathrm{a}} < 0.2$.

damping time-scales. This is expected as eccentricity is pumped up to higher values when q is smaller.

We will discuss condition (53) in more details in the next section, after deriving $e_{\mathrm{i,\,res}}$ from the numerical simulations.

When $\tau_{\mathrm{ei}} \to \infty$, a necessary condition for the system to enter an inclination-type resonance is $e_{\mathrm{o,\,res}} < e_{\mathrm{o,\,eq}}$. As can be seen from Fig. 2, and if we adopt for $q \lesssim 1$ the value of $e_{\mathrm{o,\,res}} \simeq 0.2$ found numerically, which is about twice as large as the value derived analytically, we find that the system cannot enter an inclination-type resonance when $\tau_{\mathrm{eo}}/\tau_{\mathrm{a}} < 0.2$.

3 NUMERICAL SIMULATIONS

The analysis presented above is valid only for small eccentricities. We now perform numerical simulations of a pair of migrating planets in the vicinity of a 2:1 MMR to extend the study to arbitrarily high eccentricities.

3.1 Equations of motion

We consider a system consisting of a primary star and two planets initially embedded in a gaseous disc surrounding the star. The planets undergo gravitational interaction with each other and the star and are acted on by tidal torques from the disc. To study the evolution of the system, we use the *N*-body code described in Papaloizou & Terquem (2001) in which we have added the effect of the disc torques (see also Terquem & Papaloizou 2007).

The equations of motion for the inner and outer planets are

$$\frac{\mathrm{d}^2\boldsymbol{r}_{\mathrm{i}}}{\mathrm{d}t^2} = -\frac{Gm_\star \boldsymbol{r}_{\mathrm{i}}}{|\boldsymbol{r}_{\mathrm{i}}|^3} - \frac{Gm_{\mathrm{o}}(\boldsymbol{r}_{\mathrm{i}} - \boldsymbol{r}_{\mathrm{o}})}{|\boldsymbol{r}_{\mathrm{i}} - \boldsymbol{r}_{\mathrm{o}}|^3} - \sum_{\gamma=\mathrm{i,o}} \frac{Gm_\gamma \boldsymbol{r}_\gamma}{|\boldsymbol{r}_\gamma|^3} + \boldsymbol{\Gamma}_{\mathrm{d,i}} + \boldsymbol{\Gamma}_{\mathrm{GR,i}}, \tag{54}$$

$$\frac{\mathrm{d}^2\boldsymbol{r}_{\mathrm{o}}}{\mathrm{d}t^2} = -\frac{Gm_\star \boldsymbol{r}_{\mathrm{o}}}{|\boldsymbol{r}_{\mathrm{o}}|^3} - \frac{Gm_{\mathrm{i}}(\boldsymbol{r}_{\mathrm{o}} - \boldsymbol{r}_{\mathrm{i}})}{|\boldsymbol{r}_{\mathrm{o}} - \boldsymbol{r}_{\mathrm{i}}|^3} - \sum_{\gamma=\mathrm{i,o}} \frac{Gm_\gamma \boldsymbol{r}_\gamma}{|\boldsymbol{r}_\gamma|^3} + \boldsymbol{\Gamma}_{\mathrm{d,o}} + \boldsymbol{\Gamma}_{\mathrm{GR,o}}, \tag{55}$$

where $\boldsymbol{r}_{\mathrm{i}}$ and $\boldsymbol{r}_{\mathrm{o}}$ denote the position vector of the inner and outer planets, respectively, and we have included the acceleration of the coordinate system based on the central star (third term on the right-hand side). Acceleration due to tidal interaction with the disc is dealt with through the addition of extra forces as in Papaloizou & Larwood (2000, see also Terquem & Papaloizou 2007),

$$\boldsymbol{\Gamma}_{\mathrm{d,i}} = -\frac{2}{t_{\mathrm{ei}}|\boldsymbol{r}_{\mathrm{i}}|^2}\left(\frac{\mathrm{d}\boldsymbol{r}_{\mathrm{i}}}{\mathrm{d}t}\cdot\boldsymbol{r}_{\mathrm{i}}\right)\boldsymbol{r}_{\mathrm{i}}, \tag{56}$$

$$\boldsymbol{\Gamma}_{\mathrm{d,o}} = -\frac{2}{t_{\mathrm{eo}}|\boldsymbol{r}_{\mathrm{o}}|^2}\left(\frac{\mathrm{d}\boldsymbol{r}_{\mathrm{o}}}{\mathrm{d}t}\cdot\boldsymbol{r}_{\mathrm{o}}\right)\boldsymbol{r}_{\mathrm{o}} - \frac{1}{t_{\mathrm{m}}}\frac{\mathrm{d}\boldsymbol{r}_{\mathrm{o}}}{\mathrm{d}t}, \tag{57}$$

where t_m, t_{eo} and t_{ei} are the time-scales over which the angular momentum of the outer planet, its eccentricity and the eccentricity of the inner planet, respectively, are damped through tidal interaction with the disc. As mentioned in Section 2.3, the $1/t_m$ term is applied to the outer planet only. We show in Appendix B that these forces do indeed lead to exponential damping of the eccentricities and outer semimajor axis. Note however that the migration time-scale t_m defined through equation (57) is equal to twice the semimajor axis damping time-scale defined through equation (39). In other words, $t_m = 2t_a$, where $t_a = \tau_a T$ and T is given by equation (21). For the eccentricity damping time-scales, we simply have that t_{ei} and t_{eo} defined through equations (56) and (57) are equal to $\tau_{ei} T$ and $\tau_{eo} T$, respectively, where τ_{ei} and τ_{eo} are the dimensionless damping time-scales defined in Section 2.3.

Relativistic effects are included through the following acceleration:

$$\boldsymbol{\Gamma}_{GR,i,o} = -\frac{6G^2 m_\star^2}{c^2} \frac{\boldsymbol{r}_{i,o}}{|\boldsymbol{r}_{i,o}|^4}, \tag{58}$$

with c being the speed of light. It is found that this term, which induces a precession of the arguments of pericentres, does not affect significantly the results. This is because the planets do not approach the star closely enough. For this reason also, tidal interaction between the planets and the star can be neglected.

The effect of inclination damping due to planet–disc interaction, which also has not been included here, will be discussed in Section 3.8 below.

3.2 Initial setting

In all the runs presented below, unless mentioned otherwise, we consider a one Jupiter-mass outer planet ($m_o = 1$ M$_J$) and start the two planets slightly outside a 2:1 MMR at $a_{i0} = 3.05$ au and $a_{o0} = 5$ au, corresponding to a period ratio of 2.1. The initial eccentricities and inclinations are small: $e_{i0} = e_{o0} = 5 \times 10^{-3}$, $I_{i0} = 0.^\circ 01$ and $I_{o0} = 0.^\circ 02$. The longitudes of pericentres and of ascending nodes are all equal to 0° initially. We fix $t_m = 1.4 \times 10^6$ yr which corresponds to a semimajor axis damping time-scale $t_a = 7 \times 10^5$ yr. This is roughly equal to the disc evolution time-scale at 3 au, as should be the case for type II migration. To start with, we fix for simplicity $t_{ei} = t_{eo} \equiv t_e$, i.e. $\tau_{ei} = \tau_{eo} \equiv \tau_e$, and consider different values of t_e ranging from $\sim 10^5$ to $\sim 10^6$ yr. In Section 3.7, we will consider $t_{ei} \to \infty$ and finite values of t_{eo}. The dependence of our results on the choice of initial conditions will be discussed in Section 3.6.

3.3 Illustrative cases

In this section, we illustrate the main features of the dynamical evolution of two planets migrating in 2:1 MMR as a function of the damping eccentricity time-scale. We consider strong, moderate and weak eccentricity damping, corresponding to $t_e/t_a \equiv \tau_e/\tau_a = 0.25$, 0.8 and 4, respectively. Here, the inner planet has a mass $m_i = 0.7$ M$_J$, so that the mass ratio is $q = 0.7$.

3.3.1 Strong eccentricity damping: no inclination-type resonance

We first consider the case $t_e = 1.75 \times 10^5$ yr, corresponding to $\tau_e/\tau_a = 0.25$. Fig. 3 shows the evolution of $a_{i,o}$, $e_{i,o}$, $I_{i,o}$, $\Delta\varpi = \varpi_i - \varpi_o$, $\Delta\Omega = \Omega_i - \Omega_o$, ϕ_1, ϕ_2, ϕ_6, ϕ_7 and ϕ_8 between 0 and 10^6 yr. Very quickly after the beginning of the simulation, the planets capture each other in a 2:1 eccentricity-type resonance. From equation (47), we expect the eccentricity of the inner planet to reach an equilibrium value $e_{i,eq} = 0.2$, in good agreement with the value observed in the simulation. At first, the resonant angles ϕ_1 and ϕ_2 librate about 0°. However, after about 8×10^5 yr, as the planets get closer to each other during their convergent migration, e_o starts to increase significantly while e_i decreases, and the value about which ϕ_2 librates switches rather abruptly to 180°, which is indicative of a regime with smaller eccentricities. As expected from the analysis, e_i does not become large enough for an inclination-type resonance to develop. Accordingly, the inclinations remain small and the resonant angles ϕ_6, ϕ_7 and ϕ_8, associated with inclination-type resonances, behave chaotically.

3.3.2 Moderate eccentricity damping: inclination-type resonance with small eccentricities

We now consider the case $t_e = 5.6 \times 10^5$ yr, corresponding to $\tau_e/\tau_a = 0.8$. The evolution of $a_{i,o}$, $e_{i,o}$, $I_{i,o}$, $\Delta\varpi$, $\Delta\Omega$ and the resonant angles between 0 and 4×10^6 yr are displayed in Fig. 4. In this case, equation (47) predicts that the eccentricity of the inner planet should reach an equilibrium value $e_{i,eq} = 0.35$, in good agreement with the numerical result. We see that, at first, e_i grows very quickly, until it reaches the equilibrium value. At the same time, ϕ_1 and ϕ_2 librate about 0°. Like in the previous case, after a certain time (here $t \simeq 3.2 \times 10^6$ yr), e_i starts decreasing while e_o gets larger, and the value about which ϕ_2 librates switches to 180°. When $e_i \simeq 0.3$, an inclination-type resonance starts to develop, in very good agreement with the expectation from equation (51). Accordingly, the resonant angles ϕ_6, ϕ_7 and ϕ_8 start librating about 180°, 0° and 180°, respectively, while $\Delta\Omega$ librates about 180°. The inclinations grow quickly, maintaining a ratio in agreement with equation (50). The inclination-type resonance is triggered when $e_o \simeq 0.18$, which is a bit larger than the value of 0.1 predicted by equation (52).

Note that, in this particular case, the inclination-type resonance occurs at $t \sim 3.5 \times 10^6$ yr, which is likely to be longer than the disc's lifetime.

We observe that the system does not enter an inclination-type resonance when e_i first reaches 0.3, at about $t = 2 \times 10^5$ yr. This is because at that point e_o is still smaller than $e_{o,res}$. For $q < 1$, e_o can reach $e_{o,res}$ only when the two planets get close enough during their convergent migration for the perturbation on to the outer planet to become significant.

3.3.3 Weak eccentricity damping: inclination-type resonance with large eccentricities

We finally consider the case $t_e = 2.8 \times 10^6$ yr, corresponding to $\tau_e/\tau_a = 4$. The evolution of $a_{i,o}$, $e_{i,o}$, $I_{i,o}$, $\Delta\varpi$, $\Delta\Omega$ and the resonant angles between 0 and 3×10^6 yr are displayed in Fig. 5. In this case, equation (47) predicts that the eccentricity of the inner planet should reach an equilibrium value $e_{i,eq} = 0.8$. As this is very large, the analysis presented in Section 2.4 is probably not valid. In any case, equilibrium is not attained during the time of the simulation. Here, ϕ_1 and ϕ_2 librate about 0° throughout the simulation, which is expected for a regime with high eccentricities. Both e_i and e_o grow from the beginning of the simulation. When $e_i \simeq 0.6$, at $t \simeq 1.2 \times 10^6$ yr, the system enters an inclination-type resonance, characterized by $\Delta\Omega$, ϕ_6, ϕ_7 and ϕ_8 librating about 180°, 180°, 0° and 180°, respectively. This case is similar to those investigated by Thommes & Lissauer (2003).

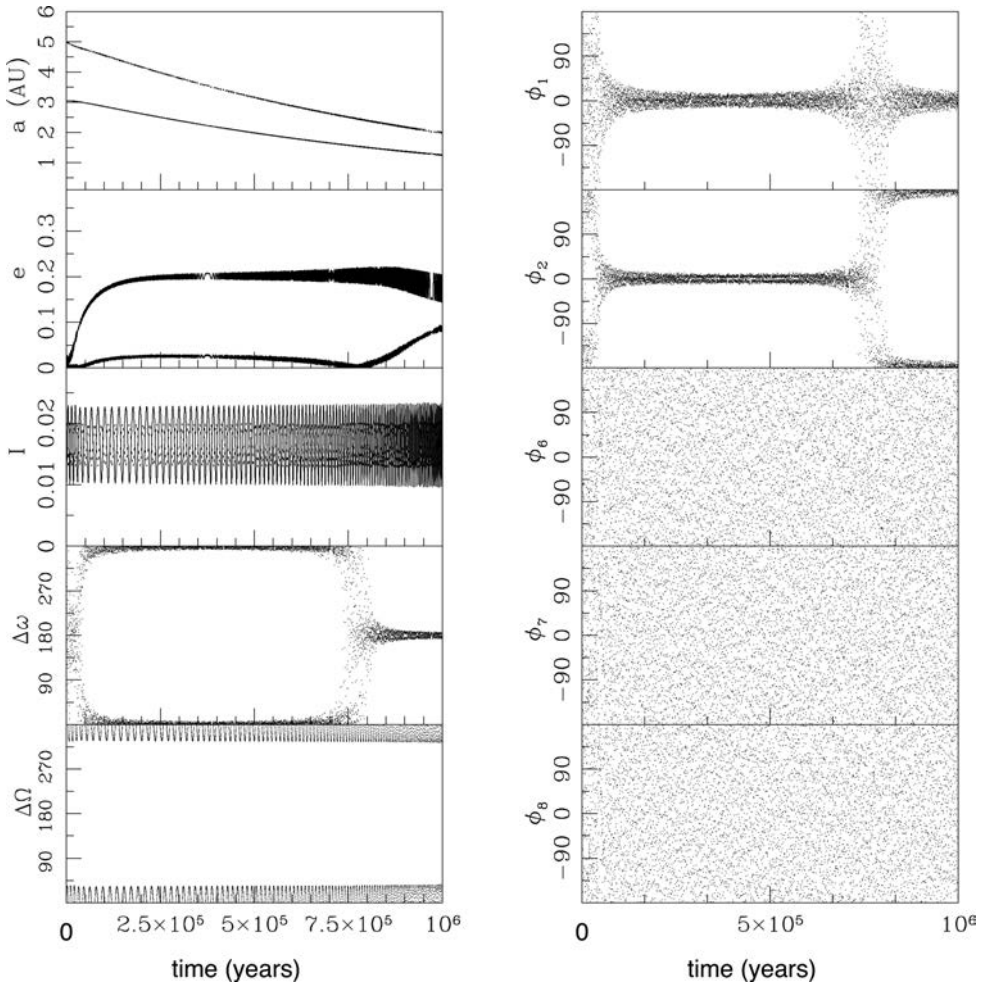

Figure 3. Evolution of a system in 2:1 MMR for $q = 0.7$ and $\tau_e/\tau_a = 0.25$ in the case $\tau_{ei} = \tau_{eo} \equiv \tau_e$. Left column, from top to bottom: semimajor axes (in au), eccentricities and inclinations of the two planets, $\Delta\varpi = \varpi_i - \varpi_o$ and $\Delta\Omega = \Omega_i - \Omega_o$ versus time (in years). Right column, from top to bottom: resonant angles ϕ_1, ϕ_2, ϕ_6, ϕ_7 and ϕ_8 versus time (in years). All the angles are given in degrees. In the plot displaying the eccentricities, the upper and lower curves represent e_i and e_o, respectively. Shortly after the beginning of the simulation, the planets are captured into an eccentricity-type resonance: e_i grows until it reaches $e_{i,\,eq} = 0.2$ and $\Delta\varpi$, ϕ_1 and ϕ_2 librate about 0°. After $t \simeq 8 \times 10^5$ yr, e_i starts decreasing while e_o gets larger, and the value about which ϕ_2 librates switches rather abruptly to 180°. Throughout the evolution, e_i stays too small to allow for inclination-type resonance. Accordingly, the inclinations remain small, the resonant angles ϕ_6, ϕ_7 and ϕ_8 behave chaotically and $\Delta\Omega = 0$ throughout the evolution.

We observe that the system does not enter an inclination-type resonance when e_i reaches 0.3 at about $t = 2 \times 10^5$ yr, as e_o is still smaller than $e_{o,\,res}$ at that time.

In the simulation reported here, the inclination of the outer planet stays smaller than the disc aspect ratio, so that migration is not interrupted. However, we expect the inclination to become larger at some later time, so that the outer planet loses contact with the disc and stops migrating.

3.4 Comparison with analytical results

In this section, we compare the numerical values of $e_{i,\,eq}$, $e_{i,\,res}$, $e_{o,\,res}$ and of the ratio s_o/s_i when the system is in an inclination-type resonance, with the analytical values given by equations (47), (51), (52) and (50), respectively.

3.4.1 Equilibrium eccentricity of the inner planet

In Section 2.4, we derived an analytical expression for the equilibrium value of e_i assuming e_o to be negligible compared to e_i. As can be seen from Figs 3 to 5, this approximation is at least marginally valid.

In Fig. 6, we compare the analytical value of $e_{i,\,eq}$ given by equation (47) with the results of the numerical integration. We consider two eccentricity damping time-scales, corresponding to $\tau_e/\tau_a = 0.5$ and 1, and different values of q ranging from 0.2 to 1. We obtain very good agreement between numerical and analytical results for these values of τ_e/τ_a, even for rather large values of $e_{i,\,eq} \sim 0.5$.

Equation (47) cannot be used for larger values of τ_e/τ_a as it would then give values of e_i too high for the second-order analysis to be valid. Anyway, as will be discussed below, larger values of τ_e/τ_a are not realistic in the context of planets migrating in discs.

3.4.2 Eccentricities of the planets when the system enters an inclination-type resonance

In the analysis conducted in Section 2.4, we found that inclination-type resonance would occur for $e_i \equiv e_{i,\,res} \sim 0.3$ (equation 51 and Fig. 1). As we have already noted, our analysis, which gives the rate

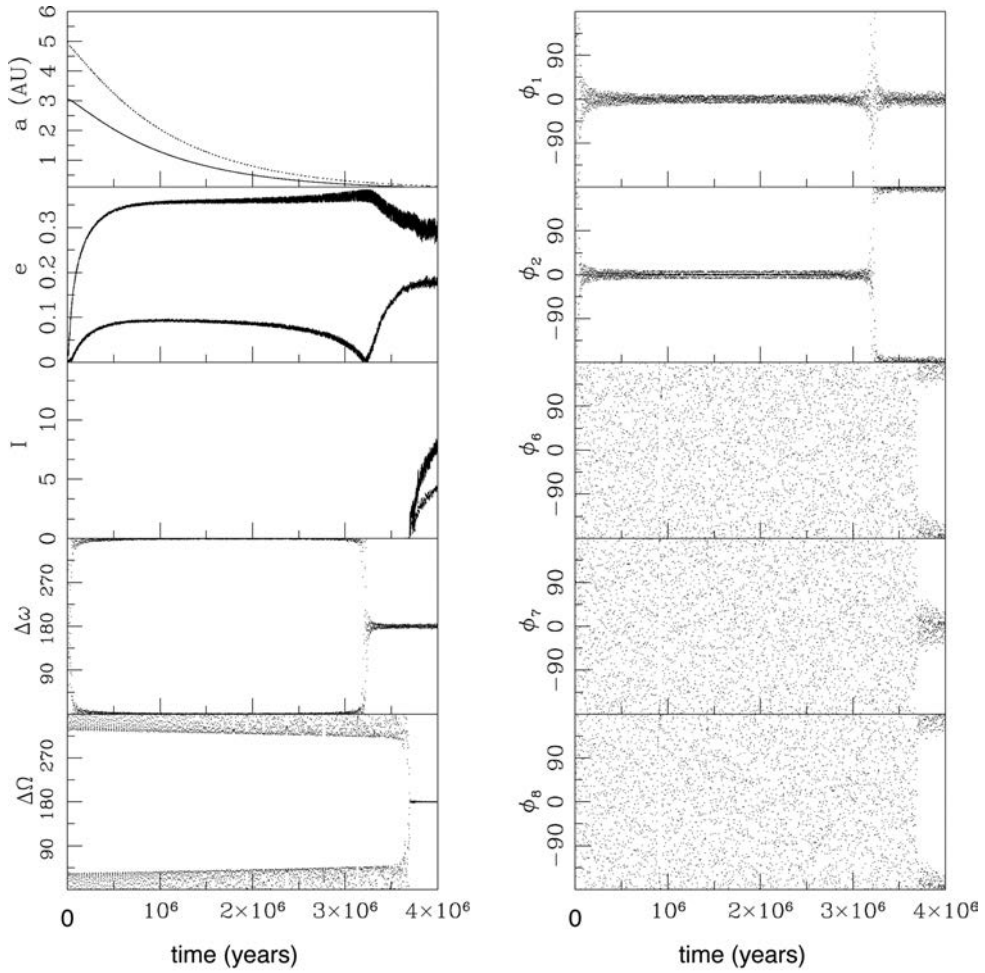

Figure 4. Same as Fig. 3 but for $\tau_e/\tau_a = 0.8$. In the plots displaying the eccentricities and inclinations, the upper curves represent e_i and I_i, respectively, whereas the lower curves represent e_o and I_o, respectively. Here again, shortly after the beginning of the simulation, the planets are captured into an eccentricity-type resonance: e_i grows until it reaches $e_{i,\,eq} = 0.35$ and $\Delta\varpi$, ϕ_1 and ϕ_2 librate about 0°. After $t \simeq 3.2 \times 10^6$ yr, e_i starts decreasing while e_o gets larger, and the value about which ϕ_2 librates switches to 180°. When $e_i \simeq 0.3$, an inclination-type resonance starts to develop. Accordingly, the resonant angles ϕ_6, ϕ_7 and ϕ_8 start librating about 180°, 0° and 180°, respectively, while $\Delta\Omega$ librates about 180°. The inclinations grow quickly.

of change of $\varpi_{i,\,o}$ and $\Omega_{i,\,o}$ only to zeroth order in $e_{i,\,o}$, is not valid in the regime of large eccentricities. The numerical simulations presented here do indeed confirm that there is a low-eccentricity regime with $e_{i,\,res} \simeq 0.3$, which corresponds to ϕ_1 and ϕ_2 librating about 0° and 180°, respectively. In addition, they show that there is a large eccentricity regime with $e_{i,\,res} \simeq 0.6$, which corresponds to ϕ_1 and ϕ_2 both librating about 0°.

The analysis also predicted that inclination-type resonance would occur for $e_o \equiv e_{o,\,res} \simeq 0.1$ for $q = 0.7$ (equation 52). This value should not be used in the regime $\phi_2 = 0$, as in that case e_i is large when the resonance is triggered and the equations are therefore not developed up to sufficient order in the eccentricities. In the low-eccentricity regime, the value found numerically for $e_{o,\,res}$, 0.18, is almost twice as large as the value derived analytically. In the large eccentricity regime, the simulations give a similar value of $e_{o,\,res} \sim 0.2$.

3.4.3 Evolution of the inclinations

After the system enters an inclination-type resonance, according to equation (50), the inclinations evolve while maintaining a constant ratio $I_o/I_i = q\sqrt{\alpha}$ (where we have used $s_{i,\,o} \simeq I_{i,\,o}/2$, valid for small inclinations).

Numerically, we find this relation to be reasonably well satisfied. This is illustrated for $\tau_e/\tau_a = 0.8$ and $q = 0.7$ in Fig. 7, which shows the evolution of I_o/I_i after the system has entered an inclination-type resonance. We have also verified that the ratio of the inclinations is essentially independent of τ_a and τ_e for the values of τ_e/τ_a for which the analysis is valid.

3.5 Conditions for the onset of inclination-type resonance

In Section 2.4, we derived a necessary condition (equation 53) for the system to enter an inclination-type resonance, which can be written as $\tau_e/\tau_a > 4e_{i,res}^2\left(1 + q\sqrt{\alpha}\right)$. With $e_{i,\,res} = 0.3$, the right-hand side of this inequality varies between 0.35 and 0.65 as q varies between 0 and 1, whereas it varies between 1.4 and 2.6 for $e_{i,\,res} = 0.6$. We now investigate whether this condition agrees with numerical results.

We performed a series of runs with q =0.2, 0.3, 0.4, 0.7, 1 and 2 and τ_e/τ_a =0.2, 0.4, 0.5, 0.6, 0.7, 0.8, 1, 1.4, 2, 2.4, 4, 10 and 20. We integrated the equations for up to $t = 6 \times 10^6$ yr, which is longer than or comparable to the age of the disc. For each run, we indicate

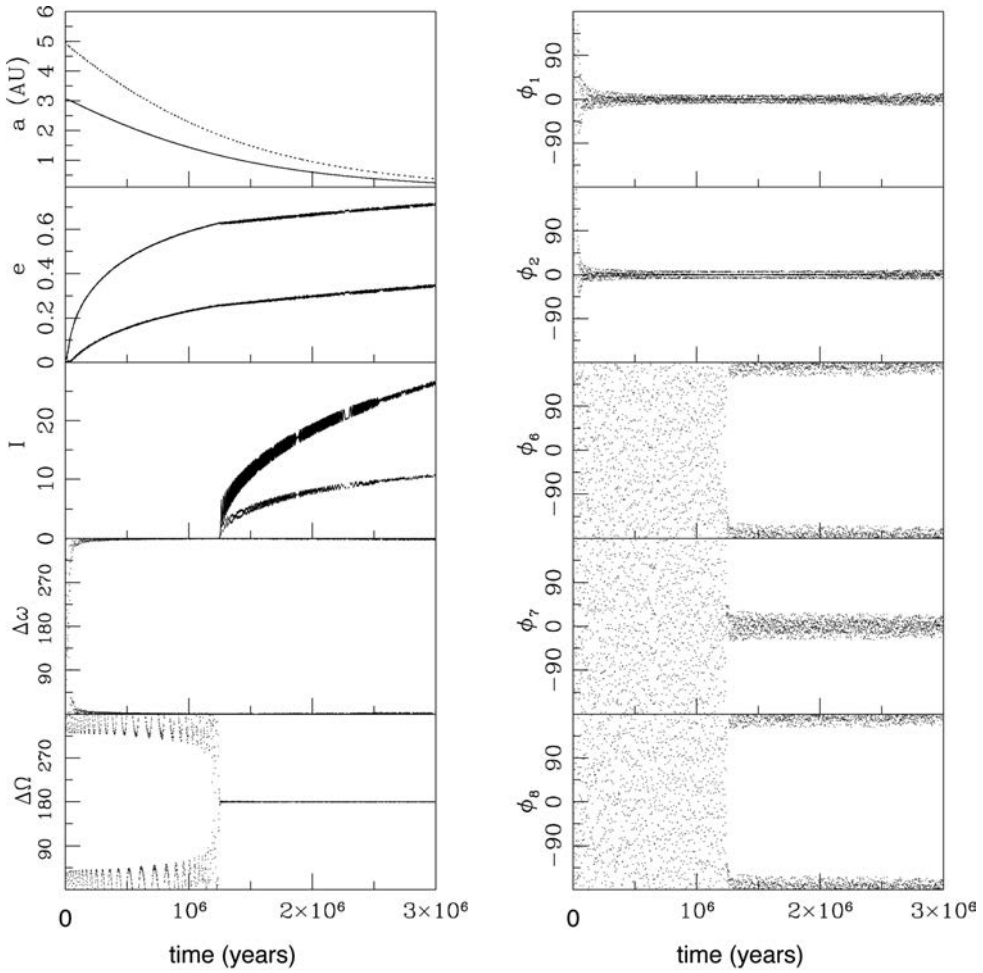

Figure 5. Same as Fig. 3 but for $\tau_e/\tau_a = 4$. In the plots displaying the eccentricities and inclinations, the upper curves represent e_i and I_i, respectively, whereas the lower curves represent e_o and I_o, respectively. Here again, shortly after the beginning of the simulation, the planets are captured into an eccentricity-type resonance and e_i and e_o grow. In the present case, ϕ_1 and ϕ_2 librate about 0° throughout the simulation. When $e_i \sim 0.6$, the system enters an inclination-type resonance and $\Delta\Omega$, ϕ_6, ϕ_7 and ϕ_8 start librating about 180°, 180°, 0° and 180°, respectively, while the inclinations start growing.

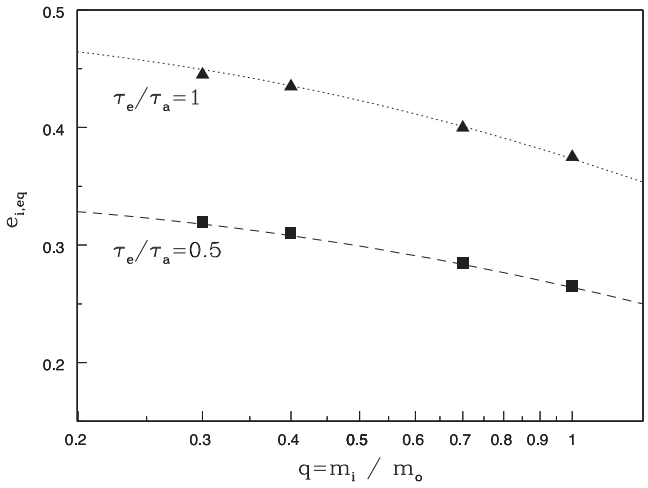

Figure 6. Equilibrium eccentricity of the inner planet versus mass ratio q for $\tau_e/\tau_a = 1$ (dotted line, triangles), and $\tau_e/\tau_a = 0.5$ (dashed line, squares) in the case $\tau_{ei} = \tau_{eo} \equiv \tau_e$. The lines represent $e_{i,eq}$, calculated using equation (47) whereas the symbols represent the numerical values.

in Fig. 8 whether the system entered an inclination-type resonance or not. Crosses represent runs in which there was no inclination-type resonance, open and filled symbols represent runs in which there was an inclination-type resonance with $(\phi_1, \phi_2) = (0°, 180°)$ or $(\phi_1, \phi_2) = (0°, 0°)$, respectively. Circles and triangles represent systems that entered an inclination-type resonance before or after $t = 3 \times 10^6$ yr, respectively.

On this diagram, the lower dashed line is the curve $\tau_e/\tau_a = 4e_{i,res}^2\left(1 + q\sqrt{\alpha}\right)$ (analytical condition 53) with $e_{i,\,res} = 0.3$. For $q \leq 0.7$, this curve approximates very well the boundary between systems which do not enter an inclination-type resonance and systems which do enter such a resonance with $(\phi_1, \phi_2) = (0°, 180°)$, i.e. while maintaining small eccentricities. These results confirm the analytical result $e_{i,\,res} \simeq 0.3$ (equation 51 and Fig. 1). We note that, as q gets larger (heavier inner planet), it takes longer for an inclination-type resonance to be excited, which is consistent with the fact that it takes longer for the eccentricity of the inner planet to grow. This probably explains why systems above the dashed curve have not entered an inclination-type resonance for the largest values of q. We would expect these systems to enter such a resonance if we carried on the integration beyond 6 Myr.

The upper dashed line is the curve $\tau_e/\tau_a = 4e_{i,res}^2\left(1 + q\sqrt{\alpha}\right)$ (analytical condition 53) with $e_{i,\,res} = 0.57$, value which gives the

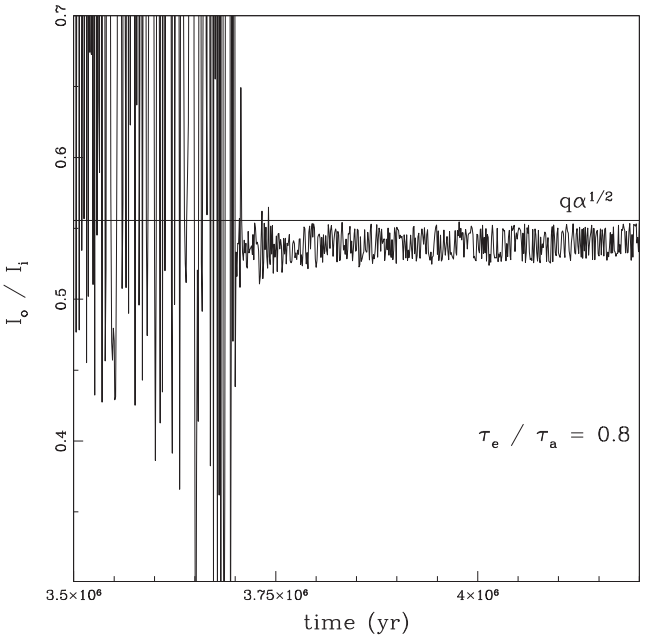

Figure 7. I_o/I_i versus time (in years) for $q = 0.7$ and $\tau_e/\tau_a = 0.8$ in the case $\tau_{ei} = \tau_{eo} \equiv \tau_e$. At $t \simeq 3.7 \times 10^6$ yr, the system enters an inclination-type resonance. The horizontal line represents $q\sqrt{\alpha}$, which is the value of I_o/I_i expected from the analysis. There is a reasonably good agreement between the numerical and analytical results.

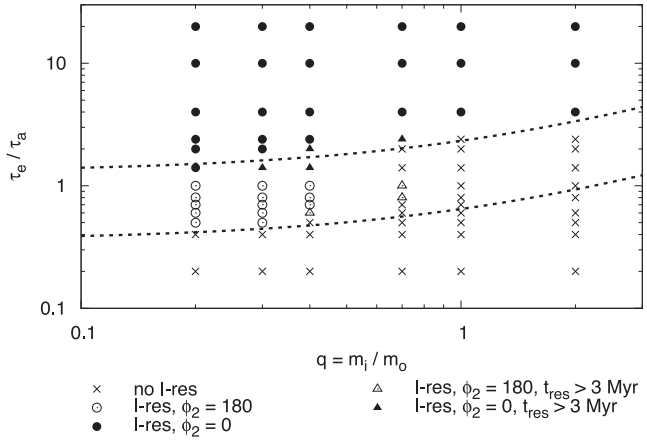

Figure 8. Occurrence of inclination-type resonance as a function of q and τ_e/τ_a in systems evolved between 0 and 6 Myr. Here, $\tau_{ei} = \tau_{eo} \equiv \tau_e$. Crosses represent systems that did not enter an inclination-type resonance, open and filled symbols represent systems that entered an inclination-type resonance with $(\phi_1, \phi_2) = (0^\circ, 180^\circ)$ or $(\phi_1, \phi_2) = (0^\circ, 0^\circ)$, respectively. Circles and triangles represent systems that entered an inclination-type resonance before or after $t = 3$ Myr, respectively. The dashed lines are the curves $\tau_e/\tau_a = 4e_{i,res}^2\left(1 + q\sqrt{\alpha}\right)$ with $e_{i,\,res} = 0.3$ (lower line) and $e_{i,\,res} = 0.57$ (upper line). In agreement with theoretical expectations, systems in between those two lines entered an inclination-type resonance with $(\phi_1, \phi_2) = (0^\circ, 180^\circ)$ if evolved long enough, whereas systems above the upper line entered an inclination-type resonance with $(\phi_1, \phi_2) = (0^\circ, 0^\circ)$.

best fit to the boundary between runs which enter an inclination-type resonance for $(\phi_1, \phi_2) = (0^\circ, 180^\circ)$ and those which enter the resonance for $(\phi_1, \phi_2) = (0^\circ, 0^\circ)$. The fact that this boundary can be fitted with this curve indicates that the analysis leading to the expression (47) of the equilibrium value of e_i (which is used in deriving equation 53) is still valid in the regime of rather large eccentricities, as already noted in Section 3.4.1, and also that $e_{i,\,res}$ is essentially independent of q and τ_e/τ_a in the large eccentricity regime (see also Thommes & Lissauer 2003).

3.6 Influence of varying t_a and m_o

In the simulations presented above, we fixed $m_o = 1$ M_J and $t_a = 7 \times 10^5$ yr (consistent with type II migration time-scale at a few au from the star). Then $q \equiv m_i/m_o$ and $\tau_e/\tau_a \equiv t_e/t_a$ were varied.

We have checked that the results reported above are unaffected if we take t_a to be 5×10^5 or 10^6 yr and m_o to be 0.5 M_J.

The *Kepler* mission has found planets with a mass comparable to or lower than that of Neptune to be very common. Fig. 9 shows the evolution of two Neptune-mass planets ($m_o = m_i = 0.05$ M_J) with $t_a = 2 \times 10^5$ yr and $\tau_e/\tau_a = 4$. As in the case of two Jupiter-mass planets illustrated above, the system enters an inclination-type resonance when $e_i \sim 0.6$.

3.7 Case where the eccentricity of the inner planet is not damped

So far, we have assumed that both planets were interacting with the disc so that both eccentricities were damped (t_{ei} and t_{eo} both finite). In this section, we consider the case where the planets evolve in a cavity, with only the outer planet maintaining contact with the disc. Eccentricity damping therefore acts only on the outer planet ($t_{ei} \to \infty$ and t_{eo} finite). This situation may arise if the planets clear-out a gap which is deep enough that the parts of the disc interior to the orbits are no longer replenished efficiently from the outer disc. The inner disc accretes on to the star over a viscous time-scale. If the outer planet migrates in over a similar time-scale, pushing in the inner planet, contact between the disc and the inner planet is maintained. However, is the outer planet migrates over a slower time-scale, which happens when the mass of the planet is larger than that of the disc in the vicinity of its orbit, the inner planet loses contact with the disc. Note that, if the pair of planets enters an inner cavity carved, e.g. by photoevaporation, migration of the outer planet ceases and eccentricities cannot grow anymore, which would prevent the onset of inclination-type resonance.

We perform the same numerical simulations as above except that now $\boldsymbol{\Gamma}_{d,i}$ in equation (54) is set to zero, whereas $\boldsymbol{\Gamma}_{d,o}$ in equation (55) remains unchanged.

Fig. 10 shows the eccentricities, inclinations and resonant angle ϕ_2 for $\tau_e/\tau_a = 0.25$, 0.3 and 0.01, where $\tau_e \equiv \tau_{eo}$.

The case $\tau_e/\tau_a = 0.25$ is the same as that shown on Fig. 3 with a finite τ_{ei}. When $\tau_{ei} \to \infty$, the eccentricities reach much larger values. However, e_i saturates just below 0.6, which is not sufficient to trigger an inclination-type resonance with $(\phi_1, \phi_2) = (0^\circ, 0^\circ)$. Note that e_i passed through the value 0.3, which we found to be, in principle, sufficient to trigger an inclination-type resonance with $(\phi_1, \phi_2) = (0^\circ, 180^\circ)$. However, when $e_i = 0.3$, e_o is only about 0.05, below the value $e_{o,\,res}$ required for the resonance to be excited.

For $\tau_e/\tau_a = 0.3$, the inclination-type resonance is not excited when the eccentricity of the inner planet is damped (see Fig. 8). Here, however, we see that e_i grows to large values and eventually reaches 0.6, at which point an inclination-type resonance with $(\phi_1, \phi_2) = (0^\circ, 0^\circ)$ is triggered. Therefore, in this case, suppressing eccentricity damping on the inner planet significantly affects the evolution of the system.

Fig. 10 also shows the case $\tau_e/\tau_a = 0.01$. Damping of the outer planet eccentricity is too strong for either $e_{i,\,res}$ or $e_{o,\,res}$ to be reached.

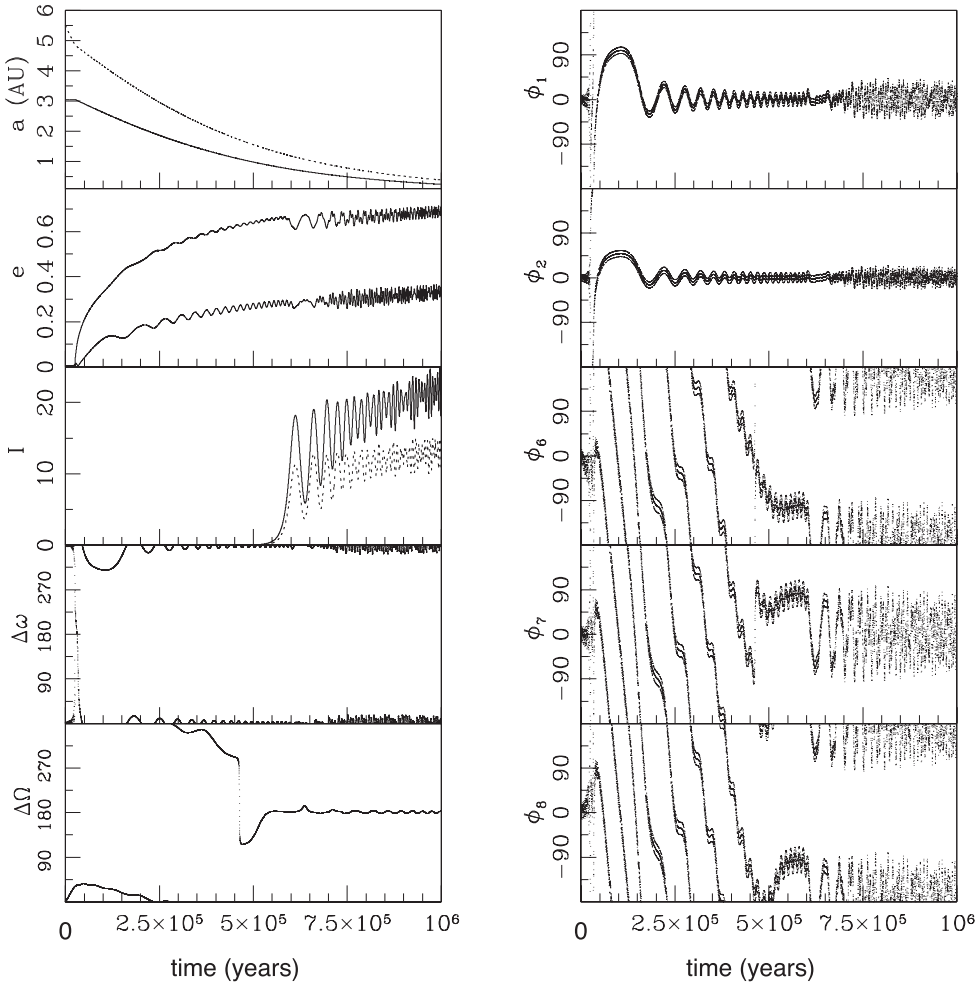

Figure 9. Same as Fig. 5 but for $m_o = m_i = 0.05$ M$_J$ and $t_a = 2 \times 10^5$ yr (and $\tau_e/\tau_a = 4$ as in Fig. 5). The evolution is very similar to that observed in Fig. 5 for two Jupiter-mass planets.

We see on Fig. 10 that the values at which e_o saturates agree very well with the expectation from equation (48).

The value of $e_{o,\,res}$ we have calculated analytically is not valid in the regime $\phi_2 = 0°$ which is observed here. In this regime however, numerical simulations performed for finite values of τ_{ei} and $q = 0.7$ indicate that $e_{o,\,res} \simeq 0.2$. We see on Fig. 2 that e_o cannot reach this value for $\tau_e/\tau_a < 0.2$, which is in good agreement with the results displayed in Fig. 10.

3.8 Effect of inclination damping

So far, we have ignored damping of the inclinations due to interaction with the disc. For the range of inclinations and eccentricities considered here, inclination and eccentricity damping are expected to occur over similar time-scales (Bitsch et al. 2013 for gap opening planets, Cresswell et al. 2007 for non-gap opening planets). Inclination damping can therefore be taken into account by adding the following term on the right-hand side of equations (56) and (57) (Papaloizou & Larwood 2000):

$$-\frac{2}{t_i}\left(\frac{d\boldsymbol{r}_{i,o}}{dt}\cdot\boldsymbol{e}_z\right)\boldsymbol{e}_z, \tag{59}$$

where $\boldsymbol{e}_z$ is the unit vector perpendicular to the disc mid-plane, and t_i the inclination damping time-scale, which is of the same order as the eccentricity damping time-scale. We have run a few simulations which show that the addition of this extra force does not strongly affect the dynamics of the system. Inclination-type resonances are found to occur for the same values of the parameters as above, and are characterized by libration of the resonant angles about the same values as when there is no inclination damping.

Inclination damping has little effect because it happens over the same time-scale as eccentricity damping. When t_e is small, inclination-type resonances do not occur, and therefore inclination damping is irrelevant. In contrast, when t_e is large enough that inclination-type resonances are excited, inclination damping is too weak to affect the sudden increase of the inclinations. It would however limit the growth of the inclinations over a time-scale longer than the time during which the simulations were run.

4 DISCUSSION

4.1 Summary of the main results

In this paper, we have studied analytically the evolution of the eccentricities of a pair of planets locked in a 2:1 MMR. In the early stages of the evolution, the planets are in an eccentricity-type resonance, in which the orbits are in the plane of the disc. We have

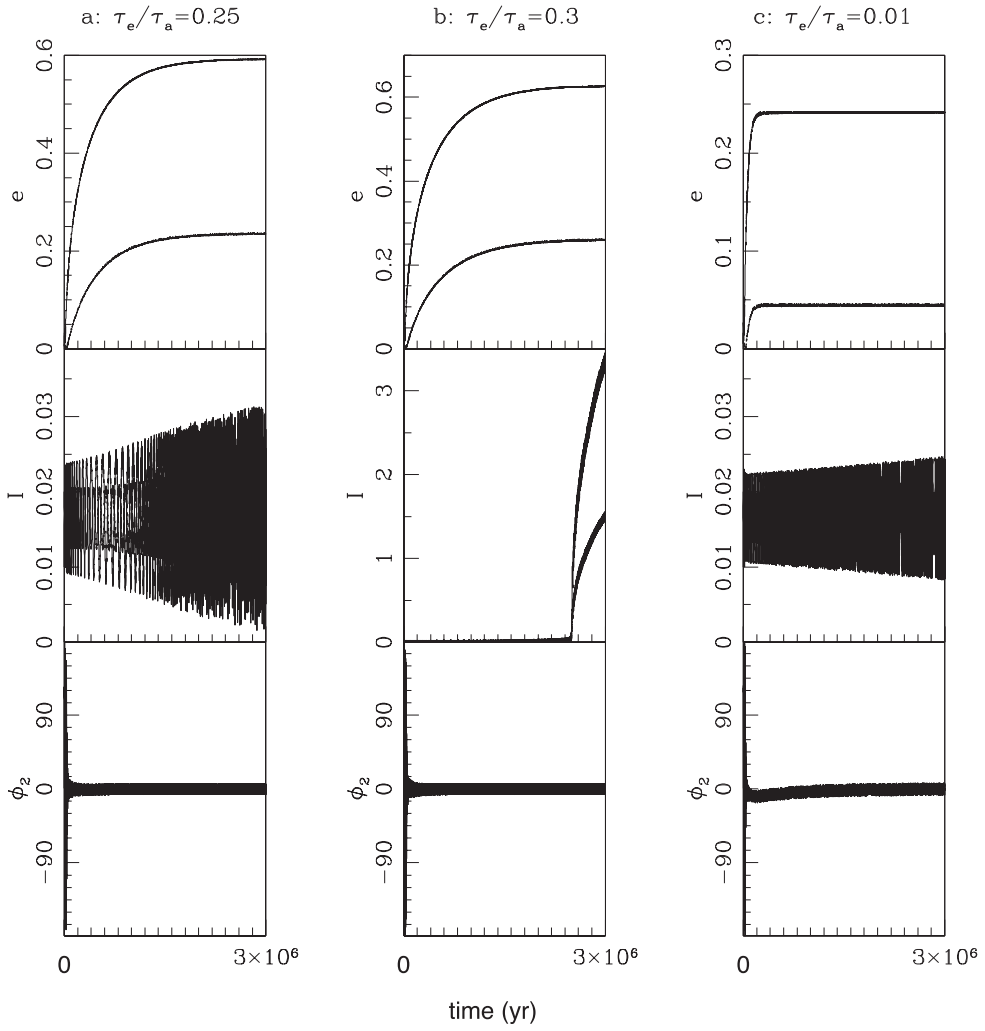

Figure 10. Evolution of a system in 2:1 MMR for $q = 0.7$ and $\tau_{ei} \to \infty$. Here, $\tau_e \equiv \tau_{eo}$. From top to bottom: eccentricities and inclinations (in degrees) of the two planets and resonant angle ϕ_2 (in degrees) versus time (in years) for $\tau_e/\tau_a = 0.25$ (left column), 0.3 (middle column) and 0.01 (right column). In the plots displaying the eccentricities, the upper and lower curves correspond to e_i and e_o, respectively. The case with $\tau_e/\tau_a = 0.25$ is the same as that displayed on Fig. 3 except for τ_{ei} which is infinite here.

derived the equilibrium eccentricity $e_{i,\,eq}$ reached by the inner planet after a time large compared to the eccentricity damping time-scale (equation 47) in the case where the eccentricities of both planets are damped. In the case where only the eccentricity of the outer planet is damped, we have calculated its equilibrium value $e_{o,\,eq}$ (equation 48).

We have shown that, for the system to enter an inclination-type resonance, the eccentricity of the inner planet has to reach a value $e_{i,\,res} \sim 0.3$, independent of the migration and eccentricity damping time-scales and only weakly dependent on the mass ratio q for $q \leq 1$ (equation 51 and Fig. 1). Numerically, we have also shown that there is another, larger, value of $e_{i,\,res} \simeq 0.6$ (which was found by Thommes & Lissauer 2003). When the system enters an inclination-type resonance with $e_{i,\,res} \simeq 0.3$ (*small eccentricity* regime), the resonant angles ϕ_1 and ϕ_2 librate about 0° and 180°, respectively. In the *large eccentricity* regime ($e_{i,\,res} \simeq 0.6$), ϕ_1 and ϕ_2 both librate about 0°.

We have also derived analytically the value $e_{o,\,res}$ that the eccentricity of the outer planet has to reach for an inclination-type resonance to be excited. In the low-eccentricity regime, we find $e_{o,\,res} \simeq 0.1$ for a mass ratio $q \lesssim 1$. This value is somewhat smaller than that found numerically, which is $\simeq 0.2$. In the large eccentricity regime, the numerical simulations also give $e_{o,\,res} \simeq 0.2$ for $q \lesssim 1$.

If e_i reaches $e_{i,res}$ while e_o is still below $e_{o,res}$, the system keeps evolving in the eccentricity-type resonance. As the planets approach each other during their convergent migration, e_o increases and may at some point reach $e_{o,res}$. The system may then enter an inclination-type resonance with either $e_i \simeq 0.3$ or $\simeq 0.6$ if the eccentricity of the inner planet has continued to increase.

Necessary conditions for the system to enter an inclination-type resonance are $e_{i,\,res} < e_{i,\,eq}$ and $e_{o,\,res} < e_{o,\,eq}$. This leads to a condition on the ratio of the eccentricity damping time-scale to the semimajor axis damping time-scale, t_e/t_a, as a function of the mass ratio $q = m_i/m_o$ (equation 53 and Fig. 1 for the case where both eccentricities are damped and Fig. 2 for the case where only the eccentricity of the outer planet is damped). For $q \leq 1$ and when both eccentricities are damped, we find that the system cannot enter an inclination-type resonance if $t_e/t_a < 0.2$. This result still holds when only the eccentricity of the outer planet is damped, at least for $q \lesssim 1$.

4.2 Implication for extrasolar planetary systems

Whether or not the orbit of an extrasolar planet embedded in a disc and locked in an MMR with a heavier outer companion may become inclined due to an inclination-type resonance depends on whether the eccentricity of the planet can become as high as 0.3. This in turn depends (weakly) on the mass ratio q and (strongly) on t_e/t_a.

For a wide range of planet masses, the eccentricity damping time-scale due to planet/disc interaction is of the order of a hundred orbits (see Papaloizou & Larwood 2000; Cresswell et al. 2007 and Bitsch & Kley 2010 for masses $\sim 1-10\,M_\oplus$, $20\,M_\oplus$ and 0.1–1 M_J, respectively), i.e. shorter than 10^3 yr for a planet at a few au from the central star. As type I and type II migration time-scales at this location are of the order of 10^5 yr, this implies that $t_e/t_a \sim 10^{-2}$, much smaller than the value needed for $e_{i,\,res}$ to be reached.

Even when the eccentricity of the inner planet is not damped, and for $q \lesssim 1$, disc torques acting on the outer planet are still too strong for enabling its eccentricity to reach the value required for the onset of an inclination-type resonance.

Lee & Peale (2002) calculated the value of τ_e/τ_a consistent with the observed eccentricities of the two giant planets around GJ 876, which are found to be in a 2:1 MMR, assuming the system had migrated inwards. They found that in the case where the semimajor axes and eccentricities of both planets were assumed to be damped, τ_e/τ_a had to be about 0.1, whereas it had to be about 0.01 in the case where only the semimajor axis and eccentricity of the outer planet were damped. According to the results presented in this paper, in neither of these cases could an inclination-type resonance be triggered.

We conclude that the excitation of inclination through the type of resonance described here is very unlikely to happen in a system of two planets migrating in a disc. If the eccentricities of both planets are damped, this conclusion does not depend on the mass ratio of the planets. If only the eccentricity of the outer planet is damped, this conclusion holds for at least $q \lesssim 1$. This is consistent with the fact that orbits in the multiplanet systems detected by *Kepler* seem to have both low inclinations (Fabrycky et al. 2012) and low eccentricities (Kane et al. 2012). It is also therefore very unlikely that inclination-type resonance is the cause of the orbital inclination observed for a number of hot Jupiters.

ACKNOWLEDGEMENTS

We thank our anonymous referee for helpful comments and suggestions that improved the manuscript.

REFERENCES

Bate M., Lodato G., Pringle J., 2010, MNRAS, 401, 1505
Batygin K., 2012, Nature, 491, 418
Beaugé C., Ferraz-Mello S., Michtchenko T., 2003, ApJ, 593, 1124
Bitsch B., Kley W., 2010, A&A, 523, 30
Bitsch B., Crida A., Libert A.-S., Lega E., 2013, A&A, 555, 124
Burns J. A., 1976, Am. J. Phys., 44, 944
Chatterjee S., Ford E., Matsumura S., Rasio F., 2008, ApJ, 686, 580
Cresswell P., Dirksen G., Kley W., Nelson R., 2007, A&A, 473, 329
Fabrycky D., Tremaine S., 2007, ApJ, 669, 1298
Fabrycky D. et al., 2012, ApJ, 750, 114
Foucart F., Lai D., 2011, MNRAS, 412, 2799
Goldreich P., 1965, MNRAS, 130, 159
Goldreich P., Schlichting H., 2014, Astron. J., 147, 32
Greenberg R., 1977, Vistas Astron., 21, 209
Kane S., Ciardi D., Gelino D., von Braun K., 2012, MNRAS, 425, 757
Kley W., Lee M., Murray N., Peale S., 2005, A&A, 437, 727
Lai D., Foucart F., Lin D., 2011, MNRAS, 412, 2790
Lee M., 2004, ApJ, 611, 517
Lee M., Peale S., 2002, ApJ, 567, 596
Lee M., Thommes E., 2009, ApJ, 702, 1662
Libert A.-S., Tsiganis K., 2009, MNRAS, 400, 1373
Lissauer J., Peale S., Cuzzi J., 1984, Icarus, 58, 159
Lissauer J. et al., 2011, ApJS, 197, 8
Lissauer J. et al., 2014, ApJ, 784, 44
Marcy G., Butler R., Fischer D., Vogt S., Lissauer J., Rivera E., 2001, ApJ, 556, 296
Murray C., Dermott S., 1999, Solar System Dynamics. Cambridge Univ. Press, Cambridge
Naoz S., Farr W., Lithwick Y., Rasio F., Teyssandier J., 2011, Nature, 473, 187
Papaloizou J., Larwood J., 2000, MNRAS, 315, 823
Papaloizou J., Terquem C., 2001, MNRAS, 325, 221
Peale S., 1976, ARA&A, 14, 215
Petrovich C., Malhotra R., Tremaine S., 2013, ApJ, 770, 24
Rowe J. et al., 2014, ApJ, 784, 45
Roy A. E., 1978, Orbital Motion, 4th edn. Institute of Physics, London, p. 212
Snellgrove M., Papaloizou J., Nelson R., 2001, A&A, 374, 1092
Terquem C., 2013, MNRAS, 435, 798
Terquem C., Papaloizou J., 2007, ApJ, 654, 1110
Thommes E., Lissauer J., 2003, ApJ, 597, 566
Wu Y., Lithwick Y., 2011, ApJ, 735, 109
Wu Y., Murray N., Ramsahai J., 2007, ApJ, 670, 820

APPENDIX A: COEFFICIENTS IN THE DISTURBING FUNCTION

In Table A1, we give the expression of the coefficients $f_i\,(i = 1, \ldots, 8)$ and $K_i\,(i = 1, \ldots, 4)$ which enter the expression of the direct part of the disturbing function in equations (3) and (4). We denote $b_s^{(j)}(\alpha)$ the Laplace coefficient defined by

$$b_s^{(j)}(\alpha) = \frac{1}{\pi}\int_0^{2\pi} \frac{\cos(j\psi)}{\left(1 - 2\alpha\cos\psi + \alpha^2\right)^s}\,\mathrm{d}\psi, \tag{A1}$$

where j is an integer and s is a half integer. We define $\mathrm{D} \equiv \mathrm{d}/\mathrm{d}\alpha$. In Table A1, we also give the numerical value of the $f_i\,(i = 1, \ldots, 8)$ and $K_i\,(i = 1, \ldots, 4)$ evaluated at the 2:1 MMR, where $\alpha = 2^{-2/3}$.

Table A1. Expression and numerical value at the 2:1 MMR of the coefficients which enter the expression of the disturbing function.

Coefficient	Expression	Numerical value at the 2:1 resonance
f_1	$-\frac{1}{2}\,(4 + \alpha\mathrm{D})\,b_{1/2}^{(2)}$	−1.190 49
f_2	$\frac{1}{2}\,(3 + \alpha\mathrm{D})\,b_{1/2}^{(1)}$	1.688 31
f_2^m	$f_2 - 2\alpha$	0.428 39
f_3	$\frac{1}{8}\left(44 + 14\alpha\mathrm{D} + \alpha^2\mathrm{D}^2\right) b_{1/2}^{(4)}$	1.695 73
f_4	$-\frac{1}{4}\left(42 + 14\alpha\mathrm{D} + \alpha^2\mathrm{D}^2\right) b_{1/2}^{(3)}$	−4.966 85
f_5	$\frac{1}{8}\left(38 + 14\alpha\mathrm{D} + \alpha^2\mathrm{D}^2\right) b_{1/2}^{(2)}$	3.593 80
f_6	$\frac{1}{2}\alpha b_{3/2}^{(3)}$	0.819 88
f_7	$-\alpha b_{3/2}^{(3)}$	−1.639 76
f_8	$\frac{1}{2}\alpha b_{3/2}^{(3)}$	0.819 88
K_1	$\frac{1}{8}\left(2\alpha\mathrm{D} + \alpha^2\mathrm{D}^2\right) b_{1/2}^{(0)}$	0.387 63
K_2	$\frac{1}{4}\left(2 - 2\alpha\mathrm{D} - \alpha^2\mathrm{D}^2\right) b_{1/2}^{(1)}$	−0.575 70
K_3	$-\frac{1}{2}\alpha b_{3/2}^{(1)}$	−1.550 51
K_4	$\alpha b_{3/2}^{(1)}$	3.101 02

APPENDIX B: DAMPING FORCES

In the *N*-body simulations performed in this paper, the damping force due to the interaction between the outer planet and the disc is given by equation (57), which we can rewrite under the form

$$\boldsymbol{\Gamma}_{\rm d} = -\left(\frac{1}{t_{\rm m}} + \frac{2}{t_{\rm e}}\right)\dot{r}\,\boldsymbol{e}_r - \frac{1}{t_{\rm m}} r\dot{\theta}\,\boldsymbol{e}_\theta, \tag{B1}$$

where we have dropped the subscript 'o' which we have used for the outer planet. Here, r and θ are the polar coordinates referred to the central star, $\boldsymbol{e}_r$ and $\boldsymbol{e}_\theta$ are the unit vectors along and perpendicular to the radius vector $\boldsymbol{r}$, respectively, in the orbital plane, and the dot denotes a time-derivative.

We now show that adding this force to the equation of motion is equivalent to adding the terms $-a/t_{\rm a} - 2ae^2/t_{\rm e}$, with $t_{\rm a} = t_{\rm m}/2$, in the expression of $\mathrm{d}a/\mathrm{d}t$ and the term $-e/t_{\rm e}$ in the expression of $\mathrm{d}e/\mathrm{d}t$, as done in Section 2.3 (see equations 39 and 41).

The total energy and angular momentum vector per unit mass of the planet are $E = -Gm_\star/(2a)$ and $\boldsymbol{H} = r^2\dot{\theta}\boldsymbol{e}_z$, respectively, where $\boldsymbol{e}_z = \boldsymbol{e}_r \times \boldsymbol{e}_\theta$. Because the planet is acted on by the perturbative force (B1), E and $\boldsymbol{H}$ vary with time according to

$$\dot{E} = \dot{\boldsymbol{r}} \cdot \boldsymbol{\Gamma}_{\rm d}, = -\left(\frac{1}{t_{\rm m}} + \frac{2}{t_{\rm e}}\right)\dot{r}^2 - \frac{1}{t_{\rm m}}(r\dot{\theta})^2, \tag{B2}$$

$$\dot{\boldsymbol{H}} = \boldsymbol{r} \times \boldsymbol{\Gamma}_{\rm d}, = -\frac{1}{t_{\rm m}} r^2\dot{\theta}\boldsymbol{e}_z. \tag{B3}$$

The rate of change of a and e is related to that of E and $\boldsymbol{H}$ through (e.g. Burns 1976)

$$\frac{\mathrm{d}a}{\mathrm{d}t} = \frac{2a^2}{Gm_\star}\dot{E}, \tag{B4}$$

$$\frac{\mathrm{d}e}{\mathrm{d}t} = \frac{1}{2e}(e^2 - 1)\left(2\frac{\dot{H}}{H} + \frac{\dot{E}}{E}\right). \tag{B5}$$

Substituting equation (B2) into equation (B4), we obtain

$$\left\langle \frac{\mathrm{d}a}{\mathrm{d}t} \right\rangle = \frac{2a^2}{Gm_\star}\left[-\left(\frac{1}{t_{\rm m}} + \frac{2}{t_{\rm e}}\right)\left\langle \dot{r}^2 \right\rangle - \frac{1}{t_{\rm m}}\left\langle (r\dot{\theta})^2 \right\rangle\right], \tag{B6}$$

where the brackets denote time-averaging over an orbital period. To perform the time-averaging, we first write $\dot{r}$ and $r\dot{\theta}$ in terms of the true anomaly f

$$\dot{r} = \frac{na}{\sqrt{1-e^2}} e \sin f, \tag{B7}$$

$$r\dot{\theta} = \frac{na}{\sqrt{1-e^2}}(1 + e\cos f). \tag{B8}$$

We then use the expansion of $\cos f$ and $\sin f$ in terms of the mean anomaly M, which is 2π-periodic and a linear function of time. To obtain $\langle \mathrm{d}a/\mathrm{d}t \rangle$ and $\langle \mathrm{d}e/\mathrm{d}t \rangle$ to second order in e, we only need to expand $\cos f$ and $\sin f$ to first order in e. This gives

$$\cos f = \cos M + e(\cos 2M - 1), \tag{B9}$$

$$\sin f = \sin M + e \sin 2M, \tag{B10}$$

so that $\left\langle \dot{r}^2 \right\rangle = n^2a^2e^2/2$ and $\left\langle (r\dot{\theta})^2 \right\rangle = n^2a^2(1 - e^2/2)$. Substituting into equation (B6) and using $Gm_\star = n^2a^3$, we finally obtain

$$\left\langle \frac{\mathrm{d}a}{\mathrm{d}t} \right\rangle = -2a\left(\frac{1}{t_{\rm m}} + \frac{e^2}{t_{\rm e}}\right). \tag{B11}$$

To calculate the rate of change of e, we now substitute equations (B3) and (B4) into equation (B5), and use the expression of E and H to obtain

$$\left\langle \frac{\mathrm{d}e}{\mathrm{d}t} \right\rangle = \frac{1}{2e}(e^2 - 1)\left(-\frac{2}{t_{\rm m}} - \frac{1}{a}\left\langle \frac{\mathrm{d}a}{\mathrm{d}t} \right\rangle\right). \tag{B12}$$

Substituting equation (B11), this gives

$$\left\langle \frac{\mathrm{d}e}{\mathrm{d}t} \right\rangle = -\frac{1}{t_{\rm e}} e. \tag{B13}$$

Therefore, as anticipated, adding the damping force (equation B1) to the equation of motion is equivalent to adding the terms in equations (B11) and (B13) to the rate of change of a and e.

This paper has been typeset from a TEX/LATEX file prepared by the author.

5.4 Complete solution in the case of strong eccentricity damping

We consider the case where the eccentricity damping is strong ($\tau_e \ll \tau_a$), in order to use a set of equations valid at lowest order in eccentricities. When the two planets are locked in resonance, $\phi_1 = 0$, $\phi_2 = \pi$, and the relation $d\varpi_\mathrm{i}/d\tau = d\varpi_\mathrm{o}/d\tau$ can be rewritten:

$$e_\mathrm{o} = -q\sqrt{\alpha} f e_\mathrm{i} \tag{5.12}$$

where $f = f_2^m/f_1$.

The equations for the semi-major axis and eccentricities now read:

$$\begin{aligned}
\frac{da_\mathrm{i}}{d\tau} &= \mathcal{C}_\mathrm{i} 2a_\mathrm{i}\left[e_\mathrm{i} f_1 \sin\phi_1 + e_\mathrm{o} f_2^m \sin\phi_2\right] - \frac{2a_\mathrm{i}e_\mathrm{i}^2}{\tau_e}, & (5.13)\\
\frac{da_\mathrm{o}}{d\tau} &= \mathcal{C}_\mathrm{o}(-4a_\mathrm{o})\left[e_\mathrm{i} f_1 \sin\phi_1 + e_\mathrm{o} f_2^m \sin\phi_2\right] - \frac{a_\mathrm{o}}{\tau_a} - \frac{2a_\mathrm{o}e_\mathrm{o}^2}{\tau_e}, & (5.14)\\
\frac{de_\mathrm{i}}{d\tau} &= -\mathcal{C}_\mathrm{i} f_1 \sin\phi_1 - \frac{e_\mathrm{i}}{\tau_e}, & (5.15)\\
\frac{de_\mathrm{o}}{d\tau} &= -\mathcal{C}_\mathrm{o} f_2^m \sin\phi_2 - \frac{e_\mathrm{o}}{\tau_e}, & (5.16)
\end{aligned}$$

where we define $f_2^m \equiv f_2 - 2\alpha = f_2 - 1/(2\alpha^2)$

Using the relation (5.12) and $\alpha = a_\mathrm{i}/a_\mathrm{o}$, we obtain the following differential equation for a_i and a_o:

$$\left(1 + 2q\sqrt{\alpha}\right)\frac{1}{a_\mathrm{i,o}}\frac{da_\mathrm{i,o}}{d\tau} = -\frac{1}{\tau_a} - 2q\sqrt{\alpha}(2 + q\sqrt{\alpha}f^2)\frac{e_\mathrm{i}^2}{te} \tag{5.17}$$

Combining equations (5.15) and (5.16) we also get

$$\left(e_\mathrm{i}\frac{de_\mathrm{i}}{d\tau} + \frac{e_\mathrm{i}^2}{\tau_e}\right)\left(1 + q\sqrt{\alpha}f^2\right) = -\mathcal{C}_\mathrm{i}\left[e_\mathrm{i}F_1 + e_\mathrm{o}F_2 - \frac{e_\mathrm{o}}{2\alpha^2}\sin\phi_2 + \mathcal{O}(3)\right] \tag{5.18}$$

which can be injected in (5.14) to give

$$\frac{1}{a_\mathrm{o}}\frac{da_\mathrm{o}}{d\tau} = 2q\sqrt{\alpha}(1 + q\sqrt{\alpha}f^2)\frac{de_\mathrm{i}^2}{d\tau} + 2q\sqrt{\alpha}\left[2(1 + q\sqrt{\alpha}f^2) - q\sqrt{\alpha}f^2\right]\frac{e_\mathrm{i}^2}{\tau_e} - \frac{1}{\tau_a} \tag{5.19}$$

By combining equations (5.17) and (5.19) we get the following differential equation:

$$\frac{de_\mathrm{i}^2}{d\tau} + \mu(q)\frac{e_\mathrm{i}^2}{\tau_e} = \eta(q)\frac{1}{\tau_a} \tag{5.20}$$

where

$$\mu(q) = \frac{2 + q\sqrt{\alpha}f^2}{1 + q\sqrt{\alpha}f^2}\left(1 + \frac{1}{1 + 2q\sqrt{\alpha}}\right)$$

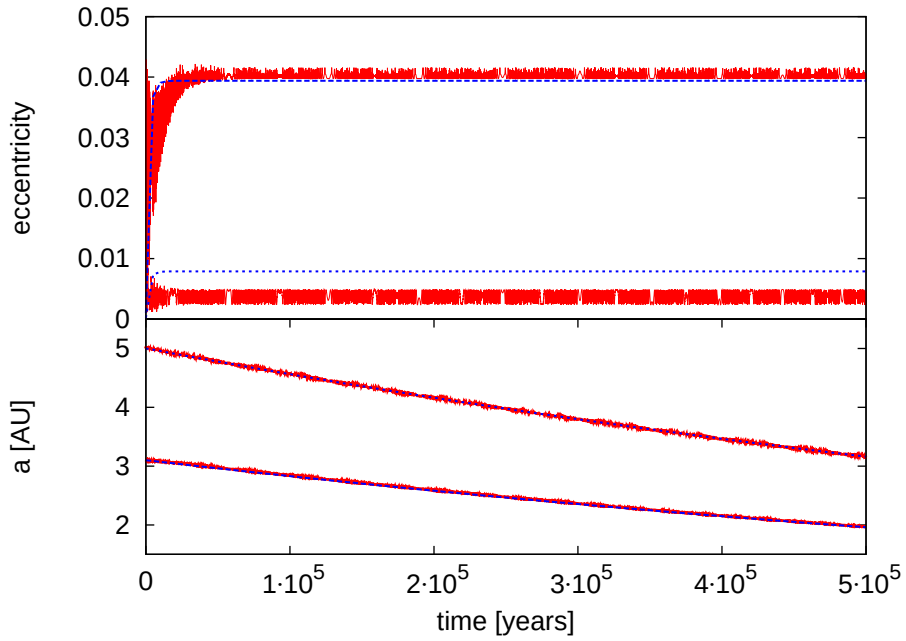

Figure 5.2: Evolution of the eccentricity (upper panel) and semi-major axis (lower panel) of two migrating planets with $q = 0.7$, $t_a = 7 \times 10^5$ yr, $t_e = 7 \times 10^3$ yr. The red curve is the result of a numerical integration, while the blue curve shows the analytical prediction from equations (5.21) and (5.23).

and

$$\eta(q) = \frac{1}{(1 + 2q\sqrt{\alpha})(1 + q\sqrt{\alpha}f^2)}$$

The straightforward integration gives

$$e_{\rm i}^2(\tau) = e_{\rm i,0}^2 \exp\left[-\mu(q)\frac{\tau}{\tau_e}\right] + \frac{\eta(q)}{\mu(q)}\frac{\tau_e}{\tau_a}\left(1 - \exp\left[-\mu(q)\frac{\tau}{\tau_e}\right]\right) \tag{5.21}$$

which has a limit for $\tau \to \infty$:

$$e_{\rm i,eq} = \left[\frac{1}{(2 + q\sqrt{\alpha}f^2)(1 + q\sqrt{\alpha})}\frac{\tau_e}{2\tau_a}\right]^{1/2} \tag{5.22}$$

The expressions for $e_{\rm o}(\tau)$ and $e_{\rm o,eq}$ follow immediately from $e_{\rm o} = -q\sqrt{\alpha}fe_{\rm i}$. In addition, one can now derive the expressions for the semi-major axis:

$$a_{\rm i,o}(\tau) = a_{\rm i0,o0} \times \tag{5.23}$$
$$\exp\left[\frac{-1}{1 + q\sqrt{\alpha}}\frac{\tau}{\tau_a} + \frac{2q\sqrt{\alpha}}{1 + 2q\sqrt{\alpha}}\frac{1}{\mu(q)}\left(e_{\rm i,0}^2(2 + q\sqrt{\alpha}f^2) - \frac{1}{2 + 2q\sqrt{\alpha}}\frac{\tau_e}{\tau_a}\right)\left(\exp\left[-\mu(q)\frac{\tau}{\tau_e}\right] - 1\right)\right]$$

On figure 5.2, we show in red a numerical integration of a system of two planets locked in a 2:1 MMR. The orbits have no inclination and the eccentricities are initially 0.001. The inner planet has a mass of $0.7\ M_{\rm J}$, and the outer one has a mass of $1\ M_{\rm J}$. We choose the

timescales to be $t_a = 7 \times 10^5$ yr and $t_e = 7 \times 10^3$ yr (equivalent to $K = 100$, regime of strong damping). Not surprisingly, we find that the eccentricities are kept to very low values throughout the integration. In blue, we also plot the analytical results given by equations (5.21) and (5.23). Regarding the semi-major axis, the agreement is very good. The inner eccentricity (upper curve) reaches an equilibrium value that agrees with the analytical estimate to within a few percent. The only major disagreement comes from the outer eccentricity, which reaches an equilibrium whose value is roughly half of that predicted by the theory. Recall that our calculation is based on the assumption that $d\varpi_{\rm i}/d\tau = d\varpi_{\rm o}/d\tau$, but the evolutions of the apses are known only to zero-th order.

Chapter 6

Conclusions

Contents

6.1 Summary

In this thesis we have studied some aspects of the planet-disc interactions. We have focused, both analytically and numerically, on the possibility for the disc to excite and/or maintain a planet, or a system of planets, at large eccentricities and inclinations.

The fate of planets inclined with respect to a disc

The first problem that we have investigated is the evolution of a planet whose orbit is misaligned with respect to a disc. We have modelled the disc as a 3D potential and included the friction that the planet undergoes when crossing the disc, twice per orbit. We have ignored the back reaction of the planet on the disc, an assumption well justified as long as the disc is more massive than the planet. We show that the disc naturally excites the eccentricity and inclination of the planet when the inclination between the two is larger than a critical angle, whose value can be as low as 20°. This is equivalent to the well-known Kozai mechanism in 3-body systems. The orbital elements of the planet are damped to low values by the friction, but also undergo periodic variations caused by the Kozai mechanism. These variations excite the eccentricity that would otherwise be kept at low values by the friction. However, the same variations cause the inclination to go to low values, where it spends more time in the disc (i.e., where it is more affected by friction). Therefore, damping by friction is overall enhanced by this process.

We find that Jupiter mass planets and above realign with the plane of the disc on a timescale shorter than the disc's lifetime. However, Neptune mass planets are kept on inclined orbits for longer than the disc's lifetime. In addition, the Kozai mechanism causes

their eccentricity to reach high values. Therefore, Neptune mass planets can naturally remain misaligned and eccentric. Currently, there is no observational evidence of a population of Neptune mass planets on inclined and eccentric orbits. For instance, the Kepler sample supports the idea that low-mass planets have low inclinations and low eccentricities. Once we will have removed the observational bias that does not favour the detection of long-period, low mass planets, we expect this to be confirmed. On the other hand, it is possible that Jupiter mass planets have been misaligned; their fast realignment would make it impossible for us to disentangle between them and the population of planets that formed and stayed in their disc. However, it seems that the disc-induced Kozai oscillations of a massive planet on an inclined orbit cannot explain the population of misaligned hot Jupiters.

We have also shown that when two planets orbit the star and are perturbed by the disc, the latter usually dominated their evolution. Planet-planet interaction, however, can sometimes lead to chaotic evolution of the system.

A possible mechanism to generate inclined orbits using disc migration

The second problem that we have studied naturally arises when studying planets which are misaligned with respect to their disc: "how did the planet(s) get this primordial inclination in the first place". In Teyssandier et al. (2013b) we have given a few suggestions regarding when this situation could occur. In Teyssandier and Terquem (2014), we have studied one specific scenario in details. In this scenario, two planets migrate in a disc, and enter a mean motion resonance. Exchange of angular momentum while the planets are locked in resonance leads to an increase of the eccentricities. Under the combined effects of resonant migration and damping from the disc, eccentricities eventually reach an equilibrium value. In addition, an other type of resonance can also appear when second-order terms in the disturbing function are included. They correspond to an inclination-type resonance, in which the inclinations rapidly reach very high values. We have shown that the onset of this inclination-type resonance can only be achieved if the eccentricities become higher than a critical value. This allows us to derive a criterion for the onset of inclination–type resonance: the equilibrium value reached by the eccentricity because of the disc damping has to be higher than the critical value needed to trigger the inclination–type resonance. We find that this criterion is weakly dependant on the mass ratio between the two planets. However, it is strongly dependant on the ratio of the eccentricity damping timescale and the orbital decay timescale. We find that this ratio has to be larger than a few 10^{-1} in order for inclination–type resonances to become possible. However, both observations and numerical simulations tend to indicate that this ratio cannot exceed a few 10^{-2}. We conclude that the excitation of inclinations through resonant migration of a pair of planets embedded in a disc is very unlikely. This seems to be supported by the fact that multiple systems in the Kepler sample, including those in, or close to, mean motion resonances, appear to have low inclinations and eccentricities.

Final remarks

The conclusions of this thesis seem to indicate that it is unlikely that planets as massive as Jupiter have been strongly misaligned with the disc, or that they could maintain such inclination. First, strong eccentricity damping prevents them from being kicked out of the plane of the disc through resonant migration mechanisms. In addition, even if the planet manages to become misaligned (for instance if they have formed by fragmentation of the envelope, or if they are captured during a close encounter with another star), they would tend to realign quickly with the disc. Only low mass planets could remain inclined and eccentric.

These results give constraints on the early stages of the evolution of planetary systems. They support the evidence that eccentricity damping in a disc is strong enough to keep the planets in the disc. They also indicate that Neptune mass planets are not expected to have been misaligned with their disc, otherwise we could still see consequences of this misalignment today. However, if massive planets have formed through gravitational collapse in the protostellar envelope, their should be very little evidence to support this theory, as they are expected to realign with the disc, and therefore mix with the population of massive planets formed in a disc.

6.2 Perspectives

There are several points in this thesis that currently remain unsolved. As we have seen, it is hard to do a global parametric survey of the interactions between two planets on orbits that are inclined with respect to a disc. If those planets formed via gravitational collapse of a protostellar envelope, then we can actually expect more than two massive planets to be formed, making the evolution even harder to predict. In addition, the action of a population of massive planets on a disc could significantly alter the structure of the latter, making our model unreliable. A way of avoiding this issue could be to properly model the response of the disc using hydrodynamical simulations. Such simulations have already been conducted for a single massive planet (see, e.g., Xiang-Gruess and Papaloizou, 2013; Bitsch et al., 2013), but could be extended to the low-mass planets regime. It should also be noted that these simulations have note explored yet multiplanet systems.

Following on the work we have presented in section 4.6, we have noticed that numerical simulations of systems of two planets inclined with respect to a disc often lead to unstable orbits. The question of the stability of such systems should be addressed more carefully, and requires high-precision numerical simulations, in order to insure a good conservation of energy.

In addition, we have noted in our simulations that the resonant capture of an inner planet by an outer, inward migrating planet can also happen if the mutual inclination between the two planets is initially high. Hence, if an inner planet has cleared a cavity between the inner

edge of the disc and the star, and is highly inclined with respect to the plane of the disc (because of some possible scattering event), it could in principle be pushed even further in following its subsequent capture in resonance by an outer planet. This could further increase its inclination and eccentricity and produce a short-period misaligned planet. However, the probability of such event to occur is expected to be rather low, but should be tested in more details.

To finish, our work could also be extended to other types of resonances. It could be interesting, for instance, to test configurations like the 3:2 MMR of the planets orbiting HD 45364. The 3:2 MMR being interior to the 2:1, this configuration probably required a fast migration, which would reduce the probability of capture in the 2:1 MMR. As we have seen, the onset of inclination-type resonance strongly depends on the ratio between the eccentricity damping timescale and the migration timescale. For a fast type III migration, this ratio could be closer to unity than in the case of the "slow" type II migration, and it would be interesting the investigate the behaviour of the inclinations in this regime. In addition, we have not investigated higher order resonances such as the 3:1 MMR. While they are difficult to investigate analytically, because of the necessity of including several high-order terms in inclinations and eccentricities, they can be studied numerically. Finally, we remark that we have used prescriptions for the migration and damping. However, planet migration can be more complicated, with stochastic terms that depart from the smooth inward migration scenario we have envisioned here. Again, it would be interesting to see if full 3D hydrodynamical simulations also reveal the onset of inclination-type resonances in specific regimes.

More globally, the study of planetary systems (including that of our own solar system) still comes with many unsolved problems. Many of them require a good understanding of planet-disc interactions. For instance, the importance of the corotation torque on the evolution of migrating planets was only fully appreciated in the last few years and is now a very active field of research. In addition, complex physical behaviours, resulting for instance from magnetic fields or turbulence in the disc, can affect the migration. As a result, the resonant locking of a pair of planets might be complicated, and brief episodes of divergent migration might explain some of the observed statistical properties of exoplanets, such as the excess of pairs just outside mean-motion resonances seen by Kepler. More generally, it is certain that planet-disc interactions will shape the planetary system, by distributing the semi-major axis, eccentricities and inclinations in a way that is not fully understood today. As such, they are a key component to understand the subsequent evolution of planetary systems once the disc has vanished, and to explain the wonderful variety of planetary systems as we presently see them.

Bibliography

Adams, F. C. and Laughlin, G. (2003). Migration and dynamical relaxation in crowded systems of giant planets. *Icarus*, 163:290–306.

Albrecht, S., Winn, J. N., Johnson, J. A., Howard, A. W., Marcy, G. W., Butler, R. P., Arriagada, P., Crane, J. D., Shectman, S. A., Thompson, I. B., Hirano, T., Bakos, G., and Hartman, J. D. (2012). Obliquities of Hot Jupiter Host Stars: Evidence for Tidal Interactions and Primordial Misalignments. *ApJ*, 757:18.

Artymowicz, P. (1993). On the Wave Excitation and a Generalized Torque Formula for Lindblad Resonances Excited by External Potential. *ApJ*, 419:155.

Barnes, J. W., van Eyken, J. C., Jackson, B. K., Ciardi, D. R., and Fortney, J. J. (2013). Measurement of Spin-orbit Misalignment and Nodal Precession for the Planet around Pre-main-sequence Star PTFO 8-8695 from Gravity Darkening. *ApJ*, 774:53.

Batygin, K. and Morbidelli, A. (2013). Dissipative Divergence of Resonant Orbits. *Astronomical Journal*, 145:1.

Belorizky, D. (1938). Le Soleil, Etoile Variable. *L'Astronomie*, 52:359–361.

Binney, J. and Tremaine, S. (1987). *Galactic dynamics*.

Bitsch, B., Crida, A., Libert, A.-S., and Lega, E. (2013). Highly inclined and eccentric massive planets. I. Planet-disc interactions. *A&A*, 555:A124.

Bitsch, B. and Kley, W. (2010). Orbital evolution of eccentric planets in radiative discs. *A&A*, 523:A30.

Bitsch, B. and Kley, W. (2011). Evolution of inclined planets in three-dimensional radiative discs. *A&A*, 530:A41.

Boss, A. P. (1997). Giant planet formation by gravitational instability. *Science*, 276:1836–1839.

Bouvier, J., Alencar, S. H. P., Boutelier, T., Dougados, C., Balog, Z., Grankin, K., Hodgkin, S. T., Ibrahimov, M. A., Kun, M., Magakian, T. Y., and Pinte, C. (2007). Magnetospheric accretion-ejection processes in the classical T Tauri star AA Tauri. *A&A*, 463:1017–1028.

Brouwer, D. and Clemence, G. M. (1961). *Methods of celestial mechanics*. Academic Press.

Burns, J. A. (1976). Elementary derivation of the perturbation equations of celestial mechanics. *American Journal of Physics*, 44:944–949.

Cassan, A., Kubas, D., Beaulieu, J.-P., Dominik, M., Horne, K., Greenhill, J., Wambsganss, J., Menzies, J., Williams, A., Jørgensen, U. G., Udalski, A., Bennett, D. P., Albrow, M. D., Batista, V., Brillant, S., Caldwell, J. A. R., Cole, A., Coutures, C., Cook, K. H., Dieters, S., Prester, D. D., Donatowicz, J., Fouqué, P., Hill, K., Kains, N., Kane, S., Marquette, J.-B., Martin, R., Pollard, K. R., Sahu, K. C., Vinter, C., Warren, D., Watson, B., Zub, M., Sumi, T., Szymański, M. K., Kubiak, M., Poleski, R., Soszynski, I., Ulaczyk, K., Pietrzyński, G., and Wyrzykowski, Ł. (2012). One or more bound planets per Milky Way star from microlensing observations. *Nature*, 481:167–169.

Charbonneau, D., Brown, T. M., Latham, D. W., and Mayor, M. (2000). Detection of Planetary Transits Across a Sun-like Star. *ApJL*, 529:L45–L48.

Correia, A. C. M., Udry, S., Mayor, M., Benz, W., Bertaux, J.-L., Bouchy, F., Laskar, J., Lovis, C., Mordasini, C., Pepe, F., and Queloz, D. (2009). The HARPS search for southern extra-solar planets. XVI. HD 45364, a pair of planets in a 3:2 mean motion resonance. *A&A*, 496:521–526.

D'Alessio, P., Canto, J., Calvet, N., and Lizano, S. (1998). Accretion Disks around Young Objects. I. The Detailed Vertical Structure. *ApJ*, 500:411.

Davies, M. B., Adams, F. C., Armitage, P., Chambers, J., Ford, E., Morbidelli, A., Raymond, S. N., and Veras, D. (2013). The Long-Term Dynamical Evolution of Planetary Systems. *ArXiv e-prints*.

Fabrycky, D. and Tremaine, S. (2007). Shrinking Binary and Planetary Orbits by Kozai Cycles with Tidal Friction. *ApJ*, 669:1298–1315.

Fabrycky, D. C., Lissauer, J. J., Ragozzine, D., Rowe, J. F., Agol, E., Barclay, T., Batalha, N., Borucki, W., Ciardi, D. R., Ford, E. B., Geary, J. C., Holman, M. J., Jenkins, J. M., Li, J., Morehead, R. C., Shporer, A., Smith, J. C., Steffen, J. H., and Still, M. (2012). Architecture of Kepler's Multi-transiting Systems: II. New investigations with twice as many candidates. *ArXiv e-prints*.

Fendyke, S. M. and Nelson, R. P. (2014). On the corotation torque for low-mass eccentric planets. *MNRAS*, 437:96–107.

Fernandez, J. A. and Ip, W.-H. (1984). Some dynamical aspects of the accretion of Uranus and Neptune - The exchange of orbital angular momentum with planetesimals. *Icarus*, 58:109–120.

Fischer, D., Howard, A., Laughlin, G., Macintosh, B., Mahadevan, S., Sahlmann, J., and Yee, J. (2013). Exoplanet Detection Techniques. *Protostars and Planet VI*.

Goldreich, P. (1965). An explanation of the frequent occurrence of commensurable mean motions in the solar system. *MNRAS*, 130:159.

Goldreich, P. and Tremaine, S. (1979). The excitation of density waves at the Lindblad and corotation resonances by an external potential. *ApJ*, 233:857–871.

Goldreich, P. and Tremaine, S. (1980). Disk-satellite interactions. *ApJ*, 241:425–441.

Greaves, J. S., Kennedy, G. M., Thureau, N., Eiroa, C., Marshall, J. P., Maldonado, J., Matthews, B. C., Olofsson, G., Barlow, M. J., Moro-Martín, A., Sibthorpe, B., Absil, O., Ardila, D. R., Booth, M., Broekhoven-Fiene, H., Brown, D. J. A., Cameron, A. C., del Burgo, C., Di Francesco, J., Eislöffel, J., Duchêne, G., Ertel, S., Holland, W. S., Horner, J., Kalas, P., Kavelaars, J. J., Lestrade, J.-F., Vican, L., Wilner, D. J., Wolf, S., and Wyatt, M. C. (2014). Alignment in star-debris disc systems seen by Herschel. *MNRAS*, 438:L31–L35.

Greenberg, R. (1977). Orbit-orbit resonances in the solar system - Varieties and similarities. *Vistas in Astronomy*, 21:209–239.

Hahn, J. M. and Malhotra, R. (1999). Orbital Evolution of Planets Embedded in a Planetesimal Disk. *Astronomical Journal*, 117:3041–3053.

Hébrard, G., Bouchy, F., Pont, F., Loeillet, B., Rabus, M., Bonfils, X., Moutou, C., Boisse, I., Delfosse, X., Desort, M., Eggenberger, A., Ehrenreich, D., Forveille, T., Lagrange, A.-M., Lovis, C., Mayor, M., Pepe, F., Perrier, C., Queloz, D., Santos, N. C., Ségransan, D., Udry, S., and Vidal-Madjar, A. (2008). Misaligned spin-orbit in the XO-3 planetary system? *A&A*, 488:763–770.

Henry, G. W., Marcy, G. W., Butler, R. P., and Vogt, S. S. (2000). A Transiting "51 Peg-like" Planet. *ApJL*, 529:L41–L44.

Howell, S. B., Everett, M. E., Esquerdo, G., Davis, D. R., Weidenschilling, S., and van Lew, T. (1999). Photometric Search for Extra-Solar Planets. In Craine, E. R., Crawford, D. L., and Tucker, R. A., editors, *Precision CCD Photometry*, volume 189 of *Astronomical Society of the Pacific Conference Series*, page 170.

Innanen, K. A., Zheng, J. Q., Mikkola, S., and Valtonen, M. J. (1997). The Kozai Mechanism and the Stability of Planetary Orbits in Binary Star Systems. *Astronomical Journal*, 113:1915.

Kley, W. and Nelson, R. P. (2012). Planet-Disk Interaction and Orbital Evolution. *Annual Review of Astronomy and Astrophysics*, 50:211–249.

Kley, W., Peitz, J., and Bryden, G. (2004). Evolution of planetary systems in resonance. *A&A*, 414:735–747.

Knutson, H. A., Fulton, B. J., Montet, B. T., Kao, M., Ngo, H., Howard, A. W., Crepp, J. R., Hinkley, S., Bakos, G. Á., Batygin, K., Johnson, J. A., Morton, T. D., and Muirhead, P. S. (2014). Friends of Hot Jupiters. I. A Radial Velocity Search for Massive, Long-period Companions to Close-in Gas Giant Planets. *ApJ*, 785:126.

Kozai, Y. (1962). Secular perturbations of asteroids with high inclination and eccentricity. *Astronomical Journal*, 67:591.

Lee, M. H. and Peale, S. J. (2002). Dynamics and Origin of the 2:1 Orbital Resonances of the GJ 876 Planets. *ApJ*, 567:596–609.

Lee, M. H. and Thommes, E. W. (2009). Planetary Migration and Eccentricity and Inclination Resonances in Extrasolar Planetary Systems. *ApJ*, 702:1662–1672.

Levison, H. F., Morbidelli, A., Gomes, R., and Backman, D. (2007). Planet Migration in Planetesimal Disks. *Protostars and Planets V*, pages 669–684.

Libert, A.-S. and Tsiganis, K. (2009). Trapping in high-order orbital resonances and inclination excitation in extrasolar systems. *MNRAS*, 400:1373–1382.

Lidov, M. L. (1962). The evolution of orbits of artificial satellites of planets under the action of gravitational perturbations of external bodies. *Planetary and Space Science*, 9:719–759.

Lin, D. N. C. and Papaloizou, J. (1979). Tidal torques on accretion discs in binary systems with extreme mass ratios. *MNRAS*, 186:799–812.

Lin, D. N. C. and Papaloizou, J. (1986). On the tidal interaction between protoplanets and the protoplanetary disk. III - Orbital migration of protoplanets. *ApJ*, 309:846–857.

Lithwick, Y. and Wu, Y. (2011). Theory of Secular Chaos and Mercury's Orbit. *ApJ*, 739:31.

Lithwick, Y. and Wu, Y. (2012). Resonant Repulsion of Kepler Planet Pairs. *ApJL*, 756:L11.

Lubow, S. H. and D'Angelo, G. (2006). Gas Flow across Gaps in Protoplanetary Disks. *ApJ*, 641:526–533.

Malmberg, D., Davies, M. B., and Heggie, D. C. (2011). The effects of fly-bys on planetary systems. *MNRAS*, 411:859–877.

Marcy, G. W., Butler, R. P., Fischer, D., Vogt, S. S., Lissauer, J. J., and Rivera, E. J. (2001). A Pair of Resonant Planets Orbiting GJ 876. *ApJ*, 556:296–301.

Masset, F. S. and Papaloizou, J. C. B. (2003). Runaway Migration and the Formation of Hot Jupiters. *ApJ*, 588:494–508.

Mayor, M. and Queloz, D. (1995). A Jupiter-mass companion to a solar-type star. *Nature*, 378:355–359.

McLaughlin, D. B. (1924). Some results of a spectrographic study of the Algol system. *ApJ*, 60:22–31.

Morbidelli, A., Tsiganis, K., Crida, A., Levison, H. F., and Gomes, R. (2007). Dynamics of the Giant Planets of the Solar System in the Gaseous Protoplanetary Disk and Their Relationship to the Current Orbital Architecture. *Astronomical Journal*, 134:1790–1798.

Murray, C. D. and Dermott, S. F. (1999). *Solar system dynamics*. Cambridge University Press.

Naoz, S., Farr, W. M., Lithwick, Y., Rasio, F. A., and Teyssandier, J. (2011). Hot Jupiters from secular planet-planet interactions. *Nature*, 473:187–189.

Naoz, S., Farr, W. M., Lithwick, Y., Rasio, F. A., and Teyssandier, J. (2013). Secular dynamics in hierarchical three-body systems. *MNRAS*, 431:2155–2171.

Nobili, A. and Roxburgh, I. W. (1986). Simulation of general relativistic corrections in long term numerical integrations of planetary orbits. In Kovalevsky, J. and Brumberg, V. A., editors, *Relativity in Celestial Mechanics and Astrometry. High Precision Dynamical Theories and Observational Verifications*, volume 114 of *IAU Symposium*, pages 105–110.

Ogilvie, G. I. and Lubow, S. H. (2002). On the wake generated by a planet in a disc. *MNRAS*, 330:950–954.

O'Toole, S. J., Tinney, C. G., Jones, H. R. A., Butler, R. P., Marcy, G. W., Carter, B., and Bailey, J. (2009). Selection functions in doppler planet searches. *MNRAS*, 392:641–654.

Papaloizou, J. C. B. and Larwood, J. D. (2000). On the orbital evolution and growth of protoplanets embedded in a gaseous disc. *MNRAS*, 315:823–833.

Papaloizou, J. C. B., Nelson, R. P., and Masset, F. (2001). Orbital eccentricity growth through disc-companion tidal interaction. *A&A*, 366:263–275.

Papaloizou, J. C. B. and Terquem, C. (2001). Dynamical relaxation and massive extrasolar planets. *MNRAS*, 325:221–230.

Papaloizou, J. C. B. and Terquem, C. (2010). On the dynamics of multiple systems of hot super-Earths and Neptunes: tidal circularization, resonance and the HD 40307 system. *MNRAS*, 405:573–592.

Peale, S. J. (1976). Orbital resonances in the solar system. *Annual Review of Astronomy and Astrophysics*, 14:215–246.

Pollack, J. B., Hubickyj, O., Bodenheimer, P., Lissauer, J. J., Podolak, M., and Greenzweig, Y. (1996). Formation of the Giant Planets by Concurrent Accretion of Solids and Gas. *Icarus*, 124:62–85.

Queloz, D., Eggenberger, A., Mayor, M., Perrier, C., Beuzit, J. L., Naef, D., Sivan, J. P., and Udry, S. (2000). Detection of a spectroscopic transit by the planet orbiting the star HD209458. *A&A*, 359:L13–L17.

Quillen, A. C. (2006). Reducing the probability of capture into resonance. *MNRAS*, 365:1367–1382.

Rasio, F. A. and Ford, E. B. (1996). Dynamical instabilities and the formation of extrasolar planetary systems. *Science*, 274:954–956.

Raymond, S. N., Barnes, R., Armitage, P. J., and Gorelick, N. (2008). Mean Motion Resonances from Planet-Planet Scattering. *ApJL*, 687:L107–L110.

Rein, H. (2012). Planet-disc interaction in highly inclined systems. *MNRAS*, 422:3611–3616.

Rein, H. and Papaloizou, J. C. B. (2009). On the evolution of mean motion resonances through stochastic forcing: fast and slow libration modes and the origin of HD 128311. *A& A*, 497:595–609.

Rein, H., Papaloizou, J. C. B., and Kley, W. (2010). The dynamical origin of the multi-planetary system HD 45364. *A&A*, 510:A4.

Rivera, E. J., Laughlin, G., Butler, R. P., Vogt, S. S., Haghighipour, N., and Meschiari, S. (2010). The Lick-Carnegie Exoplanet Survey: a Uranus-Mass Fourth Planet for GJ 876 in an Extrasolar Laplace Configuration. *ApJ*, 719:890–899.

Rossiter, R. A. (1924). On the detection of an effect of rotation during eclipse in the velocity of the brigher component of beta Lyrae, and on the constancy of velocity of this system. *ApJ*, 60:15–21.

Shakura, N. I. and Sunyaev, R. A. (1973). Black holes in binary systems. Observational appearance. *A&A*, 24:337–355.

Snellgrove, M. D., Papaloizou, J. C. B., and Nelson, R. P. (2001). On disc driven inward migration of resonantly coupled planets with application to the system around GJ876. *A&A*, 374:1092–1099.

Takeda, G., Kita, R., and Rasio, F. A. (2008). Planetary Systems in Binaries. I. Dynamical Classification. *ApJ*, 683:1063–1075.

Terquem, C. and Ajmia, A. (2010). Eccentricity pumping of a planet on an inclined orbit by a disc. *MNRAS*, 404:409–414.

Terquem, C. and Papaloizou, J. C. B. (2002). Dynamical relaxation and the orbits of low-mass extrasolar planets. *MNRAS*, 332:L39–L43.

Terquem, C. and Papaloizou, J. C. B. (2007). Migration and the Formation of Systems of Hot Super-Earths and Neptunes. *ApJ*, 654:1110–1120.

Terquem, C. E. J. M. L. J. (2003). Stopping inward planetary migration by a toroidal magnetic field. *MNRAS*, 341:1157–1173.

Teyssandier, J., Naoz, S., Lizarraga, I., and Rasio, F. A. (2013a). Extreme Orbital Evolution from Hierarchical Secular Coupling of Two Giant Planets. *ApJ*, 779:166.

Teyssandier, J. and Terquem, C. (2014). Evolution of eccentricity and orbital inclination of migrating planets in 2:1 mean motion resonance. *To appear in MNRAS*.

Teyssandier, J., Terquem, C., and Papaloizou, J. C. B. (2013b). Orbital evolution of a planet on an inclined orbit interacting with a disc. *MNRAS*, 428:658–669.

Thommes, E. W. and Lissauer, J. J. (2003). Resonant Inclination Excitation of Migrating Giant Planets. *ApJ*, 597:566–580.

Triaud, A. H. M. J., Collier Cameron, A., Queloz, D., Anderson, D. R., Gillon, M., Hebb, L., Hellier, C., Loeillet, B., Maxted, P. F. L., Mayor, M., Pepe, F., Pollacco, D., Ségransan, D., Smalley, B., Udry, S., West, R. G., and Wheatley, P. J. (2010). Spin-orbit angle measurements for six southern transiting planets. New insights into the dynamical origins of hot Jupiters. *A&A*, 524:A25.

Trilling, D. E., Benz, W., Guillot, T., Lunine, J. I., Hubbard, W. B., and Burrows, A. (1998). Orbital Evolution and Migration of Giant Planets: Modeling Extrasolar Planets. *ApJ*, 500:428.

Valtonen, M. and Karttunen, H. (2006). *The Three-Body Problem*.

Vokrouhlicky, D. and Karas, V. (1998). Stellar dynamics in a galactic centre surrounded by a massive accretion disc - I. Newtonian description. *MNRAS*, 298:53–66.

Ward, W. R. (1997). Protoplanet Migration by Nebula Tides. *Icarus*, 126:261–281.

Watson, C. A., Littlefair, S. P., Diamond, C., Collier Cameron, A., Fitzsimmons, A., Simpson, E., Moulds, V., and Pollacco, D. (2011). On the alignment of debris discs and their host stars' rotation axis - implications for spin-orbit misalignment in exoplanetary systems. *MNRAS*, 413:L71–L75.

Weidenschilling, S. J. and Marzari, F. (1996). Gravitational scattering as a possible origin for giant planets at small stellar distances. *Nature*, 384:619–621.

Williams, J. P. and Cieza, L. A. (2011). Protoplanetary Disks and Their Evolution. *Annual Review of Astronomy and Astrophysics*, 49:67–117.

Winn, J. N., Johnson, J. A., Fabrycky, D., Howard, A. W., Marcy, G. W., Narita, N., Crossfield, I. J., Suto, Y., Turner, E. L., Esquerdo, G., and Holman, M. J. (2009). On the Spin-Orbit Misalignment of the XO-3 Exoplanetary System. *ApJ*, 700:302–308.

Wolszczan, A. and Frail, D. A. (1992). A planetary system around the millisecond pulsar PSR1257 + 12. *Nature*, 355:145–147.

Wu, Y. and Lithwick, Y. (2011). Secular Chaos and the Production of Hot Jupiters. *ApJ*, 735:109.

Xiang-Gruess, M. and Papaloizou, J. C. B. (2013). Interaction between massive planets on inclined orbits and circumstellar discs. *MNRAS*, 431:1320–1336.

Appendix A

Laplace coefficients

We saw that writting down the disturbing function leads to terms of the following form:

$$\left(r_1^2 + r_2^2 - 2r_1 r_2 \cos\phi\right)^{-1/2}.$$

Using a Taylor series expansion, some terms appear of the form

$$\rho(\alpha) = \left(1 + \alpha^2 - 2\alpha\cos\psi\right)^{-s}, \tag{A.1}$$

where α, in this case, would be the semi-major axis ratio (see, e.g., Murray and Dermott, 1999, for more details). The function ρ is 2π periodic in ψ.

We recall that if f_s is a periodic function of period P, then it can be expanded in Fourier series:

$$f_s(x) = \frac{1}{2}a_s^0 + \sum_{j=1}^{\infty} a_s^j \cos(k\psi). \tag{A.2}$$

where the a_s^j are the Fourier coefficients, defined by:

$$a_s^j = \frac{2}{P}\int_0^P f_s(x)\cos\left(\frac{2\pi j x}{P}\right)\mathrm{d}x. \tag{A.3}$$

In our case we have

$$\left(1 + \alpha^2 - 2\alpha\cos\psi\right)^{-s} = \frac{1}{2}b_s^{(0)}(\alpha) + \sum_{j=1}^{\infty} b_s^{(j)}(\alpha)\cos(j\psi) \tag{A.4}$$

where the Laplace coefficients, noted $b_s^{(j)}$ are defined by:

$$b_s^{(j)}(\alpha) = \frac{1}{\pi}\int_0^{2\pi} \frac{\cos(j\psi)\mathrm{d}\psi}{(1 - 2\alpha\cos\psi + \alpha^2)^s} \tag{A.5}$$

where s is a half-integer. They can also be expressed by a series always convergent for

$\alpha < 1$:

$$\frac{1}{2}b_s^{(j)}(\alpha) = \frac{s(s+1)...(s-j+1)}{1.2.3...j}\alpha^j \times \left[1 + \frac{s(s+j)}{1(1+j)}\alpha^2 + \frac{s(s+1)(s+j)(s+j+1)}{1.2(j+1)(j+2)}\alpha^4 + ...\right] \tag{A.6}$$

More properties of the Laplace coefficients, and useful relations, including calculation of their derivatives, can be found in Brouwer and Clemence (1961) and Murray and Dermott (1999).

Appendix B

Complements on the Kozai mechanism

In this appendix we solve the integral which gives the relation between the argument of pericenter ω and the time τ, and show that its solution depends upon the value of the inclination with respect to a critical value of $39.23°$.

The argument of pericenter is linked to the time variable τ via the following equation:

$$\tau = \int_{\omega_0}^{\omega} \frac{\mathrm{d}\omega'}{a + b\sin^2\omega'}, \tag{B.1}$$

where $a = 3/2$ and $b = -(15/4)\sin^2 I$. We therefore seek the solutions of the following integral:

$$\mathcal{I} = \int_{x_1}^{x_2} \frac{\mathrm{d}x}{a + b\sin^2 x}. \tag{B.2}$$

Using the relation $\sin^2 x = (1 - \cos 2x)/2$, this integrale can be re-written

$$\mathcal{I} = \int_{2x_1}^{2x_2} \frac{\mathrm{d}x}{c + d\cos x}, \tag{B.3}$$

with $c = 2a + b$ and $d = -b$. We now set $t = \tan(x/2)$, such as $\cos x = (1 - t^2)/(1 + t^2)$ and $\mathrm{d}x = 2\mathrm{d}t/(1 + t^2)$. It follows that:

$$\mathcal{I} = \frac{2}{c + d} \int_{t_1}^{t_2} \frac{\mathrm{d}t}{1 + \frac{c-d}{c+d}t^2}. \tag{B.4}$$

From here we have two distinct cases, depending on the sign of $(c - d)/(c + d)$.

Case $(c - d)/(c + d) > 0$

If $(c - d)/(c + d) > 0$, we set $y = \beta t$, with $\beta = \sqrt{(c - d)/(c + d)}$. Hence:

$$\mathcal{I} = \frac{2}{\sqrt{(c + d)(c - d)}} \int_{y_1}^{y_2} \frac{\mathrm{d}y}{1 + y^2}. \tag{B.5}$$

Finally, in terms of the initial variables, we get

$$\mathcal{I} = \frac{1}{\sqrt{a(a+b)}} \left[\arctan\left(\sqrt{\frac{a+b}{a}} \tan\left(\frac{x}{2}\right) \right) \right]_{2x_1}^{2x_2}. \tag{B.6}$$

Case $(c-d)/(c+d) < 0$

If $(c-d)/(c+d) < 0$, we set $y = \beta t$, with $\beta = \sqrt{-(c-d)/(c+d)}$. Hence:

$$\mathcal{I} = \frac{2}{\sqrt{-(c+d)(c-d)}} \int_{y_1}^{y_2} \frac{\mathrm{d}y}{1-y^2}. \tag{B.7}$$

Using the identity

$$\frac{1}{1-y^2} = \frac{1}{2(1-y)} + \frac{1}{2(1+y)}, \tag{B.8}$$

we find

$$\mathcal{I} = \frac{2}{\sqrt{d^2-c^2}} \left[\ln \frac{y+1}{y-1} \right]_{y_1}^{y_2}, \tag{B.9}$$

which we re-write:

$$\mathcal{I} = \frac{1}{2\sqrt{-a(a+b)}} \left[\ln \frac{(a+b)\tan\frac{x}{2} - \sqrt{-a(a+b)}}{(a+b)\tan\frac{x}{2} + \sqrt{-a(a+b)}} \right]_{2x_1}^{2x_2}. \tag{B.10}$$

We note that the condition $(c-d)/(c+d) > 0$ is equivalent to $c^2 > d^2$, which in turn is the same as $a(a+b) > 0$. Similarly, $(c-d)/(c+d) < 0$ is equivalent to $a(a-b) < 0$. Therefore, all the quantities in the square roots and logarithms are well-defined. Hence we have:

$$\int_{\omega_0}^{\omega} \frac{\mathrm{d}\omega}{a + b\sin^2\omega} = \begin{cases} \frac{1}{\sqrt{a(a+b)}} \arctan\left[\frac{(a+b)\tan\omega}{\sqrt{a(a+b)}} \right] & \text{if } a(a+b) > 0 \\ \frac{1}{2\sqrt{-a(a+b)}} \ln\left[\frac{(a+b)\tan\omega - \sqrt{-a(a+b)}}{(a+b)\tan\omega + \sqrt{-a(a+b)}} \right] & \text{if } a(a+b) < 0. \end{cases} \tag{B.11}$$

To derive this solution we have assumed $w_0 = \pi/2$ when $\tau = 0$ for the case $I > 39.23°$, and $w_0 = 0$ when $\tau = 0$ for the case $I < 39.23°$. This allows us to get rid of integration constants without loss of generality.

Futhermore, we have:

$$a(a+b) > 0 \iff \frac{3}{2}\left(\frac{3}{2} - \frac{15}{4}\sin^2 I\right) > 0 \iff \sin^2 I < \frac{2}{5} \iff I < 39.23° \text{ or } I > 140.77°$$

and similarly

$$a(a+b) < 0 \iff 39.23° < I < 140.77°.$$

We restrict ourselves to the case $I < 90°$ but symmetrical results yield for $I > 90°$. The

solution can be inverted to give ω as a function of time:

$$\omega = \begin{cases} \arctan\left[\sqrt{\frac{2}{A}}\frac{e^{\frac{3}{2}\sqrt{2A}\tau}+1}{e^{\frac{3}{2}\sqrt{2A}\tau}-1}\right] & \text{if } I > 39.23^\circ \\ \arctan\left[\sqrt{\frac{2}{-A}}\tan\left(\frac{3}{4}\sqrt{-2A}\tau\right)\right] & \text{if } I < 39.23^\circ. \end{cases} \tag{B.12}$$

where we recall that $A = 5\sin^2 I - 2$.